

# Coordinated Control of Marine Craft

Ivar-André Flakstad Ihle

Thesis for the degree of philosophiae doctor



NORWEGIAN UNIVERSITY OF SCIENCE AND TECHNOLOGY  
FACULTY OF INFORMATION TECHNOLOGY, MATHEMATICS AND  
ELECTRICAL ENGINEERING  
DEPARTMENT OF ENGINEERING CYBERNETICS



# Summary

This thesis contains new results on the problem of coordinating a group of vehicles. The main motivation driving this work is the development of control laws that steer individual members of a formation, such that desired group behavior emerges. Special attention is paid to analysis of coordination issues, in particular formation control of marine craft where robustness to unknown environmental forces is important. Coordinated control applications for marine craft include: underway replenishment, maintaining a formation for increased safety during travel and instrument resolution, and cooperative transportation. A review of formation control structures is given, together with a discussion of special issues that arise in coordination of independent vehicles.

The main contributions of this thesis may be grouped into two categories:

- Path-following designs for controlling a group of vehicles
- Multi-body motivated formation modeling and control

A previously developed path following design is used to control a group of vehicles by synchronizing the individual path parameters. The path following design is advantageous since the path parameter, i.e., that parameter which determines position along a path, is scalar; hence coordination is achieved with a little amount of real-time communication. The path following design is also extended to the output-feedback case for systems where only parts of the state vector are known.

The path following scheme is exploited further in a passivity-based design for coordination where the structural properties render an extended selection of functions for synchronization available. Performance and robustness properties in different operational conditions can be enhanced with a careful selection of these functions. Two designs are presented; a cascaded interconnection where a consensus system provides synchronized path parameters as input to the individual path following systems renders time-varying formations possible and increases robustness to communication problems; a feedback interconnection which is more robust to vehicle failures. Both designs are extended to sampled-data designs where plant and controller dynamics are updated in continuous-time and path parameters are

exchanged over a communication network where transmission occurs at discrete intervals. Bias estimation is included to provide integral action against slowly-varying environmental forces and model uncertainties.

A scheme for formation modeling and control, inspired by analytical mechanics of multi-body systems and Lagrangian multipliers, is proposed. In this approach to formation control, various formation behaviors are determined by imposing constraint functions on group members. Several examples illustrate these formation behaviors. The stabilization scheme presented is made more robust with respect to unknown time-varying disturbances. In addition, the scheme is extended towards adaptive estimation of unknown plant and parameters. Furthermore, it can be applied with no major modifications to the case of position control for a single vehicle.

The formation control scheme is such that it may be used in combination with a set of position control laws for a single vessel, thus enabling the designer to choose from a large class of control laws available in the literature. The input-to-state stability (ISS) framework is utilised to investigate robustness to environmental and communication disturbances. A loop-transform, together with the ISS framework, yields an upper bound on the inter-vessel time delay below which formation stability is maintained.

# Preface

This thesis is based on the results of my research from 2003 through 2006, primarily at the Norwegian University of Science and Technology under the guidance of Professor Thor I. Fossen and Dr. Jérôme Jouffroy, and partly at the Rensselaer Polytechnical Institute (RPI) under the guidance of Professor Murat Arcak. My funding has been supported by the Norwegian Research Council through the Centre for Ships and Ocean Structures–Centre of Excellence directed by Professor Torgeir Moan.

Research is never a solitary task and my work has benefitted significantly from the supervision of Thor I. Fossen whose motivational skills and contacts have proved very valuable and should not be underestimated. Thanks to my co-supervisor Jérôme Jouffroy for putting the *ph* in philosophiae. I am particularly grateful to Murat Arcak who invited me to RPI and introduced me to many valuable topics and researchers. Thanks to Roger Skjetne for being an unofficial supervisor during the first stumbling steps of my career as a researcher.

I deeply appreciated the discussions with my colleagues from Department of Engineering Cybernetics and Centre for Ships and Ocean Structures. A special thanks to Morten Breivik for the many discussions regarding science and the reasonably quiet office for the last three years; Frank Jakobsen, Johannes Tjønnås & Jostein Bakkeheim for the highly philosophical questions, nonstop motivation and many laughs; Andreas Egeberg & Jon Espen Ingvaldsen for their technical, financial and musical advice; Andrew Ross & Mícheál Ó. Catháin for improving my English; Øyvind Smogeli for debugging SWP; Per Ivar Berntsen for improving my caffeine and lactic acid level, Kari Unneland, Anders Wroldsen & Anne Marthine Rustad for the great skiing; Jon Refsnes for his riddles, Tristan Perez for the great scientific anecdotes; Filippo Arrichiello for interesting discussions; Emrah Biyik & Aranya Chakraborty for welcoming me to their lab at RPI.

I would like to thank my entire family for their love and support. Finally, I am deeply grateful to my girlfriend Siri Nelson whose enchanting smile and laughter have helped me through the many steps involved in obtaining a Ph.D.

Fredrikstad, Norway  
September 2006

IVAR-ANDRE FLAKSTAD IHLE



# Contents

<b>Summary</b>	<b>iii</b>
<b>Preface</b>	<b>v</b>
<b>1 Introduction</b>	<b>1</b>
1.1 Motivation . . . . .	1
1.2 Background . . . . .	5
1.3 New Developments . . . . .	12
1.4 Marine Control Systems . . . . .	15
1.5 Mathematical Preliminaries . . . . .	18
<b>2 Formation and Output-Feedback Maneuvering Control</b>	<b>23</b>
2.1 Introduction . . . . .	23
2.2 Formation Maneuvering Design . . . . .	27
2.3 Maneuvering Design for Output-Feedback Systems . . . . .	34
2.4 Experimental Evaluation with Cybership II . . . . .	40
2.5 Concluding Remarks . . . . .	45
<b>3 Passivity-Based Designs for Synchronized Path Following</b>	<b>47</b>
3.1 Introduction . . . . .	47
3.2 Path-Following Design and Synchronization . . . . .	48
3.3 Passivation Designs for Synchronization . . . . .	49
3.4 Sampled-Data Design with Discrete-Time Update for $\theta$ . . . . .	56
3.5 Integral Action by Adaptive Backstepping . . . . .	60
3.6 Examples . . . . .	63
3.7 Concluding Remarks . . . . .	71
<b>4 Multi-Body Interpretation of Formation Control</b>	<b>73</b>
4.1 Introduction . . . . .	73
4.2 Formation Modeling . . . . .	75
4.3 Stabilization of Constraint Functions . . . . .	79

4.4	Extensions to Other Control Schemes . . . . .	87
4.5	Discussion . . . . .	89
4.6	Examples . . . . .	92
4.7	Concluding Remarks . . . . .	99
<b>5</b>	<b>Combined Position and Formation Control</b>	<b>101</b>
5.1	Preliminaries . . . . .	102
5.2	Formation Modeling and Control of Marine Surface Vessels . . . . .	103
5.3	Robustness to Disturbances . . . . .	106
5.4	Robustness to Time-Delays . . . . .	110
5.5	Case Study: Rendezvous operation . . . . .	111
5.6	Concluding Remarks . . . . .	114
<b>6</b>	<b>Final Remarks</b>	<b>117</b>
<b>A</b>	<b>Mathematical Toolbox</b>	<b>119</b>
A.1	Lyapunov Stability . . . . .	119
A.2	Input-to-State Stability . . . . .	124
A.3	Passivity . . . . .	125
A.4	Stability of Interconnected Systems . . . . .	128
A.5	Useful Inequalities . . . . .	132
<b>B</b>	<b>Mathematical Modeling of Marine Vessels</b>	<b>133</b>
B.1	Vessel Kinematics . . . . .	133
B.2	Vessel Kinetics . . . . .	135
B.3	3 DOF Vessel Model . . . . .	140
B.4	Autopilot Models . . . . .	140
B.5	Environmental Forces . . . . .	141
<b>C</b>	<b>Detailed Proofs</b>	<b>145</b>
C.1	Proof of Theorem 5.2 . . . . .	145
C.2	Proof of Theorem 5.3 . . . . .	148
C.3	Proof of Theorem 5.4 . . . . .	150
	<b>References</b>	<b>155</b>

# Chapter 1

## Introduction

This thesis considers the problem of coordinating a group of marine craft, that is, we want to steer the motion of each craft such that the group's overall motion is governed by a desired behavior. Thus, independent motion is coordinated as a *formation* according to the behavior, decided by the designer. Such control problems have attracted increasing attention during the last decade due to the many benefits of distributed vehicles controlled as a formation.

Some of the reasons to consider the use of formations is their characteristics of: structural flexibility, safety, reliability through redundancy, increased instrument resolution, tactical advantages, reduced cost (several simple, inexpensive systems can compete with single sophisticated expensive systems), and faster resource location (a group of vehicles can rapidly search a large area than a single vehicle).

### 1.1 Motivation

The benefits of formations were realized by military leaders a long time ago and has been used in land, sea and air—see Figure 1.1 for a marine example. Examples of different tactical formations are arrowhead, square, single column, or line abreast. Examples of medieval or ancient formations include shield walls (skjaldborg in Old Norse), phalanxes (lines of battle in close order), and skirmishers. Examples of military aircraft tactical formations are the V formation, the combat box, the fluid four formation, and the loose deuce formation. Increased safety and armed defensive support were parts of the motivation to use group of ships travelling together, also known as *convoys*, for transporting supplies during World War II.

Formations also have the benefit of improved instrumentation: the Navstar Global Positioning System use 24 satellites in intermediate circular orbits, and the orbits are designed so at least four satellites are always within line of sight from almost any place on earth. The receiver reception is better when more signals are

available. Furthermore, the US Air Force is increasingly using unmanned aerial vehicles (UAVs) equipped with cameras and sensors to automate reconnaissance, surveillance and target acquisition and as communication relays. Lately, groups of UAVs are used such that one vehicle investigates a particular location while the rest secure the widest area possible. For the *Terrestrial Planet Finder* to be launched in 2014, NASA considers spacecraft formation flying that will work together to function as a single huge telescope. The spacecraft will be virtually connected and autonomously position themselves in a rigid formation—see Wang & Hadaegh (1996), Beard, Lawton & Hadaegh (2001) and references therein.



Figure 1.1: Six of the U.S. Navy’s seven Amphibious assault ships in formation. Courtesy of U.S. Navy, [www.navy.mil](http://www.navy.mil).

During migration season it is common to observe flocks of birds flying in formations. The V-shaped formation, shown in Figure 1.2, used by some of the larger birds, such as ducks and geese, reduces energy expenditure and flight power demands. The energy savings arise from longer periods of gliding during flight and a reduction of the induced drag. Flying in a formation also favours communication and coordination within the group and may explain why some configurations of bird flocks are neutral or even disadvantageous compared to solitude flight—see e.g. Badgerow & Hansworth (1981) and Weimerskirch, Martin, Clerquin, Alexandre & Jiraskova (2001). The induced drag energy savings has motivated researchers, such as Hoerner (1958), to theoretically and experimentally reduce drag forces in formation airplane flight. This work is extendable to marine vehicles.

Animal groups such as schools of fish, flocks of birds, and herds of ungulates have also other purposes and benefits than increased efficiency of locomotion. Evolutionary ecologists and sociobiologists try to understand coordination of natural

groupings by modeling the social aggregation behavior of each individual: Such behavior depends on group structure, nearby obstacles and predators (detect and avoid), and resource location to name a few. Such individual-based models are found in e.g. Partridge (1982), Okubo (1986) and Grünbaum, Viscido & Parrish (2005). Vicsek, Czirók, Ben-Jacob, Cohen & Shochet (1995) develop a model based on nearest-neighbor rules which has been used as a basis for many papers in control systems theory.

Interesting topics regarding coordinated action amongst humans are behavior in traffic, the Mexican wave, and panic control—considered in Dirk & Huberman (1998), Farkas, Helbing & Vicsek (2002), and Helbing, Farkas & Vicsek (2000), respectively. Gladwell’s (2000) best-seller *The Tipping Point* describes collective human behavior in various situations and relates *social epidemics* to how manufacturers can create a market-winning product.



Figure 1.2: Flock of geese.

These observations have motivated control systems engineers to develop feedback control laws that synchronize and govern formations of autonomous vehicles. Applications in the literature cover a wide area of operation. Robot manipulators, mobile robots, satellites, and unmanned (aerial or underwater) vehicles are among the systems considered. Schoenwald (2000) points out that, in these applications, communication constraints and environmental disturbances pose challenges for control design. A more detailed introduction to the field of coordinated control and related problems is given in the following section.

This thesis approaches the coordinated control problem in two directions: The first is based on a *maneuvering* design from Skjetne, Fossen & Kokotović (2004) and Skjetne (2005), where mechanical systems are designed to follow a given path with a dynamic assignment along the path (time, speed, or acceleration). By performing an individual design for each system in a group and then control the positions along the paths we *synchronize* the maneuvering systems. The second approach is a multi-body interpretation of formation control: a group is held together by forces which are given by a set of functions that describe group member’s behavior. This latter approach is valid for both formation modeling and control purposes. For both schemes, emphasis has been placed on robustness to com-

munication constraints and environmental disturbances. Parts of the design and examples are aimed towards marine craft, but are extendable to other mechanical systems with similar structural properties. By working with marine craft we remain in the framework of Fossen (2002) and thus consider marine and offshore applications where robustness is highly important.

**Example 1.1 (Icebreaker Escort)** *During winter, the sea of Bothnia freezes over so vessels without icebreaking capabilities must be escorted by an icebreaker to and from Finnish and Estonian harbors—see Figure 1.3. Large vessels, such as tankers, may require two icebreakers. The vessel and the escort must be within a certain range of each other: too far away and the passage in the ice may close; too close and they might collide. This can be solved by either designing a desired path through the ice and steering the group of vessel and icebreaker(s) along it. Or, we can control the vessel to keep a fixed distance, or remain in a range relative, to the icebreakers.*



Figure 1.3: Ice Breaker and Drillship in the Beaufort Sea. Courtesy of Minerals Management Service, [www.mms.gov](http://www.mms.gov).

**Example 1.2 (Underway Replenishment)** *Underway replenishment, see Figure 1.4, also called replenishment at sea, is a method of transferring fuel, munitions, and stores from a supply ship to a combat ship while underway. For more information, see Wikipedia (2006a) and Coombe (2005). The idea of supplying ships at sea started as sail gave way to steam and became more important as oil became the principal fuel<sup>1</sup>. Both astern or abeam (side-by-side) methods are used for under-way refuelling. With the abeam method multiple transfer rigs are set up so that more than one type of supplies are transferred at the same time. However,*

<sup>1</sup>The first practical plans for coaling vessels at sea were put forward by two Royal Navy officers in 1887. The US Navy were the first to carry out under-way coaling experiments in 1899.

*one of the principal problems in abeam refuelling is the suction effect caused by the bow waves of the two vessels which cause the vessels to be drawn together. These forces are effectively zero when the vessels are a certain distance from each other and it seems natural that control laws can improve replenishment operations by coordinating the vessels such that they hold the same course and speed and maintain the required distance. A civilian application of this concept is offshore loading (tandem and side-by-side) where oil and gas are transported from a production or storage unit to another vessel for transportation.*



Figure 1.4: Double underway replenishment. Courtesy of U.S. Navy, [www.navy.mil](http://www.navy.mil).

**Example 1.3 (Coordinated Transportation)** *A possible future application for coordinated control of marine surface vessels is cooperative manipulation, that is, coordinate the motion of tugboats to manipulate the position and orientation of a large object, such as, a oil platform, an aircraft carrier (see Figure 1.5) or a barge, by pushing or pulling. Such operations require very high positioning accuracy, and by using a control system to quickly counteract undesired movements, safety is improved.*

Other examples of coordinated control of marine craft are formation control of AUVs and autonomous ocean-sampling networks—see e.g., Curtin & Bellingham (2001), Leonard & Graver (2001), and other articles in that issue.

## 1.2 Background

Coordinated control implies motion control of several independent objects towards a common goal. Agreement protocols, consensus algorithms, synchronization, cooperative and formation control are other terms used to describe similar control



Figure 1.5: Tug boats helping the USS John F. Kennedy into port. Courtesy of U.S. Navy, [www.navy.mil](http://www.navy.mil).

problems in the current literature, and the amount of control system papers in these fields is vast. This section gives a brief background to these topics from a control system theoretic point of view, reviews some of the main approaches, and presents examples for marine control systems. In addition some related challenges and topics are discussed.

### 1.2.1 From Models to Feedback Control

Researchers have been inspired by natural phenomena when finding models for group behavior. The animation model by Reynolds (1987) appears to be an important motivation for many results on coordinated systems. It produces realistic crowd behavior and has been used in movies such as *The Lion King* and *Batman Returns*. The idea is simple and beautiful. Each model consists of three steering behaviors that describe the individual maneuvers based on its neighbors:

- Separation: steer to avoid crowding local flockmates
- Alignment: steer towards the average heading of local flockmates
- Cohesion: steer to move toward the average position of local flockmates

Vicsek et al. (1995) propose a discrete-time model of  $n$  autonomous agents moving in the plane with a heading that is updated using a local rule based on the

average of its own heading and its neighbors (The model turns out to be a special case of Reynold's model). Jadbabaie, Lin & Morse (2002) provide theoretical explanations for the observed behavior and convergence results for a set of similar models.

Biologists have been working on modeling for flocking, schooling and swarming behavior for a long time, and mathematicians prove stability of these models: Gazi & Passino (2004) present an overview of biological swarm models and study the stability properties of an aggregating swarm where an attraction/repulsion function, called an artificial social potential, determines the individual motion. Stable flocking is reported in Tanner, Jadbabaie & Pappas (2003a) and Tanner, Jadbabaie & Pappas (2003b) for a fixed and dynamic topology respectively using inter-agent potential functions. Olfati-Saber (2006) present an algorithm for flocking in the presence of multiple obstacles. According to Ögren, Fiorelli & Leonard (2004) it is expected that a cooperative mobile network of sensors can outperform a single large vehicle with multiple sensors when the goal is to climb the gradient of an environmental field to locate resources.

The models from biology show structural equalities with many of the models found in the control literature. Full and partial synchronization of coupled time invariant systems has been studied in Pogromsky, Santoboni & Nijmeijer (2002). In addition, it shows how the concept of *feedback* for control systems couple individual systems and asymptotically stabilize a network of systems.

### 1.2.2 Group Coordination and Control

There exists a large number of publications on feedback in the fields of cooperative control of autonomous systems—recent results are found in Beard et al. (2001), Nijmeijer & Rodriguez-Angeles (2003), Fax & Murray (2004), Spry & Hedrick (2004), Ögren et al. (2004), Kingston, Wei & Beard (2005), Kumar, Leonard & Morse (2005), and references therein. A recent survey paper by Ren, Beard & Atkins (2005) connects various coordinated control problems with consensus problems known from other scientific fields. While the applications are different, some common fundamental parts can be extracted from the many approaches to vehicle formation control. Roughly three approaches are found in the literature.

#### Leader-Follower

Briefly explained, the *leader-following* architecture defines a leader in the formation while the other members of the formation follow that leader's position and orientation with some prescribed offset. One of the first studies on leader-following formation control for mobile robots is reported in Wang (1991). Sheikholeslam & Desoer (1992) formulate decentralized control laws for the highway congestion

problem using information from the leader's dynamics and the distance to the proceeding vehicle. Variations on this theme include multiple leaders, forming a chain, and other tree topologies. This approach has the advantage of simplicity in that the internal stability of the formation is implied by stability of the individual vehicles, but is heavily dependent on the leader for achieving the control objective. Over-reliance on a single vehicle in the formation may be disadvantageous, and the lack of explicit feedback from the formation to the leader may destabilize the formation. A leader-follower architecture for marine craft has been approached in Encarnação & Pascoal (2001a), where an autonomous underwater vehicle is forced to track the motion of an autonomous surface craft, projected down to a fixed depth.

### Behavioral Methods

The *behavioral* approach prescribes a set of desired behaviors for each member in the group, and weighs them such that desirable group behavior emerges without an explicit model of the subsystems or the environment. Possible behaviors include trajectory and neighbor tracking, collision and obstacle avoidance, and formation keeping. One paper that describes the behavioral approach for multi-robot teams is Balch & Arkin (1998) where formation behaviors are implemented with other navigational behaviors to derive control strategies for goal seeking, collision avoidance and formation maintenance. In formation control, several objectives need to be met and from the behavioral approach it is expected that averaging the weighted (perhaps competing) behaviors give a control law that meets the control objectives. This approach motivates a decentralized implementation where feedback to the formation is present, since a vehicle reacts according to its neighbors.

When the behavioral rules are given as algorithms, this approach is hard to analyze mathematically: the group behavior is not explicit, and characteristics such as stability cannot generally be guaranteed. System-theoretic approaches to behavioral control can be found in Stilwell & Bishop (2002) and Antonelli & Chiaverini (2004). The authors use a set of functions and control techniques for redundant robotic manipulators given in Siciliano & Slotine (1991) to control a platoon of autonomous vehicles. Different tasks can be merged, according to their priority, with an inverse kinematics algorithm.

### Virtual Structures

In the *virtual structure* approach, the entire formation is treated as a single, virtual, structure and acts as a single rigid body. The control law for a single vehicle is derived by defining the dynamics of the virtual structure and then translate the motion of the virtual structure into the desired motion for each vehicle. Virtual

structures have been achieved by, for example, having all members of the formation tracking assigned nodes which move through space in the desired configuration, and using formation feedback to prevent members leaving the formation as in Beard et al. (2001) and Ren & Beard (2004). In Egerstedt & Hu (2001) each member of the formation tracks a virtual element, while the motion of the elements are governed by a formation function that specifies the desired geometry of the formation. This approach makes it easy to prescribe a coordinated behavior for the group, while formation keeping is naturally assured by the approach. However, if the formation has to maintain the exact same virtual structure at all times, the potential applications are limited. Skjetne, Moi & Fossen (2002) create a virtual structure of marine surface vessels by using a centralized control law that maneuvers the formation along a predefined path. More details on synchronized path following are found in Chapter 2.

### 1.2.3 Group Coordination Issues

#### Formation Control System Architecture

According to Beard et al. (2001) coordinated control of independent systems involves at least two layers of abstraction as in Figure 1.6. The highest level of abstraction is a mechanism that coordinates the motion of each system to synthesize the desired group behavior, while at the lower level the individual systems are controlled to be consistent with the coordinating mechanism. The local controller might also incorporate a control law for solving a local control objective, and dynamic path planning for collision and obstacle avoidance.

This representation encompasses both *centralized* and *decentralized* control designs and implementations: A centralized controller has a supervisor (coordination scheme) at a centralized location, and decentralized control implies that a local version of the coordination scheme must be implemented for each system. A centralized control system is dependent on all system states and requires high-bandwidth communication. For decentralized control the local coordination schemes must be synchronized, often with a subset of the systems, e.g., the neighbors. A low-bandwidth solution can be accomplished by constructing a local observer that estimate states needed for coordination.

With formation feedback the formation is able to adjust overall speed and position online, and remain in a coordinated state if something unexpected should occur. With no formation feedback, the architecture takes on a cascaded structure.

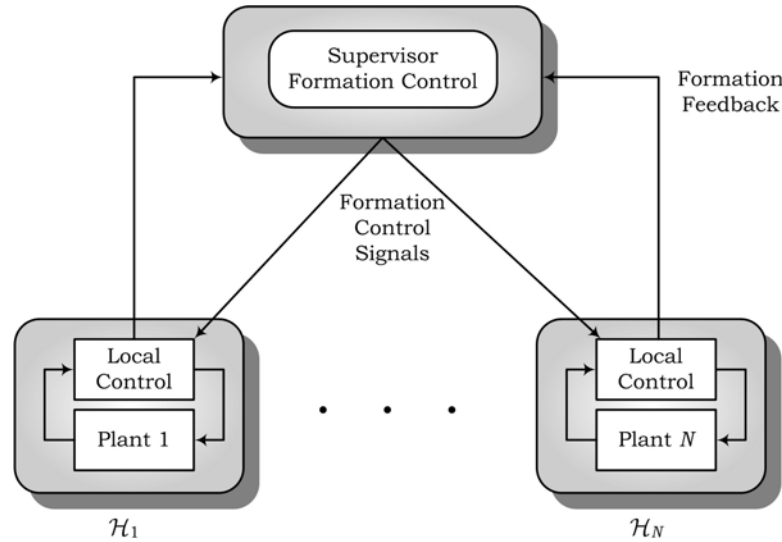


Figure 1.6: A two-level architecture for coordinated control of  $N$  systems.

### Formation Configuration

Depending on its current coordination goal a formation can have many different shapes. For example, marine surface vessels can be in a side-by-side formation during underway replenishment operations or in a V formation during transit (to save energy). Thus, formation control systems should be able to encompass changing configurations during operation. In addition, with a stable dynamic formation topology, vehicles are permitted to leave and join the formation without changing the formation stability properties. This can further be extended to allow formations to split and merge. Dynamic topologies are considered in, e.g., Tanner et al. (2003b), Fax & Murray (2004), Olfati-Saber & Murray (2004), and Arcaik (2006).

### Sharing Information And Communication

When several control systems are to be coordinated, information must be exchanged between them in order to complete the control task. Ren, Beard & McLain (2005) states the following intuitive axiom:

**Axiom 1.1** *Shared information is a necessary condition for coordination.*

The amount of communicated information depends on the coordination task: if two system must synchronize their position, some information about the other

systems position must be known. If the goal is synchronized motion (both position and velocity), the systems must also share information about their velocity.

**Example 1.4** *An effective approximation of the relationship between yaw  $r$  and rudder action  $\delta$  is the first order Nomoto model*

$$\frac{r}{\delta}(s) = \frac{K}{(1 + Ts)} \quad (1.1)$$

where  $T$  and  $K$  are known as the Nomoto time and gain constants. Consider the autopilot model for two ships

$$r_i(s) = \frac{K_i}{1 + T_i s} \delta_i(s), \quad i = 1, 2$$

Neglecting the roll and pitch modes such that  $\dot{\psi}_i = r_i$ , we obtain

$$\frac{\psi_i}{\delta_i}(s) \approx \frac{K_i}{s(1 + T_i s)}$$

If we define the coordination goal to be equal heading, that is  $\psi_1 = \psi_2$ , the ships must exchange their heading information. We choose a proportional-derivative structure for the rudder actions:

$$\delta_i = -k_p(\psi_i - \psi_j) - k_d \dot{\psi}_i, \quad i, j = 1, 2, i \neq j$$

where  $k_p$  and  $k_d$  are positive scalars. Starting with initial headings  $\psi_{10} = -10^\circ$  and  $\psi_{20} = 30^\circ$  the synchronization is shown in Figure 1.7. The ships move with parallel heading by only communicating the scalar heading variable, but to control their position a different model and control law must be used since no position information is present. Thus, more information than just the headings must be shared.

The coordination goal might be: assembling into a desired formation configuration, ending up at a given location at an appointed time, or synchronized motion. An alternative to sharing both position and velocity information during operations, is to consider synchronized paths which incorporates information of not only position but also velocity and acceleration assignments. Thus, motion can be coordinated with a smaller amount of shared information since a position on the path implies fixed speed and velocity assignments. In order to achieve proper synchronization, the individual paths must be coordinated at the start of the operation.

Information must be exchanged over a communication channel. Typically, for a set of independent vehicles, a communication protocol is set up over a physical medium, e.g., using radio-, acoustic, or optic signals. Moreau (2005) study

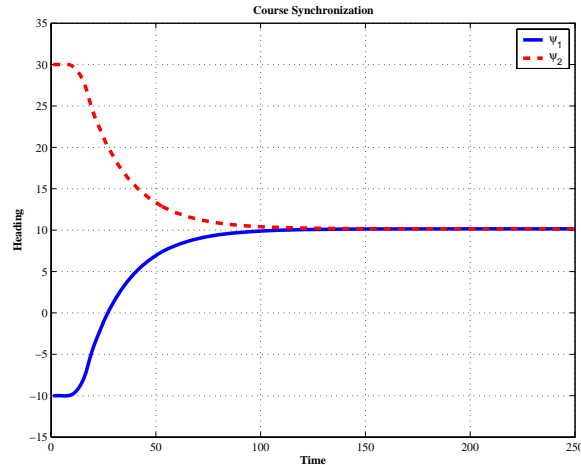


Figure 1.7: Synchronization of two Nomoto autopilot models.

multi-agent systems with time-dependent communication links; Olfati-Saber & Murray (2004) investigate consensus problems with time-delays. Standard communication protocols offer robustness to signal loss, delays, etc., but communication issues such as inconsistent delays, noise, signal dropouts, and possible asynchronous updates should be taken into account in the formation control architecture. Stojanovic (2003) and Akyildiz, Pompili & Melodia (2005) consider underwater communication for autonomous ocean-sampling networks: since electromagnetic waves propagate very poorly in sea water, acoustic and seismic technology provides the most important means of communication, navigation and imaging below the sea surface. Acoustic communication, however, is influenced by noise, path loss, multi-path, Doppler spread, and high and variable propagation delay. In environments with limited bandwidth a formation control design with a minimal amount of information exchange is desired.

Information can also be transmitted through the environment: the tension of a wire between two ships can indicate whether the relative position is changing, and if so, in which direction. We will only consider dedicated communication links but Kube & Bonabeau (2000) contains information about environmental communication and its application to cooperative control for the interested reader.

Although the data is typically transmitted in discrete-time, controllers and internal dynamics may be continuous time, which means a sampled-data analysis of the system is necessary. A sampled-data design for synchronized path following is presented in Section 3.4. However, the other designs in this thesis are in continuous time.

## 1.3 New Developments

### 1.3.1 Contributions of this Thesis

An overall motivation for this thesis has been *adaptability* – the proposed designs should be able to benefit from previous results that can be used in a new setting – and *flexibility* – designs should be flexible such that designers can choose from a wide set of available methods to perform the desired control action. The contributions can be summarized as follows:

- Chapter 2: The previously developed maneuvering problem is extended to the *formation maneuvering problem* such that multiple maneuvering systems are controlled as a formation. With careful path planning, the design covers a wide range of applications. An output-feedback design is proposed to solve the maneuvering problem when only parts of the state vector are available for feedback. The theoretical results are experimentally validated with Cybership II in the Marine Cybernetics Laboratory. This chapter is based on joint work with Roger Skjetne and Thor Inge Fossen.
- Chapter 3: By combining the results on path following and passivity schemes for group coordination we obtain a larger set of functions that can be used for formation control. This new set can be exploited to a design which increases robustness to known disturbances, thruster saturations, environmental forces, communication disturbances and delays. The *passivity framework* for coordinated control is further extended to a sampled-data design where inter-vessel communication occur at discrete time-intervals while each member's controllers and internal dynamics may be continuous-time. Bias estimation is analyzed to counteract environmental disturbances. The scheme's passivity properties preserve stability for time-varying configurations, e.g., when vessels enter or leave the formation and enables the designer to exploit a set of filters to achieve enhanced robustness and performance properties. This chapter is based on joint work with Murat Arcak and Thor Inge Fossen.
- Chapter 4: A scheme for formation modeling and control is developed to encompass the benefits of behavioral methods and virtual structures and address some of their weaknesses. The control scheme is inspired by multi-body dynamics and *Lagrangian* mechanics and the resulting control laws have an intuitive structure. Several formation behaviors, given as a class of functions, can be simulated. The formation configuration can be adjusted by using time-varying constraint functions. Furthermore, the same approach has been applied with no major modification to position control purposes for a single system. A robustifying design to counteract known disturbances on

the formation is proposed. This chapter is based on joint work with Jérôme Jouffroy and Thor Inge Fossen.

- Chapter 5: The formation control scheme is used in closed-loop with a position control law for a single vessel. This suggests a *modularity* approach for coordinated control and allows the designer to consider control laws from the existing literature. Robustness to environmental loads and communication noise is investigated, and stability in the presence of time delays is discussed. The detailed proofs are given in Appendix C. This chapter is based on joint work with Jérôme Jouffroy and Thor Inge Fossen.

### 1.3.2 Publications

The following is a complete list of the author's publications written during 2003-2006. This includes both accepted and submitted papers.

#### Journal Papers & Book Chapters

- Ihle, I.-A. F., Jouffroy, J. & Fossen, T. I. (2006), 'Formation control of marine surface craft: A Lagrangian approach', *IEEE Journal of Oceanic Engineering* 31(3).
- Ihle, I.-A. F., Jouffroy, J. & Fossen, T. I. (2006), Robust formation control of marine craft using Lagrange multipliers, *in* K. Y. Pettersen, T. Gravdahl & H. Nijmeijer, eds, 'Group Coordination and Cooperative Control', number 336 *in* 'Lecture Notes in Control and Information Sciences', Springer-Verlag, Berlin Heidelberg, chapter 7, pp. 113—130.
- Ihle, I.-A. F., Arcak, M. & Fossen, T. I. (2006), 'Passivity-based designs for synchronization of path following systems', *Automatica*. Submitted.

#### Conference Papers

- Skjetne, R., Ihle, I.-A. F. & Fossen, T. I. (2003), Formation Control by Synchronizing Multiple Maneuvering Systems, *in* 'Proc. 6th IFAC Conference on Manoeuvring and Control of Marine Crafts', Girona, Spain, pp. 280—285
- Ihle, I.-A. F., Skjetne, R. & Fossen, T. I. (2004), Nonlinear formation control of marine craft with experimental results, *in* 'Proc. 43rd IEEE Conf. on Decision & Control', Atlantis, Paradise Island, The Bahamas, pp. 680—685.

- Ihle, I.-A. F., Skjetne, R. & Fossen, T. I. (2005), Output feedback control for maneuvering systems using observer backstepping, *in* ‘Proc. IEEE International Symposium on Intelligent Control, Mediterranean Conference on Control and Automation’, Limassol, Cyprus, pp. 1512—1517.
- Ihle, I.-A. F., Jouffroy, J. & Fossen, T. I. (2005), Formation control of marine craft using constraint functions, *in* ‘IEEE Marine Technology and Ocean Science Conference Oceans05’, Washington D.C., USA.
- Ihle, I.-A. F., Jouffroy, J. & Fossen, T. I. (2005), Formation control of marine surface craft using Lagrange multipliers, *in* ‘Proc. 44rd IEEE Conference on Decision & Control and 5th European Control Conference’, Seville, Spain, pp. 752—758.
- Ihle, I.-A. F., Arcaç, M. & Fossen, T. I. (2006), Passivity-based designs for synchronization of path following systems, *in* ‘Proc. 45th IEEE Conference on Decision & Control’, San Diego, CA, USA.

The remainder of this chapter briefly reviews marine control systems and some mathematical preliminaries that are used in this thesis. Appendix A presents the mathematical definitions, lemmas, and theorems in detail, and Appendix B provides the necessary marine vessel models. Chapters 2–5 can all be read independently, but Chapters 3 and 5 benefit from some familiarity with their preceding chapter.

## 1.4 Marine Control Systems

This thesis uses the hydrodynamic notation from SNAME (1950) and vectorial notation from Fossen (2002) which has become standard for marine control systems. The mathematical vessel models used in this work are presented here, while a more detailed explanation is found in Appendix B. The *Guidance-Navigation-Control* structure for marine control systems is also presented.

**6 DOF Model** A vessel has 6 degrees of freedom (DOF), three coordinate axes to determine the position and a rotation around each axis, as in Figure 1.8. The generalized position, velocity, and force vectors in 6 DOF are

$$\begin{aligned}\eta &:= [x, y, z, \phi, \theta, \psi]^\top \in \mathbb{R}^3 \times \mathcal{S}^3 \\ \nu &:= [u, v, w, p, q, r]^\top \in \mathbb{R}^6 \\ \tau &:= [X, Y, Z, K, M, N]^\top \in \mathbb{R}^6\end{aligned}$$

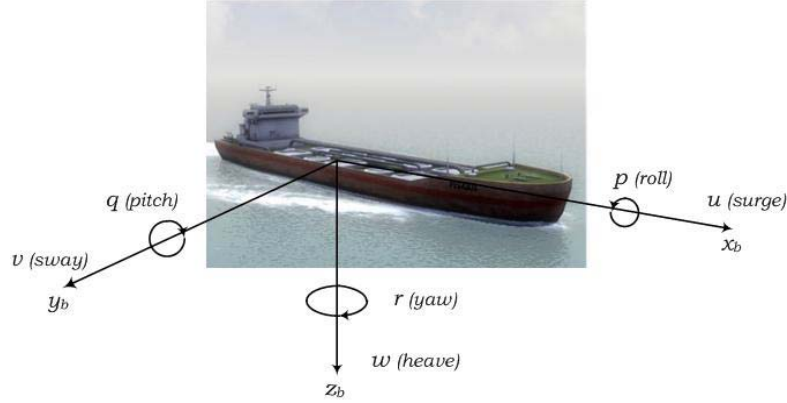


Figure 1.8: A ship and its six degrees of freedom.

where  $\mathbb{R}^n$  is the Euclidean  $n$ -dimensional space and  $\mathcal{S}^3$  is a three-dimensional sphere.

The generalized position  $\eta$  is defined with respect to an Earth-fixed reference frame, while the velocity  $\nu$  is given with respect to a body-fixed frame. The transformation between the two frames is given as

$$\dot{\eta} = J(\eta) \nu \quad (1.2)$$

where the transformation matrix is block-diagonal,

$$J(\eta) = \begin{bmatrix} R(\Theta) & 0 \\ 0 & T_{\Theta}(\Theta) \end{bmatrix}, \quad \Theta = [\phi, \theta, \psi]^{\top},$$

and consists of a linear velocity transformation  $R(\Theta) \in SO(3)$  and the angular velocity transformation  $T_{\Theta}(\Theta)$ .

The rigid-body equations of motion are expressed in the non-inertial body-frame as

$$M_{RB} \dot{\nu} + C_{RB}(\nu) \nu = \tau_{RB} \quad (1.3)$$

where  $M_{RB} = M_{RB}^{\top} > 0$  and  $C_{RB}(\nu) = -C_{RB}(\nu)^{\top}$ . It is common to assume that the forces and moments  $\tau_{RB}$  can be separated into components according to their originating effects and studied independently by assuming linear superposition:

$$\tau_{RB} = \tau_H + \tau + \tau_{env} \quad (1.4)$$

where  $\tau_H$  is the generalized hydrodynamic force,  $\tau$  represents the control forces and moments, and  $\tau_{env}$  is the resulting environmental force and moment vector due to wind, waves and currents.

The low-frequency hydrodynamic forces can be expressed as

$$\tau_H = -M_A \dot{\nu} - C_A(\nu) \nu - D(\nu) \nu - g(\eta) \quad (1.5)$$

where the subscript  $A$  represents the added mass effect due to the inertia of the surrounding fluid. The damping matrix  $D(\nu) \nu$  is caused by potential, viscous, wave drift damping, and skin friction, and the restoring forces  $g(\eta)$  is due to gravity and buoyancy forces.

Thus, by combining (1.3), (1.4) and (1.5) the resulting 6 DOF model is given as

$$M \dot{\nu} + C(\nu) \nu + D(\nu) \nu + g(\eta) = \tau + \tau_{\text{env}} \quad (1.6)$$

where  $M = M_{RB} + M_A$  is positive definite and  $C(\nu) = C_{RB}(\nu) + C_A(\nu)$  is skew-symmetric.

**3 DOF Model** A horizontal plane model in surge, sway and yaw is a common approximation for surface vessels. From the 6 DOF model the horizontal plane model is found by isolating these components and setting heave, roll and pitch to zero. With  $\eta = [x, y, \psi]^T$ ,  $\nu = [u, v, r]^T$ ,  $J(\eta) = R(\psi)$ , and matrices of appropriate dimensions, (1.2) and (1.6) are still a valid model representation.

**Guidance, Navigation and Control Structure, Fossen (2002)** Many implemented control systems consist of sensors, reference signals, and the feedback control system. To improve modularity and usability, a marine vessel control system is constructed by three independent blocks denoted as the guidance, navigation and control (GNC) systems—see Figure 1.9.

The GNC blocks represent three interconnected systems:

- The **Guidance** block supplies the control system with reference signals, i.e., the vessel's *desired* position, velocity and acceleration. This data is computed using information from the human operator, the navigation system and other external sources, such as weather forecast, fleet management systems, etc. The guidance system also supplies the human operator with information about the control system.
- The **Navigation** block estimates the position, course and distance traveled which in turn is needed to control the vessel's course. In some cases, the velocity and acceleration are also computed. Thus, this block is dependent on sensors which can provide measurements to be used for estimation. Possible sensors include inertial measurements, satellite systems, and acoustic systems, etc. In control systems terms, an estimator for reconstructing unknown states is called an *observer*. An important task for observers in marine

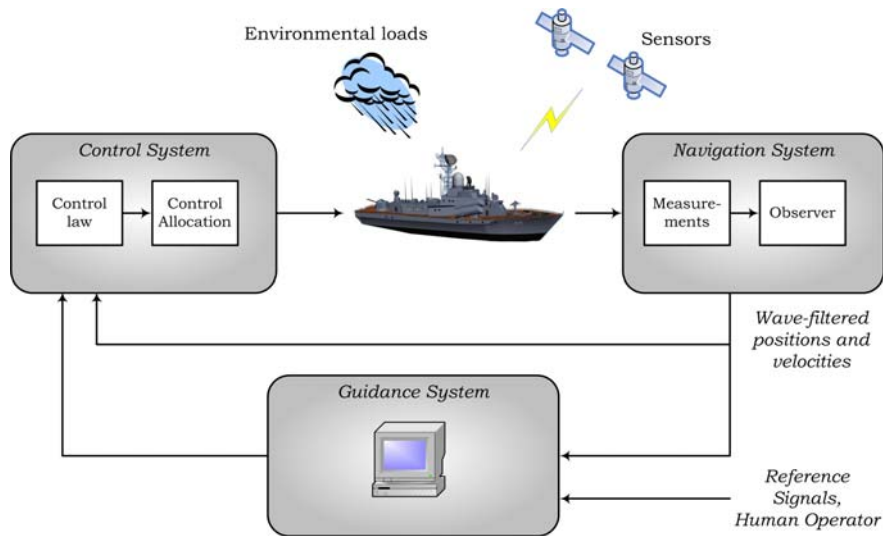


Figure 1.9: The Guidance-Navigation-Control structure for marine control systems

control systems is to prevent the high-frequency components of waves from entering the control loop, since the vessel should only counteract the slowly-varying disturbances.

- The **Control** block determines the necessary control forces and moments produced by the vessel to satisfy a certain control objective, which is often coordinated with the guidance block. The control block typically consists of two sub-blocks: the control law and the control allocation block. Whereas the control law provides the *generalized forces and moments*, the control allocation block has to *distribute* these forces among the available actuators in an optimal manner.

## 1.5 Mathematical Preliminaries

This section introduces the notation and some of the definitions used throughout this thesis.

- Time derivatives of a function  $x(t)$  are denoted  $\dot{x}$ ,  $\ddot{x}, \dots, x^{(n)}$ . A superscript with an argument variable denote partial differentiation with respect to that argument, i.e.,  $\alpha^t(x, \theta, t) := \frac{\partial \alpha}{\partial t}$ ,  $\alpha^{x^2} := \frac{\partial^2 \alpha}{\partial x^2}$ , etc.
- A function  $f : X \rightarrow Y$  is of class  $\mathcal{C}^r$ , written  $f \in \mathcal{C}^r$ , if  $f^{x^k}(x)$ ,  $k \in \{0, 1, \dots, r\}$  is defined and continuous for all  $x \in X$ . In addition,  $f$  is

continuous if  $f \in \mathcal{C}^0$ , continuously differentiable if  $f \in \mathcal{C}^1$ , and  $f$  is smooth if  $f \in \mathcal{C}^\infty$ .

- A function  $\alpha : \mathbb{R}_{\geq 0} \rightarrow \mathbb{R}_{\geq 0}$  is of class  $\mathcal{K}$  if it is continuous, strictly increasing and  $\alpha(0) = 0$ . It is of class  $\mathcal{K}_\infty$  if it is of class  $\mathcal{K}$  and in addition  $\lim_{s \rightarrow \infty} \alpha(s) = \infty$ . A function  $\beta : \mathbb{R}_{\geq 0} \times \mathbb{R}_{\geq 0} \rightarrow \mathbb{R}_{\geq 0}$  is of class  $\mathcal{KL}$  if, for each fixed  $s$ , the function  $\beta(r, s)$  belongs to class  $\mathcal{K}$  with respect to  $r$  and, for each fixed  $r$ , the function  $\beta(r, s)$  is decreasing with respect to  $s$  and  $\beta(r, s) \rightarrow 0$  as  $s \rightarrow \infty$ .
- Let  $\mathcal{L}_p$  denote the set of all piecewise continuous functions  $y : [0, \infty) \rightarrow \mathbb{R}^n$  being  $p$ -integrable on  $[0, \infty)$ , that is

$$\mathcal{L}_p = \left\{ y(t) : \int_0^\infty |y(t)|^p dt < \infty \right\}$$

- The Euclidean vector norm is  $|x| := \sqrt{(x^\top x)}$ , and the  $\mathcal{L}_p$ -norm of  $x(t)$  is

$$|x|_{\mathcal{L}_p} = \left( \int_0^\infty |y(t)|^p dt \right)^{\frac{1}{p}}$$

and in the limit  $|x|_{\mathcal{L}_\infty} = \sup_{t \geq 0} |u(t)|$ . Whenever convenient  $|(x, y, z)|$  indicates the norm of the vector  $[x^\top, y^\top, z^\top]^\top$ .

- The distance to the set  $\mathcal{M}$  is  $|x|_{\mathcal{M}} := \inf_{y \in \mathcal{M}} |x - y|$ , and the induced matrix 2-norm of  $A \in \mathbb{R}^{n \times n}$  is

$$\|A\| = \sup_{|x|=1} |Ax| = \sqrt{\lambda_{\max}(A^\top A)},$$

- For a matrix  $P = P^\top > 0$ , we let  $\lambda_{\min}(P)$  and  $\lambda_{\max}(P)$  be the minimum and maximum eigenvalue of  $P$ , respectively

### 1.5.1 Graph Theory

A brief introduction to the terminology and definitions of algebraic graph theory that we need is given here. See Godsil & Royle (2001) for a detailed treatment of algebraic properties of graphs.

- A graph  $\mathcal{G}$  consists of a *vertex* set  $\mathcal{V}$  and an *edge* set  $\mathcal{E}$  where an edge is an unordered pair of distinct vertices of  $\mathcal{G}$ .
- If  $(x, y) \in \mathcal{V}$  and  $(x, y) \in \mathcal{E}$ , then  $x$  and  $y$  are said to be adjacent or *neighbors*.

- A graph is *complete* if every pair of vertices are neighbors.
- A *cycle* is a connected graph where every vertex has exactly two neighbors.
- A *path* from  $x$  to  $y$  is a sequence of distinct vertices (starting with  $x$ , ending with  $y$ ) such that consecutive vertices are adjacent.
- If there is a path between any two vertices of a graph  $\mathcal{G}$ , then  $\mathcal{G}$  is *connected*.

We assign an orientation to the graph by considering one of the vertices to be the positive end of the edge. For a group of  $n$  members with  $p$  edges, the  $n \times p$  incidence matrix  $B(\mathcal{G})$  is defined as

$$b_{ik} = \begin{cases} +1 & \text{if } i\text{th vertex is the positive end of the } k\text{th edge} \\ -1 & \text{if } i\text{th vertex is the negative end of the } k\text{th edge} \\ 0 & \text{otherwise} \end{cases} .$$

The Laplacian of  $\mathcal{G}$  is defined as  $L(\mathcal{G}) = B(\mathcal{G})B(\mathcal{G})^\top$  and is independent on the choice of orientation. An interesting property of  $L(\mathcal{G})$  is that  $L$  is always symmetric and positive semi-definite. The algebraic multiplicity of its zero eigenvalue is equal to the number of connected components in  $\mathcal{G}$ . Another interesting fact is the second smallest eigenvalue of  $L(\mathcal{G})$ , known as the algebraic connectivity, that is positive if and only if  $\mathcal{G}$  is connected.

### 1.5.2 Stability Tools

The primary requirement for control systems is stability. We now briefly review some stability concepts from Khalil (2002). The tools for stability analysis used in this thesis are summarized in Appendix A.

**Lyapunov Stability** Consider the unforced system

$$\dot{x} = f(t, x), \quad x(t) \in \mathbb{R}^n \tag{1.7}$$

- The system (1.7) is forward complete if its solution can be continued for all time. Equivalently, the system is said to have no finite escape times.
- An equilibrium point of the system (1.7) is *uniformly globally asymptotically stable* (UGAS) if there exists a class- $\mathcal{KL}$  function  $\beta$  such that,  $\forall x_0 \in \mathbb{R}^n$ , the solution  $x(t, x_0)$  satisfies

$$|x(t, x_0)| \leq \beta(|x_0|, t), \quad \forall t \geq 0 \tag{1.8}$$

- An equilibrium point of the system (1.7) is *uniformly globally exponentially stable* (UGES) if there exists strictly positive real numbers  $k > 0$  and  $\lambda > 0$  such that,  $\forall x_0 \in \mathbb{R}^n$ , the solution  $x(t, x_0)$  satisfies

$$|x(t, x_0)| \leq k |x_0| e^{-\lambda t}, \quad \forall t \geq 0$$

**Input-to-State Stability** Consider the following system with input  $u(t)$

$$\dot{x} = f(t, x, u) \quad x(t) \in \mathbb{R}^n, \quad u(t) \in \mathbb{R}^p \quad (1.9)$$

- The system (1.9) is said to be *Input-to-State Stable* (ISS) if there exists functions  $\beta \in \mathcal{KL}$ ,  $\rho \in \mathcal{K}$  such that for any initial state  $x_0$  and any bounded input  $u(t)$ , the solution  $x(t)$  exists for all  $t \geq 0$  and satisfies

$$|x(t)| \leq \beta(|x_0|, t) + \rho\left(\sup_{\tau \leq t} |u(\tau)|\right). \quad (1.10)$$

When the input vanishes, the origin is UGAS.

- Alternatively: For  $d \in \mathcal{L}_\infty$ , we define

$$|d|_a = \limsup_{t \rightarrow \infty} |d(t)| \quad (1.11)$$

Then, the system (1.9) is said to be ISS if there exist class  $\mathcal{K}$  functions  $\gamma_0(\cdot)$ ,  $\gamma(\cdot)$ , such that, for any input  $u(\cdot) \in \mathcal{L}_\infty^m$  and  $x_0 \in \mathbb{R}^n$ , the response  $x(t)$  in the initial state  $x(0) = x_0$  satisfies

$$|x|_{\mathcal{L}_\infty} \leq \gamma_0(|x_0|) + \gamma(|u|_{\mathcal{L}_\infty}) \quad (1.12)$$

$$|x|_a \leq \gamma(|u|_a). \quad (1.13)$$

**Passivity** Consider the following system with input  $u(t)$  and output  $y(t)$

$$\dot{x} = f(x, u) \quad (1.14)$$

$$y = h(x, u), \quad x(t) \in \mathbb{R}^n, \quad u(t), y(t) \in \mathbb{R}^p$$

- The dynamic system is said to be *passive* if there exists a continuously differentiable storage function  $V(x) \geq 0$  such that

$$\dot{V} \leq -W(x) + u^\top y$$

for some positive semidefinite function  $W(x)$ . We say that (1.14) is *strictly passive* if  $W(x)$  is positive definite.

- A static nonlinearity  $y = h(u)$  is passive if, for all  $u \in \mathbb{R}^m$ ,

$$u^\top y = u^\top h(u) \leq 0; \quad (1.15)$$

and strictly passive if (1.15) holds with strict inequality  $\forall u \neq 0$ .

- The transfer function

$$G(s) = D + C(sI - A)^{-1} B,$$

where  $(A, B)$  is controllable and  $(A, C)$  is observable, is said to be *strictly positive real* if and only if there exists matrices  $P = P^\top > 0$ ,  $L$  and  $W$  such that

$$\begin{aligned} PA + A^\top P &= -L^\top L \\ PB &= C^\top - L^\top W \\ W^\top W &= D + D^\top. \end{aligned}$$

- The system (1.14) is *zero-state observable* if no solution of  $\dot{x} = f(x, 0)$  can stay identically in the subset  $S = \{x \in \mathbb{R}^n : h(x, 0) = 0\}$ , other than the trivial solution  $x(t) \equiv 0$ .

# Chapter 2

## Formation and Output-Feedback Maneuvering Control

### 2.1 Introduction

Steering the position of an object is an interesting control problem and has been the topic of many research papers. Applications range from hard-drive reading heads to robot manipulators. When the objective is to be positioned at a fixed location the control problem is often referred to as *set-point regulation*, and one way to move an object could be to regulate it along a sequence of way-points. Another solution is to construct a *path* (perhaps from the given way-points) and design a control law that forces the object to follow it. This approach is called *path-following* and the object follows the path instead of being stabilized at each point. A detailed introduction to path following is found in Skjetne et al. (2004) and Skjetne (2005).

A path is typically given as a set of coordinates and the dimensions should match the degrees of freedom for the object to be controlled: A robot arm operating on a horizontal surface should follow a path with at least two dimensions. If the orientation of the robot arm is important, more dimensions should be added. To determine the position on the path it can for example be parameterized by a path variable:

**Definition 2.1** *A parameterized path is a geometric curve*

$$Y_d := \{y \in \mathbb{R}^m : \exists \theta \in \mathbb{R} \text{ such that } y = y_d(\theta)\}$$

where  $y_d$  is continuously parameterized by the path variable  $\theta$ .

For a path  $y_d(\theta)$  parameterized by  $\theta$ , the assignment  $\theta = \theta_1$  means that the object should be at the location given by  $y_d(\theta_1)$ —see Figure 2.1. After the path is

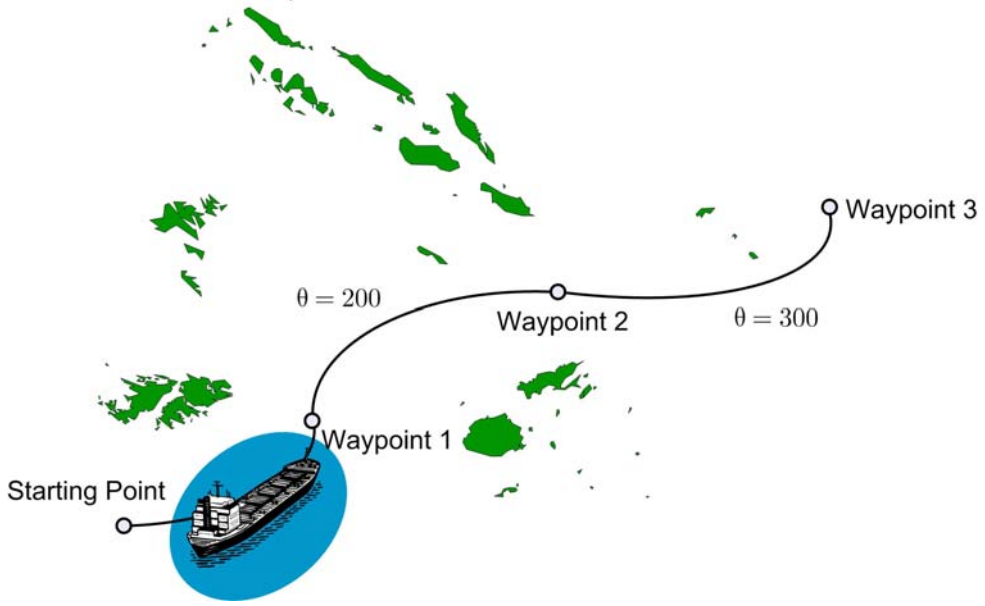


Figure 2.1: A vessel follow a path  $y_d$  constructed by using waypoints and a path algorithm. The path variable  $\theta$  determines the position on the path: e.g., when  $\theta$  is 200 or 300 the vessel is at the corresponding position  $y_d(\theta)$ .

constructed, the question of speed and accelerations along the path remains. In *trajectory tracking*, the desired path is parameterized by time  $t$ , i.e.,  $\theta(t) = t$ , and the speed along the path is then simply the time derivative  $\dot{y}_d(t)$ . Thus, there is an implicit speed (and acceleration) assignment in trajectory tracking schemes.

*Maneuvering* separates the speed assignment from the path following by constructing an update law for  $\theta$  and force the speed along the path,  $\dot{\theta}$ , to follow a speed assignment  $v_s$ . *The maneuvering problem* is defined in Skjetne et al. (2004) where the path following is referred to as the geometric task and time, speed or acceleration assignments are referred to as dynamic tasks. Design examples in this thesis assume fully actuated vessels and we consider the maneuvering problem for subclasses of the dynamic system

$$\begin{aligned}\dot{x} &= f(x, u) \\ y &= h(x)\end{aligned}$$

where the dynamic task is a speed assignment:

**Definition 2.2 (The Maneuvering Problem)** *Design a controller that solves the two tasks,*

1. **The Geometric Task:** For any continuous function  $\theta(t)$ , force the output  $y$  to converge to a desired path  $y_d(\theta)$ ,

$$\lim_{t \rightarrow \infty} |y(t) - y_d(\theta(t))| = 0 \quad (2.1)$$

2. **The Dynamic task:** Force the path speed  $\dot{\theta}$  to converge to a desired speed assignment  $v_s(\theta, t)$ ,

$$\lim_{t \rightarrow \infty} \left| \dot{\theta}(t) - v_s(\theta(t), t) \right| = 0 \quad (2.2)$$

An area where maneuvering design is of specific interest is in marine control systems. Applications include a single ship following a path (for instance in difficult maneuvering environments where it is important to move along a safe route), replenishment operations between several ships, docking operations, or seabed scanning. See e.g. Fossen, Breivik & Skjetne (2003) for path following for under-actuated systems. Other path following designs are found in Aguiar, Hespanha & Kokotović (2005), Al-Hiddabi & McClamroch (2002), Do, Jiang & Pan (2002), Encarnação & Pascoal (2001*b*), and Hauser & Hindman (1995).

The first sections of this chapter look into the formation maneuvering problem where several maneuvering systems are synchronized such that they are controlled as a formation. The paths are synchronized such that equal path parameters imply correct vessel configuration. When the paths are constructed in this manner, the vessels only need to communicate their path variable and bandwidth demand is reduced. The results are based on Skjetne, Ihle & Fossen (2003) and Ihle, Skjetne & Fossen (2004). Reported results on synchronized path following are found in, e.g., Egerstedt & Hu (2001), Ren & Beard (2004), Ghabcheloo, Pascoal, Silvestre & Kaminer (2005), Breivik, Subbotin & Fossen (2006) and Børhaug, Pavlov & Pettersen (2006).

Furthermore, we apply an output-feedback design from Ihle, Skjetne & Fossen (2005) to solve the maneuvering problem when not all states are available for feedback. Thus, an *observer* is used to estimate the unknown states using model information and system output measurements. Our design depends on the existence of a stable observer for our system, of which many are available in the literature, see Nijmeijer & Fossen (1999) for examples. The design follows along the lines of observer backstepping—explained in detail in Chapter 7 of Krstić, Kanelakopoulos & Kokotović (1995); used for output-feedback control of ships in Fossen & Grøvlen (1998). Examples of other output-feedback strategies are based on passivity, cascaded non-autonomous systems, and the certainty-equivalence principle (see e.g., Berghuis & Nijmeijer (1993), Loría, Fossen & Panteley (2000), and Arcak & Kokotović (2001)).

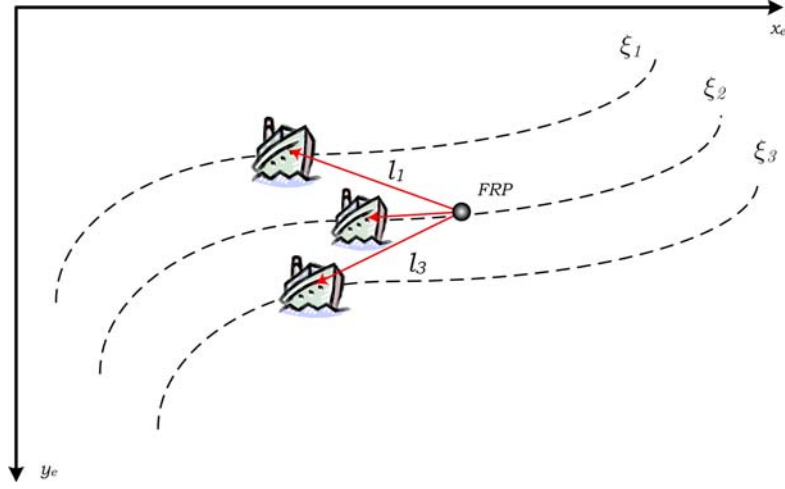


Figure 2.2: Example of formation setup for three vessels. The configuration is defined by the designation vectors  $l_1, \dots, l_3$ .

### 2.1.1 Formation setup for ships

A formation of  $r$  vessels have  $r$  individual paths. In this chapter, we generalize the setup of a single path  $\xi$  to  $r$  paths by introducing a Formation Reference Point (FRP) and create a set of  $r$  designation vectors  $l_i$  relative to the FRP. Let the FRP be the origin of a moving path frame  $\{p\}$  and denote the earth fixed frame  $\{e\}$ . The desired path for the FRP is  $\xi(\theta)$ , and Vessel  $i$  will then follow the individual desired path

$$\xi_i(\theta_i) = \xi(\theta_i) + R_p^e(\theta_i) l_i, \quad (2.3)$$

where  $R_p^e(\theta_i)$  is a rotation matrix from  $\{p\}$  to  $\{e\}$ . For a vessel on the ocean surface, the output is  $\eta = [x, y, \psi]^\top$  where  $(x, y)$  is the position and  $\psi$  is the heading. The desired path for each vessel is then given by

$$\xi_i(\theta_i) = [x_{id}(\theta_i), y_{id}(\theta_i), \psi_{id}(\theta_i)]^\top.$$

The paths are parameterized so that when the path variables are synchronized, the vessels are in their desired positions relative to the others, see Figure 2.2. The tangent vector along the path is chosen as the  $x$ -axis of the moving frame  $\{p\}$ , that is  $T(\theta_i) = [x_d^{\theta_i}(\theta_i), y_d^{\theta_i}(\theta_i)]^\top$ . The desired heading is then be computed as the angle of the tangent vector in the  $\{e\}$  frame

$$\psi_d(\theta_i) = \arctan 2 \left( \frac{T_y(\theta_i)}{T_x(\theta_i)} \right) = \arctan 2 \left( \frac{y_d^{\theta_i}(\theta_i)}{x_d^{\theta_i}(\theta_i)} \right) \quad (2.4)$$

where  $x_d(\theta_i)$  and  $y_d(\theta_i)$  are three times differentiable with respect to  $\theta_i$  and  $\arctan 2 : \mathbb{R} \times \mathbb{R} \rightarrow \langle -\pi, \pi \rangle$ . The rotation matrix  $R_p^e(\theta_i) = R(\psi_d(\theta_i))$  for the vessels is given by

$$R(\psi_d(\theta_i)) := \begin{bmatrix} \cos \psi_d(\theta_i) & -\sin \psi_d(\theta_i) & 0 \\ \sin \psi_d(\theta_i) & \cos \psi_d(\theta_i) & 0 \\ 0 & 0 & 1 \end{bmatrix}.$$

The range of applications can be further extended by considering paths with different shapes.

## 2.2 Formation Maneuvering Design

A general mechanical system is represented by the vector relative degree two model

$$\begin{aligned} \dot{x}_{1i} &= f_{1i}(x_{1i}) + G_{1i}(x_{1i})x_{2i} \\ \dot{x}_{2i} &= f_{2i}(x_i) + G_{2i}(x_{2i})u_i \\ y_i &= h_i(x_{1i}) \end{aligned} \quad (2.5)$$

where the subscript  $i$  denotes the  $i$ 'th system.  $x_{ji} \in \mathbb{R}^m$  are the states,  $x_i$  denotes the full state vector  $x_i := [x_{1i}^\top, x_{2i}^\top]^\top \in \mathbb{R}^n$  where  $n = 2m$ ,  $y_i \in \mathbb{R}^m$  are the system outputs,  $u_i$  are the controls, and the functions  $G_{1i}$ ,  $G_{2i}$ ,  $f_{1i}$ , and  $f_{2i}$  are smooth, and the matrices  $G_{1i}$ ,  $G_{2i}$ ,  $h_i^{x_{1i}}$  are invertible.

The control objective is to solve a maneuvering problem for a group of  $r$  vessels, each with a model of the form (2.5). In addition, the maneuvering systems must be synchronized such that they converge to and remain in their desired positions within the formation. By constructing the paths with a FRP we solve this by synchronizing the path parameters and the overall control objective is then to solve the *Formation Maneuvering Problem*:

**Definition 2.3 (The Formation Maneuvering Problem)** *Given a formation with  $r$  members. Then, for desired paths  $\xi_i(\theta)$ ,  $i = 1, \dots, r$ , design a controller that solves the two tasks,*

1. **The Geometric Task:** *For any continuous function  $\theta_i(t)$ , force the output  $y_i$  to converge to a desired path  $\xi_i(\theta)$ ,*

$$\lim_{t \rightarrow \infty} |y_i(t) - \xi_i(\theta(t))| = 0 \quad (2.6)$$

2. **The Dynamic task:** *Force the path speed  $\dot{\theta}_i$  to converge to a desired speed assignment  $v_i(\theta, t)$ ,*

$$\lim_{t \rightarrow \infty} \left| \dot{\theta}_i(t) - v_i(\theta(t), t) \right| = 0 \quad (2.7)$$

and force the path variables to converge,

$$\lim_{t \rightarrow \infty} \theta_i(t) - \theta_j(t) = 0, \quad i, j \in \{1, \dots, r\}, i \neq j.$$

The paths and speed assignments for the individual vessels are  $\xi_i(\theta_i)$ , according to (2.3), and  $v_i(\theta_i, t)$ , respectively. Throughout this thesis we assume that the path and speed assignment  $\xi_i(\theta_i)$ ,  $v_i(\theta_i, t)$  and their partial derivatives,  $\xi_i^\theta(\theta)$ ,  $\xi_i^{\theta^2}(\theta)$ ,  $v_i^\theta(\theta, t)$ ,  $v_i^t(\theta, t)$  are uniformly bounded, formally stated as:

**Assumption 2.1** *The following hold:*

1. For a path  $\xi(\theta) \in \mathcal{C}^n$  there exists  $K < \infty$  such that  $|\xi^{\theta^i}(\theta)| \leq K \quad \forall \theta \in \mathbb{R}, i \in \{0, 1, \dots, n\}$ .
2. For  $v_s(\theta, t) \in \mathcal{C}^{n-1}$  there exists  $L < \infty$  such that  $|v_s^{\theta^i t^j}(\theta, t)| \leq L \quad \forall (\theta, t) \in \mathbb{R} \times \mathbb{R}_{\geq 0}, i, j \in \{0, 1, \dots, n-1\}$ .

We will now go through the individual maneuvering control design for each vehicle that uses the backstepping technique from Krstić et al. (1995) in two steps. The first part of the control design solves the geometric task and follows a recursive backstepping design described in Skjetne et al. (2004). The dynamic task is solved by finding a control law that achieves (2.7) and synchronizes the path variables.

**Step 1** The error variables are defined as

$$z_{1i} = z_{1i}(x_{1i}, \theta_i) := y_i - \xi_i(\theta_i) \quad (2.8)$$

$$z_{2i} = z_{2i}(x_{1i}, x_{2i}, \theta_i, t) := x_{2i} - \alpha_{1i} \quad (2.9)$$

$$\omega_i := v_i(\theta_i, t) - \dot{\theta}_i, \quad (2.10)$$

where  $\alpha_{1i}$  are virtual controls to be specified later. Differentiating (2.8) with respect to time gives

$$\dot{z}_{1i} = \dot{y}_i - \xi_i^{\theta_i} \dot{\theta}_i = h_i^{x_{1i}} G_{1i} z_{2i} + h_i^{x_{1i}} G_{1i} \alpha_{1i} + h_i^{x_{1i}} f_{1i} - \xi_i^{\theta_i} \dot{\theta}_i.$$

Choose Hurwitz design matrices  $A_{1i}$ , so that  $P_{1i} = P_{1i}^\top > 0$  are the solutions of

$$P_{1i} A_{1i} + A_{1i}^\top P_{1i} = -Q_{1i}, \quad Q_{1i} = Q_{1i}^\top > 0.$$

Define the Step 1 control Lyapunov function (CLF)

$$V_{1i}(x_{1i}, \theta_i) := z_{1i}(x_{1i}, \theta_i)^\top P_{1i} z_{1i}(x_{1i}, \theta_i),$$

whose time derivative becomes

$$\dot{V}_{1i} = 2z_{1i}^\top P_{1i} [h_i^{x_{1i}} G_{1i} \alpha_{1i} + h_i^{x_{1i}} f_{1i} - \xi_i^\theta v_i] + 2z_1^\top P_1 h_i^{x_{1i}} G_{1i} z_{2i} + 2z_1^\top P_1 \xi_i^\theta \omega_i.$$

The first virtual controls are chosen as

$$\alpha_{1i} = \alpha_{1i}(x_{1i}, \theta_i, t) = G_{1i}^{-1} (h_i^{x_{1i}})^{-1} [A_{1i} z_{1i} - h_i^{x_{1i}} f_{1i} + \xi_i^{\theta_i}(\theta_i) v_i(\theta_i, t)].$$

Define the first tuning function,  $\tau_{1i} : \mathbb{R}^m \times \mathbb{R} \rightarrow \mathbb{R}$ , as

$$\tau_{1i}(x_{1i}, \theta_i) := 2z_{1i}^\top P_{1i} \xi_i^{\theta_i}.$$

Then, the derivative  $\dot{V}_{1i}$  becomes

$$\dot{V}_{1i} \leq -z_{1i}^\top Q_{1i} z_{1i} + 2z_{1i}^\top P_{1i} h^{x_{1i}} G_{1i} z_{2i} + \tau_{1i} \omega_i.$$

In aid of the next step, we differentiate  $\alpha_{1i}$  w.r.t. time to get

$$\dot{\alpha}_{1i} = \sigma_{1i} + \alpha_{1i}^\theta \dot{\theta}_i,$$

where  $\sigma_{1i}$  collects all terms in  $\dot{\alpha}_{1i}$  not containing  $\dot{\theta}_i$ :

$$\sigma_{1i} := \alpha_{1i}^{x_{1i}} [G_{1i}(x_{1i}) x_{2i} + f_{1i}(x_{1i})] + \alpha_{1i}^t(x_{1i}, \theta_i, t).$$

**Step 2** Differentiating (2.9) with respect to time gives

$$\dot{z}_{2i} = \dot{x}_{2i} - \dot{\alpha}_{1i} = G_{2i} u_i + f_{2i} - \sigma_{1i} - \alpha_{1i}^{\theta_i} \dot{\theta}_i$$

Again, choose Hurwitz design matrices  $A_{2i}$ , so that  $P_{2i} = P_{2i}^\top > 0$  are the solutions of

$$P_{2i} A_{2i} + A_{2i}^\top P_{2i} = -Q_{2i}, \quad Q_{2i} = Q_{2i}^\top > 0,$$

and define

$$V_{2i}(x_{1i}, \theta_i) := V_{1i} + z_{2i}(x_{2i}, \theta_i)^\top P_{2i} z_{2i}(x_{2i}, \theta_i)$$

whose time derivative becomes

$$\dot{V}_{2i} = -z_{1i}^\top Q_{1i} z_{1i} + 2z_{1i}^\top P_{1i} h^{x_{1i}} G_{1i} z_{2i} + \tau_{1i} \omega_i + z_{2i}^\top P_{2i} [G_{2i} u_i + f_{2i} - \sigma_{1i} - \alpha_{1i}^{\theta_i} \dot{\theta}_i].$$

This results in the control law

$$u_i = \alpha_{2i}(x_i, \theta_i, t) = G_{2i}^{-1} \left[ A_{2i} z_{2i} - P_{2i}^{-1} G_{1i}^\top (h^{x_{1i}})^\top P_{1i} z_{1i} - f_{2i} + \sigma_{1i} + \alpha_{1i}^{\theta_i} v_i \right], \quad (2.11)$$

and the closed-loop system

$$\begin{aligned}\dot{z}_i &= F_i(x_i) z_i + g_i(x_i, \theta_i, t) \omega_i \\ F_i &= \begin{bmatrix} A_{1i} & h^{x_{1i}} G_{1i} \\ -P_{2i}^{-1} G_{1i}^\top (h^{x_{1i}})^\top P_{1i} & A_{2i} \end{bmatrix} \\ g_i &= \begin{bmatrix} \xi_i^{\theta_i} \\ \alpha_i^{\theta_i} \end{bmatrix},\end{aligned}$$

where  $z_i := [z_{1i}^\top, z_{2i}^\top]^\top$ . By defining  $P_i := \text{diag}(P_{1i}, P_{2i})$ ,  $Q_i := \text{diag}(Q_{1i}, Q_{2i})$ , and the final tuning functions,  $\tau_i : \mathbb{R}^n \times \mathbb{R} \rightarrow \mathbb{R}$ , as

$$\tau_i(x_i, \theta_i) := \tau_{1i} + 2z_{2i}^\top P_{2i} \alpha_{1i}^{\theta_i},$$

the corresponding CLFs with time derivatives become

$$V_i = z_i^\top P_i z_i \quad (2.12)$$

$$\dot{V}_i \leq -z_i^\top Q_i z_i + \tau_i \omega_i. \quad (2.13)$$

Equation (2.11) defines the static part of the control laws and solves the geometric task of the formation maneuvering problem. The dynamic part in traditional maneuvering design for single ships, see Skjetne, Fossen & Kokotović (2005), would now proceed by designing an update law for  $\omega_i$  to render the term  $\tau_i \omega_i$  non-positive, such that the speed assignments are satisfied. For the formation maneuvering problem, however, it is now necessary to ensure both synchronization of the path variables  $\theta_i$  as well as satisfying the speed assignments.

For a cleaner presentation, we collect all states and functions into vector notation. Define the vectors  $x := [x_1^\top, \dots, x_r^\top]^\top \in \mathbb{R}^{rn}$ ,  $z := [z_1^\top, \dots, z_r^\top]^\top \in \mathbb{R}^{rn}$ ,  $\theta := [\theta_1, \dots, \theta_r]^\top \in \mathbb{R}^r$ ,  $\omega := [\omega_1, \dots, \omega_r]^\top \in \mathbb{R}^r$ ,  $\tau(x, \theta, t) := [\tau_1, \dots, \tau_r] \in \mathbb{R}^{1 \times r}$ , the composite path vector  $\xi(\theta) := [\xi_1(\theta_1)^\top, \dots, \xi_r(\theta_r)^\top]^\top \in \mathbb{R}^{rm}$  and the composite speed assignment vector  $v(\theta, t) := [v_1(\theta_1, t), \dots, v_r(\theta_r, t)]^\top$ . Also, define the matrices  $F := \text{diag}(F_1, \dots, F_r)$ ,  $G := \text{diag}(g_1, \dots, g_r)$ ,  $P := \text{diag}(P_1, \dots, P_r)$  and  $Q = \text{diag}(Q_1, \dots, Q_r)$ . The closed-loop including all vessels is then

$$\begin{aligned}\dot{z} &= F(x) z + G(x, \theta, t) \omega \\ \dot{\theta} &= v(\theta, t) - \omega,\end{aligned}$$

where  $\omega = \omega(x, \theta, t)$  is not yet determined.

Let the composite CLF be  $V(x, \theta, t) := V_1(x_1, \theta_1, t) + \dots + V_r(x_r, \theta_r, t)$  so that

$$\begin{aligned}V(x, \theta, t) &= z(\theta, t)^\top P z(\theta, t) \\ \dot{V} &\leq -z^\top Q z + \tau(x, \theta, t) \omega(x, \theta, t).\end{aligned}$$

Skjetne, Teel & Kokotović (2002a) show that the tuning function  $\tau$  is the gradient of the composite Lyapunov function  $V$  with respect to the path parameter vector  $\theta$ :

$$\tau(x, \theta, t) = -\frac{\partial V}{\partial \theta}(x, \theta, t) = -V^\theta(x, \theta, t)$$

and this gives

$$\dot{V} \leq -z^\top Qz - V^\theta(x, \theta, t) \omega(x, \theta, t), \quad (2.14)$$

where  $V^\theta(x, \theta, t) = [V_1^{\theta_1}(x_1, \theta_1, t), \dots, V_r^{\theta_r}(x_r, \theta_r, t)]$ . Skjetne, Teel & Kokotović (2002b) exploit this fact by constructing update laws for  $\omega$  with gradient optimization.

To make sure that the  $\theta_i$  variables synchronize, we introduce the *synchronization constraint function* for  $\theta$  as  $\Phi_p : \mathbb{R}^r \rightarrow \mathbb{R}^{r-1}$ ,

$$\Phi_p(\theta) = \begin{bmatrix} \phi_1(\theta) \\ \phi_2(\theta) \\ \vdots \\ \phi_{r-1}(\theta) \end{bmatrix} = \begin{bmatrix} (\theta_1 - \theta_2)^p \\ (\theta_2 - \theta_3)^p \\ \vdots \\ (\theta_{r-1} - \theta_r)^p \end{bmatrix}, \quad p \geq 1$$

where  $p$  is a power on the weight. The synchronization constraint function has the Jacobian  $\Phi_p^\theta : \mathbb{R}^r \rightarrow \mathbb{R}^{(r-1) \times r}$

$$\Phi_p^\theta(\theta) = \begin{bmatrix} \phi_1^{\theta_1} & \phi_1^{\theta_2} & 0 & \dots & 0 \\ 0 & \phi_2^{\theta_2} & \phi_2^{\theta_3} & \dots & 0 \\ & \vdots & & \ddots & \vdots \\ 0 & 0 & 0 & \dots & \phi_{r-1}^{\theta_{r-1}} & \phi_{r-1}^{\theta_r} \end{bmatrix}.$$

Notice that the null-space of  $\Phi_p^\theta$  has dimension 1 and is given by

$$\mathcal{N}(\Phi_p^\theta(\theta)) = \left\{ n \in \mathbb{R}^r : n = k [1, \dots, 1]^\top, k \in \mathbb{R} \right\}. \quad (2.15)$$

The formation maneuvering problem can now be properly stated as rendering the set

$$\mathcal{M} = \{(z, \theta, t) : z = 0, \Phi_p(\theta) = 0\}$$

UGAS under the additional requirement that  $(z, \theta, t) \in \mathcal{M} \Rightarrow \omega = 0$  so that the speed assignment is satisfied in  $\mathcal{M}$ . Synchronizing  $\theta_1 = \dots = \theta_r$  is equivalent to the constraint  $\Phi_p(\theta) = 0$ .

Define the *synchronization CLF*

$$V_s(x, \theta, t) = V(x, \theta, t) + \frac{1}{2} \Phi_p(\theta)^\top \Lambda \Phi_p(\theta) \quad (2.16)$$

where  $\Lambda = \Lambda^\top > 0$  is a weight matrix. The time-derivative of  $V_s$  is

$$\begin{aligned}\dot{V}_s &= \dot{V} + \Phi_p(\theta)^\top \Lambda \Phi_p^\theta \dot{\theta} \\ &\leq -z^\top Qz - V^\theta(x, \theta, t) \omega(x, \theta, t) + \Phi_p(\theta)^\top \Lambda \Phi_p^\theta (v(\theta, t) - \omega) \\ &= -z^\top Qz + \Phi_p(\theta)^\top \Lambda \Phi_p^\theta(\theta) v - \left[ V^\theta + \Phi_p(\theta)^\top \Lambda \Phi_p^\theta(\theta) \right] \omega.\end{aligned}\quad (2.17)$$

From (2.15) we see that when all speed assignments  $v_i(\theta_i, t)$  are equal, the vector of speed assignments lies in the null-space of  $\Phi_p^\theta$

$$v(\theta(t), t) \in \mathcal{N}(\Phi_p^\theta(\theta(t))) \quad \forall t \geq 0.$$

This ensures that the sign indefinite term  $\Phi_p(\theta)^\top \Lambda \Phi_p^\theta(\theta) v(\theta, t)$  vanishes from (2.17). One way to achieve this is to let all speed assignments be dependent on time only, i.e.  $v_i(\theta_i, t) = v_s(t)$ ,  $i = 1, \dots, r$ . Various choices are made depending on the shape and the parametrization of the path. If the path is parameterized in terms of e.g. path length,  $\theta$  will have the unit ‘meter’, and a speed assignment corresponds directly to the speed of the vessel. In this case, a purely time-dependent speed assignment is very feasible.

**Gradient update law** Consider the last sign indefinite term in (2.17) and notice that  $V^\theta(x, \theta, t) + \Phi_p(\theta)^\top \Lambda \Phi_p^\theta(\theta) = V_s^\theta(x, \theta, t)$ . Motivated by the gradient algorithm described in Skjetne et al. (2004), we choose

$$\omega(x, \theta, t) = \Gamma \left[ V^\theta(x, \theta, t) + \Phi_p(\theta)^\top \Lambda \Phi_p^\theta(\theta) \right]^\top = \Gamma V_s^\theta(x, \theta, t),$$

where  $\Gamma = \text{diag}(\gamma_1, \dots, \gamma_r) > 0$  is a gain matrix. Hence, we have the following time-derivative of  $V_s$  along the solutions of the closed-loop system

$$\dot{V}_s \leq -z^\top Qz - V_s^\theta(x, \theta, t) \Gamma V_s^\theta(x, \theta, t)^\top. \quad (2.18)$$

The path speed controller becomes

$$\dot{\theta} = v - \omega = v(\theta, t) - \Gamma V_s^\theta(x, \theta, t). \quad (2.19)$$

If we choose  $\gamma_i = 0$ ,  $i = 1, \dots, r$  not only would the vessels become decoupled, without any synchronization, but the dynamic part of the control law becomes  $\dot{\theta} = v(\theta, t)$  which is equivalent to trajectory tracking, since the speed assignment is dependent on time  $t$  only. This reduces performance, as the update law for  $\dot{\theta}$  has no information about the states of the vessels.

Skjetne, Moi & Fossen (2002) consider a tracking update law by choosing  $\omega = 0 \Rightarrow \dot{\theta} = v(\theta, t)$ . This choice solves the centralized version of the formation maneuvering problem (FMP), since the control design only depends on a

single path variable. In our case this solves the geometric task of the maneuvering problem for the individual ships, but not the FMP since synchronization of the  $\theta_i$ s is disabled.

Before we proceed with the formal proof, we state the following lemma from Skjetne et al. (2003, Lemma 2):

**Lemma 2.1** *Given  $\Phi_p(\theta) : \mathbb{R}^r \rightarrow \mathbb{R}^q$ , let  $\Psi(\theta) = \Phi_p^\theta(\theta)^\top \Lambda \Phi_p(\theta) \in \mathbb{R}^r$ . Then  $\Psi(\theta) = 0$  if and only if  $\Phi_p(\theta) = 0$ . For each pair  $0 < \delta_0 < \Delta_0$  there exist  $\delta_1, \Delta_1 > 0$  such that*

$$\delta_0 \leq |\Phi_p(\theta)| \leq \Delta_0 \Rightarrow \delta_1 \leq |\Psi(\theta)| \leq \Delta_1.$$

We are now ready to state our result in the following theorem:

**Theorem 2.1** *The overall closed-loop formation maneuvering system*

$$\begin{aligned} \dot{z} &= Fz + G\Gamma V_s^\theta(x, \theta, t)^\top \\ \dot{\theta} &= v(\theta, t) - \Gamma V_s^\theta(x, \theta, t)^\top \end{aligned} \quad (2.20)$$

*is forward complete and solves the formation maneuvering problem, i.e. the set*

$$\mathcal{M} = \{(z, \theta, t) : z = 0, \Phi_p(\theta) = 0\}$$

*is UGAS.*

**Proof:** To check that the proposed speed assignment is satisfied in  $\mathcal{M}$ , we notice that for  $\phi_i = 0 \forall i$  and  $z = 0$ ,  $\Phi_p(\theta) = 0$  and  $V^\theta(x, \theta, t) = 2z^\top Pz^\theta = 0$ . This implies that  $(z, \theta, t) \in \mathcal{M} \Rightarrow \omega = 0$  as required. Let  $Z := [z^\top, \Phi_p(\theta)^\top]^\top$ . For the synchronization Lyapunov function (2.16), we have the bounds

$$\begin{aligned} p_1 |Z|^2 &\leq V_s \leq p_2 |Z|^2 \\ \dot{V}_s &\leq -q_m |z|^2 \end{aligned}$$

where  $p_1 = \min(p_m, 0.5\lambda_m)$  and  $p_2 = \max(p_M, 0.5\lambda_M)$ . This implies that for all  $t$  in the maximal interval of definition  $[0, T)$ ,

$$|Z(t)| \leq \sqrt{\frac{p_2}{p_1}} |Z(0)|.$$

Hence, by the assumed smoothness of the plant dynamics and boundedness of all path signals and speed assignment signals, implying that the right-hand side of (2.20) depends continuously on  $(\theta, t)$  through bounded functions, and with  $z$  bounded, it follows that (2.20) is bounded on the maximal interval of definition. This excludes finite escape times so  $T = \infty$ . It is verified that  $|(z, \theta, t)|_{\mathcal{M}} = |Z|$ . We now proceed by checking if there exists a class  $\mathcal{K}$  function  $\alpha_3$  such that  $\dot{V}_s \leq -\alpha_3(|Z|)$ . Consider (2.18): By setting  $z = 0$  we see that  $\dot{V}_s|_{z=0} = -\Psi(\theta)^\top \Gamma \Psi(\theta)$ . By Lemma 2.1, we see that  $\dot{V}_s = 0$  if and only if  $Z = 0$ . Otherwise, the r.h.s. of (2.18) is negative. With  $V_s$  radially unbounded and  $\alpha_3$  positive definite we conclude, since the closed-loop is forward complete, that  $\mathcal{M}$  is UGAS.  $\square$

**Decentralized controller realization** Theorem 2.1 establishes that all path variables  $\theta_i$  synchronize and the formation moves along the path in the desired setup. For a single vessel, the controller realizations (2.11), with gradient update law (2.19), are

$$\begin{aligned} u_i &= \alpha_{2i}(x_i, \theta_i, t) \\ \dot{\theta}_i &= v_i(\theta_i, t) - \gamma_i \left\{ V_i^{\theta_i}(x_i, \theta_i, t) + \Phi_p^\theta(\theta)_i^\top \Lambda \Phi_p(\theta) \right\} \end{aligned} \quad (2.21)$$

where  $\Phi_p^\theta(\theta)_i^\top$  is the  $i$ 'th row of  $\Phi_p^\theta(\theta)^\top$ .

Notice that the control laws only depend on the vessel's own states and the path variables  $\theta_i$  from other vessels in the formation. From (2.21) it is seen that  $\Lambda = 0$  renders the update law for  $\dot{\theta}_i$  identical to the dynamic update laws in Skjetne et al. (2005) for maneuvering a single ship. This choice of  $\Lambda$  decouples the vessels by disabling synchronization. On the other hand, in the limit as  $\|\Lambda\| \rightarrow \infty$ , the path variables are synchronized at all times. As a result, this design generalizes maneuvering of ships with the extra feature of formation control.

The following section introduces an output-feedback design for a single maneuvering system before experimental results on formation maneuvering is presented.

## 2.3 Maneuvering Design for Output-Feedback Systems

The control objective in this section is to solve the maneuvering problem with output feedback for the class of *output-feedback systems*, whose output  $y$  is the only measured signal. Hence, an observer is used in the closed-loop control design to estimate the unknown states. These systems are transformed into the *output-feedback form*, in which nonlinearities depend only on  $y$ . Consider the vectorial case  $x_{1,2} \in \mathbb{R}^n$  and let  $x := [x_1^\top, x_2^\top]^\top \in \mathbb{R}^m$ .

$$\begin{aligned} \dot{x} &= Ax + f(y) + G(y)u \\ y &= c^\top x, \end{aligned} \quad (2.22)$$

where

$$A = \begin{bmatrix} 0 & I \\ 0 & 0 \end{bmatrix}, f(y) = \begin{bmatrix} f_1(y) \\ f_2(y) \end{bmatrix}, G(y) = \begin{bmatrix} 0 \\ G_2(y) \end{bmatrix}, \text{ and } c = [I, 0]^\top.$$

Assume that the functions  $G_2$ ,  $f_1$ ,  $f_2$  are smooth, and the matrix  $G_2$  is invertible which implies that (2.22) is fully actuated. Since only  $x_1$  is measured, an observer that provides information about the unknown state  $x_2$  must be designed. This

particular class of nonlinear systems is chosen since there exist exponentially stable observers for this class

$$\begin{aligned}\dot{\hat{x}} &= A\hat{x} + K(y - \hat{y}) + f(y) + G(y)u \\ \hat{y} &= c^\top \hat{x}\end{aligned}\quad (2.23)$$

where  $K = [K_1^\top, K_2^\top]^\top$  is chosen so that

$$A_o = A - Kc^\top$$

is Hurwitz. The resulting error dynamics of (2.22) and (2.23) is

$$\dot{\tilde{x}} = A_o \tilde{x}, \quad \tilde{x} = x - \hat{x}.$$

Then, there exists a  $P_o = P_o^\top > 0$  such that  $A_o^\top P_o + P_o A_o = -I$ . Note that  $|\tilde{x}| \geq |\tilde{x}_i|$  for  $i = 1, 2$ .

**Output-feedback Control Design** Consider the system

$$\begin{aligned}\dot{x}_1 &= x_2 + f_1(y) = \hat{x}_2 + \tilde{x}_2 + f_1(y) \\ \dot{\hat{x}}_2 &= G_2(y)u + f_2(y) + K_2 \tilde{y}.\end{aligned}$$

where the unknown state  $x_2$  is replaced with the estimate  $\hat{x}_2$  and the estimation error  $\tilde{x}_2$ . By using a dynamic model with the observer state  $\hat{x}_2$  and the measured state  $x_1$  we obtain an output-feedback system for control design and analysis.

**Step 1** Introduce the error variables

$$z_1(x_1, \theta) := y - y_d(\theta) = x_1 - y_d(\theta) \quad (2.24)$$

$$z_2(x, \hat{x}, \theta, t) := \hat{x}_2 - \alpha_1(x_1, \theta, t) \quad (2.25)$$

$$\omega_s := v_s(\theta, t) - \dot{\theta} \quad (2.26)$$

where  $\alpha_1$  is a virtual control to be specified later. Differentiate  $z_1$  w.r.t. time

$$\dot{z}_1 = \dot{y} - y_d^\theta \dot{\theta} = \hat{x}_2 + \tilde{x}_2 + f_1(y) - y_d^\theta \dot{\theta} = z_2 + \alpha_1 + \tilde{x}_2 + f_1(y) - y_d^\theta \dot{\theta}.$$

Define the first control Lyapunov function (clf)

$$V_1(x_1, \tilde{x}, \theta) = z_1(x_1, \theta)^\top P_1 z_1(x_1, \theta) + \frac{1}{d_1} \tilde{x}^\top P_o \tilde{x}$$

where  $d_1 > 0$ ,  $P_i = P_i^\top > 0$ ,  $i = o, 1$ , and whose time derivative is

$$\dot{V}_1 = 2z_1^\top P_1 (\alpha_1 + f_1(y) - y_d^\theta v_s) + 2z_1^\top P_1 \tilde{x}_2 + 2z_1^\top P_1 z_2 + 2z_1^\top P_1 y_d^\theta \omega_s - \frac{2}{d_1} \tilde{x}^\top P_o A_o \tilde{x}$$

Pick the virtual control law as

$$\alpha_1 = \alpha_1(x_1, \theta, t) = A_1 z_1 - f_1 + y_d^\theta v_s + \alpha_{10}.$$

The damping term  $\alpha_{10}$  will be chosen later in the design. Define the first tuning function,  $\tau_1 : \mathbb{R}^n \times \mathbb{R} \rightarrow \mathbb{R}^n$ , as  $\tau_1(x_1, \theta) = 2z_1^\top P_1 y_d^\theta$ . An application of Young's inequality yields

$$2z_1^\top P_1 \tilde{x}_2 \leq 2\kappa_1 z_1^\top P_1 P_1 z_1 + \frac{1}{2\kappa_1} \tilde{x}_2^\top \tilde{x}_2, \quad \kappa_1 > 0 \quad (2.27)$$

so

$$\dot{V}_1 \leq -z_1^\top Q_1 z_1 + 2z_1^\top P_1 z_2 + \tau_1 \omega_s + 2z_1^\top P_1 [\alpha_{10} + \kappa_1 P_1] z_1 + \frac{1}{2\kappa_1} \tilde{x}_2^\top \tilde{x}_2 - \frac{1}{d_1} \tilde{x}^\top \tilde{x}.$$

Pick first damping term as  $\alpha_{10} = -\kappa_1 P_1$  and then

$$\dot{z}_1 = A_1 z_1 + z_2 + y_d^\theta \omega_s - \kappa_1 P_1 z_1 + \tilde{x}_2$$

$$\dot{V}_1 \leq -z_1^\top Q_1 z_1 + 2z_1^\top P_1 z_2 + \tau_1 \omega_s - c_1 \tilde{x}^\top \tilde{x},$$

where  $c_1 = \frac{1}{d_1} - \frac{1}{2\kappa_1} > 0$ . To aid the design in the next step, the virtual control law is differentiated w.r.t. time

$$\dot{\alpha}_1 = \sigma_1 + \alpha_1^\theta \dot{\theta}, \quad \sigma_1 = \alpha_1^{x_1} \dot{x}_1 + \alpha_1^t.$$

**Step 2** Differentiation of  $z_2$  w.r.t. time gives

$$\dot{z}_2 = \dot{\tilde{x}}_2 - \dot{\alpha}_1 = G_2(y)u + f_2(y) + K_2 \tilde{y} - \sigma_1 - \alpha_1^\theta v_s + \alpha_1^\theta \omega_s.$$

Define the second clf

$$V_2(x, \tilde{x}, \theta, t) = V_1 + z_2^\top P_2 z_2 + \frac{1}{d_2} \tilde{x}^\top P_o \tilde{x}, \quad P_2 = P_2^\top > 0 \quad (2.28)$$

where  $d_2 > 0$ , with time derivative

$$\begin{aligned} \dot{V}_2 &= \dot{V}_1 + 2z_2^\top P_2 (G_2 u + f_2 - \sigma_1 - \alpha_1^\theta v_s) + 2z_2^\top P_2 \alpha_1^\theta \omega_s + 2z_2^\top P_2 K_2 \tilde{y} - \frac{1}{d_2} \tilde{x}^\top \tilde{x} \\ &\leq -z_1^\top Q_1 z_1 + 2z_2^\top P_2 (P_2^{-1} P_1 z_1 + G_2 u + f_2 - \sigma_1 - \alpha_1^\theta v_s) + \tau_1 \omega_s \\ &\quad + 2z_2^\top P_2 \alpha_1^\theta \omega_s + c_1 \tilde{x}^\top \tilde{x} + 2z_2^\top P_2 K_2 \tilde{y} - \frac{1}{d_2} \tilde{x}^\top \tilde{x}. \end{aligned}$$

Pick the final control law as

$$u = u(x, \tilde{x}, \theta, t) = G_2^{-1} [A_2 z_2 - P_2^{-1} P_1 z_1 - f_2 + \sigma_1 + \alpha_1^\theta v_s + u_0],$$

and define the second tuning function  $\tau_2 : \mathbb{R}^m \times \mathbb{R} \rightarrow \mathbb{R}^n$ , as

$$\tau_2(x, \hat{x}, \theta, t) = \tau_1 + 2z_2^\top P_2 \alpha_1^\theta.$$

Young's inequality yields

$$2z_2^\top P_2 K_2 \tilde{y} \leq 2\kappa_2 z_2^\top P_2 K_2 K_2^\top P_2 z_2 + \frac{1}{2\kappa_2} \tilde{y}^\top \tilde{y}, \kappa_2 > 0. \quad (2.29)$$

Hence,  $\dot{V}_2$  becomes, with  $z := [z_1, z_2]^\top$ ,  $P = \text{diag}(P_1, P_2)$ , and  $Q := \text{diag}(Q_1, Q_2)$ ,

$$\dot{V}_2 \leq -z^\top Q z + \tau_2 \omega_s + 2z_2^\top P_2 [u_0 + \kappa_2 K_2 K_2^\top P_2] z_2 + \frac{1}{2\kappa_2} \tilde{y}^\top \tilde{y} - \frac{1}{d_2} \tilde{x}^\top \tilde{x} + c_1 \tilde{x}^\top \tilde{x}.$$

Pick the second damping term as  $u_0 = -\kappa_2 K_2 K_2^\top P_2$ , and hence

$$\dot{z}_2 = A_2 z_2 - P_2^{-1} P_1 z_1 - \kappa_2 K_2 K_2^\top P_2 z_2 + K_2 \tilde{y} + \alpha_1^\theta \omega_s.$$

Then  $\dot{V}_2$  is bounded by

$$\dot{V}_2 \leq -z^\top Q z + \tau_2 \omega_s - c_2 \tilde{x}^\top \tilde{x}, \quad c_2 = c_1 + \frac{1}{d_2} - \frac{1}{2\kappa_2} > 0 \quad (2.30)$$

The final tuning function is rewritten as

$$\tau_2(x, \hat{x}, \theta, t) = 2g^\top P z(x, \hat{x}, \theta, t),$$

and the  $z$ -system as

$$\dot{z} = Fz + g\omega_s + H\tilde{y},$$

where

$$F = \begin{bmatrix} A_1 - \kappa_1 P_1 & I \\ -P_2^{-1} P_1 & A_2 - \kappa_2 K_2 K_2^\top P_2 \end{bmatrix},$$

$$g = \begin{bmatrix} y_d^\theta \\ \alpha_1^\theta \end{bmatrix}, \quad H = \begin{bmatrix} 0 \\ K_2 \end{bmatrix}.$$

The maneuvering problem with output feedback is now stated as rendering the set

$$\mathcal{M} = \{(z, \tilde{x}, \theta, t) \in \mathbb{R}^{2n} \times \mathbb{R}^{2n} \times \mathbb{R} \times \mathbb{R}_{\geq 0} : z = 0, \tilde{x} = 0\}$$

UGAS under the additional assumption that the speed assignment is fulfilled in  $\mathcal{M}$ ,  $(z, \tilde{x}, \theta, t) \in \mathcal{M} \implies \omega_s = 0$ .

Finally, the loop is closed by speed assignment design. From Skjetne et al. (2004), three different choices are available to render  $\tau_2 \omega_s$  negative in (2.30): By setting  $\omega_s = 0$ , the speed assignment is satisfied identically and is equivalent to

a trajectory tracking design with  $\dot{\theta} = v_s(\theta, t)$ . Incorporating state feedback, the *gradient update law*

$$\omega_s = -\mu\tau_2, \quad \mu > 0$$

gives

$$\dot{V}_2 \leq -z^\top Qz - \mu\tau_2^2 - c_2\tilde{x}^\top\tilde{x} \leq 0, \quad (2.31)$$

and the update law for  $\theta$  becomes

$$\dot{\theta} = v_s(\theta(t), t) + \mu\tau_2.$$

**Theorem 2.2** *The following closed-loop system with the gradient update law*

$$\begin{aligned} \dot{z} &= Fz - \mu g g^\top Pz + H\tilde{x} \\ \dot{\theta} &= v_s(\theta, t) + 2\mu g^\top Pz \\ \dot{\tilde{x}} &= A_o\tilde{x} \end{aligned} \quad (2.32)$$

*is, under the assumptions on plant and path signals, forward complete and solves the maneuvering problem with output feedback, i.e. the set*

$$\mathcal{M} = \{(z, \tilde{x}, \theta, t) : z = 0, \tilde{x} = 0\}$$

*is UGAS.*

**Proof:** The proposed speed assignment is satisfied in  $\mathcal{M}$ , since for  $z = 0$  and  $\tilde{x} = 0$  we have that  $\tau_2 = 2z^\top Pz^\theta = 0$  which further implies that  $(z, \tilde{x}, \theta, t) \in \mathcal{M} \implies \omega_s = 0 \implies \dot{\theta} = v_s$  as required. Let  $Z := [z^\top, \tilde{x}^\top]^\top$ . For the Lyapunov function (2.28), the bounds are

$$\begin{aligned} p_1 |Z|^2 &\leq V_2 \leq p_2 |Z|^2 \\ \dot{V}_2 &\leq -q_m |z|^2 - c_2 |\tilde{x}|^2 \leq -p_3 |Z|^2 \end{aligned}$$

where  $p_1 = \min(p_m, p_{o,m})$ ,  $p_2 = \max(p_M, p_{o,M})$ , and  $p_3 = \min(q_m, c_2)$ . This implies that for all  $t$  in the maximal interval of definition  $[0, T)$ ,

$$|Z(t)| \leq \sqrt{\frac{p_2}{p_1}} |Z(0)|$$

The assumed smoothness of plant dynamics and boundedness of all path and speed assignment signals imply that the right-hand side of (2.32) depends continuously on  $(\theta, t)$  through bounded functions. With  $z$  bounded it follows that (2.32) is bounded on the maximal interval of definition. This excludes finite escape times so  $T = +\infty$ , and hence

$$|(z, \tilde{x}, \theta, t)|_{\mathcal{M}} = |Z|.$$

Since  $\dot{V}_2 \leq -p_3 |Z|^2 = -\alpha_3 (|Z|)$ ,  $\alpha_3 \in \mathcal{K}$ ,  $V_2$  radially unbounded, and the closed-loop system forward complete, the set  $\mathcal{M}$  is UGAS and the maneuvering problem with output feedback is solved.  $\square$

Alternatively, the *filtered-gradient update law* is constructed, as in Skjetne et al. (2004), by augmenting the second clf to

$$V = V_2 + \frac{1}{2\mu\lambda}\omega_s^2, \quad \mu, \lambda > 0 \quad (2.33)$$

whose derivative is

$$\dot{V} \leq -z^\top Qz + \left[ \tau_2 + \frac{1}{\mu\lambda}\dot{\omega}_2 \right] \omega_s - c_2 \tilde{x}^\top \tilde{x}.$$

The second term is rendered negative by choosing the update law for  $\dot{\omega}_s$  as

$$\dot{\omega}_s = -\lambda(\omega_s + \mu\tau_2),$$

which gives

$$\dot{V} \leq -z^\top Qz - \frac{1}{\mu}\omega_s^2 - c_2 \tilde{x}^\top \tilde{x} \leq 0, \quad (2.34)$$

and the update law for  $\theta$  becomes

$$\begin{aligned} \dot{\theta} &= v_s(\theta, t) - \omega_s \\ \dot{\omega}_s &= -\lambda\omega_s - \lambda\mu\tau_2. \end{aligned}$$

Augmenting  $\mathcal{M}$  with the state  $\omega_s$ , gives the following theorem:

**Theorem 2.3** *The closed-loop system with the filtered-gradient update law*

$$\begin{aligned} \dot{z} &= F(\tilde{y})z + g\omega_s + H\tilde{x} \\ \dot{\theta} &= v_s(\theta, t) - \omega_s \\ \dot{\omega}_s &= -\lambda\omega_s - 2\lambda\mu g^\top Pz \\ \dot{\tilde{x}} &= A_o\tilde{x} \end{aligned} \quad (2.35)$$

*is, under the assumptions on plant and path signals, forward complete and solves the maneuvering problem with output feedback, i.e., the set*

$$\mathcal{M} = \{(z, \tilde{x}, \omega_s, \theta, t) : z = 0, \tilde{x} = 0, \omega_s = 0\}$$

*is UGAS.*

**Proof:** The speed assignment is now satisfied as it remains in  $\mathcal{M}$ . Let  $Z := [z^\top, \tilde{x}^\top, \omega_s]^\top$ . With the bounds

$$\begin{aligned} p_1 |Z|^2 &\leq V \leq p_2 |Z|^2 \\ \dot{V} &\leq -p_3 |Z|^2 = -\alpha_3 (|Z|) \end{aligned}$$

where  $p_1 = \min(p_m, \frac{1}{2\mu\lambda}, p_{o,m})$ ,  $p_2 = \max(p_M, \frac{1}{2\mu\lambda}, p_{o,M})$  and  $p_3 = \min(q_m, \frac{1}{\mu}, c_2)$ , the Lyapunov function  $V$  in (2.33) is bounded, and hence  $Z$  is bounded on the maximal interval of existence. The assumed smoothness of plant dynamics and boundedness of all path and speed assignment signals imply that the right-hand side of (2.35) depends continuously on  $(\theta, t)$  through bounded functions, and is bounded when  $Z$  is bounded. This implies that there are no finite escape times and  $|(z, \tilde{x}, \omega_s, \theta, t)|_{\mathcal{M}} = |Z|$ . Furthermore, with (2.35) forward complete,  $V$  radially unbounded, and  $\alpha_3 \in \mathcal{K}$ ,  $\mathcal{M}$  is UGAS and the maneuvering problem with output feedback is solved.  $\square$

## 2.4 Experimental Evaluation with Cybership II

As a demonstration of the proposed design procedure, a rendezvous maneuvering operation between Cybership II and a computer simulated ship was implemented and carried out in the Marine Cybernetics Laboratory (MCLab) where only position and heading measurements are available.

The observer objectives for a marine vessel are

- **Velocity Estimation:** With only position and heading measurements (e.g. camera and gyro compass measurements), velocity estimates are needed for feedback control.
- **Bias Estimation:** Steady-state errors are eliminated by estimating a bias term that account for slowly-varying environmental loads and unmodeled dynamics.
- **Wave filtering:** By estimating the wave-induced motion, the observer filter out the wave-frequency part of the motion (oscillatory motion components) such that only the vessel's low-frequency motion is used for feedback control.

Consider a vessel model for low-speed applications (up to 1-2 m/s) and station-keeping. For these cases the vessel is described accurately with a linear model. A nonlinear model is used for extension to maneuvering at higher speeds. Let  $\eta = [x, y, \psi]^\top$  be the Earth-fixed position vector, where  $(x, y)$  is the position on the ocean surface and  $\psi$  is the yaw angle (heading) and let  $\nu = [u, v, r]^\top$  be the

body-fixed velocity vector. The system model for a single ship with a linear wave frequency model  $x_w \in \mathbb{R}^{12}$ , bias  $b \in \mathbb{R}^3$ , and equations of motion in surge, sway, and yaw are written

$$\dot{x}_w = A_w x_w \quad (2.36a)$$

$$\dot{\eta} = R(\psi) \nu \quad (2.36b)$$

$$\dot{b} = -T_b^{-1} b \quad (2.36c)$$

$$M\dot{\nu} + D\nu = R(\psi)^\top b + u_c \quad (2.36d)$$

$$y = \eta + C_w x_w, \quad (2.36e)$$

where  $A_w$  and  $C_w$  are matrices from a linear state-space representation of a wave spectrum. The following observer structure from Fossen & Strand (1999) and Lindegaard (2003) is used:

$$\dot{\hat{x}}_w = A_w \hat{x}_w + K_1 \tilde{y}$$

$$\dot{\hat{\eta}} = R(\psi) \hat{\nu} + K_2 \tilde{y}$$

$$\dot{\hat{b}} = -T_b^{-1} \hat{b} + K_3 \tilde{y}$$

$$\dot{\hat{\nu}} = -M^{-1} D \hat{\nu} + R(\psi)^\top \hat{b} + M^{-1} u_c + K_4 R^\top(\psi) \tilde{y}$$

$$\hat{y} = \hat{\eta} + C_w \hat{x}_w, \text{ where } \tilde{y} = y - \hat{y}.$$

The model is written as

$$\dot{\eta} = R(\psi) (\nu + \tilde{\nu})$$

$$\dot{\hat{\nu}} = -M^{-1} D \hat{\nu} + R(\psi)^\top \hat{b} + M^{-1} u_c + K_4 R^\top(\psi) \tilde{y}.$$

In the remaining  $R = R(\psi)$  is used for simplicity. By choosing model matrices,  $A_w, T_b$ , and observer gains  $K_i, i = 1, \dots, 4$ , that commute with  $R(\psi)$ , the stability of the error dynamics is shown to be independent of the rotation matrix according to Property 6.1 in Fossen (2002). Denote  $\tilde{x} = [\tilde{x}_w^\top, \tilde{\eta}^\top, \tilde{b}^\top, \tilde{\nu}^\top]^\top$  and the observer error dynamics on state-space form is

$$\dot{\tilde{x}} = A_o(\psi) \tilde{x} = T(\psi)^\top A_o T(\psi) \tilde{x} \quad (2.37)$$

where

$$A_o = \begin{bmatrix} A_w - K_1 C_w & -K_1 & 0 & 0 \\ -K_2 C_w & -K_2 & 0 & I \\ -K_3 C_w & -K_3 & -T_b^{-1} & 0 \\ -K_4 C_w & -K_4 & 0 & -M^{-1} D \end{bmatrix}$$

and  $T(\psi) = \text{diag}(R(\psi)^\top, R(\psi)^\top, R(\psi)^\top, I)$  such that

$$T(\psi) A_o(\psi) T(\psi)^\top = A_o = \text{constant}. \quad (2.38)$$

If  $A_o$  is Hurwitz, and if there exists a  $P_o = P_o^\top > 0$  s.t.  $P_o A_o + A_o^\top P_o \leq -I$ , then by Lindegaard (2003, Lemma 4.1), the equilibrium  $\tilde{x} = 0$  of the observer error dynamics is UGES.

### 2.4.1 Output-feedback Control Design for Cybership II

We briefly review the output-feedback design for (2.36) and (2.37). Define the following error vectors

$$z_1(\eta, \theta) := \eta - \xi(\theta) \quad (2.39)$$

$$z_2(\eta, \hat{v}, \theta, t) := \hat{v} - \alpha_1(\eta, \theta, t) \quad (2.40)$$

$$\omega_s := v_s(\theta, t) - \dot{\theta}, \quad (2.41)$$

where  $\alpha_1$  is the virtual control law to be defined in Step 1 below.

**Step 1** Differentiate  $z_1$  :

$$\dot{z}_1 = \dot{\eta} - \xi^\theta(\theta)\dot{\theta} = R\hat{v} + R\tilde{v} - \xi^\theta v_s + \xi^\theta \omega_s = Rz_2 + R\alpha_1 + R\tilde{v} - \xi^\theta v_s + \xi^\theta \omega_s,$$

and define the step 1 clf

$$V_1(\eta, \theta, \tilde{x}) = z_1^\top P_1 z_1 + \frac{1}{d_1} \tilde{x}^\top P_o \tilde{x}, \quad d_1 > 0, \quad P_i = P_i^\top > 0, \quad i = o, 1.$$

The design procedure in Section 2.3 gives the following signals for the first step

$$\begin{aligned} \tau_1 &= \tau_1(\eta, \theta) = 2z_1^\top P_1 \xi^\theta \\ \alpha_1(\eta, \theta, t) &= R^\top [A_1 z_1 + \xi^\theta v_s + \alpha_0] \\ \alpha_0 &= -\kappa_1 P, \quad \kappa_1 > 0 \\ \dot{\alpha}_1 &= \sigma_1 + \alpha_1^\theta \dot{\theta}, \quad \sigma_1 = \alpha_1^\eta \dot{\eta} + \alpha_1^t, \end{aligned} \quad (2.42)$$

and the time-derivative of  $V_1$  becomes

$$\dot{V}_1 \leq -z_1^\top Q_1 z_1 + 2z_1^\top P_1 R z_2 + \tau_1 \omega_s - c_1 \tilde{x}^\top \tilde{x}$$

where  $c_1 = \frac{1}{d_1} - \frac{1}{2\kappa_1} > 0$ .

**Step 2** The step 2 clf is defined as

$$V_2(x, \tilde{x}, \theta, t) = V_1 + z_2^\top P_2 z_2 + \frac{1}{d_2} \tilde{x}^\top P_o \tilde{x}, \quad P_2 = P_2^\top > 0.$$

Define control law  $u_c$  and final tuning function  $\tau_2$  as

$$\begin{aligned} u_c &= u_c(x, \tilde{x}, \theta, t) = \\ &M[A_2 z_2 - P_2^{-1} R^\top P_1 z_1 + M^{-1} D \hat{v} - R^\top \hat{b} + \sigma_1 + \alpha_1^\theta v_s + u_0] \end{aligned} \quad (2.43)$$

$$\begin{aligned} u_0 &= -\kappa_2 K_4 K_4 P_2, \quad \kappa_2 > 0 \\ \tau_2(x, \hat{x}, \theta) &= \tau_1 + 2z_2^\top P_2 \alpha_1^\theta. \end{aligned}$$

Denote  $z := [z_1^\top, z_2^\top]^\top$ ,  $P := \text{diag}(P_1, P_2)$ , and  $Q := \text{diag}(Q_1, Q_2)$ . The time-derivative of  $\dot{V}_2$  is upper bounded by

$$\dot{V}_2 \leq -z^\top Q z + \tau_2 \omega_s - c_2 \tilde{x}^\top \tilde{x}, \quad c_2 = c_1 + \frac{1}{d_2} - \frac{1}{2\kappa_2} > 0.$$

The resulting  $z$ -dynamics is

$$\dot{z} = F(x)z + 2\mu g g^\top P z + H(\tilde{x}),$$

where

$$\begin{aligned} F &= \begin{bmatrix} A_1 - \kappa_1 P_1 & R \\ -P_2^{-1} R^\top P_1 & A_2 - \kappa_2 K_4 K_4 P_2 \end{bmatrix}, \\ g &= \begin{bmatrix} \xi^\theta \\ \alpha_1^\theta \end{bmatrix}, \quad H(\tilde{x}) = \begin{bmatrix} R\tilde{y} \\ K_4 R^\top \tilde{y} \end{bmatrix}. \end{aligned}$$

Finally, the gradient update law  $\omega_s = -\mu\tau_2$ ,  $\mu > 0$ , renders  $\dot{V}_2$  negative semidefinite

$$\dot{V}_2 \leq -z^\top Q z - \mu\tau_2^2 - c_2 \tilde{x}^\top \tilde{x} \leq 0.$$

The closed-loop maneuvering system

$$\begin{aligned} \dot{z} &= Fz + 2\mu g g^\top P z + H(\tilde{x}) \\ \dot{\theta} &= v_s(\theta, t) + 2\mu g^\top P z \\ \dot{\tilde{x}} &= A_o \tilde{x} \end{aligned}$$

is forward complete and solves the maneuvering problem with output feedback, i.e. the set

$$\mathcal{M} = \{(z, \tilde{x}, \theta, t) : z = 0, \tilde{x} = 0\}$$

is UGAS. The proof of this result follows along the same lines as Theorem 2.2.

A comparison of the output feedback control laws, (2.42) and (2.43), with the state feedback control designs for marine vessels in Skjetne et al. (2005), shows that they are almost identical with the exception of the damping terms  $\alpha_0, u_0$  that appear in the output-feedback design. This motivates the belief that to guarantee output-feedback stability the state-feedback control design matrices  $A_1$  and  $A_2$  must be adjusted such that observer errors are dominated, and the inequalities, (2.27) and (2.29) hold.

This design can be seen as a fully automatic control system for a ship, see Chapter 1, consisting of Guidance, Navigation and Control blocks. The navigation



Figure 2.3: Cybership II with markers for positioning.

system uses the position measurements to estimate the velocity, and feed all signals to the guidance and the control systems. The control system consists of the control law (2.43) and the update law for  $\theta$ , while the guidance system incorporates the path  $\xi(\theta)$ , speed assignment  $v_s(\theta, t)$ , and their partial derivatives.

### 2.4.2 Setup

The MCLab is an experimental laboratory for testing scale models of ships, rigs, underwater vehicles and propulsion systems located at the Norwegian University of Science and Technology (NTNU), Trondheim, Norway. It is a joint facility between the Department of Engineering Cybernetics and Marine Technology (Both at NTNU). MCLab is a 40 m x 6.45 m x 1.5 m pool and cameras are used for accurate positioning.

The software is developed using rapid prototyping techniques, and automatic code generation with Matlab, Simulink, Real-Time Workshop, and Opal RT-Lab. The simulation software was developed on a host PC under RT-Lab, and executed on the vessel in the target PC which runs the QNX Neutrino Version 6.2 RT-OS. All control commands are transferred from the control room to the ship via a wireless communication link and the experimental results are presented in real-time on the host PC using LabVIEW as a graphical user interface. Among other things, the synchronization feature can be turned on and off during experiments. The desired path is computed with a path algorithm from Corneliussen (2003) which computes a smooth path that satisfies Assumption 2.1 from a given set of waypoints.

Cybership II (Figure 2.3) is a scale-model (1:70) of an offshore supply vessel and is equipped with two rpm controlled propellers, two rudders and one bow thruster. The model ship has a mass of 23.8 kg and a length of 1.255 m. The

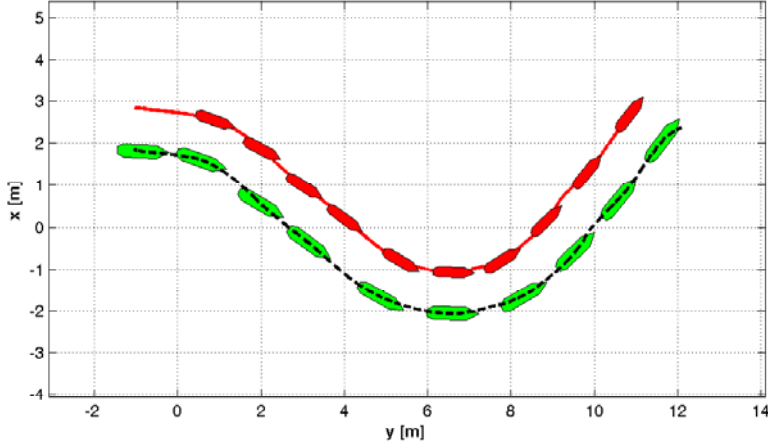


Figure 2.4: Snapshots of Cybership II (---) and the computer simulated ship (—) in the MCLab basin.

control plant parameters are from Lindegaard (2003):

$$M = \begin{bmatrix} 23.8 & 0 & 0 \\ 0 & 33.8 & 1.0948 \\ 0 & 1.0948 & 2.764 \end{bmatrix}, D = \begin{bmatrix} 2 & 0 & 0 \\ 0 & 7 & 0.1 \\ 0 & 0.1 & 0.5 \end{bmatrix}.$$

The designation vectors are  $l_1 = [0, 0, 0]^\top$  and  $l_2 = [0, 1, 0]^\top$  which means that the Formation Reference Point coincide with Cybership II. The speed assignment is a desired surge speed, set by the operator using the GUI. The controller parameters are set as:  $A_{1i} = \text{diag}(0.03, 0.03, 0.03)$ ,  $A_{2i} = \text{diag}(2.5, 2.5, 2.5)$ ,  $P_{1i} = \text{diag}(0.1, 0.1, 0.1)$ ,  $P_{2I} = I_{3 \times 3}$ ,  $\gamma_i = 0.15$ ,  $\Lambda = \text{diag}(1.5, 1.5)$  and  $p = 1$ . The initial conditions are  $\nu_1(0) = \nu_2(0) = [0, 0, 0]^\top$ ,  $\theta_1(0) = 0$  and  $\theta_2(0) = 1$ .

### 2.4.3 Results

The aim of the experiment is to verify the synchronization property of the extended maneuvering controller. Only the scalar path variables  $\theta_1$  and  $\theta_2$  are necessary to ensure synchronization, hence only two signals are communicated between the independent control systems during the experiment. The resulting position plot is shown in Figure 2.4. It shows that the virtual ship starts ahead of Cybership II and that the two ships converge to their desired paths. Until synchronization is turned on, the distance between the ships stays the same and the difference between the path variables  $\theta_1$  and  $\theta_2$  is almost constant.

After synchronization is enabled and has occurred, about halfway through the simulation, the ships move on courses parallel to each other. Figure 2.5 shows

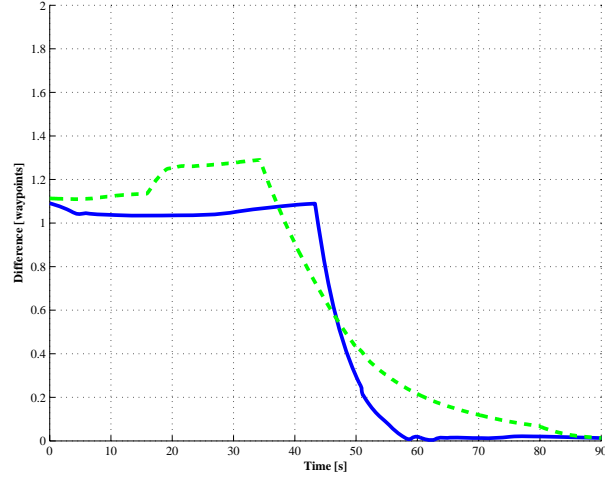


Figure 2.5: Synchronization of the path variables  $|\theta_1 - \theta_2|$  with two different synchronization gains,  $\lambda_i = 1.5$  (—) and  $\lambda_i = 1$  (- -).

the synchronization of the path variables for two different synchronization gains ( $\Lambda = 1.5I$  and  $\Lambda = I$ ). The difference between the two synchronization gains is reflected in the speed of the synchronization  $|\theta_1 - \theta_2|$ .

### Hydrodynamic Interaction

A group of ships are typically affected by forces caused by other vessels motion: both hull-hull interaction and crossing the wake of other vessels affect the movement of a vessel. The main issue of marine formations in this thesis is *control*. Coordination schemes have thus been implemented with simulation models where no interaction forces are present. More theoretical and experimental studies should be conducted to investigate these topics further.

## 2.5 Concluding Remarks

A group of independent vehicles are controlled as formation by synchronizing decentralized path following controllers. Synchronization is achieved by vehicles sharing their scalar path variables so only a small amount of real-time communication is needed. Model experiments demonstrate the performance of the proposed controller and illustrate how the synchronization speed is set by the weight matrix  $\Lambda$ .

In addition, a nonlinear output-feedback control design method is proposed for maneuvering systems. The method relies on the existence of an exponentially stable observer. Compared to state-feedback control laws, an additional damping

term is used in the control law to ensure stability of the closed-loop system when using a combination of measured and estimated states in the control law



# Chapter 3

## Passivity-Based Designs for Synchronized Path Following

### 3.1 Introduction

In this chapter, we exploit the path following flexibility with two separate goals to synchronize the path variables for a group of path-following systems. In particular, we make use of a passivity-based framework for formation control proposed in Arcaik (2006). This framework allows us to obtain a broad class of synchronization schemes for a general communication topology, and encompasses designs such as in Chapter 2. In this framework, we represent the closed-loop system as the feedback interconnection of a dynamic block for path variable synchronization and another block that incorporates the path following systems. We then prove stability by using the Passivity Theorem which states that an interconnection of two passive blocks is passive and, thus, stable in the absence of exogenous inputs. The results in this chapter are based on Ihle, Arcaik & Fossen (2006*a*, 2006*b*).

A major advantage of the passivity approach is that it allows the designer to construct filters that preserve passivity properties of the closed-loop system. This additional flexibility may be used to improve the performance and robustness of the design. We further consider a sampled-data framework where the synchronization scheme is implemented in discrete time while the path-following controllers are continuous-time systems. This formulation is meaningful because communication of path parameters between vehicles will likely occur over a digital network which introduces delays, while the path-following controllers are implemented locally in continuous-time or with fast sampling. Bias estimation fits into the passivity-based framework, and results in a control law with integral action that counteracts slowly-varying environmental loads.

With this approach the formation maneuvering problem, as defined in Chap-

ter 2, is solved using two blocks where the individual path following is performed in one block and synchronization of path variables occurs in another, also referred to as a *consensus* scheme. The main task of consensus systems is to steer variables to a common value across a network – Olfati-Saber & Murray (2004). Application areas for such problems range from natural group behaviors as described in Reynolds (1987), vehicle formations, distributed computing, and sensor networks as presented in Ren, Beard & Atkins (2005).

## 3.2 Path-Following Design and Synchronization

We briefly recapitulate the path following design that is used as a basis in this chapter. Consider a general system

$$\begin{aligned}\dot{x} &= f(x, u) \\ y &= h(x)\end{aligned}\tag{3.1}$$

where  $x \in \mathbb{R}^n$  denotes the state vector,  $y \in \mathbb{R}^m$  is the system output, and  $u \in \mathbb{R}^n$  is the control. To force  $y$  to a prescribed feasible path  $y_d(\theta)$ , and to assign a feasible speed  $v(t)$  to  $\dot{\theta}$  on this path, Skjetne (2005) studies subclasses of (3.1) and develops maneuvering design procedures based on feedback linearization and backstepping techniques. The designs in Skjetne et al. (2004) lead to a closed-loop system of the form

$$\begin{aligned}\dot{z} &= F(x)z - g(t, x, \theta)\omega \\ \dot{\theta} &= v(t) - \omega\end{aligned}\tag{3.2}$$

where  $z$  is a set of new variables that include the tracking error  $y - y_d(\theta)$  and its derivatives, and  $\omega$  is a feedback term to be designed such that the desired speed  $v(t)$  is recovered asymptotically; that is

$$\omega \rightarrow 0 \text{ as } t \rightarrow \infty.\tag{3.3}$$

$F(x) \in \mathbb{R}^{n \times n}$  and  $g(t, x, \theta) \in \mathbb{R}^n$  depend on the control design and, in particular,  $F(x)$  satisfies

$$PF(x) + F(x)^\top P \leq -I, \quad \forall x\tag{3.4}$$

for some matrix  $P = P^\top > 0$ . The uniform boundedness of the path derivatives and speed assignments implies that the function  $g(t, x, \theta)$  is uniformly bounded in its arguments. A path-following design for marine vehicles is presented in Chapter 2.

In this chapter, we consider a group of vehicles  $i = 1, \dots, r$ , each controlled by an individual path-following design with a prescribed velocity  $v(t)$  assigned to the group, resulting in the closed loop system

$$\begin{aligned}\dot{z}_i &= F_i(x_i)z_i - g_i(t, x_i, \theta_i)\omega_i \\ \dot{\theta}_i &= v(t) - \omega_i.\end{aligned}\tag{3.5}$$

Our goal is to design  $\omega_i$  to synchronize the path variables  $\theta_i$ ,  $i = 1, \dots, r$ , while achieving (3.3). The design of  $\omega_i$  depends on variables of the  $i$ th system and on the path parameters for the neighboring vehicles, so only one scalar variable needs to be transmitted from each vehicle. The communication topology between the members of the formation is described by a graph  $\mathcal{G}$ . Two members,  $i$  and  $j$ , are *neighbors* if they can access the synchronization error  $\theta_i - \theta_j$ . In this case, we let the  $i$ th and  $j$ th vertices of  $\mathcal{G}$  be connected by an edge. The information flow is bidirectional, but to simplify the derivation we assign an orientation to the graph by considering one of the vertices to be the positive end of the edge. For a group of  $r$  members with  $p$  edges, the  $r \times p$  incidence matrix  $D(\mathcal{G})$  is defined as

$$d_{ik} = \begin{cases} +1 & \text{if } i\text{th vertex is the positive end of the } k\text{th edge} \\ -1 & \text{if } i\text{th vertex is the negative end of the } k\text{th edge} \\ 0 & \text{otherwise.} \end{cases} \quad (3.6)$$

**Assumption 3.1** *We assume that  $\mathcal{G}$  is connected, i.e. a path exists between every two distinct vertices of  $\mathcal{G}$ .*

### 3.3 Passivation Designs for Synchronization

#### 3.3.1 Design 1: With Path Error Feedback

When the path error is available for feedback we design  $\omega = [\omega_1, \dots, \omega_r]^\top$  as

$$\omega_i = \mathcal{F}_i \{2z_i^\top P_i g_i + \psi_i(\theta)\} \quad (3.7)$$

where all path parameters are collected in the vector  $\theta = [\theta_1, \dots, \theta_2]^\top$  and  $\mathcal{F}_i\{\cdot\}$  denotes the output of a static or dynamic block, which will be specified. This  $\mathcal{F}_i$  can be a filter added to enhance performance and robustness properties, illustrated with examples in Section 5.5. The input to this filter is

$$u_i := 2z_i^\top P_i g_i + \psi_i(\theta) \quad (3.8)$$

where the first component is the path error feedback  $2z_i^\top P_i g_i$ , which serves to improve convergence properties to the desired path<sup>1</sup>. The second component  $\psi_i$  is for the synchronization of the path parameters, and is designed as

$$\psi_i(\theta) = \sum_{k=1}^p d_{ik} \phi_k(\theta_i - \theta_k) \quad (3.9)$$

where  $\phi_k$  is a sector nonlinearity, that is

$$x\phi_k(x) > 0 \quad \forall x \neq 0, \quad \text{and} \quad \lim_{|x| \rightarrow \infty} \int_0^x \phi_k(\sigma) d\sigma = +\infty. \quad (3.10)$$

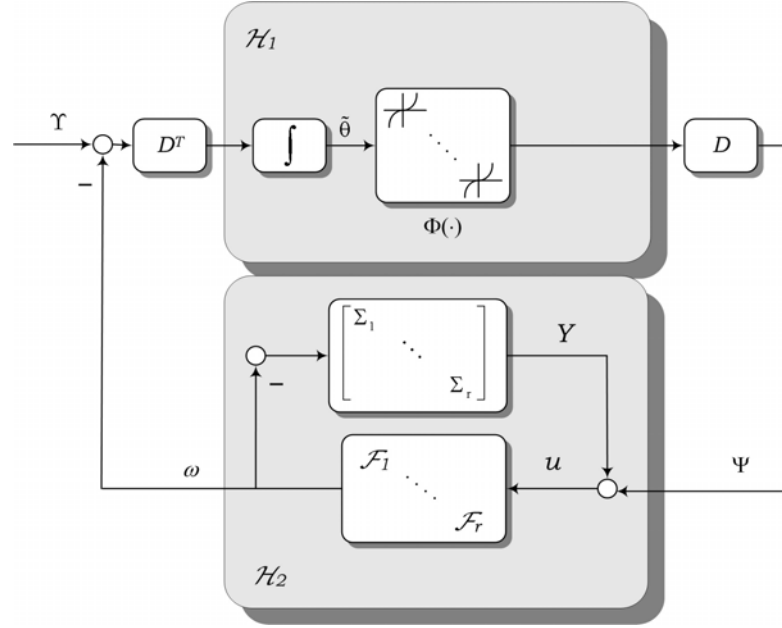


Figure 3.1: Block diagram for the synchronized path following control system.  $\Upsilon$  is a  $r \times 1$  vector with each entry equal to  $v(t)$ .

The feedback law (3.7) is implementable with local information because it depends only on the neighbors of the  $i$ th member ( $d_{ik} \neq 0$ ). With  $\omega$  as in (3.7), the total closed-loop system is represented as in Figure 3.1, where  $\Sigma_i$  is the  $z_i$ -subsystem as in (3.5),

$$\begin{aligned} \tilde{\theta} &:= D^\top \theta, \quad \mathcal{F} := \text{diag}(\mathcal{F}_1, \dots, \mathcal{F}_r), \\ \Phi(\cdot) &= [\phi_1(\cdot), \dots, \phi_p(\cdot)]^\top, \quad \Psi(\theta) = [\psi_1, \dots, \psi_r]^\top, \end{aligned} \quad (3.11)$$

and

$$Y := 2z^\top P G, \quad u = Y + \Psi \quad (3.12)$$

where  $z := [z_1^\top, \dots, z_r^\top]^\top$ ,  $P := \text{diag}(P_1, \dots, P_r)$ , for  $P_i = P_i^\top > 0$ , and  $G := \text{diag}(g_1, \dots, g_r)$ . In particular, note from (3.6) that  $\tilde{\theta}$  in (3.11) is a vector that consists of the differences between the path parameters of neighboring vehicles. Because the graph  $\mathcal{G}$  is connected,  $\tilde{\theta} = 0$  is achieved if and only if all path parameters are synchronized.

We investigate stability properties of the closed-loop by separating it into two blocks,  $\mathcal{H}_1$  and  $\mathcal{H}_2$ , as in Figure 3.1, and analyze passivity properties of each block. The Passivity Theorem guarantees stability, in the absence of exogenous inputs, for

<sup>1</sup>The reader may identify this as the gradient update law as commented before (2.14).

the negative feedback interconnection of two passive systems—see Appendix A.3. Following Arcaik (2006) we now characterize the properties that  $\mathcal{F}_i$ 's must possess to ensure passivity of  $\mathcal{H}_2$  and appropriate detectability conditions that are used to guarantee asymptotic convergence. If  $\mathcal{F}_i$  is a static block we restrict it to be of the form

$$\omega_i = h_i(u_i), \quad (3.13)$$

where  $h_i : \mathbb{R}^p \rightarrow \mathbb{R}^p$  is a locally Lipschitz function satisfying the sector property

$$u_i h_i(u_i) > 0 \quad \forall u_i \neq 0. \quad (3.14)$$

If  $\mathcal{F}_i$  is a dynamic block of the form

$$\begin{aligned} \dot{\xi}_i &= f_i(\xi_i) + g_i(\xi_i)u_i \quad \xi_i \in \mathbb{R}^{n_i} \\ \omega_i &= h_i(\xi_i) + j_i(\xi_i)u_i \end{aligned} \quad (3.15)$$

we assume  $f_i(\cdot)$ ,  $g_i(\cdot)$ ,  $h_i(\cdot)$  and  $j_i(\cdot)$  are locally Lipschitz functions such that  $f_i(0) = 0$  and  $h_i(0) = 0$ . Our main restriction on (3.15) is that it be passive with a twice continuously differentiable, positive definite, radially unbounded storage function  $S_i(\xi_i)$  satisfying

$$\dot{S}_i \leq -W_i(\xi_i) + u_i \omega_i - \nu_i u_i^2 \quad \nu_i \geq 0 \quad (3.16)$$

for some positive definite function  $W_i(\xi_i)$ . Inequality (3.16) with  $\nu_i > 0$  is an *input-strict passivity* property which is possible only when the relative degree of (3.15) is zero. Our asymptotic stability proof below allows  $\nu_i = 0$  provided that (3.15) have a well defined relative-degree-one at  $\xi_i = 0$ . According to Sepulchre, Janković & Kokotović (1997, Proposition 2.44), this is indeed the case if

$$j_i(\xi_i) \equiv 0, \quad g_i(0) \neq 0, \quad \left. \frac{\partial h_i(\xi_i)}{\partial \xi_i} \right|_{\xi_i=0} \neq 0. \quad (3.17)$$

We thus make the following assumption:

**Assumption 3.2** *If  $\nu_i = 0$  in (3.16) then (3.17) holds.*

With  $\mathcal{H}_1$  and  $\mathcal{H}_2$  designed as above, we prove UGAS for  $(\tilde{\theta}, z, \xi) = 0$  in Theorem 3.1 below. This UGAS property implies that in the limit as  $t \rightarrow \infty$  the path parameters  $\theta$  are synchronized ( $\tilde{\theta} \rightarrow 0$ ) and that each system  $i$  follows its desired path ( $z_i \rightarrow 0$ ). Furthermore  $\omega \rightarrow 0$  which means that  $\dot{\theta}$  in (3.2) recovers the speed assignment  $v(t)$ .

**Theorem 3.1** Consider the feedback interconnection shown in Figure 3.1 where members  $i = 1, \dots, r$  are interconnected in a formation as described by (3.6),  $\phi_k$ ,  $k = 1, \dots, p$  is as in (3.10), and  $\mathcal{F}_i$ ,  $i = 1, \dots, r$  are designed as in (3.13)-(3.16). Under Assumptions 3.1-3.2 the feedforward path  $\mathcal{H}_1$  is passive from  $\dot{\theta}$  to  $\Phi$ , and the feedback path  $\mathcal{H}_2$  is strictly passive from  $\Psi$  to  $\omega$ . Furthermore the origin of the feedback interconnection  $(\theta, z, \xi) = 0$  is UGAS.

**Proof:** We combine ideas from Ihle et al. (2004), Arcak (2006), and specific results for path following from Skjetne et al. (2004). To prove passivity from  $\dot{\theta}$  to  $\Phi$ , let

$$V_\psi := \sum_{i=1}^p \int_0^{\theta_i - \theta_k} \phi_k(\sigma) d\sigma. \quad (3.18)$$

Since  $\phi_k$  is as in (3.10),  $V_\psi$  is a positive definite, radially unbounded storage function for  $\mathcal{H}_1$ . Differentiating (3.18) with respect to time yields

$$\dot{V}_\psi = \sum_{i=1}^p \phi_i(\theta_i - \theta_{i+1}) \cdot (\dot{\theta}_i - \dot{\theta}_{i+1}) = \Phi^\top \dot{\theta}, \quad (3.19)$$

which proves that the mapping from  $\dot{\theta}$  to  $\Phi$  is indeed passive. It follows that the path from  $-\omega$  to  $\Psi$  is also passive. To see this, substitute  $\dot{\theta} = D(\Upsilon - \omega)$  in (3.19), and note that the sum of the rows of  $D$  being zero and the entries of  $\Upsilon$  being equal imply  $D\Upsilon = 0$ . Thus,

$$\dot{V}_\psi = -\Phi^\top D^\top \omega = -\Psi^\top \omega. \quad (3.20)$$

To prove passivity of the feedback path, we first consider the  $\Sigma_i$ -blocks. The storage function

$$V_z = \sum_{i=1}^r z_i^\top P_i z_i \quad (3.21)$$

where  $P_i$  is as in (3.4) yields the following time-derivative along the trajectories of  $z$

$$\dot{V}_z \leq - \left( \sum_{i=1}^r z_i^\top z_i \right) - Y^\top \omega \quad (3.22)$$

which proves that the  $\Sigma$ -block is strictly passive from  $-\omega$  to  $Y$ . To establish passivity of  $\mathcal{F}$ , we let  $\mathcal{I}$  denote the subset of indices  $i = 1, \dots, r$  for which  $\mathcal{F}_i$  is a dynamic block as in (3.15), and employ the storage function

$$V_f := \sum_{i \in \mathcal{I}} S_i(\xi_i) \quad (3.23)$$

which yields

$$\begin{aligned}\dot{V}_f &= \sum_{i \in \mathcal{I}} \dot{S}_i \leq \sum_{i \in \mathcal{I}} -(W_i(\xi_i) + u_i \omega_i) \\ &\leq - \left( \sum_{i \in \mathcal{I}} W_i(\xi_i) \right) + u^\top \omega - \sum_{i \notin \mathcal{I}} u_i \omega_i.\end{aligned}\quad (3.24)$$

Substitution of  $u = Y + \Psi$  then yields

$$\dot{V}_f \leq - \left( \sum_{i \in \mathcal{I}} W_i(\xi_i) \right) + Y^\top \omega + \Psi^\top \omega - \sum_{i \notin \mathcal{I}} u_i \omega_i. \quad (3.25)$$

To conclude passivity of the feedback path we use the storage function

$$V_{fb}(z, \xi) := V_z(z) + V_f(\xi) \quad (3.26)$$

and, obtain by adding (3.22) and (3.25),

$$\begin{aligned}\dot{V}_{fb} &\leq - \left( \sum_{i \in \mathcal{I}} W_i(\xi_i) \right) - \left( \sum_{i=1}^r z_i^\top z_i \right) + \Psi^\top \omega \\ &\quad - \sum_{i \notin \mathcal{I}} u_i \omega_i - \sum_{i \in \mathcal{I}} \nu_i u_i^2.\end{aligned}\quad (3.27)$$

Finally, since the static blocks satisfy (3.14),

$$\sum_{i \notin \mathcal{I}} u_i \omega_i = \sum_{i \notin \mathcal{I}} u_i h_i(u_i) \geq 0. \quad (3.28)$$

We thus obtain

$$\dot{V}_{fb} \leq - \left( \sum_{i \in \mathcal{I}} W_i(\xi_i) \right) - \left( \sum_{i=1}^r z_i^\top z_i \right) + \Psi^\top \omega \quad (3.29)$$

and conclude that the feedback path is strictly passive from  $\Psi$  to  $\omega$ .

To prove stability of  $(\tilde{\theta}, z, \xi) = 0$  we use the Lyapunov function

$$V(\tilde{\theta}, z, \xi) = V_\psi(\tilde{\theta}) + V_{fb}(z, \xi) \quad (3.30)$$

which from (3.20) and (3.27), gives the time-derivative:

$$\dot{V} \leq - \left( \sum_{i \in \mathcal{I}} W_i(\xi_i) \right) - \left( \sum_{i=1}^r z_i^\top z_i \right) - \sum_{i \notin \mathcal{I}} u_i h_i(u_i) - \sum_{i \in \mathcal{I}} \nu_i u_i^2. \quad (3.31)$$

Since the right-hand side is negative semidefinite we conclude that the trajectories  $(z(t), \xi(t), \tilde{\theta}(t))$  are uniformly bounded on the interval  $t \in [t_0, t_0 + T]$ , for any  $T$  within the maximal interval of existence. Due to the uniform boundedness of the speed assignment  $v(t)$ , it follows that  $(\theta(t), x(t))$  is bounded by a continuous function of  $T$  and, thus, there are no finite escape times. This implies that  $\tilde{\theta}(t)$  and  $z(t)$  are well defined for all  $t \geq t_0$  and, from (3.31), the equilibrium  $(z, \xi, \tilde{\theta}) = 0$  is uniformly stable.

To prove uniform asymptotic stability we use the Nested Matrosov Theorem from Loría, Panteley, Popović & Teel (2005). To this end we define the auxiliary function

$$V_2 = -\tilde{\theta}^\top D^+ \Lambda \omega \quad (3.32)$$

where  $D^+$  denotes the pseudo-inverse of the incidence matrix  $D$ , and  $\Lambda$  is a diagonal matrix with entries

$$\Lambda_{ii} = \begin{cases} (L_{g_i} h_i(0))^{-1} & \text{if } i \in \mathcal{I} \text{ and } \nu_i = 0 \\ 0 & \text{if } i \notin \mathcal{I} \text{ or } \nu_i > 0. \end{cases} \quad (3.33)$$

In particular  $L_{g_i} h_i(0) := \left. \frac{\partial h_i(\xi_i)}{\partial \xi_i} \right|_{\xi_i=0} g_i(0)$  is nonsingular and, thus, invertible because of the passivity of the  $\xi_i$ -subsystems and because of assumption (3.17) similar to Proposition 2.44 in Sepulchre et al. (1997). To apply Matrosov's Theorem we denote by  $Y_1$  the right-hand side of (3.31) and claim that

$$Y_1 = 0 \quad \Rightarrow \quad \dot{V}_2 =: Y_2 \leq 0. \quad (3.34)$$

To see this note that  $Y_1 = 0$  implies  $\xi = 0$  and  $\omega = 0$ , which mean that all terms in  $\dot{V}_2$  vanish except

$$-\tilde{\theta}^\top D^+ \Lambda \dot{\omega}|_{Y_1=0}. \quad (3.35)$$

Because  $\dot{\omega}_i|_{\xi=0} = L_{g_i} h_i(0) u_i$  when  $i \in \mathcal{I}$  and  $\nu_i = 0$ , and because  $Y_1 = 0$  implies  $u_i = 0$  when  $i \notin \mathcal{I}$  or  $\nu_i > 0$ , we conclude from (3.33) that  $\Lambda \dot{\omega}|_{Y_1=0} = u$  and rewrite (3.35) as

$$-\tilde{\theta}^\top D^+ u. \quad (3.36)$$

We then substitute  $\tilde{\theta} = D^\top \theta$  in (3.36), and using the property  $DD^+D = D$  of the pseudo-inverse, and noting that  $Y_1 = 0$  means  $z = 0$  which in turn implies  $u = \Psi = D\Phi(\tilde{\theta})$ , we conclude

$$\begin{aligned} Y_1 = 0 & \Rightarrow \\ Y_2 = -\theta^\top DD^+ D\Phi(\tilde{\theta}) & = -\theta^\top D\Phi(\tilde{\theta}) = -\tilde{\theta}^\top \Phi(\tilde{\theta}). \end{aligned} \quad (3.37)$$

Because  $\tilde{\theta}^\top \Phi(\tilde{\theta})$  is positive definite in  $\tilde{\theta}$  from (3.10), equation (3.37) proves the claim (3.34). It further follows from (3.31) and (3.37) that  $Y_1 = 0$  and  $Y_2 = 0$

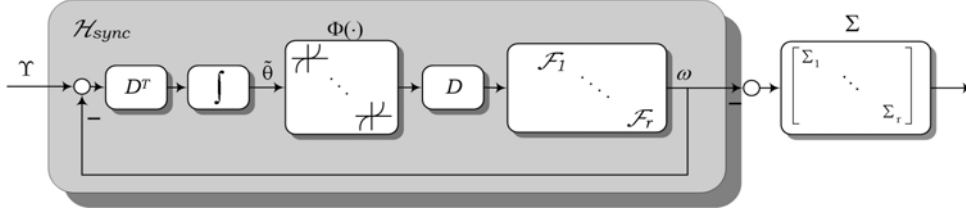


Figure 3.2: Cascade interconnection for Design 2.

together imply  $(z, \xi, \tilde{\theta}) = 0$ . All assumptions of Loría et al. (2005, Theorem 1) being satisfied we conclude UGAS of  $(z, \xi, \tilde{\theta}) = 0$ .  $\square$

**Remark 3.1** A special case of (3.7), studied in Chapter 2, is when the neighbors for system  $i$  are system  $i - 1$  and system  $i + 1$ , i.e., the synchronization error is  $\tilde{\theta} = [\theta_1 - \theta_2, \dots, \theta_{r-1} - \theta_r]^\top$ . Ihle et al. (2004) further assume that  $\mathcal{F}$  is a constant gain matrix and  $\phi_i(r) = r^{2p-1}$ , for  $p = 1, 2, 3, \dots$ . In contrast, in this paper we have considered a general communication topology, and derived relaxed conditions on the feedback block and synchronization function. In particular,  $\mathcal{F}_i$ 's are not necessarily constant gains and  $\phi_i$ 's are not necessarily polynomials.

### 3.3.2 Design 2: Without Path Error Feedback

We next consider a design where  $\omega_i$  only depends on the synchronization terms, and not on the path error. The update law for  $\omega_i$  is now

$$\omega_i = \mathcal{F}_i \{ \psi_i(\theta) \} \quad (3.38)$$

where  $\mathcal{F}_i$  and  $\psi_i$  are as in Section 3.3.1. Without the path error feedback, the closed-loop system becomes a cascade of  $\mathcal{H}_{\text{sync}}$  and  $\Sigma$  as in Figure 3.2. The origin of  $\mathcal{H}_{\text{sync}}$ ,  $(\tilde{\theta}, \xi) = 0$ , is proved to be GAS in Arcak (2006) which means that  $\omega \rightarrow 0$ . In Theorem 3.2 below we prove that the  $\Sigma$ -block is Input-to-State Stable (ISS) w.r.t.  $\omega$ . Stability of the closed-loop system then follows because a cascade of an ISS and a UGAS system is UGAS—see Appendix A.4 .

**Theorem 3.2** Consider the cascaded system in Figure 3.2, where members  $i = 1, \dots, r$  are interconnected in a formation as described by (3.6),  $\phi_k$ ,  $k = 1, \dots, p$  are as in (3.10), and  $\mathcal{F}_i$ ,  $i = 1, \dots, r$  are designed as in (3.13)-(3.16). Then, the origin of  $\mathcal{H}_{\text{sync}}$ -block is GAS, the  $\Sigma$  block is ISS with respect to  $\omega$ , and the origin  $(\tilde{\theta}, \xi, z) = 0$  is UGAS.

**Proof:** For completeness, the stability proof for  $\mathcal{H}_{\text{sync}}$  is given here: The feed-forward path of the  $\mathcal{H}_{\text{sync}}$ -block is an interconnection of a passive and a strictly

passive block. Since pre- and post-multiplication of a matrix and its transpose does not change passivity properties the forward path is passive and with negative feedback the block is output strictly passive from  $\nu$  to  $\omega$ . Moreover, when  $\Upsilon = 0$ , due to (3.17):

$$\omega \equiv 0 \Rightarrow \mathcal{F} \left\{ D\Phi(\tilde{\theta}) \right\} \equiv 0 \Rightarrow D\Phi(\tilde{\theta}) \equiv 0 \quad (3.39)$$

which implies that  $\Phi(\tilde{\theta})$  lies in the nullspace  $\mathcal{N}(D)$ . When  $D$  has linearly independent columns  $\mathcal{N}(D) = 0$  and hence  $\Phi(\tilde{\theta}) \equiv 0 \Rightarrow \tilde{\theta} \equiv 0$  due to (3.10). When  $D$  has linearly dependent columns, the null space of  $D$  is nontrivial. However, a simultaneous solution to  $\Phi(\tilde{\theta}) \in \mathcal{N}(D)$  and  $\tilde{\theta} \in \mathcal{R}(D^\top)$  is possible only when  $\tilde{\theta} = 0$ . This is because  $\mathcal{R}(D^\top)$  and  $\mathcal{N}(D)$  are orthogonal to each other, which means  $\tilde{\theta}^\top \Phi(\tilde{\theta}) = 0$ , and we conclude from (3.10) that  $\tilde{\theta} = 0$ . Hence, the  $\mathcal{H}_{\text{sync}}$ -block is zero-state observable. From Khalil (2002, Lemma 6.7) we obtain GAS of the origin  $\tilde{\theta} = 0$ .

To prove the ISS-property we rewrite the time-derivative (3.22) as

$$\begin{aligned} \dot{V}_z &\leq \sum_{i=1}^r -z_i^\top z_i - 2z_i^\top P_i g_i \omega_i \\ &\leq \sum_{i=1}^r -|z_i|^2 + 2p_{iM} \delta_{gi} |z_i| |\omega_i| \end{aligned}$$

where  $\delta_{gi}$  is an upper bound on  $g_i$  due to Assumption 2.1. Furthermore, we get

$$|z_i| \geq \frac{2p_{iM} \delta_{gi} |\omega_i|}{\varepsilon} \Rightarrow \dot{V}_z \leq \sum_{i=1}^r - (1 - \varepsilon) |z_i|^2 \quad (3.40)$$

where  $0 < \varepsilon < 1$ . Thus, the system is ISS from  $\omega_i$  to  $z_i$  with  $\rho(r) = \frac{2p_{iM} \delta_{gi}}{\varepsilon} r$ . Since the origin of  $\mathcal{H}_{\text{sync}}$  is GAS and  $\Sigma$  is ISS with respect to  $\omega$ , it follows from Lemma A.8 that the origin  $(\tilde{\theta}, \xi, z) = 0$  is UGAS.  $\square$

**Remark 3.2** *Given the results on agreement protocols in Arcak (2006), the results in this section can be extended to a time-varying communication topology given by the incidence matrix  $D(t)$  as long as  $\mathcal{G}$  remains connected for all  $t > 0$ . A further result in Arcak (2006) allows the graph to lose connectivity pointwise in time as long as it is established in an integral sense. This means that signal dropouts in the communication links are tolerated if connectivity is eventually re-established.*

Another example where consensus schemes are applied for the purpose of coordinated control is Kingston et al. (2005). The authors prove that a class of

consensus schemes with linear synchronization functions are Input-to-State Stable with respect to communication noise and design cooperative timing strategies. ISS of leader/follower systems is discussed in Tanner, Pappas & Kumar (2004) and Chen & Serrani (2004) where the leader's motion is related to formation errors, that is, the interconnections errors observed inside the formation.

### 3.4 Sampled-Data Design with Discrete-Time Update for $\theta$

We now study the situation where the path parameters  $\theta_i$  are updated in discrete-time. Such an implementation is practically relevant, because path parameters are to be exchanged over a communication network where the transmission occurs at discrete time-intervals. Since the path following controllers are implemented locally by each vehicle with fast sampling, we consider the  $\Sigma$ -blocks in Figure 3.1 to be continuous time. This implementation thus results in the sampled-data closed-loop system:

$$\begin{aligned} \dot{z}_i &= F_i(x_i) z_i - g_i(t, x_i, \theta^{\text{zoh}}) \omega_i^{\text{zoh}} \\ \theta_i((n+1)T) &= \theta_i(nT) + v(nT) - \omega_i(nT) \end{aligned} \quad (3.41)$$

where  $n = 0, 1, 2, \dots$  is the time index, and  $\omega_i^{\text{zoh}}$  and  $\theta^{\text{zoh}}$  denote the zero-order-hold equivalent continuous-time signals generated from the discrete-time signals  $\theta$  and  $\omega_i$ .

Because  $\theta$  is now updated in discrete-time the integral block in the feedforward path of Figure 3.1 is replaced by a summation block, and  $\dot{\tilde{\theta}}$  is replaced by

$$\delta\tilde{\theta} := \tilde{\theta}(n) - \tilde{\theta}(n-1). \quad (3.42)$$

As discussed in Arcak (2006), passivity of the feedforward path  $\mathcal{H}_1$  cannot be achieved in discrete-time because the phase lag of a summation block exceeds  $90^\circ$ . In the feedforward system we restrict the slope of the nonlinearity  $\phi_k(\tilde{\theta}_k)$  by

$$\phi'_k(\tilde{\theta}_k) \leq \mu \quad (3.43)$$

for some constant  $\mu > 0$ . With this assumption it is shown in Arcak (2006) that the storage function  $V_\psi(\theta)$  in (3.18) satisfies

$$V_\psi(\tilde{\theta}((n+1)T)) - V_\psi(\tilde{\theta}(nT)) \leq -\Psi^\top \omega + \frac{\mu \lambda_N}{2} \omega^\top \omega \quad (3.44)$$

where  $\lambda_N$  denotes the largest eigenvalue of the graph Laplacian matrix  $DD^\top$  and the second term on the right hand side of (3.44) quantifies the shortage of passivity. Then, the  $\mathcal{H}_2$ -block must achieve an excess of passivity in the feedback path to guarantee stability for the interconnected system.

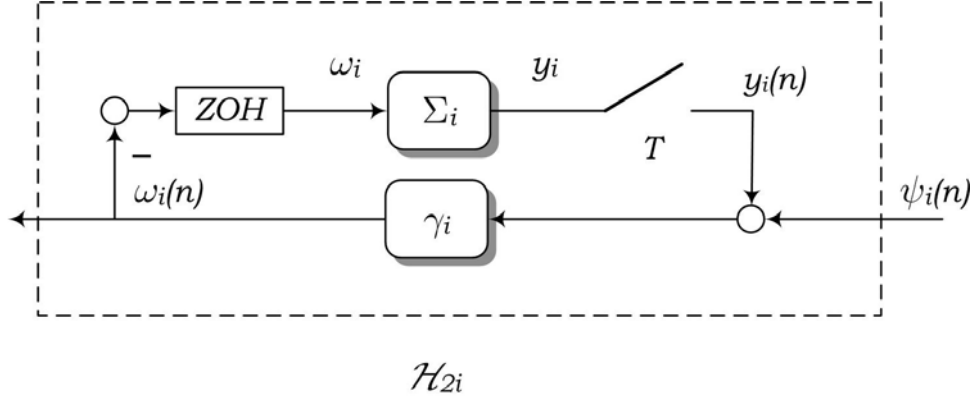


Figure 3.3: A block diagram representation of the sampled-data dynamical block  $\mathcal{H}_{2i}$  where  $ZOH$  stands for the "Zero-Order-Hold" function and  $T$  is the sampling period. The  $\theta$ -dynamics is omitted.

### 3.4.1 Design 1: With Path Error Feedback

When  $z(t)$  is available for feedback we design  $\omega_i$  in (3.41) as

$$\omega_i(nT) = \gamma_i \left( 2z_i(nT)^\top P_i g_i(nT, x_i(nT), \theta(nT)) + \psi_i(\theta(nT)) \right) \quad (3.45)$$

where  $\gamma_i > 0$  is an adaptation gain to be specified and  $\psi_i(\cdot)$  is as in (3.9). With this design the  $\mathcal{H}_2$  block is as in Figure 3.3 and, as we shall see, its excess of passivity compensates for the shortage in (3.44) when  $\gamma_i$  and  $T$  are sufficiently small. To make this claim precise we need the following lemma, proven in Biyik & Arcak (2006) using the techniques of Laila, Nešić & Teel (2002):

**Lemma 3.1** *Biyik & Arcak (2006): Consider members  $i = 1, \dots, r$  interconnected as described by the graph representation (3.6), and let  $\tilde{\theta}_k$ ,  $k = 1, 2, \dots, p$  denote the differences between the variables  $\theta_i$  of neighboring members. Let  $\phi_k(\tilde{\theta}_k)$ 's be designed as a first-third quadrant nonlinearity satisfying (3.43) for some constant  $\mu > 0$ . Suppose that  $\mathcal{H}_i$ 's are sampled-data dynamic blocks as in Figure 3.3, and satisfy the following two assumptions:*

**L1.** For  $\omega_i = 0$ , the time-derivative of  $V_{z_i}$  for  $\Sigma_i$  is upper bounded by  $\dot{V}_{z_i}(z_i) \leq -C|z_i|^2$  for some  $C > 0$ ,

**L2.**  $\Sigma_i$ -subsystems,  $i = 1, \dots, r$  are Input-to-State Stable from  $\omega_i$  to  $y_i$ , i.e., there exist class- $\mathcal{KL}$  and class- $\mathcal{K}$  functions  $\beta(\cdot, \cdot)$  and  $\rho(\cdot)$ , respectively, such that

$$|z_i(t)| \leq \beta(|z_i(t_0)|, t - t_0) + \rho \left( \sup_{t_0 \leq \tau \leq t} |\omega_i(\tau)| \right).$$

Then given compact set  $\mathcal{D}_{\tilde{\theta}}$  and  $\mathcal{D}_z$  there exist positive constants  $\bar{T}$  and  $\bar{\gamma}$  such that for all sampling periods  $T < \bar{T}$  and  $\gamma_i \leq \bar{\gamma}$ , the feedback law (3.45) achieves asymptotic stability of the origin  $(\tilde{\theta}, z) = 0$  with a region of attraction that includes  $\mathcal{D}_{\tilde{\theta}} \times \mathcal{D}_z$ .  $\square$

Lemma 3.1 proves a semiglobal asymptotic stability property in  $T$  and  $\gamma_i$  for the equilibrium point  $(\tilde{\theta}, z) = 0$ , which means that any prescribed region of attraction can be achieved by sufficiently reducing the sampling period  $T$  and the adaptation gain  $\gamma_i$ . In particular, increasing the size of the prescribed region of attraction or increasing the parameters  $\mu$  and  $\lambda_N$  in (3.44) dictate smaller values for  $\bar{T}$  and  $\bar{\gamma}$  (See Biyik & Arcak (2006) for formulas that estimate  $\bar{T}$  and  $\bar{\gamma}$ ). The proof in Biyik & Arcak (2006) (see also Laila et al. (2002)) is also applicable to time-varying sampling periods that are upper bounded by  $\bar{T}$ . We now apply Lemma 3.1 to our system and state the main result of this section:

**Theorem 3.3** Consider members  $i = 1, \dots, r$  interconnected in a formation as described by (3.6). Let  $\phi_k$ 's be as in (3.10) and (3.43), and suppose that  $\mathcal{H}_2$  consists of sampled-data dynamic blocks as in Figure 3.3 where the continuous-time  $\Sigma_i$ -block and the discrete-time updates for  $\theta_i$  are as given in (3.41). Then, given compact sets  $\mathcal{D}_z$  and  $\mathcal{D}_{\theta}$  there exist positive constants  $\bar{T}$  and  $\bar{\gamma}$  such that for all sampling periods  $T < \bar{T}$  and  $\gamma_i \leq \bar{\gamma}$ , the feedback law (3.45) achieves UAS of the origin  $(z, \tilde{\theta}) = 0$  with a region of attraction that includes  $\mathcal{D}_z \times \mathcal{D}_{\tilde{\theta}}$ .

**Proof:** First, we know from the proof of Theorem 3.1 that each  $\Sigma_i$ -block is strictly passive with a positive definite storage function  $V_{z_i}(z_i)$  such that

$$\dot{V}_{z_i} \leq -W(z_i) - y_i \omega_i$$

where  $W(z_i) = z_i^\top z_i$ . Hence, we find a lower bound on  $W(z_i) \geq C|z_i|^2$  where  $C = 1 > 0$  so L1 of Lemma 3.1 holds. Second, L2 holds since Input-to-State Stability from  $\omega_i$  to  $z_i$  is proved in Theorem 3.2 using the same storage function. We thus conclude that the origin  $(z, \tilde{\theta}) = 0$  is UAS with a region of attraction that includes the prescribed set  $\mathcal{D}_z \times \mathcal{D}_{\tilde{\theta}}$ .  $\square$

### 3.4.2 Design 2: Without Path Error Feedback

We next consider the case where  $z_i(t)$  is not employed in discrete-time  $\theta_i$  updates. In this case we have

$$\omega_i(nT) = \mathcal{F}_i \{ \psi_i(\theta(nT)) \}, \quad (3.46)$$

where  $\mathcal{F}_i$  is a discrete-time dynamic or static block. In order to guarantee excess of passivity in the feedback path, we restrict static  $\mathcal{F}_i$  blocks  $y_i = h_i(t, u_i)$  by

$$u_i y_i - \tau_i y_i^2 \geq \varpi_i(u_i) \quad (3.47)$$

where  $\varpi_i(u_i)$  is a positive definite function and  $\tau_i > 0$  quantifies the excess of passivity. When  $\mathcal{F}_i$  is a dynamic block of the form

$$\begin{aligned}\xi_i((n+1)T) &= f_i(\xi_i(nT), u_i(nT)) \quad \xi_i \in \mathbb{R}^{n_i} \\ y_i &= h_i(\xi_i, u_i)\end{aligned}\quad (3.48)$$

we assume that (3.17) holds and that there exists a positive definite and radially unbounded storage function  $S_i(\xi_i)$  satisfying

$$S_i(\xi_i((n+1)T)) - S_i(\xi_i(nT)) \leq -W_i(\xi_i) + u_i y_i - \tau_i y_i^2 \quad (3.49)$$

for some positive definite function  $W_i(\cdot)$ . We then guarantee stability of the feedback system by choosing

$$\tau_i \geq \frac{\mu \lambda_N}{2} \quad i = 1, \dots, r. \quad (3.50)$$

As before, GAS of  $\tilde{\theta} = 0$  implies  $\omega \rightarrow 0$  and stability of the path errors follows from the cascade structure and the ISS-property of the  $\Sigma_i$ -subsystems driven by  $\omega$ :

**Theorem 3.4** *Consider members  $i = 1, \dots, r$  interconnected in a formation as described by (3.6). Let  $\phi_k$ ,  $k = 1, \dots, p$  be as in (3.10) and (3.43), and suppose that  $\mathcal{H}_2$  consists of sampled-data dynamic blocks where the continuous-time  $\Sigma_i$ -blocks are as given in (3.5) and  $\mathcal{F}_i$ 's are as in (3.47)-(3.49). Under these conditions if (3.50) holds then the update law (3.46) renders the the origin  $(\tilde{\theta}, \xi, z) = 0$  UGAS.*

**Proof:** When (3.50) holds asymptotic stability of  $(\tilde{\theta}, \xi) = 0$  follows from Arcak (2006). Furthermore, from Theorem 3.2 we know that each  $z_i$  is Input-to-State Stable with respect to  $\omega_i$  so  $z(t)$  is bounded within each sampling period and constant between the sampling points. It then follows from arguments similar to those in Theorem 3.2 that the origin  $(\tilde{\theta}, \xi, z) = 0$  is UGAS.  $\square$

## 3.5 Integral Action by Adaptive Backstepping

Many practical control systems include integral control to remove constant steady-state offsets and alleviate problems with unmodeled dynamics, parameter deviations, and slowly varying disturbances—see Ortega, Loría, Nicklasson & Sira-Ramirez (1998) and Fossen, Loría & Teel (2001). The most common way to include integral action in backstepping is to employ parameter adaptation. Thus, the path-following design is extended to counteract unknown slowly-varying environmental forces by compensating for a dynamic bias estimate.

We consider a special case of Skjetne et al. (2005):

$$\begin{aligned}\dot{x} &= f(x) + H(g(x, u) + \Xi(x)b) \\ \dot{b} &= 0 \\ y &= h(x)\end{aligned}\tag{3.51}$$

where  $\Xi(x) \in \mathbb{R}^{n \times n}$  is nonsingular and  $b \in \mathbb{R}^n$  is a constant (or slowly varying) unknown bias due to external environmental forces. The bias  $b$  is matched to the control  $u$  via the matrix  $H$  which has full column rank. If  $b = 0$  the plant is undisturbed and identical to (3.1).

An additional step in the control design used to obtain (3.2) in Section 3.3.1 is needed to obtain an adaptive law for  $\hat{b}$ . The adaptive update law for  $\hat{b}$  is designed as Skjetne et al. (2005)

$$\dot{\hat{b}} = 2\Pi\Xi(x)^\top H^\top Pz$$

where  $\Pi = \Pi^\top > 0$  is a gain matrix,  $\Xi(x)$  is the adaptive regressor matrix from (3.51),  $H$  is as in (3.51), and  $P$  satisfies (3.4). For each system  $i$  we have a closed-loop system of the following form, similar to (3.2) but with parameter error dynamics

$$\begin{aligned}\dot{z}_i &= F_i(x_i)z_i - g_i(t, x_i, \theta_i)\omega_i - H_i\Xi_i(x_i)\tilde{b}_i \\ \dot{\tilde{b}}_i &= 2\Pi_i\Xi_i(x_i)^\top H_i^\top P_i z_i \\ \dot{\theta}_i &= v(t) - \omega_i\end{aligned}\tag{3.52}$$

where  $\tilde{b} = b - \hat{b}$  is the parameter estimation error and previous assumptions on the system hold. Figure 3.4 shows the block-diagram of system  $i$  without the  $\theta$ -dynamics.

We design  $\omega = [\omega_1, \dots, \omega_r]^\top$  with path error feedback as in (3.7), that is,

$$\omega_i(z_i, \theta) := \mathcal{F}_i\{2z_i^\top P_i g_i + \psi_i(\theta)\}$$

where  $\mathcal{F}_i$  and  $\psi_i$  are as in Section 3.3.1. The block diagram representation is as in Figure 3.1 where the path following systems  $\Sigma_i$  is extended with a loop for bias estimation as shown in Figure 3.4. With the previous assumptions on the blocks in the feedback interconnection, passivity is preserved and we prove UGS of the origin and convergence of  $(\tilde{\theta}, \xi, z) \rightarrow 0$ :

**Theorem 3.5** *Consider the feedback interconnection shown in Figure 3.1 where members  $i = 1, \dots, r$  have a closed-loop system as in (3.52) and interconnected in a formation as described by (3.6),  $\phi_k$ ,  $k = 1, \dots, p$  is as in (3.10), and  $\mathcal{F}_i$ ,  $i = 1, \dots, r$  are designed as in (3.13)-(3.16). Then the interconnection is passive and its origin  $(\tilde{\theta}, z, \xi, \tilde{b}) = 0$  is UGS, and*

$$\lim_{t \rightarrow \infty} |(\tilde{\theta}(t), \xi(t), z(t))| = (0, 0, 0)$$

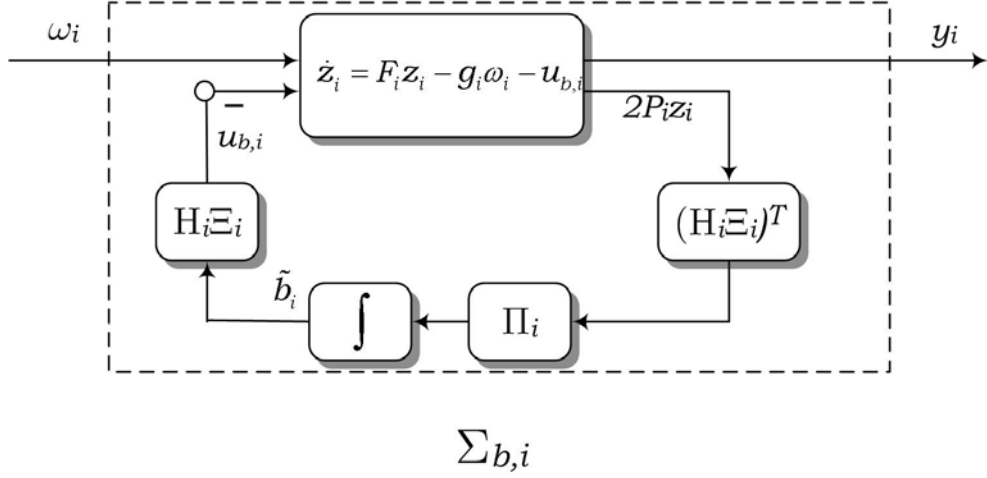


Figure 3.4: Disregarding the  $\theta$ -dynamics, the  $\Sigma_{b,i}$ -block consists of the closed-loop path following system and the bias estimation error  $\tilde{b}$ .

**Proof:** From the proof of Theorem 3.1 we know that the forward path is passive with storage function and time-derivative as in (3.18)-(3.19). Strict passivity of the feedback-loop is proved with (3.26) and (3.29). To investigate passivity of the feedback loop with bias estimation, let

$$V_b(\tilde{b}) = \sum_{i=1}^r \tilde{b}_i^\top \Pi_i^{-1} \tilde{b}_i \quad (3.53)$$

be a positive storage function, with the following time-derivative along the trajectories of the bias estimation error (3.52)

$$\dot{V}_b = \sum_{i=1}^r \tilde{b}_i^\top \Pi_i^{-1} \dot{\tilde{b}}_i = \sum_{i=1}^r \tilde{b}_i^\top \Xi_i(x_i)^\top H_i^\top P_i z_i = 2u_b^\top Pz. \quad (3.54)$$

This shows that the path from  $z$  to  $u_b$  is passive. The storage function (3.21) yields now the following time-derivative along the trajectories of  $z$  and  $\tilde{b}$

$$\dot{V}_z \leq - \left( \sum_{i=1}^r z_i^\top z_i \right) - Y^\top \omega - 2u_b^\top Pz \quad (3.55)$$

and by adding (3.54) and (3.55) we obtain (3.22). It follows as in the proof of Theorem 3.1 that the feedback path, and hence the feedback interconnection, is passive.

To prove UGS of  $(\tilde{\theta}, z, \xi, \tilde{b}) = 0$  we add (3.53) to (3.30)

$$V(\tilde{\theta}, z, \xi, \tilde{b}) = V_\psi(\tilde{\theta}) + V_{fb}(z, \xi) + V_b(\tilde{b}) \quad (3.56)$$

which, from (3.20), (3.27), and (3.54), gives the same time-derivative as (3.31). Since the right-hand side is negative semidefinite the trajectories  $(\tilde{\theta}(t), z(t), \xi(t), \tilde{b}(t))$  are uniformly bounded on the maximal interval of existence. It follows from similar arguments as in Theorem 3.1 that the equilibrium  $(\tilde{\theta}, z, \xi, \tilde{b}) = 0$  is uniformly globally stable. The conclusion follows from the LaSalle-Yoshizawa theorem (see Krstić et al. (1995, Theorem 2.1)).  $\square$

A analogous result for Design 2 can be obtained, but is omitted to save space.

## 3.6 Examples

A formation maneuvering operation between marine surface vessels is considered to illustrate the proposed framework. The passivity framework is applied to obtain an extended class of feedback functions  $\mathcal{F}_i$  that can address performance properties and increase robustness to thruster saturation, environmental disturbances and delays for a group of vessels.

We consider a model of a fully actuated tugboat in three degrees of freedom where the surge mode is decoupled from the sway and yaw mode due to port/starboard symmetry. The body-fixed equations of motion for vessel  $i = 1, \dots, r$  are given as (see Appendix B for details)

$$\dot{\eta}_i = R\nu_i \quad (3.57a)$$

$$M_i \dot{\nu}_i + C_i(\nu_i)\nu_i + D_i(\nu_i)\nu_i = \tau_i + R^\top b \quad (3.57b)$$

where the unknown constant or slowly-varying disturbances are collected in the bias  $b_i$ .

The backstepping design for each ship model gives the static part of the control signal when we assume  $b_i = 0$

$$\tau_i = -z_{1i} - K_{di}z_{2i} + D(\nu_i)\nu_i + C_i(\nu_i)\nu_i + M_i(\sigma_{1i} + \alpha_{1i}^{\theta_i}v)$$

where  $K_{di} = K_{di}^\top > 0$ ,  $\alpha_{1i}$  is a virtual control determined by the backstepping procedure, and  $\dot{\alpha}_{1i} = \sigma_{1i} + \alpha_{1i}^{\theta_i} \dot{\theta}$ —see Skjetne et al. (2004) for details. The resulting closed-loop system is given by (3.5) where  $x_i = [\eta_i^\top, \nu_i^\top]^\top$  and

$$F_i(\nu_i) := \begin{bmatrix} -K_{pi} - r_i S & I \\ -M_i^{-1} & -M_i^{-1}(K_{di} + D_i(\nu_i) + C_i(\nu_i)) \end{bmatrix}$$

$$g(\eta_i, \theta_i, t) := \begin{bmatrix} R(\psi_i) \eta_{di}^{\theta_i}(\theta_i) \\ \alpha_{1i}^{\theta_i}(\eta_i, \theta_i, t) \end{bmatrix}.$$

for  $K_{pi} = K_{pi}^\top > 0$ .

### 3.6.1 Feedback Function Design

The passivity approach expands the selection of update laws for  $\omega$ . The class of strictly positive real (SPR) systems include the *filtered gradient update law* considered in Skjetne et al. (2004) (but not previously considered for a formation): We design the dynamic block  $\mathcal{F}_i$  with output  $\omega_i$  and dynamics

$$\dot{\omega}_i = -\lambda_i \omega_i + \gamma_i u_i, \quad \lambda_i, \gamma_i > 0. \quad (3.58)$$

With the storage function

$$V_{\omega_i} = \frac{1}{2} \omega_i^2$$

we obtain

$$\dot{V}_{\omega_i} = -\lambda_i \omega_i^2 + \gamma_i \omega_i u_i$$

and since (3.15)-(3.16) are fulfilled we invoke Theorem 3.1 to conclude UGAS of  $(\tilde{\theta}, \omega, z) = 0$ . Equation (3.58) is essentially a low-pass filter where the cut-off frequency can be designed in a trade-off fashion of measurement noise attenuation versus bandwidth as determined by the choice of  $\lambda_i$  and  $\gamma_i$ .

Skjetne et al. (2003) discuss how thruster saturation constraints in a single vessel cause steady-state errors in the path variables synchronization. This error is eliminated by employing integral feedback from the synchronization error. In the proposed framework of Section 3.3.1 the thruster saturation can be handled with a proportional-integral-derivative (PID) control structure with limited integral and derivative effect, also known as a lead-lag controller,

$$\omega_i(s) = H_{pid,i}(s) u_i(s)$$

given by

$$H_{pid,i}(s) = \gamma_i \beta_i \frac{1 + \mu_i s}{1 + \beta_i \mu_i s} \frac{1 + T_{d,i} s}{1 + \alpha_i T_{d,i} s} \quad (3.59)$$

where  $\gamma_i > 0$ ,  $0 \leq T_{d,i} \leq \mu_i$ ,  $1 \leq \beta_i < \infty$  and  $0 < \alpha_i \leq 1$ . Then, (3.59) is Hurwitz and satisfies  $\text{Re}[H_{pid,i}(j\omega)] \geq \nu_i > 0$  for all  $s = j\omega$  and it follows that the PID controller structure falls into the class of input strictly passive systems and stability of the interconnection follows from Theorem 3.1.

### 3.6.2 Simulation: Saturation in Thrust

We consider a simulation where the propellers of one vessel saturates and are only able to produce a surge speed less than the speed assignment. We use Design 1 in Section 3.3.1 and compare the synchronization error for the original control scheme in Ihle et al. (2004), i.e.  $T_{d,i} = 0 = \mu_i$  in (3.59) while  $\gamma_i = 10$ , with the

PID structure with  $T_{d,i} = 10$ ,  $\mu_i = 1$ ,  $\gamma_i = 10$ ,  $\alpha_i = 0.1$ , and  $\beta_i = 10$ . The other control parameters are set as  $P_i = \text{diag}(0.2, 0.2, 1, 10, 10, 40)$  and  $\phi_i(x) = x^3$ . The desired speed is  $v = 4$ , and the desired path for Vessel 2 is given by  $x_d(\theta_2) = \theta_2$ ,  $y_d(\theta_2) = 1200 \sin \frac{2\pi}{4000} \theta_2$ , and (2.4). The other paths are constructed such that the vessels move parallel when  $\tilde{\theta} = 0$ . The initial conditions are  $\eta_1(0) = [573, 222.5, 0]^\top$ ,  $\eta_2(0) = [0, 0, 0]^\top$ ,  $\eta_3(0) = [320, 420, 0]^\top$ , and  $\nu_i = 0$  for  $i = 1, 2, 3$ . The communication topology is given by the incidence matrix

$$D(\mathcal{G}) = \begin{bmatrix} 1 & 0 \\ -1 & 1 \\ 0 & -1 \end{bmatrix} \quad (3.60)$$

that is only vehicles 1 and 2, and 2 and 3 are exchanging their path parameters. The initial synchronization errors are  $\tilde{\theta}_1(0) = 500$  and  $\tilde{\theta}_2(0) = -400$ .

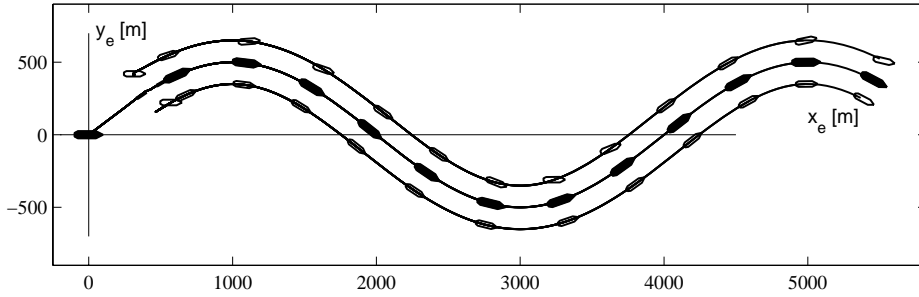


Figure 3.5: Position snapshots of three tugboats where one vessel saturates. The feedback function  $\mathcal{F}_i$  is as in (3.59).

Figure 3.5 shows that the formation follows the path as desired. The synchronization of  $\tilde{\theta}_1$  for the two  $\mathcal{F}_i$ -structures are shown in Figure 3.6 and shows that the PID-structure yields a smaller error when one vessel saturates.

### 3.6.3 Simulation: Synchronization in the presence of environmental loads

To reduce wear and tear of actuators and propulsion system the ship control system should counteract the slowly-varying environmental motion components: model uncertainties, wave drift, currents and mean wind forces. The unknown mean environmental force and its direction are assumed to be constant (or at least slowly varying).

If we assume that  $b \neq 0$ , an adaptive backstepping design for each ship model as in Section 3.5 gives the the static part of the control signal and the adaptive

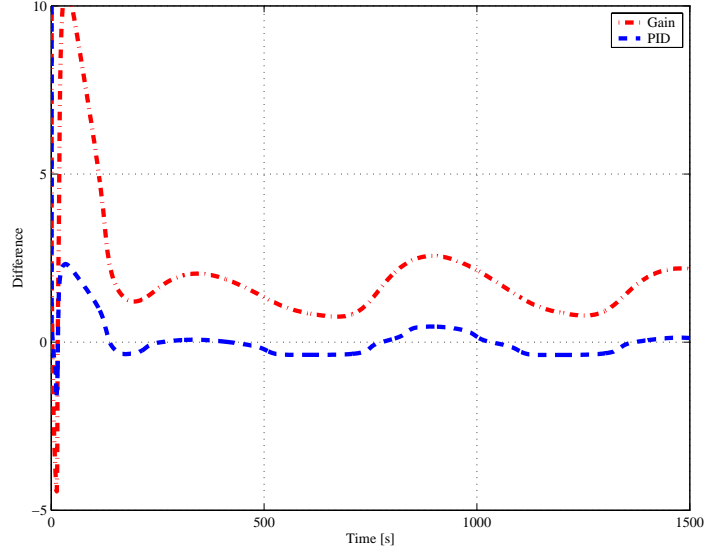


Figure 3.6: Synchronization of  $\tilde{\theta}_1$  when one vessel saturates. The result when  $\mathcal{F}_i$  is a gain is shown in red (dashed-dot) and a PID structure for  $\mathcal{F}_i$  results in the blue (dashed) plot.

update law for  $\hat{b}_i$  (integral action):

$$\begin{aligned}\tau_i &= -z_{1i} - K_{di}z_{2i} + D(\nu_i)\nu_i + C_i\nu_i + M_i(\sigma_{1i} + \alpha_{1i}^{\theta_i}v) - HR_i^\top \hat{b}_i \\ \dot{\hat{b}}_i &= \Pi_i R_i H^\top P_i z_i\end{aligned}$$

where  $K_{di} = K_{di}^\top > 0$ , the adaptive regressor matrix  $\Xi_i = R_i^\top$ , and  $\alpha_{1i}$  is a virtual control determined by the backstepping procedure.

The group of vessels is in a triangular formation that reduces drag forces, see e.g. Hoerner (1958), and the communication topology is given by (3.60). To counteract the environmental forces,  $b_i = [-10^7, 10^6, 0]^\top$  N, the bias estimate update gain is chosen as  $\Pi_i = \text{diag}(15, 15, 15)$  for  $i = 1, 2, 3$ . We use Design 1 where the feedback function is chosen as a constant gain  $\gamma_i = 10$ , and the initial bias estimate is  $\hat{b}_i(0) = 0$ , while the remaining control gains and initial conditions are as in Section 3.6.2.

The position plot in Figure 3.7 shows the vessels converge to and follow their desired path with the desired forward speed. Due to the bias the vessels converge slower to their paths than in the previous simulation. But as the bias estimation converges after the initial transient the ships follow the path in the desired triangular formation. Simulations without bias estimation show that the ships experienced serious problems when trying to counteract the unknown disturbances and follow the path.

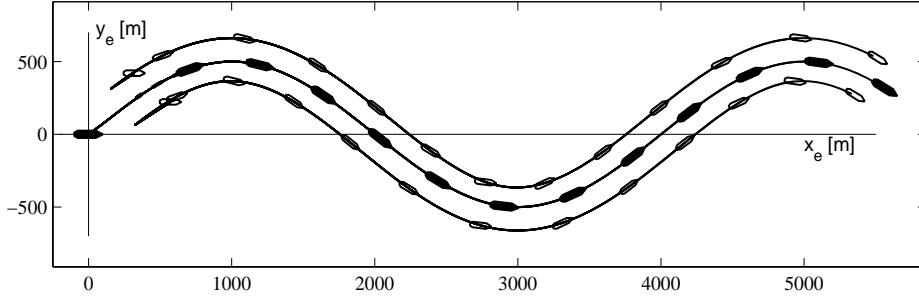


Figure 3.7: Position response during simulation.

### 3.6.4 Simulation: Time-Varying Communication Topology

This section studies a formation with changing communication topology. Link failures and/or vessels entering and leaving the formation change the incidence matrix  $D$  and the connectivity of the formation. We apply results from Arcak (2006) where convergence properties for time-varying communication topology are studied for a class of agreement protocols.

The time-varying incidence matrix  $D(t)$  is piecewise continuous because step changes occur when the communication topology changes. Consider the Design 2 synchronization scheme without path error feedback in Section 3.3.2: When the class of feedback functions  $\mathcal{F}_i$  is restricted to be of the form

$$\omega_i = \gamma_i \psi_i(\theta) \quad (3.61)$$

where  $\gamma_i$  is a positive scalar, it is shown in Arcak (2006) that, if the second smallest eigenvalue for the graph Laplacian matrix  $D(t)D(t)^\top$  satisfies

$$\lambda_2 \{D(t)D(t)^\top\} \geq \sigma > 0 \quad \forall t \geq 0 \quad (3.62)$$

for some constant time-independent  $\sigma > 0$ , the path parameters  $\tilde{\theta}_i$  reach an agreement. It is a standard result in algebraic graph theory that the graph is *connected* if and only if the Laplacian's second smallest eigenvalue is strictly positive. Thus, for the design considered in Section 3.3.2 with feedback functions as in (3.61), the vessels synchronize if the graph remains connected for all  $t \geq 0$ .

Arcak (2006) relaxes this connectivity assumption with a persistency of excitation property. The graph can then lose connectivity pointwise in time as long as it is established in an integral sense. To illustrate stability properties we consider six vessels that are initially grouped as two formations. After some time the two groups merge into one, and at the same time one vessel experiences communication problems and is only able to communicate 10% of the time. The communication

topology is given by the incidence matrix

$$D(t) = \begin{bmatrix} 1 & 0 & 0 & 0 & 0 \\ -1 & 1 & 1 & 0 & 0 \\ 0 & -1 & 0 & 0 & 0 \\ 0 & 0 & -1 & c(t) & 0 \\ 0 & 0 & 0 & -c(t) & 1 \\ 0 & 0 & 0 & 0 & -1 \end{bmatrix} \quad (3.63)$$

where

$$c(t) = \begin{cases} 0 & t < t_{change} \\ 1 & t \geq t_{change}. \end{cases} \quad (3.64)$$

Vessel 2 (shown in black in Figure 3.8) shall follow a circle-shaped path given by

$$\eta_{d2}(\theta_2) = \begin{bmatrix} x_d(\theta_2) \\ y_d(\theta_2) \\ \psi_d(\theta_2) \end{bmatrix} = \begin{bmatrix} r \cos\left(\frac{\theta_2}{r}\right) \\ r \sin\left(\frac{\theta_2}{r}\right) \\ \arctan\left(\frac{x_d^{\theta_2}(\theta_2)}{y_d^{\theta_2}(\theta_2)}\right) \end{bmatrix}$$

where  $r = 1200$  is the radius. The other paths are scaled such that equal speed assignments imply that, after synchronization has occurred, the vessels move along their respective paths parallel to each other. The initial values for the vessels are  $\eta_1 = [1350, 0, \pi/2]^\top$ ,  $\eta_2 = [1109, -459, \pi/2]^\top$ ,  $\eta_3 = [742, -742, \pi/4]^\top$ ,  $\eta_4 = [636, -363, \pi/4]^\top$ ,  $\eta_5 = [530, -530, \pi/4]^\top$ , and  $\eta_6 = [0, -600, 0]^\top$  with zero initial speeds. The initial synchronization errors, given by  $\tilde{\theta} = D^\top \theta$ , is  $\tilde{\theta} = [471, 471, 471, 0, 942]^\top$ . The synchronization function is  $\psi(x) = 0.1x$  and  $\gamma_i = 5$ .

From (3.63) and (3.64) we see that for  $t < t_{change} = 250$ s vessels 1, 3 and 4 communicate with vessel 2 while vessel 4 communicates with vessel 5. Thus, there are initially two decoupled formations as seen in Figure 3.8 where the two innermost vessels, that is vessels 5 and 6, and the other group synchronize separately. This is also seen in Figure 3.9 which shows the time-response of  $\tilde{\theta}_1, \tilde{\theta}_2, \tilde{\theta}_4$ . Before  $t_{change}$  we see that, e.g.,  $\tilde{\theta}_1$  tend to zero while  $\tilde{\theta}_4 = \theta_4 - \theta_5$  reaches a non-zero value even though the initial condition is zero. When  $t = t_{change}$  the entire formation is connected, but vessel 2 is now only able to send and receive the path parameters 10% of the time. The time-response of the path parameters in Figure 3.10 shows that the vessel synchronize and stay that way throughout the simulation.

To compare performance the same scenario has been simulated in the framework of Design 1 where path error information is used in the synchronization scheme (3.7). Figure 3.10 shows that all  $\tilde{\theta}_i$  tend to zero in the presence of link failures which cause some oscillations in the path parameters as the vessels synchronize. Both designs synchronize the vessels in the formation, but the plots

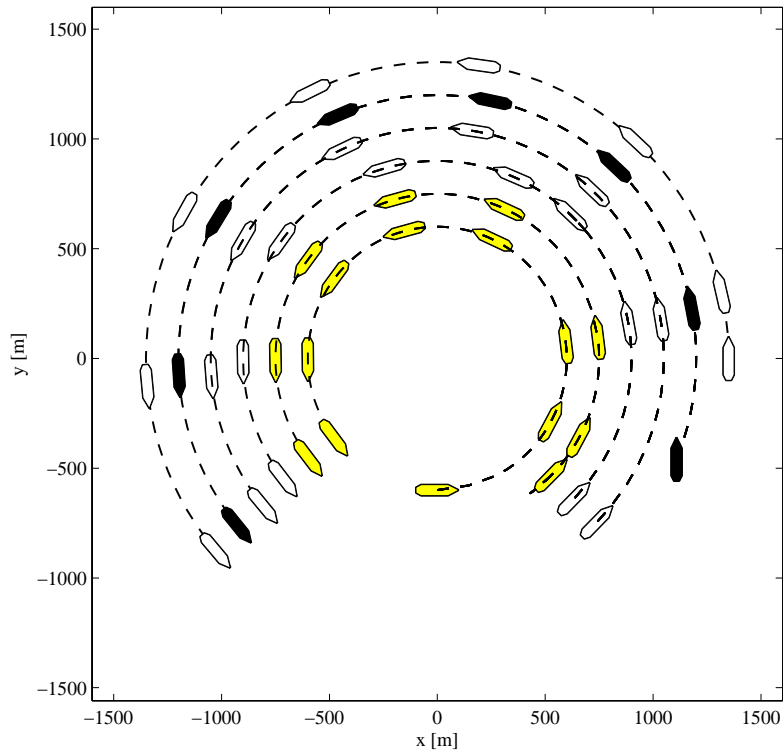


Figure 3.8: Eight position snapshots of formation. The vessels are in the beginning synchronized into two groups (second snapshot). After  $t_{change}$  all vessels are synchronized and move in parallel. Vessel 2 is shown in black.

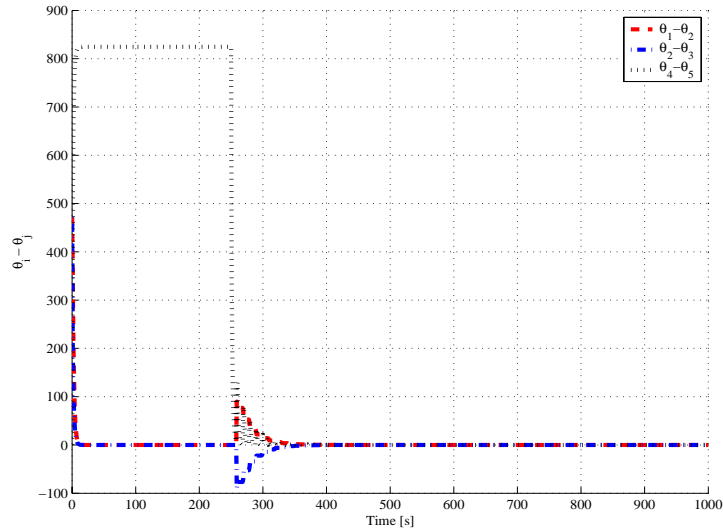


Figure 3.9: Synchronization of path parameters with time-varying communication topology.

in Figure 3.9 and 3.10 show that Design 2 is less sensitive to communication constraints as the vessels synchronize faster and with less oscillations than with Design 1.

### 3.6.5 Extensions

The passivity approach offers the flexibility to shape the feedback function in many other ways than in the previous examples. Below are some possible extensions and suggestions to illustrate how the proposed framework handles possible extensions and enhance robustness and performance properties.

**Synchronization with Output Feedback** Since interconnected passive systems remain passive, passivity is a useful tool for studying stability of systems that consists of several blocks. The full state feedback design in Section 3.3 is extended to the output feedback case by performing an output feedback design for each path-following system  $\Sigma_i$ . An example of such a design is found in Chapter 2. If the input-output properties satisfy the assumptions in Section 3.3, stability can be concluded using the same arguments as in the state feedback case. For marine surface vessels, the passive nonlinear observer in Fossen & Strand (1999) yields the desired result as demonstrated in Section 2.4.

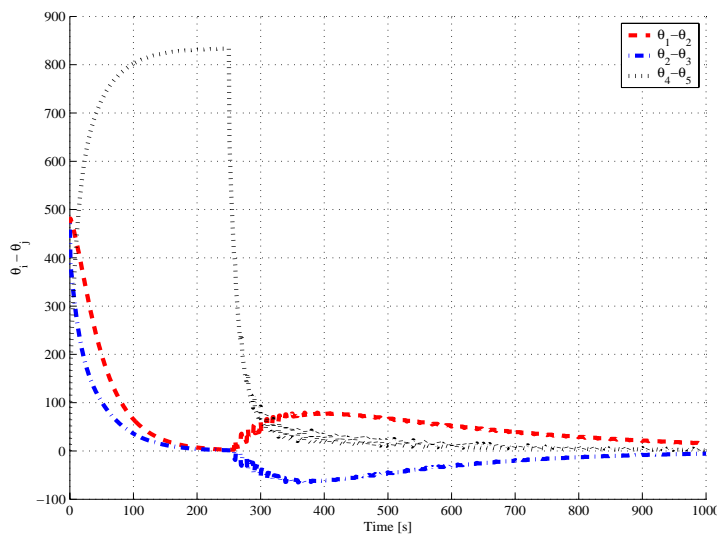


Figure 3.10: Synchronization of path parameters with time-varying communication topology.

**Robustness to Communication Disturbances** Suppose there are disturbances acting on the communication link between two or more systems. Such a disturbance can affect the synchronization of these systems and cause misalignments in a formation. One remedy to minimize such errors is to linearize the overall system and find the transfer function from the disturbance to the path error. Then, linear system tools such as frequency analysis can determine feedback functions that minimize the errors caused by these disturbances.

**Robustness to Time-Delays** The system can be robustified against time-delays by obtaining transfer functions and designing feedback functions to maximize the maximum delay  $T_{\max}$  in the feedback loop that does not destabilize the system, given by Franklin, Powell & Emami-Naeini (2002)

$$T_{\max} = \frac{PM}{\omega_{gc}}$$

for single-input single-output linear systems where  $PM$  is the phase margin, and  $\omega_{gc}$  is the gain crossover frequency. Thus, increasing the phase margin and/or decreasing the bandwidth improve delay robustness. This approach has been investigated for networked systems in Wen & Arcak (2004).

### 3.7 Concluding Remarks

This chapter has used passivity properties to design a formation control scheme where path following systems are synchronized using a bidirectional communication structure. The passivation design offers the flexibility to consider several redesigns for synchronization where robustness and performance issues can be addressed. An extension to adaptive bias estimation for integral action fits into the passivity framework.

The first design used feedback from both the path error and the synchronization error in the update law for the path parameter, while the second only employed information about the synchronization error. The path error feedback in Design 1 emphasizes convergence to the path, as a result of the gradient update law for the path parameter considered in Skjetne, Teel & Kokotović (2002*b*), while the synchronization error feedback achieves the desired formation. This scheme thus enables the designer to prioritize path convergence or synchronization by choosing the relative terms of the two feedback terms. Furthermore, the system employs its own path error information to handle situations where a trajectory tracking scheme has limitations as demonstrated in Aguiar et al. (2005). Another example, given in Fossen (2002, Chapter 10), is control saturation where an infeasible speed assignment cause instabilities. However, our analysis for Design 1 is only valid for time-invariant graph structures.

Design 2 inherits the properties of the coordination scheme in Arcak (2006) where a time-varying formation configuration is tolerated. In addition, since the incidence matrix  $D$  does not have to be pointwise connected for all times, communication dropouts are allowed, and similarly, vehicles are permitted to enter or leave the formation. We can then establish properties such that stability is guaranteed when communication only occurs at low rates. This is of interest for underwater vehicles where the available bandwidth is very low. Simulations show that synchronization occurs faster with Design 2 and is less sensitive to communication constraints since synchronization occurs faster when only path parameters are employed in the design. However, by disregarding the path error information the designer has less control on the convergence to the path.

A sampled-data approach to synchronization, where the synchronization scheme is updated in discrete time and the path following systems in continuous time, is considered. The main motivation is that communication of path variables will likely occur over a digital network and a discrete-time system is more natural to address communication issues.

# Chapter 4

## Multi-Body Interpretation of Formation Control

### 4.1 Introduction

The main topic in this chapter is formation control of marine craft in a multi-body setting: show how classic and powerful tools, from analytical mechanics of multi-body systems, can be used for coordinated control. A group of independent vehicles is controlled as a formation by introducing holonomic functions that describe a vehicle's behavior with respect to other group members. By treating these functions as mechanical constraint functions in an analytical setting, stable control laws that maintain the structure of a formation emerge. In this way, the coordinated movement of the formation is decided by forces that maintain the constraints at all times.

Mechanical constraint forces, which cause the bodies to act in accordance with the constraints, are well known from the early days of analytical mechanics, Lagrange (1811), and have been used with success, e.g. in computer graphics applications—see Baraff (1996) and Barzel & Barr (1988). This chapter shows how constraint functions impose constraint forces that maintain the formation configuration. The formation is also maintained when some, or all, of the members are exposed to external forces and disturbances. The same approach is used with several, non-conflicting, constraint functions.

The method is used both for modeling and control and gives a closed-loop structure that is part of the motivation for using this approach. Together, the constraints form control laws that both govern the movement of the entire formation and solve a motion control task given by the imposed constraint function(s). The equations of motion clearly show how individual objects are controlled by the constraint forces as they appear as a single term on the right hand side of the

equations of motion. Thus, it can be superimposed with other forces working on the system.

The variety of constraint functions applicable for formation control makes the approach flexible and leaves much freedom to the designer. Furthermore, it is easy to link the constraint stabilization to traditional motion control systems which enables us to control the overall group motion at the same time as we control the position of objects inside the formation. The main results in this chapter are based on Ihle, Jouffroy & Fossen (2006a). Additional results are reported in Ihle, Jouffroy & Fossen (2005a, 2005b, 2006b).

**Motivation** To introduce the main idea of this chapter and illustrate how the constraint function affects the motion of independent systems we consider an example:

**Example 4.1 (Formation Assembling)** Consider a formation of two point masses,  $\eta_1, \eta_2 \in \mathbb{R}^2$ , with kinetic energy  $\mathcal{T} = \frac{1}{2} \dot{\eta}^\top M \dot{\eta}$ , where  $\eta = [\eta_1^\top, \eta_2^\top]^\top$  and  $M = M^\top > 0$  is the mass matrix;  $M = \text{diag}(m_1 I_2, m_2 I_2)$  where  $I_2$  denotes the  $2 \times 2$ -identity matrix. The goal for the formation is to let the two point masses operate at a specified length away from each other. When their relative positions violate the specified length, the masses should move such that this length is rectified. This distance requirement between the points is formulated as a constraint function

$$\mathcal{C}(\eta) = (\eta_1 - \eta_2)^\top (\eta_1 - \eta_2) - r^2 = 0 \quad (4.1)$$

where  $r > 0$  is the desired distance between  $\eta_1$  and  $\eta_2$ . The procedure in the next sections gives the following equations of motion when (4.1) is satisfied

$$M \ddot{\eta} = \tau - W(\eta)^\top \lambda \quad (4.2)$$

where  $W(\eta)$  is the Jacobian of the constraint function (4.1),  $\lambda$  is the corresponding Lagrangian multiplier with stabilizing feedback from the constraints and  $\tau$  are the external forces.

If the system has initial conditions that violate the constraint (4.1) the masses move such that (4.1) is met. When  $\tau$  in (4.2) is zero at all times, the system converge to a position between the initial positions of  $\eta_1$  and  $\eta_2$  where the distance between  $\eta_1$  and  $\eta_2$  is  $r$ . If both masses are initially perturbed with a small amount of force, the motion of the masses still satisfy the constraint function eventually. As seen in Figure 4.1 the masses move such that (4.1) is satisfied – they assemble into a formation defined by the constraint function. We are now ready to apply this method to more general systems.

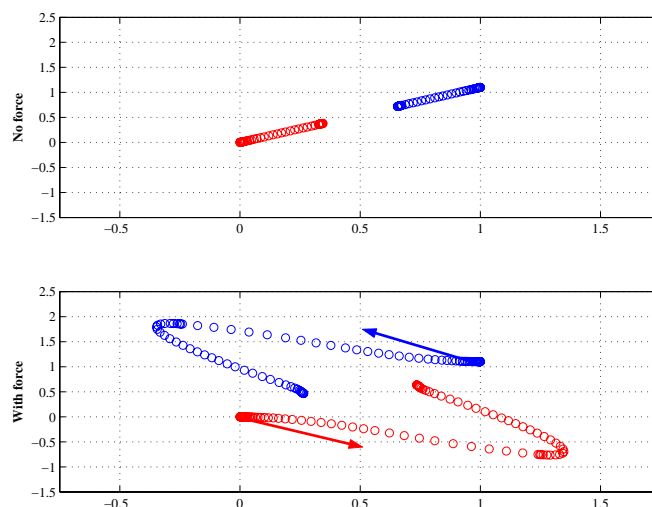


Figure 4.1: Position plot of  $\eta_1$  and  $\eta_2$  – starts in  $(0, 0)$  and  $(1, 1)$  respectively.  $r = 0.5$ . The lower plot includes the initial force disturbances shown as arrows.

## 4.2 Formation Modeling

Consider  $n$  systems, each of order  $m$ , with kinetic and potential energy,  $\mathcal{T}_i$  and  $\mathcal{U}_i$ , respectively. The Lagrangian of the total system is then

$$\mathcal{L} = \mathcal{T} - \mathcal{U} = \sum_{i=1}^n \mathcal{T}_i - \mathcal{U}_i.$$

There exist holonomic relations

$$\mathcal{C}(\eta) = 0, \quad \mathcal{C}(\eta) \in \mathbb{R}^p, \quad 1 \leq p < 2nm \quad (4.3)$$

between the coordinates which restrict the state space to a constraint manifold  $\mathcal{M}_c$  with  $2n \cdot m - p$  dimensions. We denote  $\mathcal{C}(\eta)$  the *constraint function*, where  $\eta \in \mathbb{R}^{nm}$  contains the generalized positions,  $\eta_1, \dots, \eta_n$ . From Lanczos (1986) we know that the forces that maintain the kinematic constraints add potential energy to the system according to

$$\bar{\mathcal{U}} = \mathcal{U} + \lambda^\top \mathcal{C}(\eta),$$

which gives the modified Lagrangian

$$\bar{\mathcal{L}} = \mathcal{T} - \bar{\mathcal{U}} - \lambda^\top \mathcal{C}(\eta)$$

where  $\lambda \in \mathbb{R}^p$  is the Lagrangian multiplier(s). To obtain the equations of motion, we apply the Euler-Lagrange differential equations with auxiliary conditions for

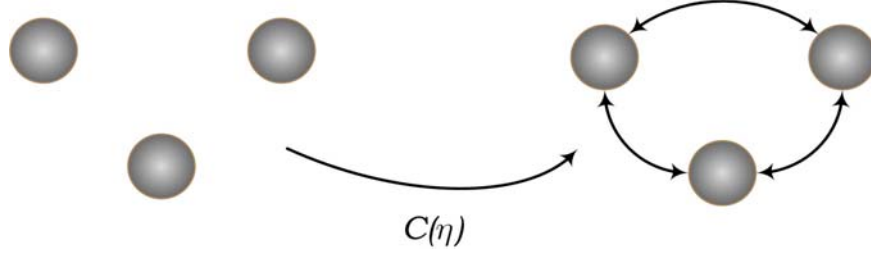


Figure 4.2: Imposed constraints transform a group of independent bodies to a formation.

$i = 1, \dots, nm,$

$$\begin{aligned} \frac{d}{dt} \frac{\partial \mathcal{L}}{\partial \dot{\eta}_i} - \frac{\partial \mathcal{L}}{\partial \eta_i} + \lambda^\top \frac{\partial \mathcal{C}(\eta)}{\partial \eta_i} + \left( \frac{\partial \lambda}{\partial \eta_i} \right)^\top \mathcal{C}(\eta) &= \tau_i \\ \mathcal{C}(\eta) &= 0 \end{aligned}$$

which implies

$$\frac{d}{dt} \frac{\partial \mathcal{L}}{\partial \dot{\eta}_i} - \frac{\partial \mathcal{L}}{\partial \eta_i} = \tau_i - \lambda^\top \frac{\partial \mathcal{C}(\eta)}{\partial \eta_i} \quad (4.4)$$

where  $\tau_i$  is the generalized external force associated with coordinate  $\eta_i$ . Figure 4.2 shows how three independent bodies are coupled with a constraint function.

Equation (4.3) constrains the systems motion to a subset,  $\mathcal{M}_c \subseteq \mathbb{R}^{2nm-p}$ , of the state space where  $\mathcal{C}(\eta) = 0$ . Since we want to keep the systems on  $\mathcal{M}_c$ , neither the velocity nor the acceleration should violate the constraints. To find the kinematic admissible velocities that correspond to (4.3), the velocities, the constraint function is differentiated with respect to time. Similarly, we differentiate twice to find the acceleration of the constraints. This gives the constrained velocities and accelerations

$$\begin{aligned} \dot{\mathcal{C}}(\eta) &= W(\eta) \dot{\eta} = 0 \\ \ddot{\mathcal{C}}(\eta) &= W(\eta) \ddot{\eta} + \dot{W}(\eta) \dot{\eta} = 0 \end{aligned} \quad (4.5)$$

where  $W(\eta) \in \mathbb{R}^{m \times p}$  is the Jacobian of the constraint function, i.e.,  $W(\eta) = \frac{\partial \mathcal{C}(\eta)}{\partial \eta}$ . An expression for the Lagrangian multiplier is found by obtaining an expression for  $\ddot{\eta}$  in (4.4) and insert it into (4.5).

**Constraint Forces** An expression for the forces that maintain the constraints, the constraint forces, is found from the right hand side of (4.4):

$$\tau_{\text{constraint}} = - \left( \frac{\partial \mathcal{C}(\eta)}{\partial \eta} \right)^\top \lambda = -W(\eta)^\top \lambda.$$

The forces are also found from the principle of virtual work. From Chapter III.5 in Lanczos (1986) we have: The gradient  $W(\eta)$  is normal to the constraint  $\mathcal{C}(\eta) = 0$ , and since the forces between independent bodies that maintain a kinematic constraint (equilibrium) are required to do no virtual work, it follows that

$$\tau_{\text{constraint}} \cdot \dot{\eta} = 0, \quad \forall \eta | W(\eta) \dot{\eta} = 0. \quad (4.6)$$

Hence, the constraint force must be a linear combination of the columns in  $W(\eta)$ :

$$\tau_{\text{constraint}} = - \left( \frac{\partial \mathcal{C}(\eta)}{\partial \eta} \right)^\top \lambda. \quad (4.7)$$

The Lagrangian multiplier is then found by combining the equations of motion with the constrained accelerations. The Lagrangian  $\lambda$  term thus provides the force of reaction which maintains the kinematic constraint.

For marine craft<sup>1</sup>, we consider the 3 DOF horizontal motion for a single vessel in the body-fixed frame (see Appendix B)

$$\begin{aligned} \dot{\eta} &= R(\psi) \nu \\ M_{RB} \dot{\nu} + C_{RB}(\nu) \nu &= \underbrace{-M_A \dot{\nu} - C_A(\nu) \nu - D(\nu) \nu - g(\eta)}_{\tau_H} + \tau_{\text{constraint}} + \tau_{\text{env}} \end{aligned}$$

where  $\eta = [x, y, \psi]^\top$  is the Earth-fixed position vector,  $(x, y)$  is the position on the ocean surface and  $\psi$  is the heading (yaw) angle, and  $\nu = [u, v, r]^\top$  is the body-fixed velocity vector. The model matrices  $M$ ,  $C$ , and  $D$  denote system inertia, Coriolis plus centrifugal and damping, respectively. Next, consider a formation of  $n$  vessels with position given by  $\eta_i$ , inertia matrix  $M_i = M_{RB,i} + M_{A,i}$ , and so on for  $i = 1, \dots, n$ . We collect the vectors into new vectors, and the matrices into new, block-diagonal, matrices by defining  $\eta = [\eta_1^\top, \dots, \eta_n^\top]^\top$ ,  $M = \text{diag}\{M_1, \dots, M_n\}$ , and similarly for the other vectors and matrices. Assume there are constraint functions between the ships' position, corresponding to the case in (4.4). Adding the potential energy from the constraints gives

$$\dot{\eta} = R(\psi) \nu \quad (4.8a)$$

$$M \dot{\nu} + C(\nu) \nu + D(\nu) \nu + g(\eta) = \tau_{\text{env}} + \tau_{\text{constraint}} \quad (4.8b)$$

$$\mathcal{C}(\eta) = 0 \quad (4.8c)$$

where

$$\tau_{\text{constraint}} = - \left( \frac{\partial \mathcal{C}(\eta)}{\partial \eta} \right)^\top \lambda = -W(\eta)^\top \lambda$$

---

<sup>1</sup>Note that this approach is also valid for mechanical systems such as  $M(q) \ddot{q} + C(q, \dot{q}) \dot{q} = \tau$  (robot manipulator).

is the expression for the constraint forces which maintain the constraint function (4.8c) and  $\tau_{\text{env}} \in \mathbb{R}^{3n}$ .

A vessel  $i$  is neighbor with a vessel  $j$  if they share each other's information. In our setting, vessels are neighbors if they appear in the same constraint function. Given a set of constraint functions  $\mathcal{C}(\eta) = [\mathcal{C}_1(\eta), \dots, \mathcal{C}_k(\eta), \dots]^\top$  with corresponding Lagrangian multipliers  $\lambda = [\lambda_1, \dots, \lambda_k, \dots]^\top$ , the resulting constraint forces for an individual ship  $i$  are

$$\tau_{\text{constraint},i} = \sum_{k \in \mathcal{A}_c} - \left( \frac{\partial \mathcal{C}_k(\eta)}{\partial \eta_i} \right)^\top \lambda_k = \sum_{k \in \mathcal{A}_c} -W_{ki}^\top \lambda_k \quad (4.9)$$

where  $\mathcal{A}_c$  is the set of indices where constraint functions with  $\eta_i$  appear and  $W_{ki} = 0$  for  $k \notin \mathcal{A}_c$ .

The equations of motion are transformed to the Earth-fixed frame by the kinematic transformation in Section 1.4 which results in

$$M_\eta(\eta) \ddot{\eta} + n(\nu, \eta, \dot{\eta}) = \tau_\eta - R(\psi) W(\eta)^\top \lambda. \quad (4.10)$$

Combining (4.5) and (4.10) gives a differential algebraic equation (DAE). Solving for  $\ddot{\eta}$  and substituting gives (the arguments have been omitted to ease the presentation)

$$WM_\eta^{-1}RW^\top \lambda = WM_\eta^{-1}(\tau_\eta - n) + \dot{W}\dot{\eta}. \quad (4.11)$$

Then, Equation (4.10), with the above expression for  $\lambda$ , gives the equations of motion for the systems subject to (4.3). To make sure that we can solve (4.11) to find  $\lambda$  we use the following property and assumption on the model and the constraint function; respectively

**Property 4.1** *The mass matrix  $M$  is positive definite, i.e.,  $M = M^\top > 0$ . Hence,  $M_\eta(\eta) = M_\eta^\top(\eta) > 0 \quad \forall \eta$  since  $R(\psi)$  is orthogonal.*

**Assumption 4.1** *The constraint function (4.3) has a unique equilibrium. The Jacobian  $W(\eta)$  has full row-rank and is limited by a linear growth rate condition, e.g.,  $k_1|\eta| \leq |W| \leq k_2|\eta|$ .*

Property 4.1 and Assumption 4.1 guarantee that  $WM_\eta^{-1}RW$  exists since  $M_\eta$  is positive definite, hence  $M_\eta^{-1}$  exists and  $WM_\eta^{-1}RW^\top$  is nonsingular. Thus, the expression is solved for  $\lambda$  and used in (4.10). Note that redundant or conflicting constraints arise when one, or more, row (column) in  $\mathcal{C}$  is a linear combination of other rows (columns), or when the functions are contradicting. An example would be the same constraint function appearing twice in  $\mathcal{C}(\eta)$ .

The above conditions yield a Jacobian with full row rank and we solve (4.11) to obtain the Lagrangian multiplier. The results can be extended to a time-varying formation topology as long as  $W$  has full row rank for all  $t \geq 0$ .

### 4.3 Stabilization of Constraint Functions

If the system starts on the constraint manifold  $\mathcal{M}_c$ , that is, the initial conditions  $(\eta(0), \dot{\eta}(0)) = (\eta_0, \dot{\eta}_0) \in \mathcal{M}_c$  such that

$$\mathcal{C}(\eta_0) = 0 \text{ and } \dot{\mathcal{C}}(\eta_0) = 0$$

and the force  $\tau$  does not perturb the system, then the solutions  $(\eta(t), \dot{\eta}(t)) \in \mathcal{M}_c$  for all times. However, if the initial conditions are not in  $\mathcal{M}_c$ , or the system is perturbed s.t.  $(\eta, \dot{\eta}) \notin \mathcal{M}_c$ , feedback must be used to stabilize the constraint function.

We want to investigate stability of the constraint function, that is, we look at stability of

$$\mathcal{M}_c = \{(\eta, \dot{\eta}) : \mathcal{C}(\eta) = 0, W(\eta)\dot{\eta} = 0\}.$$

Consider the case when  $\tau \neq 0$  in (4.10), and suppose that  $(\eta_0, \dot{\eta}_0) \notin \mathcal{M}_c$ . From Section 4.2 it follows that

$$\ddot{\mathcal{C}}(\eta) = 0 \tag{4.12}$$

which is unstable – when  $\mathcal{C}(\eta)$  is a scalar function its transfer function contains two poles at the origin. Hence, if  $\mathcal{C}(\eta) = 0$  is not fulfilled initially, the solutions might blow up in finite time. Even if  $\mathcal{C}(\eta_0) = 0$ , this may happen if there is measurement noise on  $\eta$ . This instability is, in fact, an inherent property of higher-index DAEs, pointed out in e.g. Tarraf & Asada (2002), and is one of the reasons numerical methods for differential-algebraic equations has received special attention, see Petzold (1982) and references therein, and particular in modelling of mechanical systems as in Ten Dam (1992).

This is solved by using feedback from the constraints in the expression for the Lagrangian multiplier (4.11). Moreover

$$WM_\eta^{-1}RW^\top\lambda = WM_\eta^{-1}\{\tau_\eta - n\} + \dot{W}\dot{\eta} + K_d\dot{\mathcal{C}}(\eta) + K_p\mathcal{C}(\eta) \tag{4.13}$$

where  $K_p, K_d \in \mathbb{R}^{p \times p}$  are positive definite. The constraint force for vessel  $i$  is given by

$$\begin{aligned} \tau_{\text{constraint},i} = & \sum_{k \in \mathcal{A}_c} \sum_{j \in \mathcal{C}_k} -W_{ki}^\top (W_k M_{\eta,ij}^{-1} R_{ij} W_k^\top)^{-1} \times \\ & \left( W_{ki} M_{\eta,ij} (\tau_{\eta,ij} - n_{ij}) + k_d \dot{\mathcal{C}}_k + k_p \mathcal{C}_k \right) \end{aligned}$$

where the subscript  $ij$  represents an block-diagonal matrix  $A_{ij}$  with blocks  $A_i$  and  $A_j$ , or an augmented column vector  $a_{ij} := [a_i^\top, a_j^\top]^\top$  and is essentially information

about  $i$  and its neighbor  $j$ . When we add the stabilizing terms, we consider a stabilized version of (4.12)

$$\ddot{\mathcal{C}} = -K_d \dot{\mathcal{C}}(\eta) - K_p \mathcal{C}(\eta) \quad (4.14)$$

which ensures that  $\mathcal{C}(\eta)$  and  $\dot{\mathcal{C}}(\eta)$  converge to zero:

We rewrite (4.14) using

$$\phi_1(t) = \mathcal{C}(\eta(t)), \quad \phi_2(t) = \dot{\mathcal{C}}(\eta(t)), \quad \phi = \begin{bmatrix} \phi_1 \\ \phi_2 \end{bmatrix}$$

such that

$$\begin{bmatrix} \dot{\phi}_1 \\ \dot{\phi}_2 \end{bmatrix} = \begin{bmatrix} 0 & I \\ -K_p & -K_d \end{bmatrix} \begin{bmatrix} \phi_1 \\ \phi_2 \end{bmatrix} \quad \text{or} \quad \dot{\phi} = A\phi, \quad A \in \mathbb{R}^{2p \times 2p} \quad (4.15)$$

By appropriate choice of  $K_p$  and  $K_d$ ,  $A$  is Hurwitz. Then, by choosing a design matrix  $Q = Q^\top > 0$ , we find a  $P = P^\top > 0$  such that

$$PA + A^\top P = -Q.$$

Hence

$$V(\phi) = \phi^\top P \phi > 0, \quad \forall \phi \neq 0 \quad (4.16)$$

$$\dot{V}(\phi) = -\phi^\top Q \phi < 0, \quad \forall \phi \neq 0 \quad (4.17)$$

and the set  $\mathcal{M}_c$  is by Theorem A.1 a GES set of equilibrium points of the system

$$\begin{aligned} M_\eta(\eta) \ddot{\eta} + n(\nu, \eta, \dot{\eta}) &= -R(\psi) W(\eta)^\top \lambda \\ \mathcal{C}(\eta) &= 0 \end{aligned} \quad (4.18)$$

under Property 4.1 and Assumption 4.1.

By applying feedback from the constraints we have converted (4.12) to (4.14) and the formation is stabilized when the initial values do not fulfill the constraint function.

**Remark 4.1** Consider the case in the motivating example in Section 4.1 and set  $K_p = \beta^2$  and  $K_d = 2\alpha$ , such that  $\ddot{\mathcal{C}} + 2\alpha\dot{\mathcal{C}} + \beta^2\mathcal{C} = 0$ ,  $\alpha, \beta > 0$ . In the numerical scientific community this is referred to as the Baumgarte (1972) stabilization technique—used for stabilization of numerical simulations of multi-body and constrained systems and DAEs.

There exists a wide number of numerical methods that stabilizes DAEs, see e.g. Petzold, Ren & Maly (1997) and references therein. Applying feedback, such as in (4.14), is intuitive and familiar from a control point of view, which serves as a motivation for this approach. The same method for stabilization has also been applied in Lee, Bhatt & Krovi (2005).

### 4.3.1 Constraint Functions for Control Purposes

So far the topic of this chapter has been systems with constraints in general without addressing how the constraint functions arise. In the control literature, a major research area has been constrained robot manipulators with physical contact between the end effector and a constraint surface. This occurs in many tasks, including scribing, writing, grinding, and others as described in Krishnan & McClamroch (1994), McClamroch & Wang (1988) and references therein. These constraints are inherently in the system as they are all based on how the model or the environment constrains the dynamics. Some of the difficulties related to simulations of constrained systems and ways to solve them are presented in Yun & Sarkar (1998).

However, if a control objective is defined as a constraint function and if these *constraints are imposed* on the system, feedback is used for stabilization of the constraint functions as shown in the previous section. In this way, the control law forces the system to behave according to the constraint function. As an example, consider stabilization of a point mass to a desired location:

**Example 4.2 (Point stabilization)** *Consider a single point mass subject to the constraint*

$$\mathcal{C}(\eta) = \eta = 0, \eta \in \mathbb{R}$$

*but not exposed to any external forces, i.e.  $\tau = 0$ ,*

$$m\ddot{\eta} = -W(\eta)\lambda$$

*where  $W(\eta) = 1$ ,  $m = 1$ , and  $\lambda$  is given as in (4.13):*

$$\lambda = 2\alpha\dot{\eta} + \beta^2\eta, \quad \alpha, \beta \in \mathbb{R}.$$

*The constraint manifold is now the origin, i.e.  $\mathcal{M}_c = (0, 0)$ , the dynamics is*

$$\ddot{\eta} = -2\alpha\dot{\eta} - \beta^2\eta$$

*and the origin is GES for  $\alpha, \beta > 0$ . Given an initial condition  $(\eta(0), \dot{\eta}(0)) \notin \mathcal{M}_c$ , the trajectory  $\eta(t)$  converges exponentially fast to the origin. In this case, the constraint function corresponds to a proportional-derivative (PD) controller. This approach for control design, and its combination with formation constraints, is explained further below.*

### 4.3.2 Kinematic Singularities - Rank Deficient Jacobian

To avoid a Jacobian with less than full rank, which again leads to singularities in (4.13), Assumption 4.1 yields no redundant constraints to be imposed on the

system. Thus, no singular positions are encountered. However, for situations with redundant constraints, singularities have to be avoided. The problem of kinematic singularities has been intensively studied in robotics, and one strategy is the damped least-squares (DLS) technique reported in Maciejewski & Klein (1988) and Chiaverini, Siciliano & Egeland (1994). The method corresponds to instead of solving (4.13) as

$$\lambda = A_1^{-1}b,$$

where  $A_1(\eta) = W(\eta)M_\eta^{-1}(\eta)R(\psi)W(\eta)^\top$  and  $b$  is the right-hand side of (4.13), the equation is rewritten as

$$A_2(\eta)W(\eta)^\top\lambda = b$$

which is solved by premultiplying with  $A_2(\eta)$  and introducing an additional term

$$\left(A_2(\eta)^\top A_2(\eta) + \gamma I\right)W(\eta)^\top\lambda = A_2(\eta)^\top b \quad (4.19)$$

where  $\gamma \geq 0$  is the damping factor. When  $\gamma = 0$  the solution of (4.19) corresponds to the solution of (4.13). The damping factor must be selected carefully: small values give accurate solutions but decreased robustness to singularities. The solution of (4.19) is

$$W(\eta)^\top\lambda = \left(A_2(\eta)^\top A_2(\eta) + \gamma I\right)^{-1}A_2(\eta)^\top b.$$

The DLS technique permits a wider combination of constraint functions, which could cause singularities in the solution otherwise, and allows a set of redundant constraint functions to be used. Consequently, the DLS method relaxes the assumption on the Jacobian.

### 4.3.3 Different Types of Constraints

To explain how formation control is achieved, this section considers examples of imposed constraints that coordinate group members and control certain aspects of group behavior. Different formation configurations are useful during changing operations, such as collision avoidance, sea-bed scanning, etc. To keep the notation compact,  $\eta_i$  and  $\dot{\eta}_i$  are used for position and velocity of vehicle  $i$ , and collected into vector notation as  $\eta = [\eta_1^\top, \dots, \eta_n^\top]^\top$  and  $\dot{\eta} = [\dot{\eta}_1^\top, \dots, \dot{\eta}_n^\top]^\top$ . An illustration of different types of constraint functions is shown in Figure 4.3.

**Distance Between Members** To keep a fixed distance between members of the formation, functions arising from mathematical norms are applied. To maintain a relative distance  $r_{ij}$  between group members  $i$  and  $j$ , let the function be defined by

$$\mathcal{C}_{rd}(\eta) = (\eta_i - \eta_j)^\top (\eta_i - \eta_j) - r_{ij}^2 = 0, \quad r_{ij} \in \mathbb{R}. \quad (4.20)$$

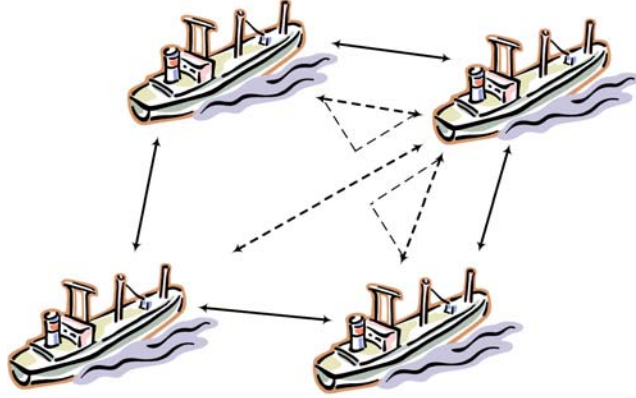


Figure 4.3: Different constraint functions acting between vessels determine collective motion. Two types of constraints functions are illustrated:  $\mathcal{C}_{rd}$  (-) and  $\mathcal{C}_{fd}$  (-).

This was used in Example 4.1. If the control objective implies a stricter formation, with fixed offsets in the direction of each coordinate axis, consider the alternative distance function

$$\mathcal{C}_{fd}(\eta) = \eta_i - \eta_j - o_{ij} = 0, \quad o_{ij} \in \mathbb{R}^m \quad (4.21)$$

where  $o_{ij}$  describes the offset between members  $i$  and  $j$ .

The formation has a time-varying configuration when the relative distance or the offset is dependent on time  $t$ . Furthermore, a combination of distance constraint functions defines the entire formation structure. For example, two vehicles with one  $\mathcal{C}_{rd}$ -function is a line-formation, three vehicles with two  $\mathcal{C}_{rd}$ -functions form a triangle, and so on. By using  $\mathcal{C}_{fd}$ -functions, constraints can also be imposed on the orientation, and the desired offset between two members can be limited to a certain coordinate axis. The last approach is applicable for a formation of AUVs moving in the horizontal plane. The resulting constraint forces between two point masses are shown in Figure 4.4.

**Position Constraints** As shown in Example 4.2, constraint functions must not necessarily be imposed between independent bodies. A vehicle  $i$  is constrained to a single stationary point  $\eta_d \in \mathbb{R}^m$  with the following function

$$\mathcal{C}_p(\eta_i) = \eta_i - \eta_d = 0. \quad (4.22)$$

This approach is extended by considering a time-dependent point

$$\mathcal{C}_{tt}(\eta_i, t) = \eta_i - \eta_d(t) = 0 \quad (4.23)$$

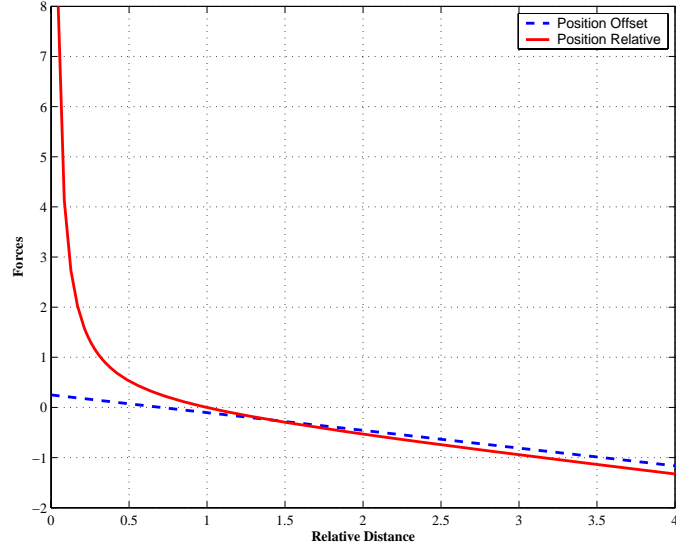


Figure 4.4: The resulting constraint forces between two point masses as a function of their relative distance. Position relative constraint function (—) as in (4.20) and position offset constraint functions (---) as in (4.21).

where  $\eta_d(t)$  now represents a path parameterized by time and at least three times differentiable with respect to time. This has now evolved into a trajectory-tracking problem for vehicle  $i$ . The addition of the time variable in the constraint function leads to a different expression for constraint velocity and acceleration, but the procedure to find the Lagrange multiplier is straightforward. Note that the expression for the constraint forces remain the same in this case, i.e.,  $\tau_{\text{constraint}} = -W^T \lambda$ .

**Combined Constraints** The position constraint is easy to combine with other constraints: Let  $W_{rd}^T \lambda_{rd}$  and  $W_p^T \lambda_p$  be forces that arise from  $\mathcal{C}_{rd}$  and  $\mathcal{C}_p$ . Then, the combination

$$W^T \lambda = \begin{bmatrix} W_{rd}^T & W_p^T \end{bmatrix} \begin{bmatrix} \lambda_{rd} \\ \lambda_p \end{bmatrix}$$

gives constraint forces that regulate the formation in accordance to both (4.20) and (4.22). The intersection of these functions forms the constraint manifold and defines the overall control objective for the group of vessels—see Figure 4.5.

Constraint functions with priority are used in Stilwell, Bishop & Sylvester (2005) where techniques for overactuated robot manipulators have been applied for platoon control. The approach has been extended by Antonelli & Chiaverini (2004) using the inverse kinematic model. The suggested approach in this chapter

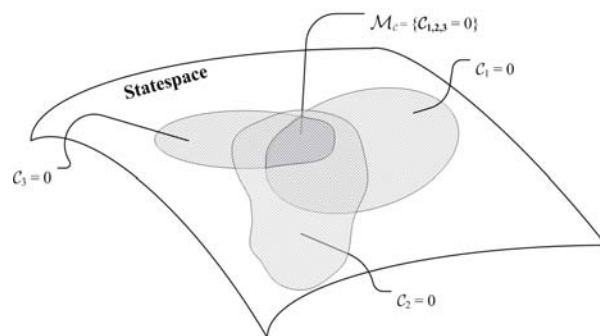


Figure 4.5: Statespace and the constraint manifold: intersection of three constraints  $\mathcal{C}_1$ ,  $\mathcal{C}_2$ , and  $\mathcal{C}_3$ .

can be implemented in the same manner.

**Formation Average Position** A constraint function that expresses the mean value of all vehicles compared to a desired position for the formation's location is given by Stilwell & Bishop (2002), Antonelli & Chiaverini (2004):

$$\mathcal{C}_a(\eta, t) = \left\{ \frac{1}{n} \sum_{i=1}^n \eta_i \right\} - \eta_d(t) = \bar{\eta} - \eta_d(t) = 0. \quad (4.24)$$

where  $\bar{\eta}$  is the average position. The time-dependent variable  $\eta_d$  is simply a reference trajectory for the desired location of the formation, and resembles a virtual leader that has been used earlier in the literature to steer the formation in the desired direction, e.g. in Leonard & Fiorelli (2001). This function is of higher interest when it is combined with the next:

**Formation Variance** As an alternative to control a formation as a rigid structure, the variance of the formation together with the average position can regulate the spreading of the vehicles around that position. The constraint function is given by

$$\mathcal{C}_v(\eta) = \frac{1}{n} \sum_{i=1}^n (\eta_i - \bar{\eta})^2 - \sigma_d^2 = 0 \quad (4.25)$$

where  $\sigma_d^2$  is the desired variance around the average position  $\bar{\eta}$ . However, controlling the formation variance does not guarantee that all vehicles stay apart nor within a bounded area of the average position, and may lead to unsafe motion. The average position  $\bar{\eta}$  and variance  $\sigma_d^2$  are global variables that must be calculated by a supervisor and communicated to all formation members. Hence, these constraint functions lead to a centralized implementation.



Figure 4.6: Examples of redundant auxiliary constraints. Consider the position offset constraints (4.21) on the left: when two constraints are given, the third is simply a linear combination of those. For the position relative constraints (4.20) on the right two of the constraints are either contradictory or redundant. In both cases, the Jacobian  $W$  has less than full row rank.

**Inequalities** Inequality constraint functions on the form  $c(q) \geq 0$  are treated within the presented framework with e.g. the logarithmic barrier function–Nocedal & Wright (1999)

$$\mathcal{C}_{ie}(q) = - \sum_i \log c_i(q) = 0 \quad (4.26)$$

where  $c_i$  is the  $i$ th function in  $c(q)$ . This type of function is used when the control objective is to keep the the formation assembled with a bound (upper and/or lower) on the inter-vessel distance instead of a fixed distance. A marine example is to keep a ship close, but not too close, to a rig.

**Formation Topology** The full row-rank assumption for the Jacobian  $W$  limits the number of constraint functions that are imposed on the formation. In addition, each imposed function reduces the degrees of freedom of the formation; the total number of constraints must thus not exceed the total degree of freedom.

The full-row rank condition of  $W$  implies that the given constraint functions can neither be contradictory nor redundant. Suppose the formation has  $n$  members, each with an  $m$  DOF system. For constraints on the form (4.21), this means that there must be  $p < n$  such constraints for  $W$  to have full row rank since a new constraint would be a linear combination of the previous. An example of a feasible formation topology is a line. A formation can be subject to  $p \leq m(n - 1)$  position relative constraints as long as they neither contradict the existing constraints nor is a linear combination of other constraints. Illustrations of constraint functions that lead to singularities are shown in Figure 4.6.

## 4.4 Extensions to Other Control Schemes

Coordinated control laws for several independent models in an unknown environment pose challenges to the designer. When the designer has some a priori knowledge of the environmental effects, they can be incorporated into the control law design.

Assume that the constraints are of the form (4.20) or (4.21) and satisfy the conditions in Section 4.3.3. Equation (4.12) is basically a double integrator which can be put into an upper-triangular form. Indeed, with  $\ddot{C} = u$ ,  $\phi_1(t) := C(\eta(t))$  and  $\phi_2(t) := \dot{C}(\eta(t))$  we obtain

$$\dot{\phi}_1 = \phi_2 \quad (4.27a)$$

$$\dot{\phi}_2 = u. \quad (4.27b)$$

The constraint stabilization problem is then to design a controller  $u$  that renders  $(\phi_1, \phi_2) = (0, 0)$  stable.

The structure of (4.27) allows us to take advantage of existing control designs. For example, with a quadratic cost function, the controller can be designed using LQR-techniques. In the presence of unknown model parameters, an adaptive control scheme can be used. The system (4.27) has an upper triangular structure and falls into the class of feedforward systems. This class of systems has been thoroughly investigated and is frequently used as a basis for systematic and constructive control design as it encompasses a large group of systems. If disturbances or unknown model parameters appear as nonlinearities we consider designs for uncertain systems and adaptive control, for example, in Krstić et al. (1995).

Consider the formation of  $r$  vessels perturbed by unknown bounded disturbances  $\delta(t)$

$$M_\eta(\eta) \ddot{\eta} + n(\nu, \eta, \dot{\eta}) = R(\psi) \tau_{\text{constraint}} + W_d^* \delta(t) \quad (4.28)$$

where  $W_d^*$  is a smooth, possibly nonlinear, function. The method in Section 4.3 transforms (4.28) to the form of (4.27)

$$\dot{\phi}_1 = \phi_2 \quad (4.29a)$$

$$\dot{\phi}_2 = u + W_d(\phi_1, \phi_2) \delta(t) \quad (4.29b)$$

where  $W_d = WM_\eta^{-1}W_d^*$ . The goal is to render the closed-loop system Input-to-State Stable from the disturbances with respect to the origin of the closed-loop system (4.29). This is achieved by applying a design procedure from Krstić et al. (1995):

**Control Design:** We define the error variable as

$$z(t) = \phi_2 - \alpha \quad (4.30)$$

where  $\alpha$  is a stabilizing function to be specified later. The time derivative of  $\phi_1$  is

$$\dot{\phi}_1 = \phi_2 = z + \alpha$$

We choose Hurwitz design matrices  $A_i$ ,  $i = 1, 2$ , such that  $P_i = P_i^\top > 0$  is the solution of  $P_i A_i + A_i^\top P_i = -Q_i$  where  $Q_i = Q_i^\top > 0$ . Let the first control Lyapunov function be

$$V_1(\phi_1, t) = \phi_1^\top P_1 \phi_1$$

The time derivative  $\dot{V}_1$  becomes, with the choice  $\alpha = A_1 \phi_1$ ,

$$\dot{V}_1 = -\phi_1^\top Q_1 \phi_1 + 2\phi_1^\top P_1 z.$$

Differentiating (4.30) with respect to time gives

$$\dot{z} = \dot{\phi}_2 - \dot{\alpha} = u + W_d(\phi_1, \phi_2) \delta(t) - A_1 \phi_2.$$

We define the second control Lyapunov function

$$V_2(\phi, t) = V_1 + z^\top P_2 z$$

with the following time derivative

$$\dot{V}_2 = -\phi_1^\top Q_1 \phi_1 + 2z^\top P_2 (u + P_2^{-1} P_1 \phi_1 + W_d \delta - A_1 \phi_2)$$

and the control law is chosen as

$$u(\phi, t) = A_2 z - P_2^{-1} P_1 \phi_1 + A_1 \phi_2 + \alpha_0 \quad (4.31)$$

where  $\alpha_0$  is a damping term to be determined. Young's inequality yields

$$2z^\top P_2 W_d \delta \leq 2\kappa z^\top P_2 W_d W_d^\top P_2 z + \frac{1}{2\kappa} \delta^\top \delta, \quad \kappa > 0$$

and we obtain

$$\dot{V}_2 \leq -\phi_1^\top Q_1 \phi_1 - z^\top Q_2 z + \frac{1}{2\kappa} \delta^\top \delta + 2z^\top P_2 (\alpha_0 + \kappa W_d W_d^\top P_2 z).$$

The choice  $\alpha_0 = -\kappa W_d W_d^\top P_2 z$  yields

$$\begin{aligned} \dot{V}_2 &\leq -\phi_1^\top Q_1 \phi_1 - z^\top Q_2 z + \frac{1}{2\kappa} \delta^\top \delta \\ &\leq -q_{\min} |y|^2 + \frac{1}{2\kappa} |\delta|^2 < 0, \quad \forall |y| > \sqrt{\frac{1}{2\kappa q_{\min}}} |\delta| \end{aligned}$$

where  $q_{\min} = \min(\lambda_{\min}(Q_1), \lambda_{\min}(Q_2))$  and  $y := [\phi_1^\top, z^\top]^\top$ . Hence, the control law (4.31) renders the closed-loop system ISS from  $\delta(t)$  to  $y$ .

In  $\phi$ -coordinates the control law (4.31) is written as

$$u = -K_p\phi_1 - K_d\phi_2 - \kappa W_d W_d^\top P_2 (\phi_2 - A_1\phi_1)$$

where  $K_d = -(A_1 + A_2)$  and  $K_p = A_2 A_1 - P_2^{-1} P_1$  so the robust backstepping design encompasses the Baumgarte stabilization technique—see Remark 4.1.

Hence, by exploiting existing design methodologies the proposed formation scheme loses the exact convergence but is rendered robust against unknown disturbances. The control scheme can also be extended to include parameter adaptation and find constant unknown biases:

**Example 4.3** *Let  $\varphi \in \mathbb{R}^x$  be a vector of constant unknown parameters*

$$M_\eta(\eta)\ddot{\eta} + n(\nu, \eta, \dot{\eta}) = R(\psi)\tau_{\text{constraint}} + W_a^* \varphi$$

where  $W_a^*$  is a smooth function. Recall that the Lagrangian multiplier  $\lambda$  is still as in (4.13). The transformed model becomes

$$\dot{\phi}_1 = \phi_2 \tag{4.32}$$

$$\dot{\phi}_2 = u + W_a(\phi_1, \phi_2)\varphi \tag{4.33}$$

where  $W_a$  is smooth. By adopting an adaptive control design procedure from Krstić et al. (1995) or Ioannou & Sun (1996) we find a control law that renders the equilibrium points  $\mathcal{C} = \dot{\mathcal{C}} = 0$  and  $\tilde{\varphi} = \varphi - \hat{\varphi}$  uniformly globally convergent and guarantees that  $\mathcal{C}, \dot{\mathcal{C}}, \tilde{\varphi} \rightarrow 0$  in the limit as  $t \rightarrow \infty$ .

## 4.5 Discussion

The motivation for using constraint functions to achieve formation control lies in the possibility to relate them with constraints in analytical mechanics which have been well-known for a long time. Hence, we want to provide an intuitive understanding of formation control. Furthermore, and contrary to Lee et al. (2005) where the analytical mechanics paradigm is also used as a starting point, the same methods that are necessary to numerically stabilize the constraints in simulations are used to stabilize a constraint manifold.

The design above, where constraint functions formulated as control objectives are put into vector form, gives control laws that regulate the entire formation. Combined with control laws for single vehicles in the formation, the design ends up with a closed-loop system that behaves according to the given constraint functions.

Moreover, stability and convergence to the constraint manifold is guaranteed by the feedback from the constraint. Hence, a control scheme which incorporates several different formation behaviors with other control laws and guarantees stability has been achieved.

#### 4.5.1 Communication Requirements

In the same setting as Section 4.3.3, consider a formation with a ring-structure where the set  $\mathcal{A}_c = \{i, i + 1\}$  for  $i = 2, \dots, n - 1$ , that is, the position of vehicle  $i$  appears in constraint functions, as in (4.20),

$$\mathcal{C} = \begin{bmatrix} \vdots \\ (\eta_{i-1} - \eta_i)^\top (\eta_{i-1} - \eta_i) - r^2 \\ (\eta_i - \eta_{i+1})^\top (\eta_i - \eta_{i+1}) - r^2 \\ \vdots \\ (\eta_n - \eta_1)^\top (\eta_n - \eta_1) - r^2 \end{bmatrix}.$$

The Lagrangian multiplier for constraint  $i$ ,  $\lambda_i$ , depends only on vehicle  $i$  and  $i + 1$ , similarly:  $\lambda_{i-1}$  depends on vehicle  $i - 1$  and  $i$ . According to (4.9), it follows that the control law for vehicle  $i$  only depends on its own and its neighbors information.

Hence, there is no explicit leader or any exogenous system in this design and the controllers are implemented in a decentralized framework. For marine surface vessels the physical link for communication channels is radio frequency.

#### 4.5.2 Extensions

##### Underactuated Ships

A common thruster configuration for marine surface vessels is rudder and propellers. In this configuration the control vector's dimension is less than the degrees of freedom. The vessel is thus underactuated and the lateral position cannot be directly controlled. For an underactuated vessel the method in Section 4.3 cannot be immediately applied to control the vessel's center of gravity. However, by controlling a point along the vessel's longitudinal axis, in the bow or ahead of the ship, the lateral position is controlled indirectly by reducing the output space. The authors of Fossen, Godhavn, Berge & Lindegaard (1998) stabilize an underactuated ship by locating a body-fixed coordinate system in the bow or ahead of the ship. A two wheeled mobile robot is controlled in the same manner in Lawton, Beard & Young (2003). Rathinam & Murray (1998) consider Lagrangian systems underactuated by one control, and characterize those systems that are configuration flat,

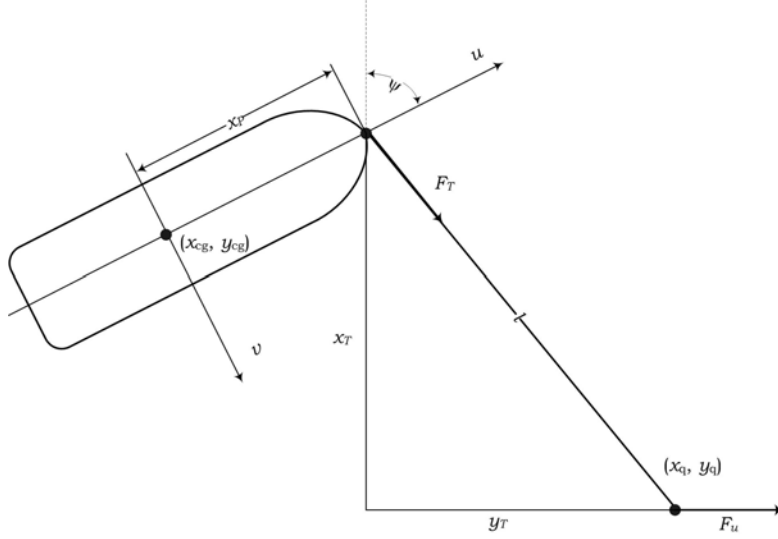


Figure 4.7: Point mass and underactuated vessel.

i.e., equivalent to a fully actuated system, while Bullo, Leonard & Lewis (2000) present a geometric framework for controllability analysis and motion control for mechanical systems on Lie form. We proceed by showing by illustration how the proposed formation control scheme is extended to underactuated vessels.

Consider a vessel and a point mass as in Figure 4.7 where  $l$  is the length between the point mass and the vessel's bow, subscript  $cg$  denotes the center of gravity, subscript  $q$  denotes the point mass,  $x_p$  is the length between bow and center of gravity and  $\eta = [x_{cg}, y_{cg}, \psi]^T$ . The distance between the bow and the mass point satisfies

$$x_T^2 + y_T^2 = l^2$$

which is equal to the constraint

$$\mathcal{C}_T(x_q, y_q, \eta) = (x_q - x_{cg} + x_p \cos(\psi))^2 + (y_q - y_{cg} + x_p \sin(\psi))^2 - l^2 = 0. \quad (4.34)$$

With a forced motion for the point mass and constraint force  $F_T$ , the vessel follows according to (4.34). For a positive  $x_p$ , the forces at the vessel's center of gravity are only longitudinal and angular around  $(x_{cg}, y_{cg})$ . Since no lateral forces are used to control the ships motion, this corresponds to a surface vessel actuated by rudders and propellers only. This is further extended to all vessels in the formation.

## Dynamic Formation Configuration

By including feedback to the constraint functions the formation configuration would be more dynamic and capable of adjusting to external inputs: if the desired inter-vessel distance  $r$  change according to the environment, operating conditions, etc., collision and obstacle avoidance can be included in the scheme.

## 4.6 Examples

### 4.6.1 Formation Control Schemes and Constraint Functions

This goal of this section is to show that, under some assumptions, constraint functions appear implicitly in some schemes for coordinated control of a group of ships.

In the formation maneuvering design given in Skjetne, Moi & Fossen (2002) the control objective is to make an error vector  $z$  go to zero – in particular, the design establishes UGES of the set  $\mathcal{M} = \{(z, \theta, t) : z = 0\}$ . The error vector contains information about both position and velocity, where the position error is defined as  $z_{1i} = \eta_i - \xi_i$ , for  $i = 1, 2$ , where  $\eta_{1i} \in \mathbb{R}^m$  is the position and  $\xi_i \in \mathbb{R}^m$  is the desired location for the  $i$ th member of the formation. We consider a formation with two members where  $\xi_i = \xi + R(\psi(\theta))l_i$ ,  $l_i \in \mathbb{R}^3$  and we assume that  $R(\psi) = I$ . This corresponds to a desired motion where the formation moves parallel to the  $x$ -axis in the inertial frame. When the systems have reached  $\mathcal{M}$ ,  $z = 0$  and the position errors are  $z_{1i} = \eta_i - \xi_i = \eta_i - \xi - l_i = 0$ .

Combining  $z_{11}$  and  $z_{12}$ , we get  $\eta_1 - \xi - l_1 = \eta_2 - \xi - l_2$ , or  $\eta_1 - \eta_2 - (l_1 - l_2) = \eta_1 - \eta_2 - r_{12} = 0$ . Similar with the velocity errors on  $\mathcal{M}$ ,  $z_{2i} = \dot{\eta}_i - \alpha_{1i}$ , where  $\alpha_{1i}$  is a virtual control law. For the two systems we get  $z_{2i} = \dot{\eta}_i - A_{1i}(\eta_i - \xi - l_i) = 0$ , where  $\dot{\eta}_i$  is the velocity and  $A_{1i}$  is a control design matrix. A combination of  $z_{21}$  and  $z_{22}$  gives, assuming that  $A_{11} = A_{12}$ ,  $\dot{\eta}_1 - \dot{\eta}_2 = A_{11}(z_{21} - z_{22}) = 0$ . Hence, on  $\mathcal{M}$ , the error variable gives constraints on the form

$$\begin{aligned} \mathcal{C}(x) &= \eta_1 - \eta_2 - r_{12} = 0 \\ \dot{\mathcal{C}}(x) &= \dot{\eta}_1 - \dot{\eta}_2 = W\dot{\eta} = 0, \quad W = [1 \quad -1]^\top. \end{aligned}$$

With the above assumptions we see that in the formation assembling phase, the set  $\mathcal{M}$  corresponds to  $\mathcal{M}_c$ .

In Kyrkjebø & Pettersen (2003) the authors use synchronization techniques to develop a control law for rendezvous control of ships. In a case study with two ships the control objective is to control the supply ship to a position relative to the main ship. The desired configuration is reached when the errors  $e = \eta_S - \eta_M$

and  $\dot{e} = \dot{\eta}_S - \dot{\eta}_M$  are zero, where the subscripts  $S$  and  $M$  stands for supply- and main ship, respectively. Both error functions fit into the framework for constraints in Section 4.2.

For a replenishment operation, we define the constraint to depend on the lateral position coordinate only. Then, the supply vessel converge to a position parallel to the course of the main ship, and this position is maintained during forward speed for replenishment purposes.

### 4.6.2 Case Study: Assembling of Marine Craft

We consider a formation of three vessels where the control objective is to assemble the craft into a predefined configuration, e.g., in order to be in position to tow a barge or another object. We assume there are no external forces or control laws acting on the formation, i.e.  $\tau = 0$ , and the purpose is to show that imposing constraint functions assemble the individual vessels into a formation.

Consider the constraint function

$$\mathcal{C}_1(\eta) = \begin{bmatrix} (x_1 - x_2)^2 + (y_1 - y_2)^2 - r_{12}^2 \\ (x_2 - x_3)^2 + (y_2 - y_3)^2 - r_{23}^2 \\ (x_3 - x_1)^2 + (y_3 - y_1)^2 - r_{31}^2 \end{bmatrix} = 0 \quad (4.35)$$

where  $x_i, y_i \in \mathbb{R}$  is the position in the Earth-fixed reference frame and  $r_{ij} \in \mathbb{R}$  is the distance between vessel  $i$  and  $j$ . The constraint manifold is now equivalent to the formation configuration, and by the previous sections we stabilize  $\mathcal{M}_c$  using feedback from the constraint functions. Hence, the proposed method provides control laws for *formation assembling*. From the ship model and the constraint, we have

$$M_\eta \ddot{\eta} + D_\eta \dot{\eta} = -R(\psi) W(\eta)^\top \lambda$$

where  $M_\eta = M_\eta(\eta) = \text{diag}(M_{\eta_1}, M_{\eta_2}, M_{\eta_3})$ ,  $D_\eta = D_\eta(\nu, \eta) = \text{diag}(D_{\eta_1}, D_{\eta_2}, D_{\eta_3})$ ,  $\eta = [\eta_1^\top, \eta_2^\top, \eta_3^\top]^\top$ , and, so on. The Lagrangian multiplier is obtained from

$$W M_\eta^{-1} R W^\top \lambda = -W M_\eta^{-1} D_\eta \dot{\eta} + \dot{W}(\eta) \dot{\eta} + K_d \dot{\mathcal{C}}(q) + K_p \mathcal{C}(q).$$

Equation (4.35) gives the configuration of the formation, but does not provide any information about location. If the control objective is to assemble the formation and position one vessel in a desired location, we add a row to (4.35), such that

$$\mathcal{C}_2(\eta) = \begin{bmatrix} (x_1 - x_2)^2 + (y_1 - y_2)^2 - r_{12}^2 \\ (x_2 - x_3)^2 + (y_2 - y_3)^2 - r_{23}^2 \\ (x_3 - x_1)^2 + (y_3 - y_1)^2 - r_{31}^2 \\ \eta_1 - \eta_{\text{des}} \end{bmatrix} = 0 \quad (4.36)$$

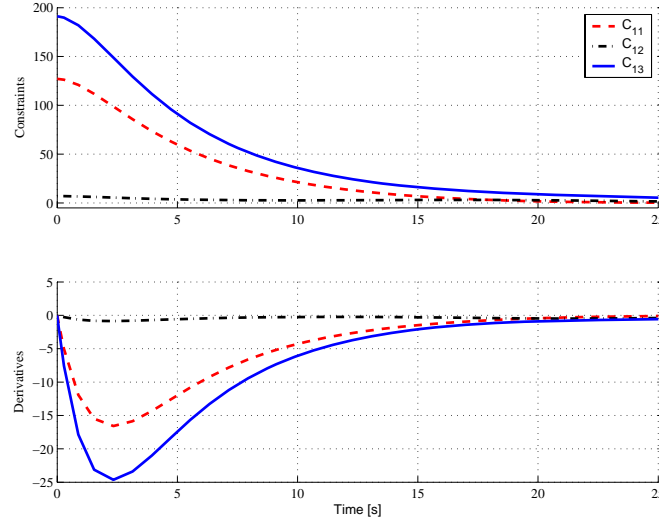


Figure 4.8: Time response of formation constraints during assembling.  $\mathcal{C}_{1i}$  corresponds to the  $i$ 'th row in  $\mathcal{C}_1$ .

where  $\eta_{\text{des}} \in \mathbb{R}^3$  is a fixed desired position and orientation for the first vessel. The closed-loop equations have the same structure as before, except that  $\mathcal{C}_1$  is replaced with  $\mathcal{C}_2$ . The last addition in the constraint function is equal to a PD-controller for the first vessel, so (4.36) leads to a combination of a formation controller and a PD-type-controller for dynamic positioning of ships. Several control laws are thus handled in one step using the constraint approach.

The control parameters chosen to stabilize the formation constraints  $\mathcal{C}_1$  and  $\mathcal{C}_2$  are ( $I = I_{3 \times 3}$ )  $K_p = 0.8I$ ,  $K_d = 0.8I$ , the formation is defined by  $r_{12} = 3$ ,  $r_{23} = 3$ ,  $r_{31} = 3$ , and the desired position for the first vessel is  $\eta_{\text{des}} = [10, 5, 0]^\top$ . The vessels start in  $\eta_{10} = [8, 8, 0]^\top$ ,  $\eta_{20} = [-2, 2, 0]^\top$ , and  $\eta_{30} = [-2, -2, 0]^\top$  – all with zero initial velocity.

Figure 4.8 shows the time-plot of the constraint function  $\mathcal{C}_1$  and its time-derivative  $W_1(\eta) \dot{\eta}$ . The constraints and velocity terms converge to zero, and the constraint manifold is reached. The vessels have converged to the nearest positions where the constraints are fulfilled, and the formation is assembled in the desired configuration, as seen in Figure 4.9.

Figure 4.10 shows the position of the three vessels with the same initial conditions as before but subject to the constraint  $\mathcal{C}_2$ . The vessels assemble according to the constraints, but this time vessel 1 is positioned at the desired position  $\eta_{\text{des}}$ . This forces the two other vessels to move to a different position compared to the first case in order to satisfy the constraint. The additional constraint slows down

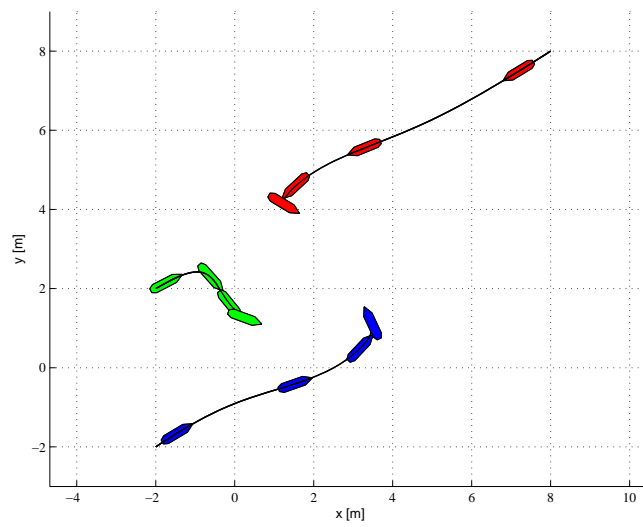


Figure 4.9: Position response of vessels during assembling.

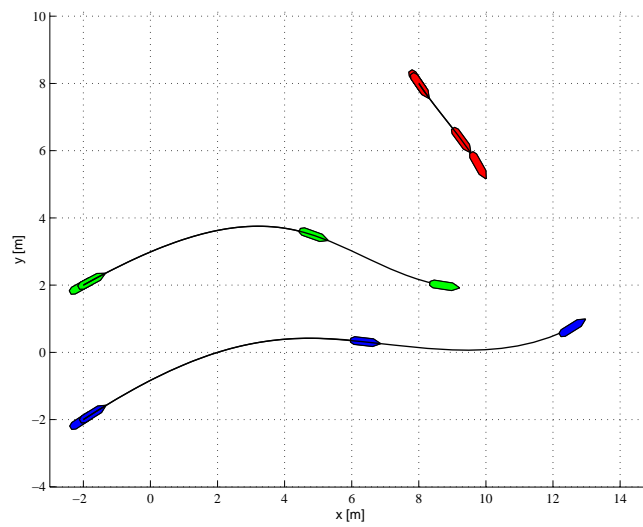


Figure 4.10: Position response of vessels subject to formation constraints when vessel 1 is to be positioned at  $\eta_{des}$ .

convergence to the constraint manifold since vessel 1 has to be positioned at  $\eta_{\text{des}}$  and this forces the other vessels to move accordingly.

### 4.6.3 Case Study: Trajectory Tracking and Formation Control

We investigate a formation of three vessels where one vessel tracks a desired path while the others follow according to the formation constraint function. All vessels are subject to unknown environmental perturbations, measurement noise and the communication channels are affected by time delays.

We use a time-varying constraint function to allow a time-varying configuration. Consider the following functions

$$\mathcal{C}_{fc}(\eta, t) = \begin{bmatrix} (x_1 - x_2)^2 + (y_1 - y_2)^2 - r_{12}^2 \\ (x_2 - x_3)^2 + (y_2 - y_3)^2 - r_{23}^2(t) \\ (x_3 - x_1)^2 + (y_3 - y_1)^2 - r_{31}^2 \end{bmatrix}, \quad \mathcal{C}_{tt}(\eta, t) = \tilde{\eta} := \eta_1 - \eta_d(t)$$

where  $r_{23}(t)$  and  $\eta_d(t)$  are three times differentiable. The first functions are on the constraint function form (5.10), while the last is a constraint function that yields a control law for trajectory tracking. Since the two functions are not conflicting we collect them into the following constraint function

$$\mathcal{C}(\eta, t) = \begin{bmatrix} \mathcal{C}_{fc}(\eta, t) \\ \mathcal{C}_{tt}(\eta, t) \end{bmatrix} = 0. \quad (4.37)$$

Together with the ship model (4.28), where  $W_d = WM_\eta^{-1}R(\psi)$ , the backstepping design in Section 4.4 yields robust control laws for formation control and trajectory tracking with  $\phi = \mathcal{C}$  and

$$V(\phi, t) = \phi^\top P \phi \quad P = P^\top > 0.$$

The closed-loop equations of motion for the three vessels are

$$M_\eta(\eta) \ddot{\eta} + n(\nu, \eta, \dot{\eta}) = -R(\psi) W_{fc}^\top \lambda_{fc} - \tau_{tt} + R(\psi) \delta(t)$$

where the formation control laws are given as

$$R(\psi) W_{fc}^\top \lambda_{fc} = (W_{fc} M_\eta^{-1} W_{fc}^\top) (-W_{fc} n + \dot{W} \dot{\eta} + K_p \mathcal{C}_{fc} + K_d \dot{\mathcal{C}}_{fc} + P_{fc2} (\dot{\mathcal{C}}_{fc} - A_{fc1} \mathcal{C}_{fc}))$$

where  $K_p, K_d \in \mathbb{R}^{3 \times 3}$  are positive definite. The trajectory tracking control law is  $\tau_{tt} = [R(\psi_1) \lambda_{tt}, 0, 0]^\top$  where  $R(\psi_1) \lambda_{tt}$  is the control law for the first vessel to track the desired path  $\eta_d$ :

$$R(\psi_1) \lambda_{tt} = -n_1(\nu_1, \eta_1, \dot{\eta}_1) - M_{\eta_1} (\ddot{\eta}_d - k_{tp} \dot{\tilde{\eta}} - k_{td} \tilde{\eta} - P_{tt2} (\dot{\tilde{\eta}} - A_{tt} \tilde{\eta}))$$

where  $k_{tp}, k_{td} \in \mathbb{R}^{3 \times 3}$  are positive definite.

### Linearized Analysis of Robustness to Time-delays

We know that the delay robustness for a single-input-single-output linear system is given by

$$T_{\max} = \frac{PM}{\omega_{gc}} \quad (4.38)$$

where  $T_{\max}$  is the maximum delay in the feedback loop that does not destabilize the system,  $PM$  is the phase margin, and  $\omega_{gc}$  is the gain crossover frequency. Thus, increasing the phase margin and/or decreasing the bandwidth improves delay robustness. We linearize by assuming small variations in the constraint functions and heading angle. The loop-gain of the linearized system (about the heading angle  $\psi \approx 0$ ) from the disturbance  $\delta$  to the constraint  $\mathcal{C}_{fc1}$  is

$$G_{c\delta}(s) = \frac{\kappa/2}{s^2 + k_d s + k_p} \quad (4.39)$$

where  $k_p$  and  $k_d$  are the  $(1, 1)$ -elements of  $K_p$  and  $K_d$ , respectively.

Using tools from linear systems theory we adjust the gains to maximize the delay that does not destabilize the system. This has to be done in a trade-off relation with other performance properties. A critically damped system is desired since it implies no overshoot, and is achieved for  $k_d = 2\sqrt{k_p}$ . The linearized analysis is no guarantee for formation stability in the presence of delays, but it gives an indication.

### Simulation Results

The desired path for vessel 1 is

$$\eta_d(t) = \begin{bmatrix} x_d(t) \\ y_d(t) \\ \psi_d(t) \end{bmatrix} = \begin{bmatrix} t \\ A \sin \omega t \\ \text{atan2} \left( \frac{\dot{y}_d}{\dot{x}_d} \right) \end{bmatrix}$$

where  $A = 200$  and  $\omega = 0.005$ , and the unknown environmental disturbances are

$$\delta_i(t) = \begin{bmatrix} 10^3 + 2 \cdot 10^3 \sin(0.1t) \\ 2 \cdot 10^3 \sin(0.1t) \\ 2 \cdot 10^3 \sin(0.1t) \end{bmatrix} + \text{white noise} \quad (4.40)$$

acting the same on all vessels.

The unknown environmental disturbances are seen to be slowly-varying while the first-order wave-induced forces (oscillatory wave motion) are assumed to be filtered out of the measurements by using a *wave filter*. This is a good assumption since a ship control system is only supposed to counteract the slowly-varying

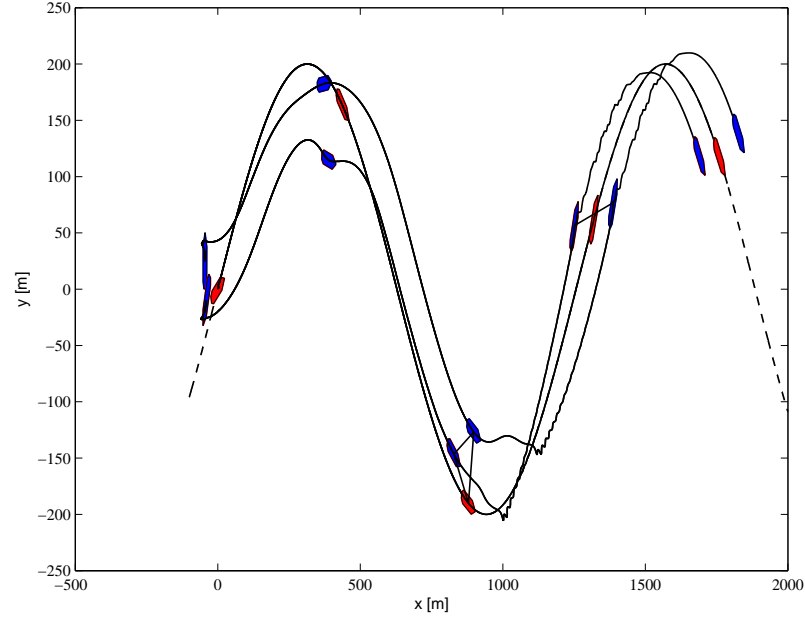


Figure 4.11: Position response of vessels during simulation. Vessel 1 follows the desired (dashed) path, and the desired configuration changes from a triangular shape to a line about halfway through the simulation.

motion components of the environmental disturbances to reduce wear and tear of actuators and propulsion system.

The desired formation configuration is given by  $r_{12} = 70$ ,  $r_{31} = 70$ , and  $r_{23}$  is initially 65 and changes smoothly to 130 at about  $1000s$ . The control gains are  $k_{tp} = 4I$ ,  $k_{td} = 2I$ ,  $K_p = \text{diag}(k_{pi})$ ,  $k_{pi} = 3.24$ ,  $K_d = \text{diag}(k_{di})$ ,  $k_{di} = 6$  and  $\kappa = 20$ . The initial values are  $\eta_1(0) = [0, 0, \frac{\pi}{2}]^\top$ ,  $\eta_2(0) = [-45, 25, \frac{\pi}{2}]^\top$ ,  $\eta_3(0) = [-40, -10, \frac{\pi}{2}]^\top$  and  $\nu_1(0) = \nu_2(0) = \nu_3(0) = 0$ .

Figure 4.11 shows the resulting position trajectories and five snapshots of the vessels during the simulation: the vessels assemble into the desired configuration and vessel 1 tracks the desired path. The position tracking and formation constraints errors due to the disturbances (4.40) were attenuated to less than 1 m, and 5 m, respectively. The time-varying configuration is seen in the third and fourth snapshot as the formation changes from a triangle to a line.

For the linearized relation (4.39) the values give a bandwidth of 0.59 rad/s and a phase margin of  $85^\circ$ . This corresponds to a maximum time delay of 2.5s. In the simulation all communication channels are affected by 2.5s time delays, and simulations show that delays larger than 3s cause instabilities in the closed-loop system. Thus, the transfer function provides a good estimate of robustness

towards time delays.

## 4.7 Concluding Remarks

We have shown how individual ships are controlled as a formation by designing constraint functions that force the vessels to assemble and remain in a desired configuration. The distance and orientation between independent vehicles are maintained by forces which arise due to the imposed constraints.

The constraint forces, which can be interpreted as control laws, are derived in an analytical setting using Lagrangian multipliers. Further, feedback from the constraints is used to render the system robust against initial position errors during formation assembling, and is extended to counteract external disturbances and measurement noise by adding further damping gains. The resulting formation constraint forces are non-zero only when the constraints are violated – when a constraint is fulfilled, the corresponding multiplier and constraint force is zero. Furthermore, the same approach has been applied with no major modification to control purposes. In particular, we have proposed control laws which maintain the formation structure and the approach is also used to combine control laws in order to simultaneously achieve desired behavior and maintain formation configuration.



# Chapter 5

## Combined Position and Formation Control

In this chapter, we consider formation control of marine surface vessels and investigate robustness to both environmental disturbances and noisy communication channels where time-delays may arise. The formation configuration is described with the framework of Chapter 4 using inter-vessel functions constraining a vessel's behavior with respect to its neighbors. Stability and convergence of the inter-vessel constraint functions imply that vessels assemble into the formation configuration.

From the marine vessel model the forces acting on the rigid body are superimposed (see Appendix B for details)

$$M_{RB}\dot{\nu} + C_{RB}(\nu)\nu = \underbrace{-M_A\dot{\nu} - C_A(\nu)\nu - D(\nu)\nu - g(\eta)}_{\tau_H} + \tau + \tau_{\text{env}}$$

where  $\tau$  consists of generalized control forces and moments. This chapter studies a group of vessels in two cases:

- We firstly consider control laws for maintaining a given formation configuration in the presence of environmental loads and communication disturbances, that is,  $\tau = \tau_{\text{formation}}$ .
- Secondly, we extend this scheme in pursuit of a modularity approach where one or more of the vessels are individually controlled by a position control law for point stabilization, trajectory tracking or path following, e.g.,  $\tau = \tau_{\text{formation}} + \tau_{\text{position}}$ .

Finally, we study this scheme's robustness to time-delays. Stability of the suggested modules enables the control designer to address motion control laws and formation maintenance separately instead of incorporating a motion control

law in the formation control framework as in Chapter 4. Thus, the literature on motion control for single vessels, see for example Fossen (2002) and Perez (2005), is utilized in a formation setting.

Even though the individual position controllers in closed-loop with the vessels and the formation control laws are stable with respect to their origins, an interconnection may not be stable unless it satisfies additional properties. Examples of such properties are given in e.g. Panteley & Loría (1998, 2001). Motivated by results on passivity design for coordinated control in Arcak (2006), and robustness for network flow control in Fan & Arcak (2004), we show that the proposed scheme can be modelled as a feedback interconnection of a block of vessels and position control laws and a block that maintains the formation configuration is maintained. Furthermore, we use a small-gain result from Jiang, Teel & Praly (1995) and Teel (1996) to prove that the interconnection is ISS with respect to environmental and inter-vessel disturbances. We finally consider a formation with time-delays and use the ISS property and a loop-transform to prove uniform global asymptotic stability of both position and formation configuration errors for sufficiently small delays.

## 5.1 Preliminaries

We consider a ship model in surge, sway, and yaw

$$\dot{\eta} = R(\psi)\nu \quad (5.1a)$$

$$M\dot{\nu} + D(\nu)\nu + C(\nu)\nu = \tau_b \quad (5.1b)$$

where  $\eta = [x, y, \psi]^\top$  is the Earth-fixed position vector,  $(x, y)$  is the position on the ocean surface and  $\psi$  is the heading (yaw) angle, and  $\nu = [u, v, r]^\top$  is the body-fixed velocity vector. The model matrices  $M$ ,  $C$ , and  $D$  denote system inertia, Coriolis plus centrifugal and damping, respectively, and  $R = R(\psi) \in SO(3)$ ,  $\|R\| = 1 \forall \psi$ , is the rotation matrix between the body and Earth coordinate frame.

**Property 5.1** *The damping matrix  $D(\nu)$  is strictly positive, i.e.,  $(1/2)x^\top(D(\nu) + D(\nu)^\top)x > 0$ ,  $\forall x \neq 0$ . It consists of a linear and a nonlinear part, i.e.,  $D(\nu) = D + D_{nonlin}(\nu)$  where  $D$  is a matrix of linear damping terms, and  $D_{nonlin}(\nu)$  is a matrix of nonlinear viscous damping terms, for instance quadratic drag.*

We characterize the passivity properties of a vessel  $i$ . Consider the positive definite, radially unbounded storage function

$$V_i = \nu_i^\top M_i \nu_i, \quad M_i = M_i^\top > 0 \quad (5.2)$$

with the following time-derivative

$$\dot{V}_i = -2\nu_i^\top (D_i(\nu_i) + C_i(\nu_i)) \nu_i + \nu_i^\top \tau_i \leq -\varepsilon_i |\nu_i|^2 + \nu_i^\top \tau_i \quad (5.3)$$

since  $C_i(\nu_i)$  is skew-symmetric,  $D_i(\nu_i)$  is strictly positive and  $\varepsilon_i > 0$ . Thus, (5.2) and (5.3) show that the vessel dynamics is passive from  $\tau_i$  to  $\nu_i$ . For low-speed applications, such as dynamic positioning, linear damping dominates such that the damping matrix is constant and the Coriolis and centripetal matrix is close to zero if currents are neglected. The dissipative property of ships is then equivalent to consider the eigenvalues of  $-M^{-1}D$ . If the resulting matrix is Hurwitz the ship is *course-stable*.

For notational convenience we rewrite the vessel dynamics (5.1) in Earth-fixed coordinates:

$$M_{\eta_i}(\eta_i) \ddot{\eta}_i + N_i(\nu_i, \eta_i) \dot{\eta}_i = R(\psi_i) \tau_{b,i} = \tau_i \quad (5.4)$$

where

$$M_{\eta_i}(\eta_i) = R(\psi_i) M_i R(\psi_i)^\top \quad (5.5)$$

$$C_{\eta_i}(\nu_i, \eta_i) = R(\psi_i) \left[ C_i(\nu_i) - M_i R(\psi_i)^\top \dot{R}(\psi_i) \right] R(\psi_i)^\top \quad (5.6)$$

$$D_{\eta_i}(\nu_i, \eta_i) = R(\psi_i) D_i(\nu_i) R(\psi_i)^\top \quad (5.7)$$

$$N(\nu_i, \eta_i) = C_{\eta_i}(\nu_i, \eta_i) + D_{\eta_i}(\nu_i, \eta_i) \quad (5.8)$$

and it follows from Appendix B that

$$\begin{aligned} M_{\eta_i}(\eta_i) &= M_{\eta_i}(\eta_i)^\top > 0 \\ s^\top \left( \dot{M}_{\eta_i} - 2C_{\eta_i} \right) s &= 0 \quad \forall s \in \mathbb{R}^3 \\ D_{\eta_i}(\nu_i, \eta_i) &> 0. \end{aligned}$$

## 5.2 Formation Modeling and Control of Marine Surface Vessels

For the remaining part of this chapter, we consider a group of  $r$  marine surface vessels

$$\Sigma_i : M_{\eta_i} \ddot{\eta}_i + N_i(\nu_i, \eta_i) \dot{\eta}_i = R(\psi_i) \tau_i, \quad i = 1, \dots, r \quad (5.9)$$

where each vessel's dynamics is as in (5.2) and (5.3)—depicted in Figure 5.1. We apply the proposed formation control procedure from Chapter 4 and consider two functions for formation purposes, the position-relative

$$C_r(\eta_i, \eta_j) = (x_i - x_j)^2 + (y_i - y_j)^2 - r_{ij}^2, \quad r_{ij} \in \mathbb{R} \quad (5.10)$$

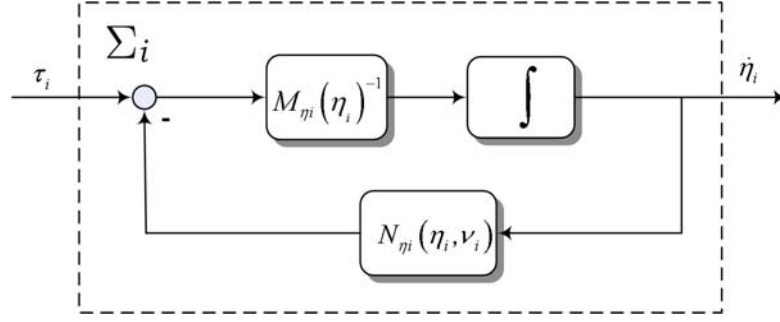


Figure 5.1: Vessel input-output dynamics.

and the orientation-fixed

$$\mathcal{C}_f(\eta_i, \eta_j) = \eta_i - \eta_j - o_{ij}, \quad o_{ij} \in \mathbb{R}^3. \quad (5.11)$$

The scalar  $r_{ij}(t)$  is the desired distance between vessel  $i$  and  $j$  while the column vector  $o_{ij}$  describes the offset between  $\eta_i$  and  $\eta_j$  in each degree of freedom (DOF). We say that two vessels are *neighbors* if they are connected by formation constraint functions such as (5.10) or (5.11), in which case they can access each others information.

Given a set of constraint functions as in (5.10) or (5.11). The desired formation structure is then given by the formation constraint function

$$\begin{aligned} \mathcal{C} &= [\mathcal{C}_1^\top, \dots, \mathcal{C}_l^\top]^\top = 0 \\ \dim \mathcal{C} &= p \end{aligned} \quad (5.12)$$

subject to

**Assumption 5.1** *The constraints  $\mathcal{C}_1, \dots, \mathcal{C}_l$  are neither redundant nor conflicting and  $\dim(\mathcal{C}) < 3(r-1)$ .*

It follows from this assumption that the Jacobian  $W(\eta)$  has full row-rank as in Assumption 4.1. The analytical approach in Chapter 4 stabilizes the formation structure with the constraint force  $\tau_{ci}$  acting on vessel  $i$

$$\tau_{ci} = \sum_{k \in \mathcal{N}_i} -W_{k,i}^\top \lambda_k \quad (5.13)$$

where  $\mathcal{N}_i$  is the set of indices of  $\mathcal{C}$  where  $\eta_i$  appears,  $W_{k,i}$  is the  $i$ th column of the Jacobian of the constraint  $\mathcal{C}_k$ , i.e.,  $W_{k,i} = \frac{\partial \mathcal{C}_k}{\partial \eta_i}$ , and  $\lambda_k$  is the Lagrangian multiplier corresponding to  $\mathcal{C}_k$ . The Lagrangian multiplier is found by combining

$$\frac{d^2}{dt^2} \mathcal{C}_k = 0$$

with the vessel model (5.9) and solve for  $\lambda_k$  – see Ihle, Jouffroy & Fossen (2006a) for details.

We write the system matrices on block-diagonal form

$$\begin{aligned} M_\eta &:= \text{diag} \{M_{\eta_1}, \dots, M_{\eta_r}\}, \quad N := \text{diag} \{N_1, \dots, N_r\}, \\ R &:= \text{diag} \{R(\psi_1), \dots, R(\psi_r)\}, \end{aligned}$$

and the vectors as concatenated vectors

$$\eta := [\eta_1^\top, \dots, \eta_r^\top]^\top, \quad \tau_c := [\tau_{c1}^\top, \dots, \tau_{cr}^\top]^\top,$$

to obtain the closed-loop dynamics for the entire formation

$$M_\eta \ddot{\eta} + N \dot{\eta} = -RW^\top \lambda \tag{5.14}$$

where

$$W = \frac{\partial \mathcal{C}}{\partial \eta}, \quad \text{and } \lambda = [\lambda_1, \dots, \lambda_p]^\top.$$

The formation members are now coupled together by the constraint forces. The analytical expression for  $\lambda$  is obtained from  $\dot{\mathcal{C}}$  and (5.14):

$$(WM_\eta^{-1}RW^\top) \lambda = \left(-WM_\eta^{-1}N\dot{\eta} + \dot{W}\dot{\eta} + K_p\mathcal{C} + K_d\dot{\mathcal{C}}\right), \quad K_p, K_d > 0 \tag{5.15}$$

where  $K_p, K_d > 0$ , and the two latter terms stabilize  $\mathcal{C} = 0$  and thus force the formation to configure accordingly.

To obtain  $\lambda$  in (5.15) the term on the left-hand side must be invertible: The transformed inertia matrix  $M_\eta$  is positive definite due to (5.2) and (5.5). Since the Jacobian  $W$  has full row rank, it follows that the product  $WM_\eta^{-1}RW^\top$  is nonsingular.

Combining (5.14) and (5.15) yields the constraint-stabilization system

$$\ddot{\mathcal{C}} = -K_d\dot{\mathcal{C}} - K_p\mathcal{C}, \tag{5.16}$$

which has a stable origin, that is, the formation assembles in the desired configuration:

**Theorem 5.1** *The constraint-stabilization system (5.16), or equivalently (5.14) and (5.15), has a GES origin  $(\mathcal{C}, \dot{\mathcal{C}}) = 0$  under Assumption 5.1.*

The proof follows from standard Lyapunov theory using

$$V_c(\phi) = \phi^\top P\phi, \quad P = P^\top > 0. \tag{5.17}$$

Furthermore, the velocity vectors are aligned, that is,  $\eta_i = \eta_j \quad \forall i, j, i \neq j$  when the entire formation is connected by constraint functions: The constraint derivative

$$\ddot{C} = W\dot{\eta} = 0$$

implies that  $\dot{\eta}_i - \dot{\eta}_j = 0$ . This is seen as follows: For both type of constraints the Jacobian  $W$  has zero-sum columns, thus  $v = k[1, \dots, 1]^\top$ ,  $k \in \mathbb{R}$ , lies in the null-space of  $W$ . Since  $W$  has full row rank it has a single nullspace vector, and  $v$  is the only null-space vector. Thus, the velocities  $\eta_i$  and  $\eta_j$  are equal,  $\dot{\eta}_i = \dot{\eta}_j$ .

Before we proceed, we state the following lemma which is needed for the results in the remainder of this chapter.

**Lemma 5.1** *The Jacobian  $W$  of (5.12) and its time-derivative  $\dot{W}$  have bounded norms under the hypothesis of Theorem 5.1.*

**Proof:** We know from matrix analysis that the matrix norm induced by the euclidean vector norm is

$$\|W\|_2 = \sqrt{\lambda_{\max}(W^\top W)}$$

When the formation configuration is given by (5.11), the Jacobian is constant so the result is trivial. When the configuration is given by (5.10), the elements of the Jacobian are either zero or a relative displacement,  $x_i - x_j$  or  $y_i - y_j$ . The norm of  $W$  is bounded when these elements are bounded and stability of (5.12) follows from (5.16) which implies that the displacements are bounded, and the result follows. Similarly, boundedness of  $\|\dot{W}\|$  follows from similar arguments as each element of  $\dot{W}$  is bounded by Theorem 5.1.  $\square$

### 5.3 Robustness to Disturbances

A ship is affected by unknown environmental loads due to wind, waves and currents. These loads are represented by a force field where

- a slowly varying mean force which attacks the ship in
- a slowly varying mean direction relative to the Earth-fixed frame.

The slowly varying terms include model uncertainties, second-order wave-induced disturbances (wave drift), currents and mean wind forces. The first-order wave-induced forces (oscillatory wave-induced motion) are assumed to be filtered out by employing a *wave filter*— see Section 2.4.

The ship control system should only counteract the slowly-varying motion components of the environmental to reduce wear and tear of actuators and propulsion

system. In addition, there are no sensors to accurately measure the mean force and direction of the environmental loads. This motivates the assumption that the unknown mean environmental force and its direction are constant (or at least slowly varying).

### 5.3.1 Robust Formation Control

We use the results in Section 5.2 to study system robustness with respect to disturbances. The closed-loop system is represented as in Figure 5.2 where the  $\Sigma$ -block consists of vessels as in (5.9). We define the output of  $\Sigma$  as

$$e := \dot{\eta} = [\dot{\eta}_1^\top, \dots, \dot{\eta}_r^\top]^\top.$$

Multiplying  $e$  with  $W_{\text{constr}}$  transforms the variables into constraint functions. The constraint functions are stabilized in  $\mathcal{H}_{\text{stab}}$  where the output is as in (5.15), and the block  $\Sigma_i$  represents the internal dynamics of vessel  $i$ . Stability of the feedback interconnection implies that, as in Theorem 5.1, the formation assembles in the desired configuration.

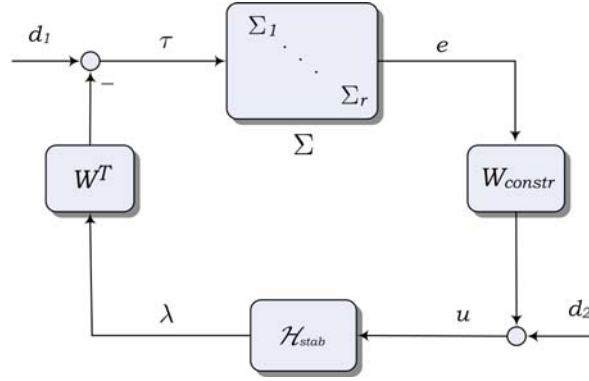


Figure 5.2: A formation of vessels,  $\Sigma$ -block, with stabilized inter-vessel constraints,  $\mathcal{H}_{\text{sync}}$ , with disturbances  $d_1$  and  $d_2$ .

We assume that the disturbances act on the system as in Figure 5.2. Each vessel in the formation is affected by the environmental loads  $d_1$  while  $d_2$  act on the stabilization of inter-vessel constraints and is interpreted as disturbances on the inter-vessel communication links. Other disturbances can be represented by using loop transformations. In Theorem 5.2 we first prove ISS of vessel dynamics in the  $\Sigma$ -block and the inter-vessel constraint in the  $\mathcal{H}_{\text{stab}}$ -block separately. Furthermore, we show that the forward path from  $\lambda$  to  $e$  has gain

$$g_1 = \frac{m_M}{m_m \varepsilon_M} \|W\| \quad (5.18)$$

where  $\epsilon_M = \max_i \{\epsilon_i\}$  and  $m_m$  ( $m_M$ ) is a lower (upper) bound for all mass matrices. The feedback path from  $e$  to  $\lambda$  has gain

$$g_2 = \delta w_e \quad (5.19)$$

where  $g_2$  is the gain from  $\dot{\eta}$  to  $\lambda$  in (5.15). Then, if the small-gain condition

$$g_1 g_2 < 1 \quad (5.20)$$

holds the interconnection is ISS with respect to  $d_1$  and  $d_2$ .

**Theorem 5.2** *Consider the feedback interconnected system (5.14), (5.16) as depicted in Figure 5.2 where  $\Sigma_i$  is as given in (5.2) and (5.3). Suppose  $d_1, d_2 \in \mathcal{L}_\infty$  and Assumption 5.1 holds. Then, the  $\Sigma$ -block is ISS with respect to  $\tau$ , and the  $\mathcal{H}_{stab}$ -block is ISS with respect to  $d_2$ . Furthermore, if (5.20) holds the feedback interconnection is ISS with respect to the disturbances  $d_1$  and  $d_2$ .*

The proof is found in Appendix C.1

### 5.3.2 Robust Combined Control

As an extension to Theorem 5.2 we consider the case where one or more vessels in  $\Sigma$  is in closed loop with individual control laws  $u_i$ , e.g., for dynamic positioning or path following. Disregarding the formation control laws, we assume that  $u_i$  renders equilibrium points of the closed-loop system  $e_i = 0$  (U)GES. ISS of the feedback interconnection implies that the vessels behave according to the individual control laws while maintaining the formation configuration in the presence of disturbances.

**Assumption 5.2** *Suppose (5.1) is in closed loop with a control law  $u_{ship,i}$  such that equilibrium points  $e_i = 0$  are ISS with respect to  $\tau_i$ , that is, for  $\Sigma_i$*

$$M_{\eta_i} \ddot{\eta}_i + D_{\eta_i}(\nu_i, \eta_i) \dot{\eta}_i = R(\psi_i) (u_{ship\_i} + \tau_i), \quad (5.21)$$

which we rewrite as

$$\Sigma_i : \dot{e}_i = F_i(\eta_i, t) e_i + b_i(\eta_i) \tau_i \quad (5.22)$$

where  $F_i(\eta_i, t) \in \mathbb{R}^{n \times n}$  and  $b_i(\eta_i) \in \mathbb{R}^n$  depend on the control design and, we have the ISS-Lyapunov function

$$V_{ship\_i} = e_i^\top P_i e_i. \quad (5.23)$$

In particular,  $F(x)$  satisfies

$$PF_i(\eta_i, t) + F_i(\eta_i, t)^\top P \leq -I \quad (5.24)$$

for some matrix  $P = P^\top > 0$ . The time-derivative of (5.23) is

$$\dot{V}_i(t, e_i) \leq -\varepsilon_i |e_i|^2 + \rho_i |e_i| |\tau_i| \quad (5.25)$$

where  $\varepsilon_i, \rho_i > 0$ . Furthermore, we assume that the individual control laws are not conflicting.  $\square$

By Assumption 5.2 the closed-loop system

$$M_{\eta_i} \ddot{\eta}_i + D_{\eta_i}(\nu_i, \eta_i) \dot{\eta}_i = R(\psi_i) u_{ship\_i}, \quad (5.26)$$

or equivalently

$$\Sigma_i : \dot{e}_i = F_i(\eta_i, t) e_i, \quad (5.27)$$

has uniformly globally exponentially stable equilibrium points  $e_i = 0$ . It further follows that for (5.23) we have

$$p_{i,m} |e_i|^2 \leq V_{ship\_i}(t, e_i) \leq p_{i,M} |e_i|^2 \quad (5.28)$$

$$\dot{V}_{ship\_i}(t, e_i) \leq -\varepsilon_i |e_i|^2 \quad (5.29)$$

$$\left| \frac{\partial V_{ship\_i}}{\partial e_i} \right| \leq p_{i,M} |e_i|. \quad (5.30)$$

As mentioned in Loría (2001, Ch. 2.3.2), a feedback interconnected system can be viewed as a cascade. If the two feedback interconnected systems  $\Sigma$  and  $H_{stab}$  are stable and, in addition, the closed-loop of vessel and controller is stable *uniformly* in  $\phi$ , we rewrite the system on a cascaded form. Thus, stability of the closed-loop system is proved with stability tools from cascaded non-autonomous systems (e.g., Panteley & Loría (2001)). However, we remain in the feedback structure to exploit a loop-transformation to consider time-delays.

The error vector  $e$  in Figure 5.2 consists now of equilibrium points  $e_i$  for the individually controlled vessels and velocities  $\dot{\eta}_i$  for the remaining vessels. Similar to the proof of Theorem 5.2, we obtain a new gain from  $\lambda$  to  $e$

$$g_{1c} = \frac{q_M \bar{\rho}}{q_m \bar{\varepsilon}} \|W\| \quad (5.31)$$

where  $q_m, q_M$  are bounds for the Lyapunov function of  $\Sigma$ ,  $\bar{\varepsilon} = \max_i \{\varepsilon_i\}$ ,  $\bar{\rho} = \max_i \{\rho_i\}$ , and prove that if the small-gain condition

$$g_{1c} g_2 < 1, \quad (5.32)$$

holds, the interconnection is ISS with respect to disturbances  $d_1$  and  $d_2$ .

**Theorem 5.3** Consider the feedback interconnected system (5.14), (5.16) as depicted in Figure 5.2 where  $\Sigma_i$  is as given in (5.2) and (5.3), or as in (5.25)-(5.28), for  $d_1, d_2 \in \mathcal{L}_\infty$ . Then, if Assumptions 5.1 and 5.2 and the small-gain condition (5.32) hold, the feedback interconnection is ISS with respect to  $d_1$  and  $d_2$ .

The proof is found in Appendix C.2

## 5.4 Robustness to Time-Delays

We next consider the case where the communication channels are affected by time-delays and analyze robustness of the feedback interconnection to such delays. Time delays may arise as a result of unanticipated changes in the medium of communication or other events inside or outside the control system.

To simplify the derivations, we only consider delays between  $\Sigma$  and the constraint stabilization scheme, that is, delays occur as vessels exchange information to calculate the constraint forces that maintain the formation configuration. We model the delays, as in Figure 5.3, by multiplying the entries of  $W_{\text{constr}}$  with  $e^{-sT_{ij}}$  where  $T_{ij}$  is the delay from vessel  $i$  to vessel  $j$ . This section consider formations where at least one of the vessels is subject to a position control law, but the analysis is also applicable to a group of vessels without positioning control law—considered in Section 5.3.1.

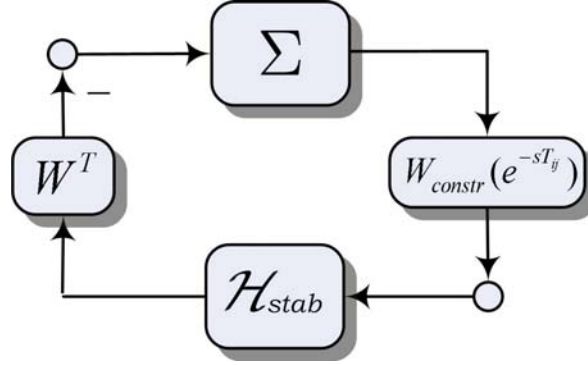


Figure 5.3: Formation control with time-delay.

We transform the delay robustness problem to the framework of the previous section by adding and subtracting  $W_{\text{constr}}$  to the forward path in Figure 5.3, and represent it as in Figure 5.4. The outer loop is then the perturbation due to delay and the inner is the same loop as we have studied in Section 5.3. Robustness with respect to  $d_2$  has been studied in Section 5.3.2 and we use a small-gain condition to establish stability of the feedback interconnection's origin.

We have from Theorem 5.3 that the path from  $d_2$  to  $\lambda$  has gain

$$g_{\text{inner}} = \frac{2\delta k_M p_M^2 p_m^{-1}}{1 - g_{1c} g_2} \quad (5.33)$$

where  $g_{c1}$  and  $g_2$  are the gains for the combined control case in Section 5.3. In the following theorem, we show that the path from  $\lambda$  to  $d_2$  has gain

$$g_{\text{outer}} = T w_e \sqrt{2pr} \left( \|F\| \frac{2\sqrt{m_M}}{m_m \varepsilon_M} + |b| \right) \|W\| \quad (5.34)$$

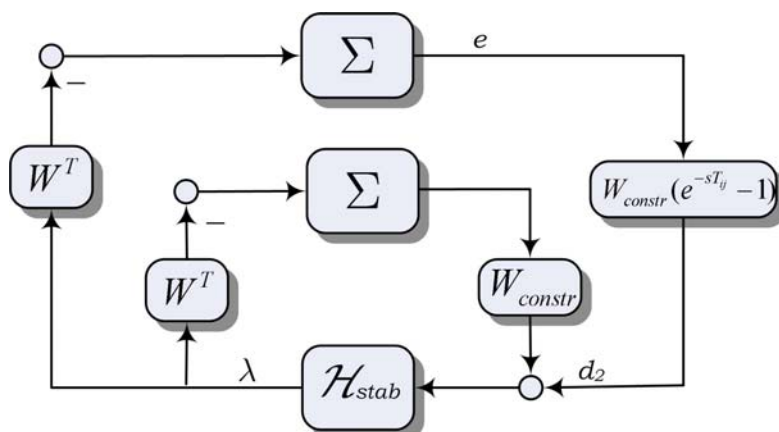


Figure 5.4: Formation control with time-delay after loop-transform.

where  $T = \max_{i,j} \{T_{ij}\}$  and  $\|F\|, |b| = \max_{\mathcal{N}_i} \{\|F_i\|\}, \{|b_i|\}$  respectively. Uniform global asymptotic stability of  $(e, \phi) = 0$  then follows from the small-gain condition

$$g_{\text{inner}}g_{\text{outer}} < 1. \quad (5.35)$$

**Theorem 5.4** Consider the interconnection in Figure 5.3 where  $\Sigma_i$  satisfy either (5.2) and (5.3) or (5.25)-(5.28) and  $\mathcal{H}_{\text{stab}}$  is as in (5.15)-(5.16). If the maximum delay  $T$  is small enough such that (5.35) is satisfied, then the origin  $(e, \phi) = 0$  is UGAS.

The proof is found in Appendix C.3.

## 5.5 Case Study: Rendezvous operation

To illustrate the theoretical results we consider a formation control law for a group of vessels where one vessel is in closed-loop with a previously developed path following controller from Chapter 2. We briefly review the closed-loop properties for the controller and show that all assumptions of Theorem 5.3 are satisfied.

Consider a general system

$$\begin{aligned} \dot{x} &= f(x, u) \\ y &= h(x) \end{aligned} \quad (5.36)$$

where  $x \in \mathbb{R}^n$  denotes the state vector,  $y \in \mathbb{R}^m$  is the system output, and  $u \in \mathbb{R}^n$  is the control. To steer  $y$  to a prescribed path  $\xi(\theta)$ , and to assign a speed  $v(t)$  to  $\dot{\theta}$  on this path, Skjetne (2005) studies subclasses of (5.36) and develops maneuvering

design procedures based on feedback linearization and backstepping techniques. The designs are based on the Lyapunov function

$$V(z, \theta, t) = z^\top Pz, \quad P = P^\top > 0 \quad (5.37)$$

with time-derivative

$$\dot{V}(z, \theta, t) \leq -z^\top Uz, \quad U = U^\top > 0 \quad (5.38)$$

They lead to a closed-loop system of the form

$$\begin{aligned} \dot{z} &= F(x)z - g(t, x, \theta)\omega \\ \dot{\theta} &= v(\theta, t) - \omega \end{aligned} \quad (5.39)$$

where  $z$  is a set of new parameters that include the tracking error  $y - \xi(\theta)$  and its derivatives, and  $\omega$  is a feedback term to be designed such that the desired speed  $v(\theta, t)$  is recovered asymptotically; that is

$$\omega \rightarrow 0 \text{ as } t \rightarrow \infty. \quad (5.40)$$

$F(x) \in \mathbb{R}^{n \times n}$  and  $g(t, x, \theta) \in \mathbb{R}^n$  depend on the control design. For the systems considered in this paper,  $F(x)$  and  $g(t, x, \theta)$  are uniformly upper bounded for bounded path and speed derivatives and there are no finite escape times for (5.39). It then follows from (5.37) and (5.38) that

$$\mathcal{M}_c = \{(z, \theta, t) : z = 0\}$$

is a UGES set of equilibrium points for (5.39). Assumption 5.2 is satisfied with  $\varepsilon = \lambda_{\min}(U)$  and  $\rho = \lambda_{\min}(P)$ .

The case study considers fully actuated tugboats in three degrees of freedom (DOF), surge, sway, and yaw. The numerical values for the vessels have been developed using the results in Fossen (2005). The 3 DOF horizontal plane vessel model is linearized for cruise speeds around  $u = 5$  m/s with nonlinear viscous quadratic damping in surge. Furthermore, the surge mode is decoupled from the sway and yaw mode due to port/starboard symmetry. The model is valid for maneuvering at cruise speed 5 m/s and the model matrices are

$$\begin{aligned} M_i &= \begin{bmatrix} 180.3 & 0 & 0 \\ 0 & 2.436 & 1.3095 \\ 0 & 1.3095 & 172.2 \end{bmatrix} \times 10^6, \\ D_i &= \begin{bmatrix} 3.883 \times 10^{-9} & 0 & 0 \\ 0 & 0.2181 & -3.434 \\ 0 & 3.706 & 26.54 \end{bmatrix} \times 10^6 \end{aligned}$$

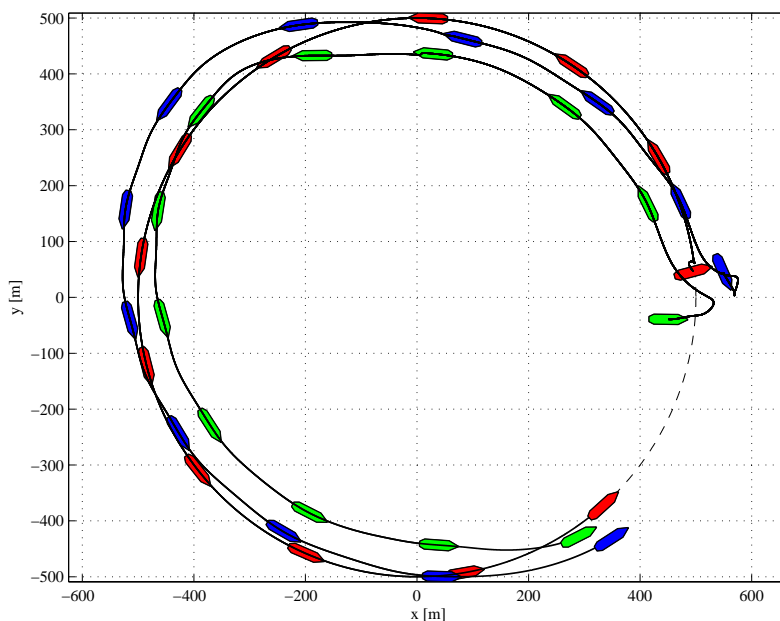


Figure 5.5: Position snapshots of three surface vessels in a formation given by (5.42) where Vessel 1 (shown in red) follows the desired path (5.41) (dashed line).

and  $D_{n,i}(\nu_i) = \text{diag}\{-2.393 \times 10^3 |u_i|, 0, 0\}$  for  $i = 1, 2, 3$ .

The goal for Vessel 1 is to follow the desired path, a circle with radius  $r = 500$ ,

$$\xi(\theta) = \begin{bmatrix} x_d(\theta) \\ y_d(\theta) \\ \psi_d(\theta) \end{bmatrix} = \begin{bmatrix} r \cos\left(\frac{\theta}{r}\right) \\ r \sin\left(\frac{\theta}{r}\right) \\ \text{atan2}\left(\frac{y_d(\theta)}{x_d(\theta)}\right) \end{bmatrix} \quad (5.41)$$

while all vessels should remain in the formation configuration given by

$$\mathcal{C}(\eta) = \begin{bmatrix} (x_1 - x_2)^2 + (y_1 - y_2)^2 - r_{12}^2 \\ (x_2 - x_3)^2 + (y_2 - y_3)^2 - r_{23}^2 \\ (x_3 - x_1)^2 + (y_3 - y_1)^2 - r_{31}^2 \end{bmatrix} = 0 \quad (5.42)$$

where  $r_{12} = 90$ ,  $r_{23} = 60$ ,  $r_{31} = 90$ . The formation is exposed to the following disturbances

$$d_1 = \begin{bmatrix} 10^5 \\ 0 \\ 0 \end{bmatrix} + \begin{bmatrix} 2 \cdot 10^4 \\ 2 \cdot 10^4 \\ 2 \cdot 10^4 \end{bmatrix} \sin(0.05t), \quad d_2 = 2 \sin(0.1t) \quad (5.43)$$

The control parameters in the maneuvering design are set as  $P = \text{diag}(0.6, 0.6, 0.6, 10, 10, 40)$  and  $U = \text{diag}(-0.6, -0.6, -0.6, -40, -40, -1600)$  while the

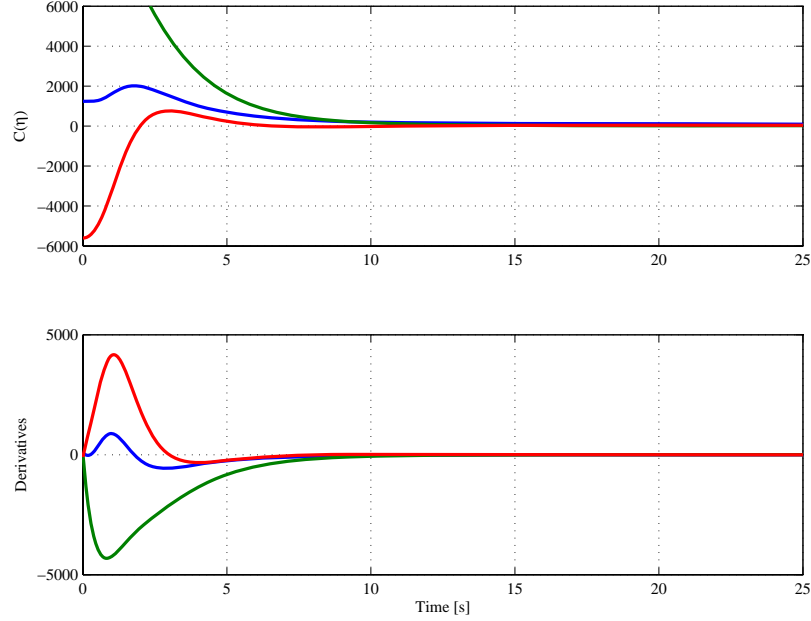


Figure 5.6: Time-response of formation constraint functions.

formation constraint functions are stabilized with  $K_p = I$  and  $K_d = 2I$ . The initial conditions for the vessels are  $\eta_1(0) = [498, 43.5, 0]^\top$ ,  $\eta_2(0) = [448, -40, \pi/2]^\top$ ,  $\eta_3(0) = [548, 48, 0, \pi/3]$ ,  $\dot{\eta}_1(0) = [1, 0, 0]$ ,  $\dot{\eta}_{2,3}(0) = 0$  and  $\theta(0) = 0$ . The speed assignment for Vessel 1,  $v_s$ , is chosen corresponding to a desired surge speed of 2 m/s along the path.

It follows from (5.19) and (5.31) that the small-gain condition (5.32) is satisfied and by Theorem 5.3 the formation with one path following controller is robust to disturbances. The position response is shown in Figure 5.5 while the constraint functions for the first 25 seconds are plotted in Figure 5.6. The plots verify that as Vessel 1 follows the desired path  $\xi(\theta)$  the vessels converge to and remain in the desired formation configuration  $\mathcal{C}(\eta) = 0$ .

## 5.6 Concluding Remarks

This chapter has considered control of a group of marine surface vessels subject to both environmental disturbances and noise and time-delays in the communication channels. We have proved robustness to external disturbances and uniform global asymptotic stability for sufficiently small time-delays by employing an ISS property.

---

The vessels in the formation are either controlled by the formation scheme only, or in addition, they are subject to a position control law. When one vessel is in closed-loop with, e.g., trajectory tracking controller, the vessel tracks its desired path while the rest of the group follows according to the formation configuration given by a set of constraint functions. The combined control approach separates the motion and formation control laws into two modules and enables the control designer to benefit from the available literature on motion control for marine systems and apply it in a formation control setting. These results can be compared to Chapter 3 where the path variables of several path following systems were synchronized using a consensus scheme: However, the approach in this chapter encompasses several motion control laws that satisfy Assumption 5.2 at the expense of communicating more signals and more conservative stability estimates.



# Chapter 6

## Final Remarks

This thesis has considered coordinated control of a group of marine vessels, and addressed related topics such as robustness to environmental disturbances and communication issues. The coordinated control problem was essentially solved by coordinating the group of individually controlled vessels such that desired formation behavior emerged, and we investigated robustness properties of schemes for coordinated control to extend the applicability of the proposed coordinated control schemes.

By exploiting the properties of a path following control system, (the *maneuvering* design controls a system along a predefined path with a dynamic assignment, often a given speed), we synchronized a group of path-following systems with little exchange of information. The position of each system was controlled by a path variable that determined the position along a corresponding path, and when the path variables had reached a consensus the group was in the desired configuration. For maneuvering systems where only parts of the state vector are measured, an output-feedback design using backstepping was proposed. The theoretical and experimental results are given in Chapter 2.

The properties of coordinated path following systems were investigated further in Chapter 3. The structural properties were exploited in a passivity approach which enables the designer to choose from an extended selection of functions for synchronization of path parameters and for fulfilling the dynamic task. These functions can be designed to enhance performance and robustness properties. Two designs, a feedback interconnected and a cascaded version, were considered in the passivity approach: the feedback interconnected version rendered the group more robust against failures in a single system while the cascaded version was more robust with respect to inter-system failures such as signal dropouts etc. The cascaded structure inherited properties from an earlier design for consensus systems, and rendered time-varying communication topologies feasible. Among other, stability was preserved when vessels entered, or left, the formation and

when signals were only communicated periodically. Both designs were extended from a continuous-time design to a sampled-data design, where path variables were communicated and updated in discrete-time and the path-following systems were updated in continuous-time. To the author's knowledge, similar results have not appeared in the literature. Finally, bias estimation was included to provide integral action to counteract environmental disturbances and model uncertainties.

A different approach to coordinated control was taken in Chapter 4 which considered a scheme for formation control using a set of constraint functions that relate group members to each other. Inspired by Lagrangian mechanics and stabilization techniques the scheme was equally useful for modeling multi-body systems as well as formation control. We have thus named this multi-body interpretation. Satisfying certain criteria a set of functions determined the formation behavior. Time-varying functions enabled shifting formation configurations. The approach was also applicable to single-vessel control, e.g., set-point regulation or trajectory tracking. A backstepping design was proposed to stabilize the formation in the presence of a priori known disturbances.

A modularity design in Chapter 5 combined the formation control scheme from Chapter 4 with a position control law for a single vessel, or with several individually controlled vessels. The group, controlled by the constraint functions, moved according to the vessel(s) with a position control law. The design was a feedback interconnection and robustness to both environmental and communication disturbances were investigated in the ISS framework. Using a loop transformation, the ISS-framework enabled us to establish a bound on the maximum delay that did not destabilize the formation.

Coordinated control is still a research field in rapid development. Future research should facilitate implementation of theoretical results to be verified experimentally. An important step is to address these topics and mathematically guarantee that a group of systems, subject to a wide range of practical challenges, can cooperate to solve a problem that is out of reach for a single system. Some interesting marine applications to consider in the future include coordinated transportation (for example of a barge or an oil rig) and distributed sensor networks. Fault tolerance should also be considered to improve robustness.

# Appendix A

## Mathematical Toolbox

This appendix contains important tools for proving stability of differential equations, or *systems* as they usually are referred to in this thesis. Some useful inequalities are also given. For completeness and convenience we repeat some of the definitions already presented in Chapter 1. The material is collected from various sources, among other, Krstić et al. (1995), Isidori (1999), Khalil (2002), Teel (2002) and Skjetne (2005). Other mathematical references used in this thesis are Meyer (2000) and Wikipedia (2006b).

### A.1 Lyapunov Stability

Consider the nonautonomous (time-varying) ordinary differential equation (ODE)

$$\dot{x} = f(t, x) \quad (\text{A.1})$$

where  $f : \mathbb{R}^n \times \mathbb{R}_{\geq 0} \rightarrow \mathbb{R}^n$  is locally Lipschitz in  $x$  and piecewise continuous in  $t$ . The ODE (A.1) is often referred to as a *system*. Locally Lipschitz implies that for a fixed  $t$  and for each point  $x \in D \in \mathbb{R}^n$ , there exists a neighborhood  $D_0 \in D$  such that

$$\|f(t, x) - f(t, y)\| \leq L \|x - y\|, \quad \forall x, y \in D_0$$

where  $L$  is called the Lipschitz constant on  $D_0$ . Let  $x(t, t_0, x(t_0))$  denote the solution of (A.1) at time  $t$  with initial time  $t_0$  and state  $x(t_0)$  where  $0 < t_0 < \infty$ . The solution is defined on some maximal interval of existence  $(-T_{\min}(x(t_0)), T_{\max}(x(t_0)))$ . The system (A.1) is called forward complete if  $T_{\max} = \infty$ , backward complete if  $T_{\min} = \infty$ , and *complete* if it is both forward and backward complete.

In Lyapunov stability we usually refer to stability of equilibrium points:

**Definition A.1** *The point  $x_e \in \mathbb{R}^n$  is the equilibrium point for (A.1) if*

$$f(t, x_e) = 0, \quad \forall t \geq 0.$$

The equilibrium point can always be shifted to the origin, so we often consider stability of  $x = 0$ . Scalar comparison functions are useful tools to define stability:

**Definition A.2** A function  $\alpha : \mathbb{R}_{\geq 0} \rightarrow \mathbb{R}_{\geq 0}$  is of class  $\mathcal{K}$  if it is continuous, strictly increasing and  $\alpha(0) = 0$ . It is of class  $\mathcal{K}_{\infty}$  if it is of class  $\mathcal{K}$  and in addition  $\lim_{s \rightarrow \infty} \alpha(s) = \infty$ .

**Definition A.3** A function  $\beta : \mathbb{R}_{\geq 0} \times \mathbb{R}_{\geq 0} \rightarrow \mathbb{R}_{\geq 0}$  is of class  $\mathcal{KL}$  if, for each fixed  $s$ , the function  $\beta(r, s)$  belongs to class  $\mathcal{K}$  with respect to  $r$  and, for each fixed  $r$ , the function  $\beta(r, s)$  is decreasing with respect to  $s$  and  $\beta(r, s) \rightarrow 0$  as  $s \rightarrow \infty$ .

We use the comparison functions to define the stability properties of the origin of (A.1), where, to ease the presentation, the solution is written as  $x(t)$ :

**Definition A.4** The equilibrium point  $x = 0$  of (A.1) is

- uniformly stable, if there exists a class function  $\alpha(\cdot)$  and a positive constant  $c$ , independent of  $t_0$ , such that

$$|x(t)| \leq \alpha(|x(t_0)|), \quad \forall t \geq t_0 \geq 0 \quad \forall x(t_0) |x(t_0) < c; \quad (\text{A.2})$$

- uniformly asymptotically stable, if there exists a class  $\mathcal{KL}$  function  $\beta(\cdot, \cdot)$  and a positive constant  $c$ , independent of  $t_0$ , such that

$$|x(t)| \leq \beta(|x(t_0)|, t - t_0), \quad \forall t \geq t_0 \geq 0 \quad \forall x(t_0) |x(t_0) < c; \quad (\text{A.3})$$

- exponentially stable, if (A.3) is satisfied with  $\beta(r, s) = kre^{-\gamma s}$ ,  $k, \gamma > 0$ ;
- uniformly globally stable (UGS), if (A.2) is satisfied with  $\alpha \in \mathcal{K}_{\infty}$  for any initial state  $x(t_0)$ ;
- uniformly globally attractive, if for each  $r, \sigma > 0$  there exists  $T > 0$  such that

$$|x(t_0)| < r \implies |x(t)| \leq \sigma, \quad \forall t = t_0 + T;$$

- uniformly globally asymptotically stable (UGAS), if it is UGS and uniformly globally attractive. This property is equal to (A.3) being satisfied for any initial state  $x(t_0)$ ; and
- globally exponentially stable, if (A.3) is satisfied with  $\beta(r, s) = kre^{-\gamma s}$ ,  $k, \gamma > 0$  and for any initial state  $x(t_0)$ .

We can the formulate the main Lyapunov stability theorem as follows

**Theorem A.1 (Lyapunov)** *Let  $x = 0$  be an equilibrium point of (A.1) and  $D = \{x \in \mathbb{R}^n : |x| < r\}$ . Let  $V : \mathbb{R}_{\geq 0} \times D \rightarrow \mathbb{R}_{\geq 0}$  be a continuously differentiable function such that  $\forall t \geq 0, \forall x \in D$ ,*

$$\begin{aligned}\alpha_1(|x|) &\leq V(t, x) \leq \alpha_2(|x|) \\ \dot{V} &= \frac{\partial V}{\partial t} + \frac{\partial V}{\partial x} f(t, x) \leq -\alpha_3(|x|),\end{aligned}$$

Then the equilibrium  $x = 0$  is

- uniformly stable, if  $\alpha_1$  and  $\alpha_2$  are class  $\mathcal{K}$  functions on  $[0, r)$  and  $\alpha_3(\cdot) \geq 0$  on  $[0, r)$ ;
- uniformly asymptotically stable, if  $\alpha_1, \alpha_2$  and  $\alpha_3$  are class  $\mathcal{K}$  functions on  $[0, r)$ ;
- exponentially stable, if  $\alpha_i(\rho) = k_i \rho^\gamma$  on  $[0, r)$ ,  $k_i > 0, \gamma > 0, i = 1, 2, 3$ ;
- globally uniformly stable; if  $D = \mathbb{R}^n$ ,  $\alpha_1$  and  $\alpha_2$  are class  $\mathcal{K}_\infty$  functions and  $\alpha_3(\cdot) \geq 0$  on  $\mathbb{R}_{\geq 0}$ ;
- uniformly globally asymptotically stable, if  $D = \mathbb{R}^n$ ,  $\alpha_1$  and  $\alpha_2$  are class  $\mathcal{K}_\infty$  functions and  $\alpha_3$  is a class  $\mathcal{K}$  function on  $\mathbb{R}_{\geq 0}$ ; and
- globally exponentially stable, if  $D = \mathbb{R}^n$  and  $\alpha_i(\rho) = k_i \rho^\gamma$  on  $\mathbb{R}_{\geq 0}$ ,  $k_i > 0, \gamma > 0, i = 1, 2, 3$ .

□

**Remark A.1** *It is not necessary to establish uniform convergence for time-invariant systems since Hale & Lunel (1993, Ch. 6, Lemma 1.1) show that, in this case, asymptotic stability implies uniform asymptotic stability.*

In many model-based control applications it is natural to use the closed-loop energy function as a candidate Lyapunov function. However, the time derivative of this function is often only negative semi-definite. For autonomous, or time-invariant, systems on the form

$$\dot{x} = f(x) \tag{A.4}$$

the Krasowskii-LaSalle invariance theorem and its stability corollary can be used to conclude global asymptotic stability – see Krasowskii (1959) and LaSalle (1960).

**Theorem A.2 (Krasowskii-LaSalle)** *Let  $\Omega$  be a positively invariant set of (A.4). Let  $V : \Omega \rightarrow \mathbb{R}_{\geq 0}$  be a continuously differentiable function  $V(x)$  such that  $\dot{V}(x) \leq 0$ ,  $\forall x \in \Omega$ . Let  $E = \{x \in \Omega : \dot{V}(x) = 0\}$ , and let  $M$  be the largest invariant set contained in  $E$ . Then, every bounded solution  $x(t)$  starting in  $\Omega$  converges to  $M$  as  $t \rightarrow \infty$ .  $\square$*

**Corollary A.1 (Asymptotic Stability)** *Let  $x = 0$  be the only equilibrium of (A.4). Let  $V : \mathbb{R}^n \rightarrow \mathbb{R}_{\geq 0}$  be a continuously differentiable, positive definite, radially unbounded function  $V(x)$  such that  $\dot{V}(x) \leq 0$ ,  $\forall x \in \mathbb{R}^n$ . Let  $E = \{x \in \mathbb{R}^n : \dot{V}(x) = 0\}$ , and suppose that no solution other than  $x(t) \equiv 0$  can stay forever in  $E$ . Then, the origin is globally asymptotically stable.*

This is often referred to as the Krasowskii-LaSalle invariance principle. For nonautonomous systems Barbalat's lemma and the following corollary can guarantee convergence.

**Lemma A.1 (Barbalat)** *Let  $\phi : \mathbb{R} \rightarrow \mathbb{R}$  be a uniformly continuous function on  $[0, \infty)$ . Suppose that  $\lim_{t \rightarrow \infty} \int_0^t \phi(\tau) d\tau$  exists and is finite. Then,*

$$\phi(t) \rightarrow 0 \text{ as } t \rightarrow \infty.$$

**Corollary A.2** *Consider the function  $\phi : \mathbb{R} \rightarrow \mathbb{R}$ . If  $\phi, \dot{\phi} \in \mathcal{L}_{\infty}$ , and  $\phi \in \mathcal{L}_p$  for some  $p \in [1, \infty)$ , then*

$$\lim_{t \rightarrow \infty} \phi(t) = 0$$

Analogous to the Krasowskii-LaSalle invariance principle, Matrosov's (1962) theorem can be used to check for uniform global asymptotic stability in the case of a negative semi-definite  $\dot{V}$  for time-variant systems. The following theorem is an adapted version from Loría et al. (2005):

**Theorem A.3 (Matrosov)** *The origin of the system (A.1) is uniformly globally asymptotically stable under the following assumptions:*

1. *The origin of the system (A.1) is uniformly globally stable.*
2. *There exist integers  $j, m > 0$  and for each  $\Delta > 0$  there exist*
  - *a number  $\mu > 0$ ,*
  - *locally Lipschitz continuous functions  $V_i : \mathbb{R} \times \mathbb{R}^n \rightarrow \mathbb{R}$ ,  $i \in \{1, \dots, j\}$ ,*
  - *a (continuous) function  $\phi : \mathbb{R}^n \times \mathbb{R} \rightarrow \mathbb{R}^m$ ,  $i \in \{1, \dots, j\}$ ,*

- continuous functions  $Y_i : \mathbb{R}^n \times \mathbb{R}^m \rightarrow \mathbb{R}$ ,  $i \in \{1, \dots, j\}$ , such that, for almost all  $(t, x) \in \mathbb{R} \times B(\Delta)$ ,

$$\begin{aligned} \max \{|V_i(t, x)|, |\phi(t, x)|\} &\leq \mu \\ \dot{V}_i(t, x) &\leq Y_i(x, \phi(t, x)) \end{aligned}$$

where  $B(r) := \{x \in \mathbb{R}^n : |x| \leq r\}$ .

3. For each integer  $k \in \{1, \dots, j\}$  we have that

$$\begin{aligned} \{(z, \psi) \in \mathcal{B}(\Delta) \times \mathcal{B}(\mu), Y_i(z, \psi) = 0, \forall i \in \{1, \dots, k-1\}\} \\ \Downarrow \\ \{Y_k(z, \psi) \leq 0\}. \end{aligned}$$

4. We have that

$$\begin{aligned} \{(z, \psi) \in \mathcal{B}(\Delta) \times \mathcal{B}(\mu), Y_i(z, \psi) = 0, \forall i \in \{1, \dots, j\}\} \\ \Downarrow \\ \{z = 0\}. \end{aligned}$$

□

**Set Stability** We can also consider other attractors than the compact equilibrium set  $\mathcal{A}_e = \{x \in \mathbb{R}^n : x = x_e\}$ . A set  $\mathcal{A}$  is forward invariant if  $\forall x(t_0) \in \mathcal{A}$  the solution  $x(t, t_0, x(t_0)) \in \mathcal{A} \quad \forall t \geq t_0$ . Such attractors can be closed, compact, or noncompact subsets of the state space. To measure the distance away from the set, the distance to the set is defined as

$$|x|_{\mathcal{A}} := d(x; \mathcal{A}) = \inf \{d(x, y) : y \in \mathcal{A}\}$$

where  $d(x, y) = |x - y|$  is the Euclidean distance. For noncompact sets a solution may escape to infinity in finite time within the set. Thus, forward completeness is a requirement in stability analysis of such sets, and can be established by using finite escape-time detectability – Teel (2002).

**Definition A.5** A nonempty closed set  $\mathcal{A} \subseteq \mathbb{R}^n$  is a forward invariant set for (A.1) if the system is forward complete and  $\forall x(t_0) \in \mathcal{A}$  the solution  $x(t, x(t_0)) \in \mathcal{A}$ ,  $\forall t \geq 0$ .

Assume that the system (A.1) is forward complete. For stability definitions of a closed forward invariant set  $\mathcal{A} \subseteq \mathbb{R}^n$ , we have equivalent statements as in Definition A.4 when we replace the equilibrium point  $x = 0$  with  $\mathcal{A}$  and  $|\cdot|$  with  $|\cdot|_{\mathcal{A}}$ . When  $\mathcal{A}$  is compact the system is finite escape time detectable and the forward completeness assumption is redundant. Several results on set stability and, in particular, converse theorems are presented in Lin, Sontag & Wang (1996) and Teel & Praly (2000).

## A.2 Input-to-State Stability

Input-to-State Stability (ISS) introduced by Sontag (1989, 2000) relates the norm of the solution to the input:

**Definition A.6** *The system*

$$\dot{x} = f(t, x, u) \quad (\text{A.5})$$

where  $f$  is piecewise continuous in  $t$  and locally Lipschitz in  $x \in \mathbb{R}^n$  and  $u \in \mathbb{R}^m$ , is said to be Input-to-State Stable if there exist a class  $\mathcal{KL}$  function  $\beta$  and a class  $\mathcal{K}$  function  $\gamma$ , such that, for any  $x(t_0)$  and for any input  $u(\cdot) \in \mathcal{L}_\infty^m$  (continuous and bounded on  $[0, \infty)$ ) the solution exists for all  $t \geq 0$  and satisfies

$$|x(t)| \leq \beta(|x(t_0)|, t - t_0) + \gamma\left(\sup_{t_0 \leq \tau \leq t} |u(\tau)|\right) \quad (\text{A.6})$$

for all  $t_0$  and  $t$  such that  $0 \leq t_0 \leq t$ .

**Remark A.2** *An alternative way to say that a system is Input-to-State Stable is that there exist a class  $\mathcal{KL}$  function  $\beta$  and a class  $\mathcal{K}$  function  $\gamma$ , such that, for any  $x(t_0)$  and for any input  $u(\cdot) \in \mathcal{L}_\infty^m$  the solution satisfies*

$$|x(t)| \leq \max\{\beta(|x(t_0)|, t - t_0), \gamma(|u(\cdot)|_\infty)\},$$

where  $|u(\cdot)|_\infty = \sup_{t_0 \leq \tau \leq t} |u(\tau)|$ , and exists for all  $t \geq 0$ . It then follows that the response  $x(t)$  to any input  $u(\cdot) \in \mathcal{L}_\infty^m$  is always bounded and, in particular,

$$\begin{aligned} |x(\cdot)|_\infty &\leq \max\{\gamma_0(|x(t_0)|), \gamma(|u(\cdot)|_\infty)\} \\ |x(t)|_a &\leq \gamma(|u(t)|_a) \end{aligned}$$

where  $|d|_a = \lim_{t \rightarrow \infty} \sup |d(t)|$  for  $d \in \mathcal{L}_\infty$ .

The inequality (A.6), with  $u(t) \equiv 0$ , reduces to

$$|x(t)| \leq \beta(|x(t_0)|, t - t_0)$$

which shows that ISS implies that the origin of the unforced system

$$\dot{x} = f(t, x, 0)$$

is uniformly globally asymptotically stable. The following Lyapunov-like theorem gives a sufficient condition for Input-to-State Stability:

**Theorem A.4** Let  $V : \mathbb{R}_{\geq 0} \times \mathbb{R}^n \rightarrow \mathbb{R}$  be a continuously differentiable function for (A.5) such that,

$$\begin{aligned} \alpha_1(|x|) &\leq V(t, x) \leq \alpha_2(|x|) \\ |x| \geq \rho(|u|) &\implies \dot{V} = \frac{\partial V}{\partial t} + \frac{\partial V}{\partial x} f(t, x) \leq -\alpha_3(|x|), \end{aligned}$$

$\forall (t, x, u) \in \mathbb{R}_{\geq 0} \times \mathbb{R}^n \times \mathbb{R}^m$ , where  $\alpha_1, \alpha_2, \rho$  are class  $\mathcal{K}_\infty$  functions and  $\alpha_3$  is a class  $\mathcal{K}$  function. Then, the system (A.5) is Input-to-State Stable with  $\gamma = \alpha_1^{-1} \circ \alpha_2 \circ \rho$ , and  $V$  is an ISS-Lyapunov function.  $\square$

## A.3 Passivity

Passivity is a structural property and not explicitly dependent on model parameters. Thus, it is a useful tool to prove stability for a system with uncertain model parameters. It became a fundamental feedback control concept in the seminal work of Popov (1966). Consider systems on the form

$$\begin{aligned} \dot{x} &= f(x, u) \\ y &= h(x, u) \end{aligned} \tag{A.7}$$

with  $x \in \mathbb{R}^n$ ,  $y \in \mathbb{R}^m$ ,  $u \in \mathbb{R}^m$ ,  $f, h$  continuous,  $f(0, 0) = 0$  and  $h(0, 0) = 0$ .

**Definition A.7** The system (A.7) is passive if there exists a continuous nonnegative (storage) function  $V : \mathbb{R}^n \rightarrow \mathbb{R}_{\geq 0}$ , which satisfies  $V(0, t) = 0$ ,  $\forall t \geq 0$ , such that for all continuous  $u$ ,  $x \in \mathbb{R}^n$ ,  $t \geq t_0 \geq 0$

$$\int_{t_0}^t y(\sigma)^\top u(\sigma) d\sigma \geq V(x(t)) - V(x(t_0)).$$

**Definition A.8** The system (A.7) is strictly passive if there exists a continuous nonnegative (storage) function  $V : \mathbb{R}^n \rightarrow \mathbb{R}_{\geq 0}$ , which satisfies  $V(0, t) = 0$ ,  $\forall t \geq 0$ , and a positive definite function (dissipation rate)  $\psi : \mathbb{R}^n \rightarrow \mathbb{R}_{\geq 0}$ , such that for all continuous  $u$ ,  $x \in \mathbb{R}^n$ ,  $t \geq t_0 \geq 0$

$$\int_{t_0}^t y(\sigma)^\top u(\sigma) d\sigma \geq V(x(t)) - V(x(t_0)) + \int_{t_0}^t \psi(x(\sigma)) d\sigma.$$

Passivity and Lyapunov stability are related through the following definition and lemma:

**Definition A.9** *The system (A.7) is passive if there exists a continuous differentiable nonnegative (storage) function  $V(x)$  such that*

$$u^\top y \geq \dot{V} = \frac{\partial V}{\partial x} f(x, u), \quad \forall (x, u) \in \mathbb{R}^n \times \mathbb{R}^m.$$

Moreover, it is said to be

- lossless if  $u^\top y = \dot{V}$ .
- output strictly passive if  $u^\top y = \dot{V} + y^\top \rho(y)$  and  $y^\top \rho(y) > 0, \quad \forall y \neq 0$ .
- strictly passive if  $u^\top y = \dot{V} + \psi(x)$  for some positive definite function  $\psi$ .

In all cases, the inequality should hold for all  $(x, u)$ .

**Lemma A.2** *Suppose the system (A.7) is (strictly) passive. If there exists  $\alpha_1, \alpha_2 \in \mathcal{K}_\infty$  such that  $\alpha_1(|x|) \leq V(x) \leq \alpha_2(|x|), \quad \forall x \in \mathbb{R}^n$ , then for  $u \equiv 0$ , the origin of (A.7) is uniformly globally (asymptotically) stable.*

The system (A.7) is *zero-state observable* if no solution of  $\dot{x} = f(x, 0)$  can stay identically in the subset  $S = \{x \in \mathbb{R}^n : h(x, 0) = 0\}$ , other than the trivial solution  $x(t) \equiv 0$ . Memoryless functions can also be characterized by their passivity properties: A static nonlinearity  $y = h(u)$  is passive if, for all  $u \in \mathbb{R}^m$ ,

$$u^\top y = u^\top h(u) \leq 0; \tag{A.8}$$

and strictly passive if (A.8) holds with strict inequality  $\forall u \neq 0$ .

**Positive Real Transfer Functions** For linear time-invariant passive systems we have

**Definition A.10** *A  $p \times p$  proper rational transfer function matrix  $G(s)$  is called positive real if*

- poles of all elements of  $G(s)$  are in  $\text{Re}[s] \leq 0$ ,
- for all real  $\omega$  for which  $j\omega$  is not a pole of any element of  $G(s)$ , the matrix  $G(j\omega) + G(-j\omega)^\top$  is positive semidefinite, and
- any pure imaginary pole  $j\omega$  of any element of  $G(s)$  is a single pole and the residue matrix  $\lim_{s \rightarrow j\omega} (s - j\omega) G(s)$  is positive semidefinite Hermitian.

**Lemma A.3** Let  $G(s)$  be a  $p \times p$  proper rational transfer function matrix, and suppose

$$\det \left[ G(s) + G(s)^\top \right]$$

is not identically zero. Then,  $G(s)$  is strictly positive real if and only if:

- $G(s)$  is Hurwitz; that is, poles of all elements of  $G(s)$  have negative real parts
- $G(j\omega) + G(-j\omega)^\top$  is positive definite for  $\omega \in R$ , and
- either  $G(\infty) + G(\infty)^\top$  is positive definite or it is positive semidefinite and

$$\lim_{\omega \rightarrow \infty} \omega^2 M^\top \left[ G(\infty) + G(\infty)^\top \right] M$$

is positive definite for any  $p \times (p - q)$  full-rank matrix  $M$  such that

$$M^\top \left[ G(\infty) + G(\infty)^\top \right] M = 0,$$

where  $q = \text{rank} \left[ G(\infty) + G(\infty)^\top \right]$ .

Passivity properties of positive real transfer functions can be shown by the following two lemmas, known as the *positive real lemma* and the *Kalman-Yakubovich-Popov lemma*:

**Lemma A.4 (Positive Real)** Let

$$G(s) = D + C(sI - A)^{-1}B,$$

be a  $p \times p$  transfer function matrix where  $(A, B)$  is controllable and  $(A, C)$  is observable. Then  $G(s)$  is positive real if and only if there exist matrices  $P = P^\top > 0$ ,  $L$  and  $W$  such that

$$\begin{aligned} PA + A^\top P &= -L^\top L \\ PB &= C^\top - L^\top W \\ W^\top W &= D + D^\top. \end{aligned}$$

**Lemma A.5 (Kalman-Yakubovich-Popov)** Let  $G(s) = D + C(sI - A)^{-1}B$ , be a  $p \times p$  transfer function matrix where  $(A, B)$  is controllable and  $(A, C)$  is observable. Then  $G(s)$  is strictly positive real if and only if there exist matrices  $P = P^\top > 0$ ,  $L$  and  $W$ , and a positive constant  $\varepsilon$  such that

$$\begin{aligned} PA + A^\top P &= -L^\top L - \varepsilon P \\ PB &= C^\top - L^\top W \\ W^\top W &= D + D^\top. \end{aligned}$$

Then,

**Lemma A.6** *The linear time-invariant minimal realization*

$$\begin{aligned}\dot{x} &= Ax + Bu \\ y &= Cx + Du\end{aligned}$$

with  $G(s) = D + C(sI - A)^{-1}B$  is (strictly) passive if  $G(s)$  is (strictly) positive real.

## A.4 Stability of Interconnected Systems

### A.4.1 Stability of Feedback Systems

**ISS Small-Gain Theorem** Jiang et al. (1995) used a small-gain argument to prove that the feedback interconnection of two ISS-systems is again an ISS system if the composition of their gain functions are smaller than the identity function. Consider the following interconnected system

$$\begin{aligned}\dot{x}_1 &= f_1(x_1, x_2) \\ \dot{x}_2 &= f_2(x_1, x_2, u)\end{aligned}\tag{A.9}$$

where  $x_1 \in \mathbb{R}^{n_1}$ ,  $x_2 \in \mathbb{R}^{n_2}$ ,  $u \in \mathbb{R}^m$  and  $f_1(0, 0) = f_2(0, 0, 0) = 0$ . Suppose that the first subsystem with is ISS with  $x_2$  as input, and the second subsystem is ISS with  $x_1$  and  $u$  as inputs. In view of the ISS results this hypothesis is equivalent to the existence of class  $\mathcal{K}$  functions  $\gamma_{01}$ ,  $\gamma_1$ ,  $\gamma_{02}$ ,  $\gamma_2$ ,  $\gamma_u$  such that, for all  $t \geq 0$ ,

$$\begin{aligned}|x_1(t)| &\leq \max\{\gamma_{01}(x_1(t_0)), \gamma_1(|x_2|_\infty)\} \\ |x_2(t)| &\leq \max\{\gamma_{02}(|x_2(t_0)|), \gamma_2(|x_1|_\infty), \gamma_u(|u|_\infty)\}\end{aligned}$$

and

$$\begin{aligned}|x_1(t)|_a &\leq \gamma_1(|x_2(t)|_a) \\ |x_2(t)|_a &\leq \max\{\gamma_2(|x_1(t)|_a), \gamma_u(|u(t)|_a)\}\end{aligned}$$

to any input  $x_2 \in \mathcal{L}_\infty^{n_2}$  and  $x_1 \in \mathcal{L}_\infty^{n_1}$ ,  $u \in \mathcal{L}_\infty^m$  respectively.

**Theorem A.5 (Small-Gain)** *If the composite function  $\gamma_1 \circ \gamma_2(\cdot)$  is a contraction, i.e. if*

$$\gamma_1(\gamma_2(r)) < r \quad \forall r > 0$$

the system (A.9), with state  $x = [x_1^\top, x_2^\top]^\top$  and input  $u$ , is Input-to-State Stable. In particular, the class  $\mathcal{K}$  functions

$$\begin{aligned}\gamma_0(r) &= \max \{2\gamma_{01}(r), 2\gamma_{02}(r), 2\gamma_1 \circ \gamma_{02}(r), 2\gamma_2 \circ \gamma_{01}(r)\} \\ \gamma(r) &= \max \{2\gamma_1 \circ \gamma_u(r), 2\gamma_u(r)\}\end{aligned}$$

are such that the response  $x(t)$  to any input  $u \in \mathcal{L}_\infty^m$  is bounded and

$$\|x\|_\infty \leq \max \{\gamma_0(\|x(t_0)\|), \gamma(\|u\|_\infty)\}.$$

**Passivity Theorems** Passivity was first used in network synthesis and is a very useful tool when studying feedback interconnections:

$$\Sigma_i : \begin{cases} \dot{x}_i = f_i(x_i, u_i) \\ y_i = h_i(x_i, u_i) \end{cases} \quad \text{for } i = 1, 2 \quad (\text{A.10})$$

connected by

$$\begin{aligned}u_1 &= -y_2 + v_1 \\ u_2 &= y_1 + v_2\end{aligned} \quad (\text{A.11})$$

where  $v_1, v_2$  are new inputs to the system.

**Theorem A.6 (Passivity Theorem)** *Suppose the system  $\Sigma_1$  is (strictly) passive with storage function  $V_1$  (and dissipation rate  $\psi_1$ ) independent of  $x_2$ . Likewise, suppose the system  $\Sigma_2$  is (strictly) passive with storage function  $V_2$  (and dissipation rate  $\psi_2$ ) independent of  $x_1$ . Then, the interconnected system (A.10)-(A.11) with input  $v_1, v_2$  and output  $y_1, y_2$  is*

1. strictly passive if both  $\Sigma_1$  and  $\Sigma_2$  are strictly passive,
2. passive if at least one of the systems  $\Sigma_1$  and  $\Sigma_2$  is passive but not strictly passive.

Moreover, when  $v_1, v_2 \equiv 0$ , if  $\Sigma_1$  is strictly passive and  $\Sigma_2$  is passive, then the equilibrium  $x = 0$  is globally stable and  $\lim_{t \rightarrow \infty} x_1(t) = 0$ .  $\square$

**Theorem A.7** *Consider the feedback interconnection of two systems as in (A.10)-(A.11). When  $v_1, v_2 \equiv 0$ , the origin of the interconnection is asymptotically stable if*

- both feedback components are strictly passive,
- both feedback components are output strictly passive and zero-state observable, or
- one component is strictly passive and the other one is output strictly passive and zero-state observable.

Furthermore, if the storage function for each component is radially unbounded, the origin is globally asymptotically stable.  $\square$

## A.4.2 Stability of Cascaded Systems

Cascaded time-invariant systems has been studied for many different classes of interconnection—e.g. Janković, Sepulchre & Kokotović (1996).

Consider the cascade nonlinear time-varying system

$$\Sigma_1 : \dot{x}_1 = f_1(t, x_1) + g(t, x) x_2 \quad (\text{A.12})$$

$$\Sigma_2 : \dot{x}_2 = f_2(t, x_2) \quad (\text{A.13})$$

where  $f_1$  and  $f_2$  are piecewise continuous in  $t$  and locally Lipschitz in  $x = [x_1, x_2]^\top$ , and  $g$  is locally Lipschitz in  $x$ . Suppose both

$$\dot{x}_1 = f_1(t, x_1) \quad (\text{A.14})$$

and (A.13) have uniformly globally asymptotically stable origins. Panteley and Loria (1998, 2001) have studied these forms of cascaded interconnections and shown that solutions must be bounded to conclude stability. That is,

$$\text{UGAS} + \text{UGAS} + \text{UGB} \implies \text{UGAS},$$

as formalized in the following lemma:

**Lemma A.7** *If the origins of (A.13) and (A.14) are UGAS and the solutions of (A.12) and (A.13) are globally uniformly bounded, then the origin of (A.12) and (A.13) is UGAS.*

The concept of Input-to-State Stability can be used to prove bounded solutions and hence stability of (A.13) and (A.14). Lemma 4.8 from Khalil (2002) shows GAS of the cascades origin  $x = 0$ .

**Lemma A.8** *Under the stated assumptions, if the system (A.12), with  $x_2$  as input, is Input-to-State Stable and the origin of (A.13) is uniformly globally asymptotically stable, then the origin of the cascade system (A.12) and (A.13) is uniformly globally asymptotically stable.*

The ISS property is invariant for cascaded interconnections and can thus be applied to a long chain of ISS systems—Sontag (1989), Sontag & Teel (1995).

Depending on the structure of  $f_1$  and  $g$ , there are different ways to show that the solutions are uniformly globally bounded. One method is to use the theorem from Panteley & Loria (1998):

**Theorem A.8** *The cascaded system (A.12) and (A.13) is UGAS if the following assumptions hold:*

- A1: a) The subsystem (A.14) is UGAS, or b) There exists a continuously differentiable function  $V(t, x) : \mathbb{R}_{\geq 0} \times \mathbb{R} \rightarrow \mathbb{R}$ ,  $\alpha_1, \alpha_2 \in K_\infty$ , a positive semi-definite function  $W(x_1)$ , and a continuous non-decreasing function  $\alpha_4(\cdot)$  such that

$$\begin{aligned} \alpha_1(|x_1|) &\leq V(t, x_1) \leq \alpha_2(|x_2|) \\ \frac{\partial V}{\partial t} + \frac{\partial V}{\partial x_1} f_1(t, x) &\leq -W(x_1) \\ \left| \frac{\partial V}{\partial x_1} \right| &\leq \alpha_4(|x_1|) \end{aligned}$$

- A2: The subsystem (A.13) is UGAS
- A3: There exists constants  $c_1, c_2, \eta > 0$  and a Lyapunov function for (A.14), such that  $V(t, x) : \mathbb{R}_{\geq 0} \times \mathbb{R} \rightarrow \mathbb{R}$  is positive definite and radially unbounded, which satisfies

$$\begin{aligned} \left| \frac{\partial V}{\partial x_1} \right| |x_1| &\leq c_1 V(t, x_1) \quad \forall x_1 \geq \eta \\ \left| \frac{\partial V}{\partial x_1} \right| &\leq c_2 \quad \forall x_1 \geq \eta \end{aligned}$$

- A4: There exist two continuous functions  $\theta_1, \theta_2 : \mathbb{R}_{\geq 0} \rightarrow \mathbb{R}_{\geq 0}$ , such that  $g(t, x)$  satisfies

$$|g(t, x)| \leq \theta_1(|x_2|) + \theta_2(|x_2|) |x_1|$$

- A5: There exist a class  $\mathcal{K}$  function  $\alpha(\cdot)$  such that, for all  $t_0 \geq 0$ , the trajectories of the system (A.13) satisfy

$$\int_{t_0}^{\infty} |x_2(t, t_0, x_2(t_0))| dt \leq \alpha(|x_2(t_0)|).$$

□

When the subsystems of the cascade has exponentially stable origins, the origin of the cascade system will be exponentially stable – Panteley, Lefeber, Loría & Nijmeijer (1998)

**Lemma A.9** *If, in addition to Assumptions A3-A5 in Theorem A.8, both subsystems are exponentially stable in any ball, then the cascaded system (A.12)-(A.13) is exponentially stable in any ball.*

## A.5 Useful Inequalities

**Cauchy-Schwarz Inequality** If  $x$  and  $y$  are elements of real or complex inner product spaces then

$$|\langle x, y \rangle|^2 \leq \langle x, x \rangle \langle y, y \rangle .$$

Inequality holds if and only if  $x$  and  $y$  are linearly dependent (or in geometrical sense they are parallel). This contrasts with a property that the inner product of two vectors is zero if they are orthogonal (or perpendicular) to each other.

Using the norm notation, we have

$$|\langle x, y \rangle| \leq |x| |y| .$$

In the case of the Euclidean space  $\mathbb{R}^n$ , we get

$$\left( \sum_{i=1}^n x_i y_i \right)^2 \leq \left( \sum_{i=1}^n x_i^2 \right) \left( \sum_{i=1}^n y_i^2 \right) .$$

For the inner product space of square-integrable complex-valued functions, one has

$$\left| \int f^*(x) g(x) dx \right|^2 \leq \int |f(x)|^2 dx \int |g(x)|^2 dx .$$

**Triangle Inequality** The triangle inequality for the inner product is often shown as a consequence of the Cauchy-Schwarz inequality:

$$\begin{aligned} |x + y|^2 &= \langle x + y, x + y \rangle \\ &= |x|^2 + \langle x, y \rangle + \langle y, x \rangle + |y|^2 \\ &\leq |x|^2 + 2|\langle x, y \rangle| + |y|^2 \\ &\leq |x|^2 + 2|x||y| + |y|^2 \\ &= (|x| + |y|)^2 . \end{aligned}$$

Taking the square root of both sides gives the triangle inequality.

**Young's Inequality** If  $a, b, p, q$  are real numbers with

$$\frac{1}{p} + \frac{1}{q} = 1$$

then we have

$$ab \leq \frac{a^p}{p} + \frac{b^q}{q} .$$

In the case where  $p = q = 2$  we obtain, for  $x, y$  positive real,

$$(x + y)^2 = x^2 + 2xy + y^2 \leq 2(x^2 + y^2) .$$

# Appendix B

## Mathematical Modeling of Marine Vessels

The notation in this thesis is adopted from SNAME (1950), Fossen (2002), Perez (2005), and Ross, Perez & Fossen (2006): The generalized position, velocity, and force vectors in six degrees of freedom are

$$\eta := [x, y, z, \phi, \theta, \psi]^T \in \mathbb{R}^3 \times \mathcal{S}^3$$

$$\nu := [u, v, w, p, q, r]^T \in \mathbb{R}^6$$

$$\tau := [X, Y, Z, K, M, N]^T \in \mathbb{R}^6$$

where  $\mathbb{R}^n$  is the Euclidean  $n$ -dimensional space and  $\mathcal{S}^3$  is a three-dimensional sphere. The longitudinal and sideways motion is referred to as surge and sway, respectively. Heading, or yaw, describes the vessels course. The following section shows how the equations of motion for a marine vessel are written as

$$\dot{\eta} = J(\eta) \nu \quad (\text{B.1a})$$

$$M\dot{\nu} + C(\nu)\nu + D(\nu)\nu + g(\eta) = \tau + \tau_{\text{env}} \quad (\text{B.1b})$$

where  $M$  is the system inertia matrix,  $C(\nu)$  is the coriolis-centripetal matrix, and  $D(\nu)$  is the damping matrix. The vector  $g(\eta)$  consists of restoring forces and moments,  $\tau$  is a vector of generalized control forces, and  $\tau_{\text{env}}$  is a vector of environmental disturbances.

### B.1 Vessel Kinematics

The kinematics describes the geometrical aspects of motion, and the main reference frames used in this thesis are

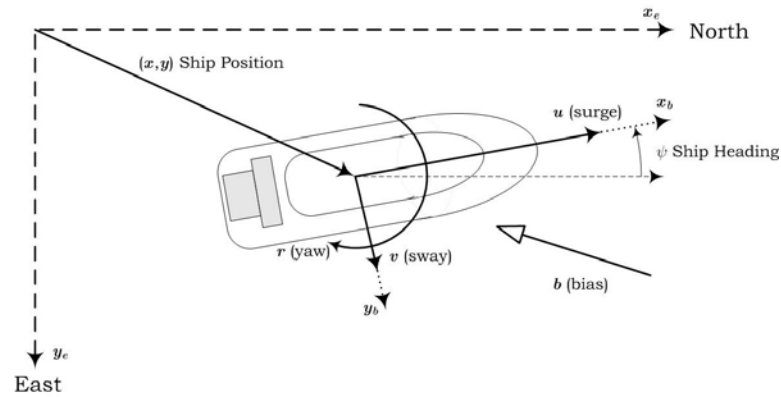


Figure B.1: A ship moving on the ocean surface. The NED and the body-fixed reference frame are related via the heading angle  $\psi$ .

- **BODY (b-frame).** The body-fixed reference frame  $x_b y_b z_b$  is a moving coordinate frame fixed to the vessel. The position and orientation of the vessel are described relative to an inertial reference frame, while the linear and angular velocities of the vessel are expressed in the body-fixed coordinate system.
- **NED (n-frame).** The North-East-Down coordinate system  $x_n y_n z_n$  is defined relative to the Earth's reference ellipsoid, and is usually defined as the tangent plane on the Earth's surface moving with the vessel. The  $x_n$ -axis points toward true North, the  $y_n$ -axis towards East, while the  $z_n$ -axis points downwards normal to the Earth's surface.

For marine vessels operating in a local area, an Earth-fixed tangent plane on the surface is used for navigation and is usually referred to as flat Earth navigation—see Figure B.1. Due to the vessel's low speed relative to the Earth's rotation we assume that the NED frame is inertial. For ships en route between continents a star-fixed reference frame is used as the inertial frame—see Perez (2005) for further details on reference frames for marine control systems..

### Transformation between the $b$ - and $n$ -frame

The body-fixed velocities are transformed to the Earth-fixed frame given by

$$\dot{\eta} = J(\eta) \nu \quad (\text{B.2})$$

where the transformation matrix is block-diagonal

$$J(\eta) = \begin{bmatrix} R(\Theta) & 0 \\ 0 & T_{\Theta}(\Theta) \end{bmatrix}$$

and  $\Theta = [\phi, \theta, \psi]^\top$  contains the Euler angles.

The linear velocity transformation  $R(\Theta)$  is usually described by three rotations about the  $z$ ,  $y$ , and  $x$  axes, the so called  $zyx$ -convention,

$$R(\Theta) := R_{z,\psi}R_{y,\theta}R_{z,\phi}$$

where  $R_{a,\beta}$  is a rotation by an angle  $\beta$  around the  $a$ -axis. Each rotation matrix is an element in  $SO(3)$ , the special orthogonal group of order 3:

$$SO(3) = \{R | R \in \mathbb{R}^{3 \times 3}, \quad RR^\top = R^\top R = I \text{ and } \det R = 1\}.$$

Since  $R$  is orthogonal, the inverse rotation matrix is given by

$$R(\Theta)^{-1} = R(\Theta)^\top.$$

Furthermore, the derivative of the rotation matrix between the BODY and NED reference frame is

$$\frac{d}{dt}R(\Theta) = R(\Theta)S(\nu)$$

where  $S : \mathbb{R}^3 \rightarrow \mathbb{R}^{3 \times 3}$  is the cross-product operator

$$S(\alpha) = -S(\alpha)^\top = \begin{bmatrix} 0 & -\alpha_3 & \alpha_2 \\ \alpha_3 & 0 & -\alpha_1 \\ -\alpha_2 & \alpha_1 & 0 \end{bmatrix}, \quad \alpha = \begin{bmatrix} \alpha_1 \\ \alpha_2 \\ \alpha_3 \end{bmatrix}.$$

$S(\nu)$  is in fact skew-symmetric, that is,  $S(\nu) = -S(\nu)^\top$ .

The angular velocity transformation is given by

$$T_\Theta(\Theta) = \begin{bmatrix} 1 & \sin \phi \tan \theta & \cos \phi \tan \theta \\ 0 & \cos \phi & -\sin \phi \\ 0 & \frac{\sin \phi}{\cos \theta} & \frac{\cos \phi}{\cos \theta} \end{bmatrix}, \quad \theta \neq \frac{\pi}{2}$$

which is singular for  $\theta = \pm 90^\circ$ . By using e.g. unit quaternions this singularity is avoided at the cost of using four, instead of three, parameters to describe the vessel's orientation.

## B.2 Vessel Kinetics

The vessel kinetics describes the forces acting on the vessel and the resulting motion. The equations of motion are derived from both rigid-body- and hydrodynamics.

### Rigid-Body Dynamics

The rigid-body equations of motion are obtained either via a Newton-Euler or a Lagrangian approach. They are expressed in the  $b$ -frame as

$$M_{RB}\dot{\nu} + C_{RB}(\nu)\nu = \tau_{RB} \quad (\text{B.3})$$

where  $\tau_{RB}$  is a generalized vector of external forces and moments. The generalized mass matrix  $M_{RB} = M_{RB}^\top > 0$  is written as

$$M_{RB} := \begin{bmatrix} mI & -mS(r_g^b) \\ mS(r_g^b) & I^b \end{bmatrix}$$

where  $m$  is the rigid body mass,  $r_g^b = [x_g, y_g, z_g]^\top$  is the vector from the origin of the  $b$ -frame to the center of gravity, and  $I_b = I_b^\top > 0$  is the rigid body inertia tensor with respect to the origin

$$I_b = \begin{bmatrix} I_x & -I_{xy} & -I_{xz} \\ -I_{yx} & I_y & -I_{yz} \\ -I_{zx} & -I_{zy} & I_z \end{bmatrix}.$$

It follows that

$$\dot{M}_{RB} = 0.$$

Since the  $b$ -frame is not an inertial frame, the equations of motion include workless forces that neither introduce nor dissipate energy. The nonlinear terms due to Coriolis and centripetal effects are contained in the  $C$ -matrix, which can always be formulated on a skew-symmetric form, i.e.,

$$C_{RB}(\nu) = -C_{RB}(\nu)^\top, \quad \forall \nu \in \mathbb{R}^6.$$

When the system inertia matrix is partitioned as

$$M_{RB} = \begin{bmatrix} M_{11} & M_{12} \\ M_{12}^\top & M_{22} \end{bmatrix}$$

the  $C$ -matrix is represented as

$$C_{RB}(\nu) = \begin{bmatrix} 0 & -S(M_{11}\nu_1 + M_{12}\nu_2) \\ -S(M_{11}\nu_1 + M_{12}\nu_2) & -S(M_{21}\nu_1 + M_{22}\nu_2) \end{bmatrix} \quad (\text{B.4})$$

### Hydrodynamic Forces and Moments

It is common to assume that the forces and moments  $\tau_{RB}$  on the right-hand side of (B.3) are separated into components according to their originating effects and studied independently by assuming linear superposition:

$$\tau_{RB} = \tau_H + \tau + \tau_{\text{env}}$$

where

$$\tau_H = \tau_R + \tau_D$$

is the hydrodynamic forces due to radiation-induced and damping forces, respectively,  $\tau$  represents the control forces and moments, and  $\tau_{\text{env}}$  is the resulting environmental force and moment vector due to wind, waves and currents. The radiation-induced forces and moments include the added mass effect due to the inertia of the surrounding fluid. As for the rigid-body equations of motion, it is advantageous to separate the added mass forces and moments in terms that belong to the added mass system inertia matrix  $M_A$  and a matrix of hydrodynamic Coriolis and centripetal terms denoted  $C_A(\nu)$ . In contrast to submerged volumes that have constant added mass, the added mass effect of surface vessels depend on the frequency of motion due to water surface effects. Under the assumption of low frequency, we assume that  $M_A$  is constant and given as

$$M_A = \lim_{\omega \rightarrow \omega_{LF}} M_A(\omega), \quad \omega_{LF} = [0 \ 0 \ \omega_{30} \ \omega_{40} \ \omega_{50} \ 0]^T$$

where  $\omega_{30}$ ,  $\omega_{40}$ ,  $\omega_{50}$  is the natural frequency in heave, roll and pitch, respectively – see Ross et al. (2006) for further details. At zero speed the added mass matrix is expressed using the hydrodynamic derivatives,

$$M_A = - \begin{bmatrix} X_{\ddot{u}} & X_{\ddot{v}} & X_{\ddot{r}} & X_{\dot{p}} & X_{\dot{q}} & X_{\dot{r}} \\ Y_{\ddot{u}} & Y_{\ddot{v}} & Y_{\ddot{r}} & Y_{\dot{p}} & Y_{\dot{q}} & Y_{\dot{r}} \\ Z_{\ddot{u}} & Z_{\ddot{v}} & Z_{\ddot{r}} & Z_{\dot{p}} & Z_{\dot{q}} & Z_{\dot{r}} \\ K_{\ddot{u}} & K_{\ddot{v}} & K_{\ddot{r}} & K_{\dot{p}} & K_{\dot{q}} & K_{\dot{r}} \\ M_{\ddot{u}} & M_{\ddot{v}} & M_{\ddot{r}} & M_{\dot{p}} & M_{\dot{q}} & M_{\dot{r}} \\ N_{\ddot{u}} & N_{\ddot{v}} & N_{\ddot{r}} & N_{\dot{p}} & N_{\dot{q}} & N_{\dot{r}} \end{bmatrix}.$$

Assuming a frequency independent model  $\omega = \omega_{LF}$  and  $M_A = M_A^T > 0$ . The  $C_A(\nu)$ -matrix is obtained using (B.4) by replacing  $M_{RB}$  with  $M_A$ .

The total damping matrix  $D(\nu)$ , mainly caused by potential, viscous, skin friction, and wave drift damping, is expressed as a sum of linear and nonlinear terms

$$D(\nu) = D + D_n(\nu)$$

where

$$D = - \begin{bmatrix} X_u & X_v & X_r & X_p & X_q & X_r \\ Y_u & Y_v & Y_r & Y_p & Y_q & Y_r \\ Z_u & Z_v & Z_r & Z_p & Z_q & Z_r \\ K_u & K_v & K_r & K_p & K_q & K_r \\ M_u & M_v & M_r & M_p & M_q & M_r \\ N_u & N_v & N_r & N_p & N_q & N_r \end{bmatrix}.$$

For vessels operating around zero speed the linear damping dominate, while quadratic damping dominates at higher speeds. However, the damping forces are always dissipative, that is,

$$\nu^\top \left( D(\nu) + D(\nu)^\top \right) \nu > 0, \quad \forall \nu \neq 0.$$

With the following expression for the hydrodynamic forces

$$\tau_H = -M_A \dot{\nu} - C_A(\nu) \nu - D(\nu) \nu - g(\eta)$$

the resulting model is given by

$$(M_{RB} + M_A) \dot{\nu} + (C_{RB}(\nu) + C_A(\nu)) \nu + D(\nu) \nu + g(\eta) = \tau + \tau_{env}$$

and we collect the rigid-body and added mass terms

$$\begin{aligned} M &= M_{RB} + M_A \\ C(\nu) &= C_{RB}(\nu) + C_A(\nu). \end{aligned}$$

Since  $M_A = M_A^\top > 0$  it follows that  $M = M^\top > 0$ . The Coriolis-centripetal matrix can always be represented such that  $C(\nu) = -C(\nu)^\top$  which means that  $x^\top C(\nu) x = 0 \quad \forall x$ .

### Restoring Forces

In addition to the rigid-body and hydrodynamic forces, a submerged vessel is also affected by gravity and buoyancy forces. In hydrodynamic terminology, they are referred to as *restoring forces* and we collect them in the vector  $g(\eta)$ . The derivation and resulting formula depends on the degree of submergence and Fossen (2002) treats underwater vehicles are different than surface vessels.

A surface vessel's restoring forces depend on the metacenter, the centre of gravity (buoyancy),  $CG$  ( $CB$ ) and the geometry of the water plane.

**Definition B.1 (Metacenter)** *The theoretical point at which an imaginary vertical line through  $CB$  intersects another imaginary vertical (with respect to the ship's horizontal plane) through a new  $CB$  created when the ship is displaced, or tilted, in the water.*

Let  $A_{wp}(\zeta)$  denote the water plane area as a function of the heave position,  $\rho$  be the water density,  $\Delta$  is the nominal displaced water volume, and

$$\begin{aligned}\overline{GM}_T &= \text{transverse metacentric height (m)} \\ \overline{GM}_L &= \text{longitudinal metacentric height (m)}\end{aligned}$$

be the decomposed distance between  $CG$  and  $CB$ . From Fossen (2002, Ch. 3.2.3), we have

$$g(\eta) = \begin{bmatrix} -\rho g \int_0^z A_{wp}(\zeta) d\zeta \sin \theta \\ \rho g \int_0^z A_{wp}(\zeta) d\zeta \cos \theta \sin \phi \\ \rho g \int_0^z A_{wp}(\zeta) d\zeta \cos \theta \cos \phi \\ \rho g \Delta \overline{GM}_T \sin \phi \cos \theta \cos \phi \\ \rho g \Delta \overline{GM}_L \sin \theta \cos \theta \cos \phi \\ \rho g \Delta (-\overline{GM}_L \cos \theta + \overline{GM}_T) \sin \phi \cos \theta \end{bmatrix}.$$

Assuming  $yz$ -symmetry, approximately constant water plane area, that is,  $A_{wp}(\zeta) = A_{wp}$ , and that  $\phi$ ,  $\theta$ , and  $z$  are small imply that

$$g(\eta) \approx \begin{bmatrix} 0 \\ 0 \\ \rho g A_{wp} z \\ \rho g \Delta \overline{GM}_T \phi \\ \rho g \Delta \overline{GM}_L \phi \\ 0 \end{bmatrix} = G\eta.$$

### Alternative Representation

The marine vessel dynamics can be expressed with a NED-vector representation

$$M_\eta(\eta) \ddot{\eta} + C_\eta(\nu, \eta) \dot{\eta} + D_\eta(\nu, \eta) \dot{\eta} + g_\eta(\eta) = J(\eta)^{-\top} \tau$$

where

$$\begin{aligned}M_\eta(\eta) &= J(\eta)^{-\top} M J(\eta) \\ C_\eta(\nu, \eta) &= J(\eta)^{-\top} \left[ C(\nu) - M J(\eta)^{-1} \dot{J}(\eta) \right] J(\eta) \\ D_\eta(\nu, \eta) &= J(\eta)^{-\top} D(\nu) J(\eta) \\ g_\eta(\eta) &= J(\eta)^{-\top} g(\eta)\end{aligned}$$

and  $J(\eta)$  is not defined for  $\theta = \pm 90^\circ$ .

It then follows that for  $M = M^\top > 0$ ,  $\dot{M} = 0$ ,  $C(\nu) = -C(\nu)^\top$ , and  $D(\nu) > 0$  we have

$$\begin{aligned} M_\eta(\eta) &= M_\eta(\eta)^\top > 0, \quad \forall \eta \in \mathbb{R}^6 \\ s^\top \left[ \dot{M}\eta(\eta) - 2C_\eta(\nu, \eta) \right] s &= 0 \quad \forall s, \eta, \nu \in \mathbb{R}^6 \\ D_\eta(\nu, \eta) &> 0 \quad \forall \eta, \nu \in \mathbb{R}^6. \end{aligned}$$

### B.3 3 DOF Vessel Model

A sea surface model with surge, sway and yaw dynamics is a common approximation for surface vessels—see Figure B.1. From the general 6 DOF model the horizontal plane model is found by isolating these components and setting heave, roll and pitch to zero. The position and orientation are then given by  $\eta = [x, y, \psi]^\top$  where  $(x, y)$  is the position on the ocean surface (North and East) and  $\psi$  is the heading, and  $\nu = [u, v, r]^\top$ . Then from Fossen (2002), we have

$$\dot{\eta} = R(\psi)\nu \quad (\text{B.5a})$$

$$M\dot{\nu} + D(\nu)\nu + C(\nu)\nu + g(\eta) = \tau + \tau_{\text{env}} \quad (\text{B.5b})$$

where the kinematic equations of motion (B.2) is reduced to one principal rotation about the  $z$ -axis:  $R(\psi) = R_{z,\psi}$ . Assuming homogeneous mass distribution and  $xz$ -plane symmetry, surge is decoupled from sway and yaw, and the individual components are

$$M = M_{RB} + M_A = \begin{bmatrix} m - X_{\dot{u}} & 0 & 0 \\ 0 & m - Y_{\dot{v}} & mx_g - Y_{\dot{r}} \\ 0 & mx_g - N_{\dot{v}} & I_z - N_{\dot{r}} \end{bmatrix} = M^\top > 0$$

$$C(\nu) = \begin{bmatrix} 0 & 0 & -(m - Y_{\dot{v}})v - m(x_g r + v) \\ 0 & 0 & (m - X_{\dot{u}})u \\ (m - Y_{\dot{v}})v + m(x_g r + v) & -(m - X_{\dot{u}})u & 0 \end{bmatrix},$$

where  $C(\nu) = -C(\nu)^\top$ , and the linear damping terms are given by

$$D = \begin{bmatrix} -X_u & 0 & 0 \\ 0 & -Y_v & -Y_r \\ 0 & -N_v & -N_r \end{bmatrix}.$$

Since heave, roll and pitch are neglected the restoring term contains mooring forces only.

## B.4 Autopilot Models

The 3DOF model (B.5) is linearized around a cruise speed  $u_0$  and decoupled into a speed equation in surge and steering equations that depends on sway and yaw only. Speed and heading are then controlled independently. Consider the linear ship steering model of Davidson & Schiff (1946)

$$M\dot{\nu} + N(u_0)\nu = b\delta \quad (\text{B.6})$$

where

$$M = \begin{bmatrix} m - Y_{\dot{v}} & mx_g - Y_{\dot{r}} \\ mx_g - N_{\dot{v}} & I_z - N_{\dot{r}} \end{bmatrix}, \quad b = \begin{bmatrix} -Y_{\delta} \\ -N_{\delta} \end{bmatrix}$$

$$N(u_0) = C(u_0) + D = \begin{bmatrix} -Y_v & mu_0 - Y_r \\ -N_v & mx_g u_0 - N_r \end{bmatrix}.$$

A transfer function between  $r$  and  $\delta$ , the 2nd-order *Nomoto-model*, is obtained by eliminating the sway velocity  $v$  from (B.6):

$$\frac{r}{\delta}(s) = \frac{K(1 + T_3s)}{(1 + T_1s)(1 + T_2s)}. \quad (\text{B.7})$$

where  $T_i$ ,  $i = 1, 2, 3$  are time constants and  $K$  is the gain constant. A first order approximation of (B.7) is obtained by defining the effective time constant

$$T = T_1 + T_2 - T_3$$

such that

$$\frac{r}{\delta}(s) = \frac{K}{(1 + Ts)}$$

where  $T$  and  $K$  are known as the Nomoto time and gain constants. Neglecting roll and pitch modes such that

$$\dot{\psi} = r$$

we obtain

$$\frac{\psi}{\delta}(s) \approx \frac{K}{s(1 + Ts)}$$

which, due to its simplicity and accuracy, is the most popular model for autopilot design.

## B.5 Environmental Forces

The motion of a ship in a seaway is affected by the action of environmental disturbances from waves, wind and current. The environmental forces have rapidly- and slowly-varying components.

### Ocean Current

A model for ocean currents in two dimensions (sea surface) is characterized by its velocity  $V_c$  and Earth-fixed direction  $\beta_c$ . We want it in the form of (B.1) and decomposed in the  $b$ -frame the model is

$$u_c = V_c \cos(\beta_c - \psi) \quad (\text{B.8})$$

$$v_c = V_c \sin(\beta_c - \psi). \quad (\text{B.9})$$

Thus, the vessel has a velocity relative to the fluid

$$\nu_r = [u - u_c, v - v_c, r]^\top$$

in a horizontal plane model. Hence, the effect of ocean currents should be incorporated in the model by considering the added mass Coriolis/centripetal  $C_A$  and the nonlinear damping matrix  $D_n$

$$\begin{aligned} C(\nu, \nu_r) &= C_{RB}(\nu)\nu + C_A(\nu_r)\nu_r \\ D(\nu_r) &= D\nu_r + D_n(\nu_r)\nu_r \end{aligned}$$

### Wind

Similar to the current model, wind is characterized by a velocity  $V_w$  and an Earth-fixed propagation direction  $\psi_w$ . Decomposed in the  $n$ -frame the components are

$$\begin{bmatrix} u_w^n \\ v_w^n \end{bmatrix} = V_w \begin{bmatrix} \cos \psi_w \\ \sin \psi_w \end{bmatrix}$$

such that the onboard experienced wind, relative to the vessel, is

$$u_r^b = V_w \cos(\psi_w - \psi) - u \quad (\text{B.10})$$

$$v_r^b = V_w \sin(\psi_w - \psi) - v. \quad (\text{B.11})$$

From (B.10) and (B.11), the experienced incoming wind direction and velocity becomes

$$\begin{aligned} \gamma_r &= \arctan\left(\frac{v_r^b}{u_r^b}\right) \\ V_r &= \sqrt{(u_r^b)^2 + (v_r^b)^2} \end{aligned}$$

Although the wind direction is slowly varying and constant for finite periods of time, the wind velocity is usually represented as the sum of a stationary and a rapidly fluctuating component with zero mean.

In the horizontal plane the forces generated by the wind is quadratic in velocity and given by

$$\tau_{\text{wind}} = \frac{1}{2}\rho_a \begin{bmatrix} C_u(\gamma_r) A_T \\ C_v(\gamma_r) A_L \\ C_r(\gamma_r) A_L L \end{bmatrix} V_r^2$$

where  $\rho_a$  is the air density,  $A_T$  and  $A_L$  are the transverse and lateral projected area, and  $L$  is the ship length. The wind coefficients  $C_u, C_v, C_r : \mathbb{R} \rightarrow \mathbb{R}$  are either found by model tests or computed by dedicated software packages.

### Waves

The wave-induced disturbances that influence a marine control system are separated into

- 1st-order effects (or linear wave theory): Oscillatory motion, often called wave frequency motion.
- 2nd-order (or higher) effects: Wave drift forces whose magnitude are proportional to the square of the wave's amplitude and with relative low frequency content compared to the 1st-order effects.

A common approximation to a wave spectrum is to send white noise  $w$  through a linear filter. The filter with transfer function  $H(j\omega)$  is designed such that the power spectral density (PSD) of the output approximates the PSD of the wave spectrum. Such methods have been applied since the 1970s and a common way to model wave-induced motion on ships and marine structures on the sea surface is to apply a second-order filter of the form

$$H(j\omega) = \frac{2\xi\omega_n(j\omega)}{(j\omega)^2 + 2\xi\omega_n(j\omega) + \omega_n^2} \tag{B.12}$$

in each of the three DOF. A state-space representation of (B.12) is

$$\begin{aligned} \dot{\xi} &= A_w \xi + E_w w \\ \eta_w &= C_w \xi_w \end{aligned}$$

where

$$A_w = \begin{bmatrix} 0 & 1 \\ -\omega_n^2 & -2\xi\omega_n \end{bmatrix}, E_w = \begin{bmatrix} 0 \\ 2\xi\omega_n \end{bmatrix}, C_w = [ 0 \quad 1 ] .$$

The wave-drift forces are usually modelled as slowly-varying bias terms (Wiener processes)

$$\dot{d} = w$$

or just a constant bias

$$\dot{d} = 0$$

in the control plant model.

# Appendix C

## Detailed Proofs

The detailed proofs for Chapter 5 are given in this appendix. We need the following lemma from Khalil (2002) for our proofs:

**Lemma C.1** *Suppose that  $S : [0, \infty) \rightarrow \mathbb{R}$  satisfies*

$$D^\dagger S \leq -\alpha S(t) + \beta(t),$$

where  $D^\dagger$  denotes the upper Dini-derivative (see Khalil (2002)),  $\alpha$  is a positive constant, and  $\beta \in \mathcal{L}_p$ ,  $p \in [1, \infty)$ . Then

$$|S|_{\mathcal{L}_p} \leq (\alpha p)^{-1/p} |S(0)| + (\alpha q)^{-1/q} |\beta|_{\mathcal{L}_p},$$

where  $q$  is the complementary index of  $p$ , i.e.,  $1/p + 1/q = 1$ . When  $p = \infty$ , the following holds

$$|S(t)| \leq e^{-\alpha t} |S(0)| + \alpha^{-1} |\beta|_{\mathcal{L}_\infty}.$$

### C.1 Proof of Theorem 5.2

To prove Input-to-State Stability (ISS) from  $\tau$  to  $e$ , we use (5.2) for each vessel so an ISS-Lyapunov function candidate is

$$V_\Sigma = \sum_{i=1}^r V_i(\dot{\eta}_i) \quad \text{where} \quad V_i = \frac{1}{2} \dot{\eta}_i^\top M_{\eta_i} \dot{\eta}_i. \quad (\text{C.1})$$

The function  $V_\Sigma$  in (C.1) is bounded by

$$m_m |\dot{\eta}|^2 \leq V_\Sigma \leq m_M |\dot{\eta}|^2 \quad (\text{C.2})$$

where

$$m_m = \min_i \{\lambda_{\min}(M_i)\} \quad \text{and} \quad m_M = \max_i \{\lambda_{\max}(M_i)\}.$$

The time-derivative of (C.1) is, from (5.5) ,

$$\dot{V}_\Sigma = \sum_{i=1}^r \dot{\eta}_i^\top M_{\eta_i} \ddot{\eta}_i$$

and it follows from (5.3) that

$$\begin{aligned} \dot{V}_\Sigma &\leq \sum_{i=1}^r -\varepsilon_i |\dot{\eta}_i|^2 + \tau_i \dot{\eta}_i = \sum_{i=1}^r -\varepsilon_i |\dot{\eta}_i|^2 + \|W\| |\lambda| |\dot{\eta}_i| + |d_{1i}| |\dot{\eta}_i| \\ &\leq -\varepsilon_M |e|^2 + (\|W\| |\lambda| + |d_1|) |e|. \end{aligned}$$

where  $d_{1i}$  is the  $i$ th element of the disturbance vector  $d_1$ . From (C.2) we obtain

$$\begin{aligned} \dot{V}_\Sigma &\leq -\frac{\varepsilon_M}{m_M} V_\Sigma + \frac{1}{\sqrt{m_m}} (\|W\| |\lambda| + |d_1|) \sqrt{V_\Sigma} \\ &\leq -2\alpha_1 V_\Sigma + 2\beta_1 \sqrt{V_\Sigma}, \end{aligned} \quad (\text{C.3})$$

where

$$\alpha_1 = \frac{\varepsilon_M}{2m_M} \quad \text{and} \quad \beta_1 = \frac{1}{2\sqrt{m_m}} (\|W\| |\lambda| + |d_1|).$$

Setting  $S_\Sigma := \sqrt{V_\Sigma}$  we obtain

$$D^\dagger S_\Sigma \leq -\alpha_1 S_\Sigma + \beta_1. \quad (\text{C.4})$$

Equation (C.4) and Lemma C.1 imply that

$$|S_\Sigma|_{\mathcal{L}_p} \leq (\alpha_1 p)^{-1/p} |S_\Sigma(0)| + (\alpha_1 q)^{-1/q} |\beta_1|_{\mathcal{L}_p}$$

and

$$|S_\Sigma(t)| \leq e^{-\alpha_1 t} |S_\Sigma(0)| + \alpha_1^{-1} |\beta_1|_{\mathcal{L}_\infty}. \quad (\text{C.5})$$

Thus, from (C.5) and

$$|e(t)| \leq \frac{1}{\sqrt{m_m}} |S_\Sigma(t)|,$$

we find the  $\mathcal{L}_\infty$ -gain of the forward path

$$|e|_{\mathcal{L}_\infty} \leq \frac{1}{\sqrt{m_m}} e^{-\frac{\varepsilon_M}{2m_M} t} |S_\Sigma(0)| + \frac{1}{\sqrt{m_m}} \left( \frac{\varepsilon_M}{2m_M} \right)^{-1} |\beta_1|_{\mathcal{L}_\infty} \quad (\text{C.6})$$

which shows that the  $\Sigma$ -block is ISS with respect to  $\beta_1$  according to (1.12). For future reference, note that (C.6) is equivalent to

$$|e|_{\mathcal{L}_\infty} \leq \frac{1}{\sqrt{m_m}} e^{-\frac{\varepsilon_M}{2m_M} t} |S_\Sigma(0)| + \frac{m_M}{m_m \varepsilon_M} (\|W\| |\lambda|_{\mathcal{L}_\infty} + |d_1|_{\mathcal{L}_\infty}) \quad (\text{C.7})$$

and the forward path has asymptotic gain

$$|e|_a \leq \frac{m_M}{m_m \varepsilon_M} (\|W\| |\lambda|_a + |d_1|_a)$$

from which we find the gain of the forward path from  $\lambda$  to  $e$  as in (5.18).

Next, we prove ISS of  $\mathcal{H}_{\text{stab}}$  with respect to  $d_2$  and find the gain from  $e$  to  $\lambda$ . The time-derivative of (5.17) in the presence of the disturbance  $d_2$  is

$$\dot{V}_c = 2\phi^\top P(A\phi + d_2) = -\phi^\top \phi + 2\phi^\top P d_2.$$

From the bounds on the Lyapunov function, we obtain

$$\dot{V}_c \leq -|\phi|^2 + 2\|P\| |\phi| |d_2| \leq -\frac{1}{p_M} V_c + \frac{2p_M}{\sqrt{p_m}} |d_2| \sqrt{V_c}$$

which we rewrite as

$$\dot{V}_c \leq -\frac{1}{p_M} V_c + 2\beta_2 \sqrt{V_c}, \quad \beta_2 = \frac{p_M}{\sqrt{p_m}} |d_2|.$$

Similar to (C.3)-(C.6), we invoke Lemma C.1 and use

$$|\phi(t)| \leq \frac{1}{\sqrt{p_m}} \sqrt{V_c(t)}$$

to obtain

$$\begin{aligned} |\phi(t)| &\leq \frac{1}{\sqrt{p_m}} e^{-\frac{1}{2p_M} t} \sqrt{V_c(0)} + \frac{2p_M^2}{p_m} |d_2|_{\mathcal{L}_\infty} \\ |\phi(t)|_a &\leq \frac{2p_M^2}{p_m} |d_2|_a \end{aligned} \quad (\text{C.8})$$

which shows that the  $\mathcal{H}_{\text{stab}}$ -block is ISS with respect to  $d_2$  according to (1.12) and (1.13).

Finally, we use a small-gain argument from Jiang et al. (1995), Teel (1996) to prove ISS of the closed-loop system with respect to  $d_1$  and  $d_2$ . We find the gain of the feedback path from  $e$  to  $\lambda$  using (5.15) and (C.8)

$$|\lambda(t)| \leq g_2 |e(t)| + \delta k_M |\phi(t)| \quad (\text{C.9})$$

where the  $g_2$ -gain is given as in (5.19) and  $w_e \geq \|\dot{W}\| + \|W\| \|D_\eta\|$ , and  $\delta = \|(WM_\eta^{-1}RW^\top)^{-1}\|$ . Boundedness of  $\delta$  and  $w_e$  follows from Assumption 5.1 and Lemma 5.1. We combine (C.8) and (C.9) to find the  $\mathcal{L}_\infty$ -gain of the feedback path from  $e$  to  $\lambda$

$$|\lambda(t)| \leq g_2 |e(t)| + \frac{\delta k_M}{\sqrt{p_m}} e^{-\frac{1}{2p_M} t} \sqrt{V_c(0)} + \frac{2\delta k_M p_M^2}{p_m} |d_2|_{\mathcal{L}_\infty} \quad (\text{C.10})$$

By combining (C.7) and (C.10), and using the small-gain condition (5.20) we find

$$|e|_{\mathcal{L}_\infty} \leq \frac{1}{1-g_1g_2} \left\{ \frac{1}{\sqrt{m_m}} e^{-\frac{\varepsilon_M}{2m_M}t} |S_\Sigma(0)| + \frac{g_1\delta k_M}{\sqrt{p_m}} e^{-\frac{1}{2p_M}t} \sqrt{V_c(0)} \right. \\ \left. + g_1 \frac{2\delta k_M p_M^2}{p_m} |d_2|_{\mathcal{L}_\infty} + \frac{2\sqrt{m_M}}{m_m\varepsilon_M} |d_1|_{\mathcal{L}_\infty} \right\} \quad (\text{C.11})$$

which shows that  $e$  is ISS with respect to  $d_1$  and  $d_2$  as in (1.12) and (1.13). Similarly, from inserting (C.8) in (C.10) when (5.20) holds, we obtain

$$|\lambda|_{\mathcal{L}_\infty} \leq \frac{1}{1-g_1g_2} \left\{ \frac{g_2}{\sqrt{m_m}} e^{-\frac{\varepsilon_M}{2m_M}t} |S_\Sigma(0)| + \frac{\delta k_M}{\sqrt{p_m}} e^{-\frac{1}{2p_M}t} \sqrt{V_c(0)} \right. \\ \left. + \frac{m_M}{m_m\varepsilon_M} |d_1|_{\mathcal{L}_\infty} + \frac{2\delta k_M p_M^2}{p_m} |d_2|_{\mathcal{L}_\infty} \right\}. \quad (\text{C.12})$$

We conclude from (C.11) and (C.12) that the interconnected system is ISS with respect to disturbances  $d_1$  and  $d_2$ .  $\square$

## C.2 Proof of Theorem 5.3

To establish ISS of the  $\Sigma$ -block, we let  $\mathcal{I}$  denote the subset of indices  $i = 1, \dots, r$  for which  $\Sigma_i$  is the closed-loop of a vessel and an individual controller and define the ISS-Lyapunov function

$$V_\Sigma := \sum_{i \in \mathcal{I}} V_{ship\_i} + \sum_{i \notin \mathcal{I}} V_i \quad (\text{C.13})$$

where  $V_{ship\_i}$  and  $V_i$  are defined in (5.2) and (5.29). The function (C.13) is bounded by

$$q_m |\dot{\eta}|^2 \leq V_\Sigma \leq q_M |\dot{\eta}|^2 \quad (\text{C.14})$$

where

$$q_m = \min_i \{ \lambda_{\min}(P_i), \lambda_{\min}(M_i) : i \notin \mathcal{I} \} \text{ and} \\ q_M = \max_i \{ \lambda_{\max}(P_i), \lambda_{\max}(M_i) : i \notin \mathcal{I} \}.$$

We first find the gain of the forward path: The time-derivative of  $V_\Sigma$  is, from (5.3) and (5.25),

$$\dot{V}_\Sigma \leq \sum_{i \notin \mathcal{I}} \{ -\varepsilon_i |\dot{\eta}_i|^2 + |\tau_i| |\dot{\eta}_i| \} + \sum_{i \in \mathcal{I}} \{ -\varepsilon_i |e_i|^2 + \rho_i |e_i| |\tau_i| \} \\ \leq - \left( \sum_{i=1}^r \varepsilon_i |e_i|^2 \right) + \bar{\rho} |e| |\tau| \leq -\bar{\varepsilon} |e|^2 + \bar{\rho} |e| |\tau|$$

which proves that  $\Sigma$  is ISS with respect to  $\tau$ . From (C.14) we get

$$\dot{V}_\Sigma \leq -\frac{\bar{\varepsilon}}{q_M} V_\Sigma + \frac{\bar{\rho}}{\sqrt{q_m}} |\tau| \sqrt{V_\Sigma} = -2\alpha_3 V_\Sigma + 2\beta_3 \sqrt{V_\Sigma}$$

where

$$\alpha_3 = \frac{\bar{\varepsilon}}{2q_M} \quad \text{and} \quad \beta_3 = \frac{\bar{\rho}}{2\sqrt{q_m}} |\tau|.$$

Setting  $S_\Sigma := \sqrt{V_\Sigma}$  we obtain

$$D^\dagger S_\Sigma \leq -\alpha_3 S_\Sigma + \beta_3,$$

which, from Lemma C.1, implies that

$$|S_\Sigma(t)| \leq e^{-\alpha_3 t} |S_\Sigma(0)| + \alpha_3^{-1} |\beta_3|_{\mathcal{L}_\infty}. \quad (\text{C.15})$$

Then, from (C.15) and

$$|e(t)| \leq \frac{1}{\sqrt{q_m}} |S_\Sigma(t)|$$

we find the gain of the forward path

$$|e|_{\mathcal{L}_\infty} \leq \frac{1}{\sqrt{q_m}} e^{-\alpha_3 t} |S_\Sigma(0)| + g_{1c} |\lambda|_{\mathcal{L}_\infty} + \frac{q_M \bar{\rho}}{q_m \bar{\varepsilon}} |d_1|_{\mathcal{L}_\infty} \quad (\text{C.16})$$

where  $g_{1c}$  are as in (5.31). Thus,  $e(t)$  is ISS with respect to  $d_1$ . The gain of the feedback path is as in (5.19), and we insert (C.10) into (C.16) and use the small-gain condition (5.32) to obtain

$$\begin{aligned} |e|_{\mathcal{L}_\infty} \leq & \frac{1}{1 - g_{1c} g_2} \left\{ \frac{1}{\sqrt{q_m}} e^{-\alpha_3 t} |S_\Sigma(0)| + \frac{g_{1c} \delta k_M}{\sqrt{p_m}} e^{-\frac{1}{2p_M} t} \sqrt{V_c(0)} \right. \\ & \left. + \frac{q_M \bar{\rho}}{q_m \bar{\varepsilon}} |d_1|_{\mathcal{L}_\infty} + g_{1c} \frac{2\delta k_M p_M^2}{p_m} |d_2|_{\mathcal{L}_\infty} \right\}. \end{aligned} \quad (\text{C.17})$$

Similarly, by inserting (C.16) into (C.10) and employing (5.32) we get

$$\begin{aligned} |\lambda|_{\mathcal{L}_\infty} \leq & \frac{1}{1 - g_{1c} g_2} \left\{ \frac{g_2}{\sqrt{q_m}} e^{-\alpha_3 t} |S_\Sigma(0)| + \frac{\delta k_M}{\sqrt{p_m}} e^{-\frac{1}{2p_M} t} \sqrt{V_c(0)} \right. \\ & \left. + g_2 \frac{q_M \bar{\rho}}{q_m \bar{\varepsilon}} |d_1|_{\mathcal{L}_\infty} + \frac{2\delta k_M p_M^2}{p_m} |d_2|_{\mathcal{L}_\infty} \right\}. \end{aligned} \quad (\text{C.18})$$

Finally, from (C.17) and (C.18) we conclude that the feedback interconnection is ISS with respect to disturbances  $d_1$  and  $d_2$ .  $\square$

### C.3 Proof of Theorem 5.4

We find the gain of the outer loop in two steps, first from  $\dot{e}$  to  $d_2$  and then from  $\lambda$  to  $e$ : We first note that

$$d_{2j}(t) = \sum_{i=1}^r W_{\text{constr}e}(t - T_{ij}) - W_{\text{constr}e}(t)$$

where  $d_{2j}$  is the  $j$ th entry of  $d_2$ . Due to Lemma 5.1, we have that

$$\begin{aligned} |d_{2j}(t)| &\leq w_e \sum_{i=1}^r \int_{t-T_{ij}}^t |\dot{e}_i(\sigma)| d\sigma \\ &\leq w_e \sum_{i=1}^r \int_{\max\{0, t-T_{ij}\}}^t |\dot{e}_i(\sigma)| d\sigma + w_e \sum_{i=1}^r \int_{\min\{0, t-T_{ij}\}}^0 |\dot{e}_i(\sigma)| d\sigma. \end{aligned}$$

Young's inequality yields

$$\begin{aligned} d_{2j}(t)^2 &\leq (2w_e \sum_{i=1}^r \int_{\max\{0, t-T_{ij}\}}^t |\dot{e}_i(\sigma)| d\sigma)^2 + (2w_e \sum_{i=1}^r \int_{\min\{0, t-T_{ij}\}}^0 |\dot{e}_i(\sigma)| d\sigma)^2 \\ &\leq 2w_e^2 r \sum_{i=1}^r \left( \int_{\max\{0, t-T_{ij}\}}^t |\dot{e}_i(\sigma)| d\sigma \right)^2 + 2w_e^2 r \sum_{i=1}^r \left( \int_{\min\{0, t-T_{ij}\}}^0 |\dot{e}_i(\sigma)| d\sigma \right)^2 \end{aligned}$$

Applying the Cauchy-Schwarz inequality to each term, we get

$$d_{2j}(t)^2 \leq 2w_e^2 r T \sum_{i=1}^r \left( \int_{\max\{0, t-T_{ij}\}}^t |\dot{e}_i(\sigma)|^2 d\sigma + \int_{\min\{0, t-T_{ij}\}}^0 |\dot{e}_i(\sigma)|^2 d\sigma \right)$$

which implies that the norm of  $d_2(t)$  is

$$\begin{aligned}
|d_2(t)| &= \sqrt{\sum_{j=1}^p d_{2j}(t)^2} \\
&\leq \sqrt{2w_e^2 r T \sum_{j=1}^p \sum_{i=1}^r \left( \int_{\max\{0, t-T_{ij}\}}^t |\dot{e}_i(\sigma)|^2 d\sigma + \int_{\min\{0, t-T_{ij}\}}^0 |\dot{e}_i(\sigma)|^2 d\sigma \right)} \\
&\leq \sqrt{2w_e^2 r T \sum_{j=1}^p \sum_{i=1}^r \left( \int_{\max\{0, t-T_{ij}\}}^t |\dot{e}_i(\sigma)|^2 d\sigma \right)} \\
&\quad + \sqrt{2w_e^2 r T \sum_{j=1}^p \sum_{i=1}^r \left( \int_{\min\{0, t-T_{ij}\}}^0 |\dot{e}_i(\sigma)|^2 d\sigma \right)}
\end{aligned}$$

By using the inequalities

$$\max\{0, t - T_{ij}\} \leq \max\{0, t - T\} \quad \text{and} \quad \min\{0, t - T_{ij}\} \leq \min\{0, t - T\}$$

we obtain

$$\begin{aligned}
|d_2(t)| &\leq \sqrt{2w_e^2 r T \sum_{j=1}^p \sum_{i=1}^r \left( \int_{\max\{0, t-T\}}^t |\dot{e}_i(\sigma)|^2 d\sigma \right)} \\
&\quad + \sqrt{2w_e^2 r T \sum_{j=1}^p \sum_{i=1}^r \left( \int_{\min\{0, t-T\}}^0 |\dot{e}_i(\sigma)|^2 d\sigma \right)}
\end{aligned}$$

Changing the sequence of the sum and integral yields

$$\begin{aligned}
|d_2(t)| &\leq \sqrt{2w_e^2 r T \sum_{j=1}^p \int_{\max\{0, t-T\}}^t \sum_{i=1}^r |\dot{e}_i(\sigma)|^2 d\sigma} \\
&\quad + \sqrt{2w_e^2 r T \sum_{j=1}^p \int_{\min\{0, t-T\}}^t \sum_{i=1}^r |\dot{e}_i(\sigma)|^2 d\sigma} \\
&\leq \sqrt{2w_e^2 p r T^2 |\dot{e}|_{\mathcal{L}_\infty}^2} + \sqrt{2w_e^2 p r T^2 \int_{\min\{0, t-T\}}^t |\dot{e}(\sigma)| d\sigma} \\
&= Tw_e \sqrt{2pr} \left( |\dot{e}|_{\mathcal{L}_\infty} + \sqrt{\sup_{-T \leq t \leq 0} |F(\eta, t) + b\tau|^2} \right) \quad (\text{C.19})
\end{aligned}$$

and

$$|d_2|_a \leq Tw_e \sqrt{2pr} |\dot{e}|_a. \quad (\text{C.20})$$

To find the gain from  $\lambda$  to  $\dot{e}$ , note that from (C.7) we have

$$|e|_{\mathcal{L}_\infty} \leq |e|_{\mathcal{L}_\infty} \leq \sqrt{m_M} e^{-\frac{m_m \varepsilon_M}{2} t} |S_\Sigma(0)| + \frac{2\sqrt{m_M}}{m_m \varepsilon_M} \|W\| |\lambda|_{\mathcal{L}_\infty}.$$

Because

$$|\dot{e}| \leq \|F\| |e| + |b| |\tau|$$

we obtain

$$|\dot{e}| \leq \|F\| \sqrt{m_M} e^{-\frac{m_m \varepsilon_M}{2} t} |S_\Sigma(0)| + \left( \|F\| \frac{2\sqrt{m_M}}{m_m \varepsilon_M} + |b| \right) \|W\| |\lambda(t)| \quad (\text{C.21})$$

and

$$|\dot{e}|_a \leq \left( \|F\| \frac{2\sqrt{m_M}}{m_m \varepsilon_M} + |b| \right) \|W\| |\lambda(t)|_a \quad (\text{C.22})$$

Combining (C.19)-(C.20) and (C.21)-(C.22), we conclude that the gain of the outer path from  $\lambda$  to  $d_2$  is

$$\begin{aligned}
|d_2|_{\mathcal{L}_\infty} &\leq Tw_e \sqrt{2pr} \|F\| \sqrt{m_M} e^{-\frac{m_m \varepsilon_M}{2} t} |S_\Sigma(0)| + g_{\text{outer}} |\lambda(t)| \quad (\text{C.23}) \\
&\quad + Tw_e \sqrt{2pr} \sqrt{\sup_{-T \leq t \leq 0} |F(\eta, t) + b\tau|^2}
\end{aligned}$$

$$|d_2|_a \leq g_{\text{outer}} |\lambda|_a \quad (\text{C.24})$$

where  $g_{\text{outer}}$  is as in (5.34). Finally, we find the gain for the inner loop and use the small-gain condition (5.35) to prove UGAS of the interconnection. For the inner loop in Figure 5.4 we have from (C.18) that

$$|\lambda|_{\mathcal{L}_\infty} \leq \frac{1}{1 - g_{1c}g_2} \{g_2\sqrt{q_M}e^{-\alpha_3 t} |S_\Sigma(0)| + \delta k_M\sqrt{p_M}e^{-\frac{pm}{2}t} \sqrt{V_c(0)}\} + g_{\text{inner}} |d_2|_{\mathcal{L}_\infty}. \quad (\text{C.25})$$

and

$$|\lambda|_a \leq g_{\text{inner}} |d_2|_a \quad (\text{C.26})$$

where  $g_{\text{inner}}$  is as in (5.33). Substituting (C.25)-(C.26) into (C.23)-(C.24) we find

$$\begin{aligned} |d_2|_{\mathcal{L}_\infty} &\leq Tw_e\sqrt{2pr} \|F\| \sqrt{m_M} e^{-\frac{mm\varepsilon M}{2}t} |S_\Sigma(0)| \\ &\quad + g_{\text{outer}} \frac{1}{1 - g_{1c}g_2} \{g_2\sqrt{q_M}e^{-\alpha_3 t} |S_\Sigma(0)| + \delta k_M\sqrt{p_M}e^{-\frac{pm}{2}t} \sqrt{V_c(0)}\} \\ &\quad + g_{\text{outer}}g_{\text{inner}} |d_2|_{\mathcal{L}_\infty} + Tw_e\sqrt{2pr} \sqrt{\sup_{-T \leq t \leq 0} |F(\eta, t) + b\tau|^2} \\ |d_2|_a &\leq g_{\text{outer}}g_{\text{inner}} |d_2|_a \end{aligned}$$

and using the small-gain condition we obtain

$$\begin{aligned} |d_2|_{\mathcal{L}_\infty} &\leq \frac{1}{1 - g_{\text{outer}}g_{\text{inner}}} \{Tw_e\sqrt{2pr} \|F\| \sqrt{m_M} e^{-\frac{mm\varepsilon M}{2}t} |S_\Sigma(0)| \\ &\quad + \frac{g_{\text{outer}}}{1 - g_{1c}g_2} \{g_2\sqrt{q_M}e^{-\alpha_3 t} |S_\Sigma(0)| \\ &\quad + \delta k_M\sqrt{p_M}e^{-\frac{pm}{2}t} \sqrt{V_c(0)}\} + Tw_e\sqrt{2pr} \sqrt{\sup_{-T \leq t \leq 0} |F(\eta, t) + b\tau|^2} \\ |d_2|_a &= 0. \end{aligned}$$

Finally, from Theorem 5.2, we have

$$\begin{aligned} |\phi|_{\mathcal{L}_\infty} &\leq \sqrt{p_M}e^{-\frac{pm}{2}t} \sqrt{V_c(0)} + \frac{2p_M^2}{p_m} |d_2|_{\mathcal{L}_\infty} \\ &\leq \sqrt{p_M}e^{-\frac{pm}{2}t} \sqrt{V_c(0)} + \frac{Tw_e\sqrt{2pr} \|F\| \sqrt{m_M} e^{-\frac{mm\varepsilon M}{2}t} |S_\Sigma(0)|}{1 - g_{\text{outer}}g_{\text{inner}}} \\ &\quad + \frac{g_{\text{outer}}}{1 - g_{\text{outer}}g_{\text{inner}}} \{g_2\sqrt{q_M}e^{-\alpha_3 t} |S_\Sigma(0)| + \delta k_M\sqrt{p_M}e^{-\frac{pm}{2}t} \sqrt{V_c(0)}\} \\ &\quad + \frac{Tw_e\sqrt{2pr}}{1 - g_{\text{outer}}g_{\text{inner}}} \sqrt{\sup_{-T \leq t \leq 0} |F(\eta, t) + b\tau|^2} \\ &\leq \gamma_{10} (|\phi_0|, |e_0|) + \gamma_1 (|d_1|_{\mathcal{L}_\infty}, |d_2|_{\mathcal{L}_\infty}) \\ |\phi|_a &= 0 \end{aligned}$$

where  $\gamma_{10}(\cdot)$ ,  $\gamma_1(\cdot)$  are  $\mathcal{K}$  functions. From Theorem 5.3 we obtain

$$|e|_{\mathcal{L}_\infty} \leq \frac{1}{1 - g_{1c}g_2} \left\{ \sqrt{q_M} e^{-\alpha_3 t} |S_\Sigma(0)| + g_{1c} \delta k_M \sqrt{p_M} e^{-\frac{p_m}{2} t} \sqrt{V_c(0)} + g_{1c} \frac{2\delta k_M p_M^2}{p_m} |d_2|_{\mathcal{L}_\infty} \right\}.$$

$$\begin{aligned} |e|_{\mathcal{L}_\infty} &\leq \frac{1}{1 - g_{1c}g_2} \left\{ \sqrt{q_M} e^{-\alpha_3 t} |S_\Sigma(0)| + g_{1c} \delta k_M \sqrt{p_M} e^{-\frac{p_m}{2} t} \sqrt{V_c(0)} + \frac{2g_{1c} \delta k_M p_M^2}{p_m} |d_2|_{\mathcal{L}_\infty} \right\} \\ &\leq \frac{1}{1 - g_{1c}g_2} \left\{ \sqrt{q_M} e^{-\alpha_3 t} |S_\Sigma(0)| + g_{1c} \delta k_M \sqrt{p_M} e^{-\frac{p_m}{2} t} \sqrt{V_c(0)} + \frac{2g_{1c} \delta k_M p_M^2 p_m^{-1}}{1 - g_{\text{outer}} g_{\text{inner}}} \left\{ \right. \right. \\ &\quad \left. \left. T w_e \sqrt{2pr} \|F\| \sqrt{m_M} e^{-\frac{m_m \varepsilon_M}{2} t} |S_\Sigma(0)| + \frac{g_{\text{outer}}}{1 - g_{1c}g_2} \left\{ g_2 \sqrt{q_M} e^{-\alpha_3 t} |S_\Sigma(0)| + \delta k_M \sqrt{p_M} e^{-\frac{p_m}{2} t} \sqrt{V_c(0)} \right\} + T w_e \sqrt{2pr} \sqrt{\sup_{-T \leq t \leq 0} |F(\eta, t) + b\tau|^2} \right\} \right\} \\ &\leq \gamma_{20}(|\phi_0|, |e_0|) + \gamma_2(|d_1|_{\mathcal{L}_\infty}, |d_2|_{\mathcal{L}_\infty}), \quad \gamma_{20}(\cdot), \gamma_2(\cdot) \in \mathcal{K} \\ |e|_a &= 0 \end{aligned}$$

Having established that the origin  $(\phi, e) = 0$  is UGS and uniformly globally attractive we have proved uniform global asymptotic stability for sufficiently small time-delays.  $\square$

# References

- Aguiar, A. P., Hespanha, J. P. & Kokotović, P. V. (2005), ‘Path-following for non-minimum phase systems removes performance limitations.’, *IEEE Transactions on Automatic Control* **50**(2), 234–239.
- Akyildiz, I. F., Pompili, D. & Melodia, T. (2005), ‘Underwater acoustic sensor networks: research challenges’, *Ad Hoc Networks* **3**(3), 257–279.
- Al-Hiddabi, S. A. & McClamroch, N. H. (2002), ‘Tracking and maneuver regulation control for nonlinear nonminimum phase systems: Application to flight control’, *IEEE Transactions on Control Systems Technology* **10**(6), 780–792.
- Antonelli, G. & Chiaverini, S. (2004), Fault tolerant kinematic control of platoons of autonomous robots, *in* ‘Proc. of the IEEE Int. Conf. on Robotics & Automation’, New Orleans, LA, USA, pp. 3313–3318.
- Arcak, M. (2006), ‘Passivity as a design tool for group coordination’, *IEEE Transactions on Automatic Control*. In print.
- Arcak, M. & Kokotović, P. (2001), ‘Observer-based control of systems with slope-restricted nonlinearities’, *IEEE Transactions on Automatic Control* **46**(7), 1146–1150.
- Badgerow, J. P. & Hansworth, F. R. (1981), ‘Energy savings through formation flight? A re-examination of the vee formation’, *Journal of Theoretical Biology* **93**, 41–52.
- Balch, T. & Arkin, R. C. (1998), ‘Behavior-based formation control for multirobot teams’, *IEEE Transactions on Robotics and Automation* **14**(6), 926–939.
- Baraff, D. (1996), Linear-time dynamics using Lagrange multipliers, *in* ‘Computer Graphics Proceedings’, SIGGRAPH, pp. 137–146.
- Barzel, R. & Barr, A. H. (1988), ‘A modeling system based on dynamic constraints’, *Computer Graphics* **22**(4), 179–188.

- Baumgarte, J. (1972), ‘Stabilization of constraints and integrals of motion in dynamical systems’, *Computer Methods in Applied Mechanical Engineering* **1**, 1–16.
- Beard, R. W., Lawton, J. & Hadaegh, F. Y. (2001), ‘A coordination architecture for spacecraft formation control’, *IEEE Transactions on Control Systems Technology* **9**(6), 777–790.
- Berghuis, H. & Nijmeijer, H. (1993), ‘A passivity approach to controller-observer design for robots’, *IEEE Transactions on Robotics and Automation* **9**(6), 740–754.
- Biyik, E. & Arcak, M. (2006), Passivity-based agreement protocols: Continuous-time and sampled-data designs, in K. Y. Pettersen, T. Gravdahl & H. Nijmeijer, eds, ‘Group Coordination and Cooperative Control’, number 336 in ‘Lecture Notes in Control and Information Sciences’, Springer-Verlag, Berlin Heidelberg, chapter 2, pp. 21–33.
- Børhaug, E., Pavlov, A. & Pettersen, K. Y. (2006), Cross-track formation control of underactuated autonomous underwater vehicles, in K. Y. Pettersen, T. Gravdahl & H. Nijmeijer, eds, ‘Group Coordination and Cooperative Control’, number 336 in ‘Lecture Notes in Control and Information Sciences’, Springer-Verlag, Berlin Heidelberg, chapter 3, pp. 35–54.
- Breivik, M., Subbotin, M. V. & Fossen, T. I. (2006), Kinematic aspects of guided formation control in 2d, in K. Y. Pettersen, T. Gravdahl & H. Nijmeijer, eds, ‘Group Coordination and Cooperative Control’, number 336 in ‘Lecture Notes in Control and Information Sciences’, Springer-Verlag, Berlin Heidelberg, chapter 4, pp. 55–74.
- Bullo, F., Leonard, N. E. & Lewis, A. D. (2000), ‘Controllability and motion algorithms for underactuated Lagrangian systems on Lie groups’, *IEEE Transactions on Automatic Control* **45**(8), 1437–1454.
- Chen, X. & Serrani, A. (2004), Remarks on iss and formation control, in ‘Proc. 43rd IEEE Conf. on Decision & Control’, Paradise Island, The Bahamas, pp. 177–182.
- Chiaverini, S., Siciliano, B. & Egeland, O. (1994), ‘Review of the damped least-squares inverse kinematics with experiments on an industrial robot manipulator’, *IEEE Transactions on Control Systems Technology* **2**(2), 123–134.
- Coombe, I. (2005), ‘Rfa tankers’, [Online, Accessed Sept. 28] <http://iancoombe.tripod.com/id8.html>.

- Corneliussen, J. (2003), Implementation of Guidance System for Cybership II, Master's thesis, Department of Engineering Cybernetics, Norwegian University of Science and Technology, Trondheim, Norway.
- Curtin, T. B. & Bellingham, J. G. (2001), 'Guest editorial - autonomous ocean-sampling networks', *IEEE Journal of Oceanic Engineering* **26**(4), 421–423.
- Davidson, K. S. M. & Schiff, L. I. (1946), Turning and course keeping qualities, in 'Transactions of SNAME'.
- Dirk, H. & Huberman, B. A. (1998), 'Coherent moving states in highway traffic', *Nature* **396**, 738–740.
- Do, K. D., Jiang, Z. P. & Pan, J. (2002), Robust adaptive path following of underactuated ships, in 'Proc. 41st IEEE Conference on Decision and Control', Las Vegas, NV, USA, pp. 3243–3248.
- Egerstedt, M. & Hu, X. (2001), 'Formation constrained multi-agent control', *IEEE Transactions on Robotics and Automation* **17**(6), 947–951.
- Encarnação, P. & Pascoal, A. (2001a), Combined trajectory tracking and path following: an application to the coordinated control of autonomous marine craft, in 'Proc. 40th IEEE Conf. on Decision & Control', Orlando, FL, USA, pp. 964–969.
- Encarnação, P. & Pascoal, A. (2001b), Combined trajectory tracking and path following for marine craft, in 'Proc. 9th Mediterranean Conference on Control and Automation', Dubrovnik, Croatia.
- Fan, X. & Arcak, M. (2004), 'Robustness of network flow control against disturbances and time-delay', *Systems and Control Letters* **53**, 13–29.
- Farkas, I., Helbing, D. & Vicsek, T. (2002), 'Mexican waves in an excitable medium', *Nature* **419**, 131–132.
- Fax, J. A. & Murray, R. M. (2004), 'Information flow and cooperative control of vehicle formations', *IEEE Transactions on Automatic Control* **49**(9), 1465–1476.
- Fossen, T. I. (2002), *Marine Control Systems: Guidance, Navigation and Control of Ships, Rigs and Underwater Vehicles*, Marine Cybernetics, Trondheim, Norway. <http://www.marinecybernetics.com>.

- Fossen, T. I. (2005), ‘A nonlinear unified state-space model for ship maneuvering and control in a seaway’, *International Journal of Bifurcation and Chaos* **15**(9).
- Fossen, T. I., Breivik, M. & Skjetne, R. (2003), Line-of-sight path following of underactuated marine craft, *in* ‘Proc. 6th IFAC Conference on Manoeuvring and Control of Marine Crafts’, Girona, Spain.
- Fossen, T. I., Godhavn, J. M., Berge, S. P. & Lindegaard, K. P. (1998), Nonlinear control of underactuated ships with forward speed compensation, *in* ‘4th IFAC Nonlinear Control Systems Design Symposium (NOLCOS)’, Enschede, The Netherlands, pp. 121–127.
- Fossen, T. I. & Grøvlén, Å. (1998), ‘Nonlinear Output Feedback Control of Dynamically Positioned Ships Using Vectorial Observer Backstepping’, *IEEE Transactions on Control Systems Technology* **6**(1), 121–128.
- Fossen, T. I., Loría, A. & Teel, A. (2001), ‘A theorem for UGAS and ULES of (passive) nonautonomous systems: Robust control of mechanical systems and ships’, *International Journal of Robust and Nonlinear Control* **11**, 95–108.
- Fossen, T. I. & Strand, J. P. (1999), ‘Passive Nonlinear Observer Design for Ships Using Lyapunov Methods: Full Scale Experiments with a Supply Vessel’, *Automatica* **35**(1), 3–16.
- Franklin, G. F., Powell, J. D. & Emami-Naeini, A. (2002), *Feedback Control of Dynamic Systems*, 4th edn, Addison-Wesley, Boston, MA, USA.
- Gazi, V. & Passino, K. M. (2004), ‘Stability analysis of social foraging swarms’, *IEEE Transactions on Systems, Man, and Cybernetics–Part B: Cybernetics* **34**(1), 539–557.
- Ghabcheloo, R., Pascoal, A., Silvestre, C. & Kaminer, I. (2005), Coordinated path following control of multiple wheeled robots with directed communication links, *in* ‘Proc. 44rd IEEE Conference on Decision & Control and 5th European Control Conference’, Seville, Spain.
- Gladwell, M. (2000), *The Tipping Point: How Little Things Can Make a Big Difference*, Little, Brown.
- Godsil, C. D. & Royle, G. F. (2001), *Algebraic Graph Theory*, Graduate texts in mathematics; 207, Springer-Verlag, New York.

- Grünbaum, D., Viscido, S. & Parrish, J. K. (2005), Extracting interactive control algorithms from group dynamics of schooling fish, *in* V. Kumar, N. Leonard & A. S. Morse, eds, ‘Cooperative Control’, number 309 *in* ‘Lecture Notes in Control and Information Sciences’, Springer-Verlag, Berlin Heidelberg, pp. 103–117.
- Hale, J. K. & Lunel, S. M. V. (1993), *Introduction to Functional Differential Equations*, Applied Mathematical Sciences, Springer, Berlin, Germany.
- Hauser, J. & Hindman, R. (1995), Maneuver regulation from trajectory tracking: Feedback linearizable systems, *in* ‘Proc. IFAC symposium on nonlinear control systems design’, Lake Tahoe, CA, USA, pp. 595–600.
- Helbing, D., Farkas, I. & Vicsek, T. (2000), ‘Simulating dynamical features of escape panic’, *Nature* **407**, 487–490.
- Hoerner, S. F. (1958), *Fluid Dynamic Drag: Pratical Information on Aerodynamic Drag and Hydrodynamic Resistance*, Published by the Author, Midland Park, NJ, USA.
- Ihle, I.-A. F., Arcak, M. & Fossen, T. I. (2006a), ‘Passivation designs for synchronization of path following systems’, *Automatica* . Submitted.
- Ihle, I.-A. F., Arcak, M. & Fossen, T. I. (2006b), Passivation designs for synchronization of path following systems, *in* ‘Proc. 45th IEEE Conference on Decision & Control’, San Diego, CA, USA. In print.
- Ihle, I.-A. F., Jouffroy, J. & Fossen, T. I. (2005a), Formation control of marine craft using constraint functions, *in* ‘IEEE Marine Technology and Ocean Science Conference *Oceans05*’, Washington D.C., USA.
- Ihle, I.-A. F., Jouffroy, J. & Fossen, T. I. (2005b), Formation control of marine surface craft using Lagrange multipliers, *in* ‘Proc. 44rd IEEE Conference on Decision & Control and 5th European Control Conference’, Seville, Spain, pp. 752–758.
- Ihle, I.-A. F., Jouffroy, J. & Fossen, T. I. (2006a), ‘Formation control of marine surface craft: A Lagrangian approach’, *IEEE Journal of Oceanic Engineering* **31**(3).
- Ihle, I.-A. F., Jouffroy, J. & Fossen, T. I. (2006b), Robust formation control of marine craft using Lagrange multipliers, *in* K. Y. Pettersen, T. Gravdahl & H. Nijmeijer, eds, ‘Group Coordination and Cooperative Control’, number 336 *in* ‘Lecture Notes in Control and Information Sciences’, Springer-Verlag, Berlin Heidelberg, chapter 7, pp. 113–130.

- Ihle, I.-A. F., Skjetne, R. & Fossen, T. I. (2004), Nonlinear formation control of marine craft with experimental results, *in* 'Proc. 43rd IEEE Conf. on Decision & Control', Atlantis, Paradise Island, The Bahamas, pp. 680–685.
- Ihle, I.-A. F., Skjetne, R. & Fossen, T. I. (2005), Output feedback control for maneuvering systems using observer backstepping, *in* 'Proc. IEEE International Symposium on Intelligent Control, Mediterranean Conference on Control and Automation', Limassol, Cyprus, pp. 1512–1517.
- Ioannou, P. A. & Sun, J. (1996), *Robust Adaptive Control*, Prentice Hall, Inc. (Out of print in 2003), Electronic copy at [http://www-rcf.usc.edu/~ioannou/Robust\\_Adaptive\\_Control.htm](http://www-rcf.usc.edu/~ioannou/Robust_Adaptive_Control.htm).
- Isidori, A. (1999), *Nonlinear Control Systems II*, Springer-Verlag, London, UK.
- Jadbabaie, A., Lin, J. & Morse, A. S. (2002), 'Coordination of groups of mobile autonomous agents using nearest neighbor rules', *IEEE Transactions on Automatic Control* **48**(6), 988–1101.
- Janković, M., Sepulchre, R. & Kokotović, P. V. (1996), 'Constructive lyapunov stabilization of nonlinear cascade systems', *IEEE Transactions on Automatic Control* **41**(12), 1723–1735.
- Jiang, Z. P., Teel, A. R. & Praly, L. (1995), 'Small gain theorem for iss systems and applications', *Mathematics of Control, Signals, and Systems* **7**, 95–120.
- Khalil, H. K. (2002), *Nonlinear Systems*, 3rd edn, Prentice-Hall, New York.
- Kingston, D. B., Wei, R. & Beard, R. W. (2005), Consensus algorithms are input-to-state stable, *in* 'Proc. 2005 American Control Conference', Portland, OR, USA, pp. 1686–1690.
- Krasowskii, N. N. (1959), *Problems of the theory of stability of motion*, Stanford University Press, Moscow. 1963; Translation of the Russian edition.
- Krishnan, H. & McClamroch, N. H. (1994), 'Tracking in nonlinear differential-algebraic control systems with applications to constrained robot systems', *Automatica* **30**(12), 1885–1897.
- Krstić, M., Kanellakopoulos, I. & Kokotović, P. V. (1995), *Nonlinear and Adaptive Control Design*, John Wiley & Sons Ltd, New York.
- Kube, C. R. & Bonabeau, E. (2000), 'Cooperative transport by ants and robots', *Robotics and Autonomous Systems* **30**, 85–101.

- Kumar, V., Leonard, N. & Morse, A. S., eds (2005), *Cooperative Control*, number 309 in 'Lecture Notes in Control and Information Sciences', Springer-Verlag, Berlin Heidelberg.
- Kyrkjebø, E. & Pettersen, K. Y. (2003), Ship replenishment using synchronization control, in 'Proc. 6th IFAC Conference on Manoeuvring and Control of Marine Crafts', Girona, Spain, pp. 286–291.
- Lagrange, J. L. (1811), *Mécanique analytique, nouvelle édition*, Académie des Sciences. Translated version: *Analytical Mechanics*, Kluwer Academic Publishers, 1997.
- Laila, D. S., Nešić, D. & Teel, A. R. (2002), 'Open and closed loop dissipation inequalities under sampling and controller emulation', *European Journal of Control* **8**(2), 109–125.
- Lanczos, C. (1986), *The Variational Principles of Mechanics*, 4th edn, Dover Publications, New York.
- LaSalle, J. (1960), 'Some extensions of liapunov's second method', *IRE Transactions on Circuit Theory* **7**(4), 520–527.
- Lawton, J. R. T., Beard, R. W. & Young, B. J. (2003), 'A decentralized approach to formation maneuvers', *IEEE Transactions on Robotics and Automation* **19**(6), 933–941.
- Lee, L.-F., Bhatt, R. & Krovi, V. (2005), Comparison of alternate methods for distributed motion planning of robot collectives within a potential field framework, in 'Proc. of the IEEE Int. Conf. on Robotics & Automation', IEEE, Barcelona, Spain.
- Leonard, N. E. & Fiorelli, E. (2001), Virtual leaders, artificial potentials and coordinated control of groups, in 'Proc. 40th IEEE Conference on Decision and Control', Orlando, FL, USA, pp. 2968–2973.
- Leonard, N. E. & Graver, J. G. (2001), 'Model-based feedback control of autonomous underwater gliders', *IEEE Journal of Oceanic Engineering* **26**(4), 633–645.
- Lin, Y., Sontag, E. D. & Wang, Y. (1996), 'A smooth converse Lyapunov theorem for robust stability', *SIAM Journal on Control and Optimization* **34**(1), 124–160.

- Lindgaard, K.-P. (2003), Acceleration Feedback in Dynamic Positioning, PhD thesis, Department of Engineering Cybernetics, Norwegian University of Science and Technology, Trondheim, Norway.
- Loría, A. (2001), Cascaded nonlinear time-varying systems: analysis and design, Tech. report, LAG UMR CNRS 5528. Lecture notes, minicourse at IPN, Mexico, Nov. 2001.
- Loría, A., Fossen, T. I. & Panteley, E. (2000), ‘A separation principle for dynamic positioning of ships: Theoretical and experimental results’, *IEEE Transactions on Control Systems Technology* **8**(2), 332–343.
- Loría, A., Panteley, E., Popović, D. & Teel, A. R. (2005), ‘A nested matrosov theorem and persistency of excitation for uniform convergence in stable nonautonomous systems’, *IEEE Transactions on Automatic Control* **50**(2), 183–198.
- Maciejewski, A. & Klein, C. (1988), ‘Numerical filtering for the operation of robotic manipulators through kinematically singular configurations’, *Journal of Robotic Systems* **5**, 527–552.
- Matrosov, V. M. (1962), ‘On the stability of motion’, *Journal of Applied Mathematics and Mechanics* **26**(5), 1337–1353.
- McClamroch, N. H. & Wang, D. (1988), ‘Feedback stabilization and tracking of constrained robots’, *IEEE Transactions on Automatic Control* **33**(5), 419–426.
- Meyer, C. D. (2000), *Matrix Analysis and Applied Linear Algebra*, Society for Industrial and Applied Mathematics, Philadelphia, USA.
- Moreau, L. (2005), ‘Stability of multiagent systems with time-dependent communication links’, *IEEE Transactions on Automatic Control* **50**(2), 619–182.
- Nijmeijer, H. & Fossen, T. I., eds (1999), *New Directions in Nonlinear Observer Design*, Springer-Verlag, London, UK.
- Nijmeijer, H. & Rodriguez-Angeles, A. (2003), *Synchronization of Mechanical Systems*, Vol. 46 of *Series on Nonlinear Science A*, World Scientific, London.
- Nocedal, J. & Wright, S. J. (1999), *Numerical Optimization*, Springer-Verlag, New York.
- Ögren, P., Fiorelli, E. & Leonard, N. E. (2004), ‘Cooperative control of mobile sensor networks: Adaptive gradient climbing in a distributed environment’, *IEEE Transactions on Automatic Control* **49**(8), 1292–1302.

- Okubo, A. (1986), ‘Dynamical aspects of animal grouping: Swarms, schools, flocks, and herds’, *Advances in Biophysics* **22**, 1–94.
- Olfati-Saber, R. (2006), ‘Flocking for multi-agent dynamic systems: Algorithms and theory’, *IEEE Transactions on Automatic Control* **51**(3), 401–420.
- Olfati-Saber, R. & Murray, R. (2004), ‘Consensus problems in networks of agents with switching topology and time-delays’, *IEEE Transactions on Automatic Control* **49**(9), 1520–1533.
- Ortega, R., Loría, A., Nicklasson, P. J. & Sira-Ramirez, H. (1998), *Passivity-Based Control of Euler-Lagrange Systems*, Springer Verlag, London, UK.
- Panteley, E., Lefeber, E., Loría, A. & Nijmeijer, H. (1998), Exponential tracking control of a mobile car using a cascaded approach, *in* ‘Proceedings of the IFAC Workshop on Motion Control’, Grenoble, France.
- Panteley, E. & Loría, A. (1998), ‘On global uniform asymptotic stability of nonlinear time-varying non autonomous systems in cascade’, *Systems and Control Letters* **33**(2), 131–138.
- Panteley, E. & Loría, A. (2001), ‘Growth rate conditions for uniform asymptotic stability of cascaded time-varying systems’, *Automatica* **37**, 453–460.
- Partridge, B. L. (1982), ‘The structure and function of fish schools’, *Scientific American* pp. 90–99.
- Perez, T. (2005), *Ship Motion Control: Course Keeping and Roll Stabilisation using Rudders and Fins*, Advances in Industrial Control, Springer-Verlag, London, UK.
- Petzold, L. (1982), ‘Differential/algebraic equations are not ODEs’, *SIAM Journal on Scientific and Statistical Computing* **3**(3), 367–384.
- Petzold, L. R., Ren, Y. & Maly, T. (1997), ‘Regularization of higher-index differential-algebraic equations with rank-deficient constraints’, *SIAM Journal on Scientific and Statistical Computing* **18**(3), 753–774.
- Pogromsky, A., Santoboni, G. & Nijmeijer, H. (2002), ‘Partial synchronization: From symmetry towards stability’, *Physica D Nonlinear Phenomena* **172**, 65–87.
- Popov, V. M. (1966), *Hyperstability of Dynamic Systems*, Springer-Verlag, New York, USA. 1973; Translated version of the Romanian edition.

- Rathinam, M. & Murray, R. M. (1998), 'Configuration flatness of lagrangian systems underactuated by one control', *SIAM Journal on Control and Optimization* **36**(1), 164–179.
- Ren, W. & Beard, R. W. (2004), 'Formation feedback control for multiple spacecraft via virtual structures', *IEE Proc. - Control Theory and Applications* **151**(3), 357–368.
- Ren, W., Beard, R. W. & Atkins, E. M. (2005), A survey of consensus problems in multi-agent coordination, in 'Proc. American Control Conference', Portland, OR, USA, pp. 1859–1864.
- Ren, W., Beard, R. W. & McLain, T. W. (2005), Coordination variables and consensus building in multiple vehicle systems, in V. Kumar, N. Leonard & A. S. Morse, eds, 'Cooperative Control', number 309 in 'Lecture Notes in Control and Information Sciences', Springer-Verlag, Berlin Heidelberg, pp. 171–188.
- Reynolds, C. W. (1987), 'Flocks, herds, and schools: A distributed behavioral model', *Computer Graphics Proceedings* **21**(4), 25–34. Boids: <http://www.red3d.com/cwr/boids/>.
- Ross, A., Perez, T. & Fossen, T. I. (2006), Clarification of the low-frequency modelling concept for marine craft, in 'Proc. 7th IFAC Conference on Manoeuvring and Control of Marine Crafts', Lisbon, Portugal.
- Schoenwald, D. A. (2000), 'Auvs: In space, air, water, and on the ground', *IEEE Control Systems Magazine* **20**(6), 15–18.
- Sepulchre, R., Janković, M. & Kokotović, P. (1997), *Constructive Nonlinear Control*, Springer-Verlag, New York.
- Sheikholeslam, S. & Desoer, C. A. (1992), 'Control of interconnected nonlinear dynamical systems: The platoon problem', *IEEE Transactions on Automatic Control* **37**, 806–810.
- Siciliano, B. & Slotine, J.-J. E. (1991), A general framework for managing multiple tasks in highly redundant robotic system, in '5th Int. Conference on Advanced Robotics', IEEE, Pisa, Italy, pp. 1211–1216.
- Skjetne, R. (2005), The Maneuvering Problem, PhD thesis, Department of Engineering Cybernetics, Norwegian University of Science and Technology, Trondheim, Norway.
- Skjetne, R., Fossen, T. I. & Kokotović, P. V. (2004), 'Robust Output Maneuvering for a Class of Nonlinear Systems', *Automatica* **40**(3), 373–383.

- Skjetne, R., Fossen, T. I. & Kokotović, P. V. (2005), ‘Adaptive maneuvering with experiments for a model ship in a marine control laboratory’, *Automatica* **41**(2), 289–298.
- Skjetne, R., Ihle, I.-A. F. & Fossen, T. I. (2003), Formation Control by Synchronizing Multiple Maneuvering Systems, *in* ‘Proc. 6th IFAC Conference on Manoeuvring and Control of Marine Crafts’, Girona, Spain, pp. 280–285.
- Skjetne, R., Moi, S. & Fossen, T. I. (2002), Nonlinear Formation Control of Marine Craft, *in* ‘Proc. 41st IEEE Conf. Decision and Control’, Las Vegas, NV, USA, pp. 1699–1704.
- Skjetne, R., Teel, A. R. & Kokotović, P. V. (2002a), Nonlinear Maneuvering with Gradient Optimization, *in* ‘Proc. 41st IEEE Conf. Decision & Control’, Las Vegas, NV, USA, pp. 3926–3931.
- Skjetne, R., Teel, A. R. & Kokotović, P. V. (2002b), Stabilization of Sets Parameterized by a Single Variable: Application to Ship Maneuvering, *in* ‘15th Int. Symp. Mathematical Theory of Networks and Systems’, Notre Dame, IN, USA.
- SNAME (1950), The society of naval architects and marine engineers. nomenclature for treating the motion of a submerged body through a fluid, *in* ‘Technical and Research Bulletin’, number 1–5.
- Sontag, E. D. (1989), ‘Smooth stabilization implies coprime factorization’, *IEEE Transactions on Automatic Control* **34**(4), 435–443.
- Sontag, E. D. (2000), The ISS philosophy as a unifying framework for stability-like behavior, *in* A. Isidori, F. Lamnabhi-Lagarrigue & W. Respondek, eds, ‘Nonlinear Control in the Year 2000’, Vol. 2 of *Lecture Notes in Control and Information Sciences*, Springer-Verlag, Berlin, Germany, pp. 443–468.
- Sontag, E. & Teel, A. (1995), ‘Changing supply functions in input/state stable systems’, *IEEE Transactions on Automatic Control* **40**, 1476–1478.
- Spry, S. & Hedrick, J. K. (2004), Formation control using generalized coordinates, *in* ‘Proc. 43rd IEEE Conf. Decision & Control’, Atlantis, Paradise Island, The Bahamas, pp. 2441–2446.
- Stilwell, D. J. & Bishop, B. E. (2002), Redundant manipulator techniques for a path planning and control of a platoon of autonomous vehicles, *in* ‘Proc. 41st IEEE Conf. Decision & Control’, Las Vegas, NV, USA, pp. 2093–2098.

- Stilwell, D. J., Bishop, B. E. & Sylvester, C. A. (2005), ‘Redundant manipulator techniques for partially decentralized path planning and control of a platoon of autonomous vehicles’, *IEEE Transactions on Systems, Man, and Cybernetics—Part B: Cybernetics* **35**(4), 842–848.
- Stojanovic, M. (2003), Acoustic underwater communications, *in* J. G. Proakis, ed., ‘Encyclopedia of Telecommunications’, John Wiley and Sons.
- Tanner, H. G., Jadbabaie, A. & Pappas, G. J. (2003a), Stable flocking of mobile agents, part i: Fixed topology, *in* ‘Proc. 42rd IEEE Conf. Decision & Control’, Maui, Hawaii, USA, pp. 2010–2015.
- Tanner, H. G., Jadbabaie, A. & Pappas, G. J. (2003b), Stable flocking of mobile agents part ii: Dynamic topology, *in* ‘Proc. 42rd IEEE Conf. Decision & Control’, Maui, Hawaii, USA, pp. 2016–2021.
- Tanner, H. G., Pappas, G. J. & Kumar, V. (2004), ‘Leader-to-formation stability’, *IEEE Transactions on Robotics and Automation* **20**(3), 443–455.
- Tarraf, D. C. & Asada, H. H. (2002), On the nature and stability of differential-algebraic systems, *in* ‘Proc. of the American Control Conference’, Anchorage, AK, pp. 3546–3551.
- Teel, A. R. (1996), ‘A nonlinear small gain theorem for the analysis of control systems with saturation’, *IEEE Transactions on Automatic Control* **41**(9), 1256–1271.
- Teel, A. R. (2002), ‘Notes on nonlinear control and analysis, Univ. of California Santa Barbara’. Lecture Notes, Course ECE236.
- Teel, A. R. & Praly, L. (2000), ‘A smooth Lyapunov function from a class- $\mathcal{KL}$  estimate involving two positive semidefinite functions’, *ESAIM: Control, Optimisation and Calculus of Variations* **5**, 313–367.
- Ten Dam, A. A. (1992), ‘Stable numerical integration of dynamical systems subject to equality state-space constraints’, *Journal of Engineering Mathematics* **26**, 315–337.
- Vicsek, T., Czirók, A., Ben-Jacob, E., Cohen, I. & Shochet, O. (1995), ‘Novel type of phase transition in a system of self-driven particles’, *Physical Review Letters* **75**(6), 1226–1229.
- Wang, P. K. C. (1991), ‘Navigation strategies for multiple autonomous robots moving in formation’, *Journal of Robotic Systems* **8**(2), 177–195.

- Wang, P. K. C. & Hadaegh, F. Y. (1996), ‘Coordination and control of multiple microspacecraft moving in formation’, *Journal of the Astronautical Sciences* **44**(3), 315–355.
- Weimerskirch, H., Martin, J., Clerquin, Y., Alexandre, P. & Jiraskova, S. (2001), ‘Energy saving in flight formation’, *Nature* **413**, 697–698.
- Wen, J. T. & Arcak, M. (2004), ‘A unifying passivity framework for network flow control’, *IEEE Transactions on Automatic Control* **49**(2), 162–174.
- Wikipedia (2006a), ‘Underway replenishment — wikipedia, the free encyclopedia’. [Online; accessed 18-May-2006].  
**URL:** [http://en.wikipedia.org/w/index.php?title=Underway\\_replenishment&oldid=37671761](http://en.wikipedia.org/w/index.php?title=Underway_replenishment&oldid=37671761)
- Wikipedia (2006b), ‘Wikipedia, the free encyclopedia’. [Online].  
**URL:** <http://en.wikipedia.org/>
- Yun, X. & Sarkar, N. (1998), ‘Unified formulation of robotic systems with holonomic and nonholonomic constraints’, *IEEE Transactions on Robotics and Automation* **14**(4), 640–650.